FACULTEIT LANDBOUWKUNDIGE EN TOEGEPASTE BIOLOGISCHE WETENSCHAPPEN
DEPARTEMENT LANDBEHEER
LABORATORIUM VOOR BODEM- EN WATERBEHEER
VITAL DECOSTERSTRAAT 102
B-3000 LEUVEN (BELGIE)

KATHOLIEKE
UNIVERSITEIT
LEUVEN

DISSERTATIONES DE AGRICULTURA

Doctoraatsproefschrift nr. 583 aan de Faculteit Landbouwkundige en Toegepaste Biologische Wetenschappen van de K.U.Leuven

PARAMETER ESTIMATION STRATEGIES IN UNSATURATED ZONE MODELLING

Proefschrift voorgedragen tot het behalen van de graad van Doctor in de Toegepaste Biologische Wetenschappen

door

Jan MERTENS

November 2003

Doctoraatsproefschrift nr. 583 aan de Faculteit Landbouwkundige en Toegepaste Biologische Wetenschappen van de K.U.Leuven

FACULTEIT LANDBOUWKUNDIGE EN TOEGEPASTE BIOLOGISCHE WETENSCHAPPEN
DEPARTEMENT LANDBEHEER
LABORATORIUM VOOR BODEM- EN WATERBEHEER
VITAL DECOSTERSTRAAT 102
B-3000 LEUVEN (BELGIE)

KATHOLIEKE
UNIVERSITEIT
LEUVEN

DISSERTATIONES DE AGRICULTURA

Doctoraatsproefschrift nr. 583 aan de Faculteit Landbouwkundige en Toegepaste Biologische Wetenschappen van de K.U.Leuven

PARAMETER ESTIMATION STRATEGIES IN UNSATURATED ZONE MODELLING

Promotoren

Prof. J. Feyen, Faculteit Landbouwkundige en Toegepaste Biologische Wetenschappen, K.U.Leuven

Prof. D. Raes, Faculteit Landbouwkundige en Toegepaste Biologische Wetenschappen, K.U.Leuven

Leden examencommissie

Prof. J. Coosemans, Faculteit Landbouwkundige en Toegepaste Biologische Wetenschappen, K.U.Leuven, Voorzitter.
Prof. G. Govers, Faculteit Wetenschappen, K.U.Leuven.
Prof. H. Madsen, Flood Management Departement, Danish Hydraulic Institute.
Prof. P. Willems, Faculteit Toegepaste Wetenschappen, K.U.Leuven.
Prof. G. Wyseure, Faculteit Landbouwkundige en Toegepaste Biologische Wetenschappen, K.U.Leuven.

Proefschrift voorgedragen tot het behalen van de graad van Doctor in de Toegepaste Biologische Wetenschappen

door

Jan MERTENS

November 2003

Word of Thanks/Dankwoord

The completion of this thesis has only been achieved through the help of a large amount of people and the support of a number of institutions.

Ik wil niet afwijken van de ‘gewoonte’ om een dankwoord te beginnen met het bedanken van de promotor. Niet omdat het beleefd is en zo hoort, maar wel omwille van wat Prof. Jan Feyen voor deze thesis betekend heeft. Hij heeft me altijd gesteund en begeleid met slechts enkele woorden die een grote impact hadden. Zowel wetenschappelijk als financieel heb ik zijn stil maar onvoorwaardelijk vertrouwen en steun in wat ik ‘probeerde’ te doen geapprecieerd. Dank je Jan en ik hoop dat we kunnen blijven samenwerken, ook in gebieden waar de zonneschijn meer voorspelbaar is. Mijn co-promotor Prof. Dirk Raes verdient ook meer dan een gewone dankjewel. Ik heb altijd zijn ‘Afrikaanse’ manier van begeleiden kunnen waarderen. Afrikaans hier te verstaan als warm, welkomend en respectvol. Dirk begeleidde me volgende de Senegalese ‘Terranga’ in combinatie met zijn realistische en praktische aanpak van onderzoeksthema’s.

During this Ph.D. research, I have greatly enjoyed my stays at the Danish Hydraulic Institute in Horsholm, Denmark. In particular, I have found it an honour to be able to work with Dr. Henrik Madsen and owe him great thanks. His guidance has increased the scientific level of this Ph.D. research drastically. I took great pleasure in his ‘Danish’ way of guiding me: not too much ‘noise’ but very efficient! Thank you very much Henrik and I really hope that sometime in future we can work together again. I also owe great thanks to Prof. Keith Beven who made me realise during his 6 months stay at our laboratory, that modelling is not straightforward and the more you get to know about models and their parameters, the less faith you have in them. Special thanks to Anthony Timmerman (Janetkat), Diederik Jacques, Ingeborg Joris, Jan Schaerlaekens, Jan Vanderborght, Luc Feyen, Michael Kristensen, Peter Viane and Sofie Herman for their scientific comments throughout the four years of this study.

I very much appreciate the people of my doctoral jury not yet mentioned above: Prof. J. Coosemans, Prof. G. Govers, Prof. G. Wyseure and Prof. P. Willems for the thorough reading and correcting of my text. I am sure their comments have improved the quality of this dissertation considerably. The assessors Prof. Gerard Govers and Prof. Guido Wyseure are additionally thanked for their useful comments throughout this doctoral research.

Dank ook aan alle collega's van het Laboratorium voor Bodem- en Waterbeheer. Bedankt voor het helpen graven van de putten, het verbeteren van teksten en vooral voor de sfeer die er heerste op ons labo gedurende de voorbije vier jaar: bezoekjes aan café Paula in Rillaar, het beruchte bezoek aan de zoo, na-doctorale 'key-west' avonden met kooidansen… Het bezinningsweekendje in de Hastière zal ik nooit vergeten omdat het nagenoeg een chiro-planningsweekend was: veel serieus besproken en nog meer gelachen; iets wat ik altijd heb weten te appreciëren …

Mijn administratieve capaciteiten zijn eerder beperkt en gelukkig kon ik rekenen op Greta Camps, Heidi Demin, Sofie Bruneel en Viviane Crabbé om deze nogal grote leemte deskundig op te vullen. Ook mag ik François Serneels niet vergeten voor zijn professionele hulp bij het veldwerk en de labometingen. Een 'lomperik' als ik wist zijn technische vernuftheid te appreciëren. Veel dank ook aan Philippe Van Ingh die ik dag en nacht mocht lastig vallen met vervelende computervragen! Nancy Nys had ik ook graag bedankt voor het onderhoud van mijn 'ordelijk' bureau en het terugvinden van portefeuilles en sleutels ...

Met plezier dank ik het Fonds Voor Wetenschappelijk Onderzoek Vlaanderen (FWO-Vlaanderen) voor hun maandelijkse financiële bijdragen, hun financiële tegemoetkomingen tijdens mijn twee verblijven in Denemarken en congresbezoeken aan EGS, Nice. Ik heb hun steun telkens in volste vertrouwen zonder bewijs van elke cent (gelukkig maar...), weten te appreciëren.

Doctoraal onderzoek is niet de meest denkbare sociale bezigheid vandaar dat mijn vrienden een heel grote bijdrage hebben in het welslagen van deze thesis. Dank aan de oud-leiding, leiding en aspiranten van Chiro G'Bergen voor de leute tijdens het

voorbereiden van activiteiten, het uitvoeren ervan en de nachtelijke uitstappen! De Ronny, de Jean en den Vandenbeirghe dank ik in het bijzonder voor hun hulp tijdens het veldwerk en het zaaien van de zonnebloemen te Rillaar... Ook de verbondsmensen van Heuvelland, Oost-Vlaanderen worden bedankt voor de wekelijkse serieuze en minder serieuze discussies op de Kwaadham in Gent en de cursusweekjes en oase-weekendjes! Verder ook nog de Leuvense kameraden: het kotleven in de Constantijn Meunierstraat en de Vandetymplestraat is me meer dan bevallen, weliswaar soms zwaar de volgende morgen ... Danten, merci ook voor de professionele hulp bij het graven van drie profielputten op 1 dag!

Mijn broer Koen en zijn vriendin Tascha dank ik voor hun steun en vertrouwen ook als ik het even moeilijker had. Het is niet eenvoudig om je ouders voor iets specifieks te danken, daarom dank voor het onvoorwaardelijk vertrouwen en de steun die ze me gaven in alles wat ik deed! Samenleven met een doctoraatsstudent en voor de zoveelste keer gezaag moeten aanhoren, is niet aan mij besteed vrees ik … Daarom dank ik Tanja met liefs, niet alleen voor het veel alléén zitten gedurende mijn verblijven in Denemarken maar vooral voor haar begeleiding op een minder wetenschappelijke maar minstens even doeltreffende manier!

CONTENTS

Summary

During the past four decades, computer based mathematical hydrological models have been widely used for a variety of applications. These models are based on general mathematical descriptions of the hydrological processes that transform natural forcings (e.g. rainfall over the landscape) into response (e.g. runoff in the river). The user of a hydrological model must specify the model parameters before the model is able to properly simulate the hydrological behaviour that it describes. In general, there are two main approaches to estimating model parameters. The first (*a-priori approach*) estimates model parameters by relying on theoretical or empirical relationships that relate such parameters to observable (measurable) characteristics of the model area (e.g. soil and vegetation properties, topography, …). The second approach (*model calibration*) adjusts model parameter values such that the model input-output (e.g. rainfall-runoff) response closely matches the observed (measured) input-output response for some historical period for which data has been collected. Ever since the development of these models, studies have shown the large complexity of estimating these parameter values, either by the a-priori or model calibration approaches. The main reason for this is the fact that our model equations and their respective parameters are idealised representations of real world processes. Furthermore, there are a variety of errors in the model structure and uncertainties in the data used for parameter estimation, which introduce considerable inaccuracy into model behaviour. These factors have made it difficult to develop reliable procedures for model parameter estimation, and to provide suitable estimates of uncertainties in the model predictions.

The parameter estimation problem for unsaturated zone modelling forms the central research topic of this PhD dissertation. After a general introduction, the set-up of a field experiment that was carried out on a hillslope in the sandy-loam belt of Belgium is described. Soil samples were taken from profile pits along the hillslope. On these samples, the soil hydraulic parameters needed for unsaturated zone modelling were estimated in the laboratory. On top of that, in-situ measurements using a single ring pressure infiltrometer prior to the start of the experiment were carried out. Based on these measurements, a mathematical procedure was developed resulting in more robust

estimates of the field-saturated hydraulic conductivity than the classical approach. Parameter estimates as a result of the laboratory measurements together with the field saturated hydraulic conductivity estimated were considered as prior information in the *a-priori* approach.

The importance of each of the soil hydraulic parameters for simulating water content profiles on the hillslope was evaluated using two different sensitivity analyses. Resulting important parameters were consequently incorporated in the SCE (Shuffled Complex Evolution) automatic calibration routine and their 'effective' values were estimated. The 'effective' parameter set is the result from the autocalibration routine and yields the best fit of the model to the observed soil moisture content on the hillslope. Initially, no use was made of the prior information in the inverse modelling or autocalibration technique. It was concluded that for the hillslope, 'effective' parameter values and the prior measured parameter values differed significantly. Furthermore, the use of this prior information in an *a-priori* context, i.e. as model parameters in the model, resulted in very poor model fits. These conclusions raised questions about the relevance of measuring prior information since the parameters needed by the model (='effective parameters') to give the best fit to the observed data, are significantly different.

To investigate the relevance of the prior information, a methodology for the incorporation of this prior parameter information in two different parameter estimation strategies, SCE and GLUE (Generalised Likelihood Uncertainty Estimation) was developed. It was shown that incorporating prior information in the SCE algorithm resulted in more 'realistic' parameter estimates and reduced the goodness-of-fit of the model negligibly. Incorporating prior information in the GLUE algorithm resulted in more behavioural parameter sets and uncertainty bounds that comprised the observed data better. Hence, it was concluded that the developed methodology of combining inverse modelling with prior parameter estimations was 'superior' to the case when both were applied individually, i.e. the direct use of prior information in the model (*a-priori approach*) and inverse modelling without the incorporation of prior information (*calibration approach*). Finally, a procedure for the incorporation of rainfall intensity into daily rainfall records was developed and tested using a synthetic hillslope model

set-up. Using this procedure, it was shown that the temporal resolution of rainfall affected the values of the effective parameters significantly.

Samenvatting

Gedurende de laaste 40 jaar worden numerieke hydrologische modellen gebruikt voor een brede waaier van toepassingen. Deze modellen zijn gebaseerd op algemene wiskundige beschrijvingen van hydrologische processen die natuurfenomenen (vb. regen) tranformeren in een respons (vb. afvoer naar rivier). De gebruiker van een hydrologisch model moet de modelparameters specifiëren alvorens het model het gesimuleerde hydrologisch process correct kan beschrijven. Het schatten van parameters kan grosso modo opgedeeld worden in twee benaderingen. De eerste (*a-priori aanpak*) schat de modelparameters op basis van theoretische of empirische relaties. Deze benadering relateert modelparameters aan observeerbare (meetbare) karakteristieken van het modelgebied (vb. bodem en vegetatie eigenschappen, topografie, ...). De tweede aanpak (*model calibratie*) past modelparameters aan zodat de model input-output (vb. regen-afvoer) respons overeenstemt met de geobserveerde (gemeten) respons voor een historisch opgemeten tijdreeks. Sinds het ontstaan van deze modellen hebben verschillende studies gewezen op de enorme complexiteit die gepaard gaat met het schatten van deze parameters, dit voor beide benaderingen. De belangrijkste reden voor deze complexiteit is het feit dat model vergelijkingen en hun respectievelijke parameters geidealiseerde representaties zijn van ‘echte wereld’ processen. Bovendien zijn fouten in model structuur niet uit te sluiten en bestaan er onzekerheden in de data gebruikt voor parameter schatting, die een aanzienlijke onzekerheid introduceren in model gedrag. Deze factoren bemoeilijken het ontwikkelen van betrouwbare procedures voor parameter schatting en schatting van onzerheidsintervallen voor modelvoorspellingen.

Het probleem van de parameter schatting voor modellen, die zich focussen op de onverzadigde zone (= bodem van maaiveld tot grondwatertafel), vormt het centraal onderzoeksthema van deze doctoraatsthesis. Na een algemene inleiding wordt er een beschrijving gegeven van het veldexperiment uitgevoerd op een hellend proefveld in Rillaar, België. Er werden onverstoorde bodemstalen genomen in 3 profielputten langsheen de helling. De bodemhydraulische parameters, vereist voor onverzadigde zone modellering, werden geschat aan de hand van metingen in het laboratorium op de

onverstoorde stalen. Bovenop deze metingen, werden er ook in-situ metingen uitgevoerd gebruik makende van enkele-ring druk infiltrometers. Gebruik makend van deze metingen werd een wiskundige inverse optimalisatie procedure ontwikkeld die resulteert in meer robuste in-situ hydraulische conductiviteit schattingen dan de klassieke analyse methode. Parameter schattingen uit het laboratorium en de in-situ hydraulische conductiviteit schattingen werden beschouwd als *prior* informatie in de *a-priori* aanpak.

Het belang van elk van bodemhydraulische parameters voor het simuleren van bodemvochtgehalte profielen werd geëvalueerd met behulp van 2 verschillende gevoeligheidsanalyses. Belangrijke parameters werden vervolgens geïncorporeerd in het SCE (Shuffled Complex Evolution) algoritme. Dit resulteerde in schattingen van de effectieve waarden van de belangrijke parameters. De set van effectieve modelparameters is het resultaat van een calibratie of in dit geval een autocalibratie (SCE) die resulteert in de beste overeenkomst tussen geobserveerde en gesimuleerde data. In dit onderzoek werden bodemvochtgehalte profielen gebruikt om deze overeenkomst na te gaan. Initieel werd er geen gebruik gemaakt van de prior informatie in de inverse modellering of autocalibratie techniek. Er werd aangetoond dat voor het hellend proefveld, effectieve parameter waarden significant verschillen van hun gemeten waarden. Bovendien resulteerde het gebruik van de *prior* informatie als rechtstreekse parameter input in het model in een slechte overeenkomst. Deze besluiten deden vragen rijzen over de relevantie van het meten van prior informatie aangezien de parameters die het model nodig heeft voor de beste overeenkomst (effectieve parameters) significant verschillen van hun gemeten waarden.

Om de relevantie van het meten van prior informatie te onderzoeken, werd een methodologie voor het incorporeren van deze prior informatie in twee verschillende parameter schatting strategiën, SCE en GLUE (Generalised Likelihood Uncertainty Estimation), ontwikkeld. Er werd aangetoond dat het incorporeren van de prior informatie in het SCE algorithme resulteerde in meer ‘realistische’ effectieve parameter schattingen terwijl de model overeenkomst met de geobserveerde bodemvochtprofielen, slechts verwaarloosbaar verminderde. Incorporeren van prior informatie in het GLUE algorithme resulteerde in meer ‘behavioural’ parameter sets en de onzekerheidsgrenzen

bevatten de geobserveerde bodemvochtprofielen beter. De ontwikkelde methodologie van het combineren van invers modelleren met prior parameter informatie werd beter bevonden dan de toepassing van beiden apart, met name het direkt gebruik van prior informatie in het model (*a-priori aanpak*) en invers modelleren zonder de inbreng van prior informatie (*calibratie aanpak*). Om te besluiten werd er een procedure ontwikkeld en getest op een synthetisch hellend veld model voor het in rekening brengen van regenintensiteit in dagelijkse regenhoeveelheden. Gebruik makende van deze procedure werd er aangetoond dat de temporele resolutie van de neerslag een significant effect heeft op de waarden van de effectieve modelparameters.

Notation

In some places throughout the text, same symbols are used for different variables to have a notation in correspondence with the general notation in literature. The exact meaning of the symbol should be clear from the context in which the variable is used. The dimensions of the symbols can be found throughout the text in square brackets ([ ]) and are copied in the following tables. In these tables, the paragraph in which the symbol first occurred or is defined, is also given.

Latin symbols

Symbol	*Definition*	*Units*	*Paragraph*
a_i	Parameter to be optimised in the analysis of single ring pressure infiltrometer measurements (related to K_{fs} at each location *i*)	T^{-1}	3.2.2.3
a_{int}	Chosen integer (Morris design)	-	5.3.2
A	Cross sectional area	L^2	2.2.1
b	Parameter to be optimised in the analysis of single ring pressure infiltrometer measurements (related to field α_m)	L	3.2.2.3
C	Soil water capacity	L^{-1}	2.2.1
C_0	Nugget variance		3.2.3
C_1	Empirical parameter of the Kristensen and Jensen evapotranspiration model	-	4.2.1.2
C_2	Empirical parameter of the Kristensen and Jensen evapotranspiration model	-	4.2.1.2
C_s	Co-variance contribution or sill value	-	3.2.3

Symbol	*Definition*	*Units*	*Paragraph*
d	Depth between the A- and B-horizon	L	5.2
$d()$	Elementary effect of the ith component (Morris design)	-	5.3.2
d_r	Depth of insertion of the ring of a single-ring pressure infiltrometer	L	3.2.2.1
E	Model Efficiency	-	7.4.2
E_{at}	Actual transpiration	LT^{-1}	4.2.1.2
E_p	Potential evapotranspiration	LT^{-1}	4.2.1.2
E_s	Soil evaporation	LT^{-1}	4.2.1.2
F	Objective function value		2.2.2
F_{agg}	Aggregated objective		6.3.2
G	Dimensionless parameter	-	3.2.2.1
h	Soil pressure head	L	2.2.1
H	Height of the ponded head	L	3.2.2.1
h_g	Flow depth above the ground surface	L	4.2.1.3
h_l	Lag distance class	L	3.2.3
j	Number of intensity classes	-	7.3
K	Hydraulic conductivity	LT^{-1}	2.2.1
k	Number of parameters (Morris design)	-	5.3.2
K_{fs}	Field saturated hydraulic conductivity	LT^{-1}	3.1
K_s	Saturated hydraulic conductivity	LT^{-1}	2.2.1
K_{x} -	Strickler coefficient x direction	$L^{-3}T^{1}$	4.2.1.3
K_{y}-	Strickler coefficient y direction	$L^{-3}T^{1}$	4.2.1.3
l	Length	L	2.2.1
L	Likelihood measure		6.3.3
m	Empirical fitting parameter of van	-	2.2.1

	Genuchten-Mualem hydraulic functions		
Symbol	*Definition*	*Units*	*Paragraph*
	No. of points in each complex (SCE	-	4.3.3.3
m	algorithm)		
$M()$	Model function		3.2.2.3
m_j	Rainfall intensity	LT^{-1}	
n	Empirical fitting parameter of van Genuchten-Mualem hydraulic functions	-	2.2.1
N	Empirical fitting parameter of Averjanov conductivity curve	-	2.2.2
n	Number of …	-	
O	Observed data vector		3.2.2.3
p	Set of parameters		3.2.2.3
P	Feasible parameter space	-	4.3.2.2
p	No. of complexes (SCE algorithm)	-	4.3.3.3
P	Significance level in the Kolgomorov-Smirnov test	-	5.3.1
P	Vector containing the transformed parameters		6.3.2
P_i	Rainfall record on day i	L	
	Minimum No. of complexes required as the search proceeds	-	4.3.3.3
p_{min}	(SCE algorithm)		
Q	Flow capacity	L^3T^{-1}	2.2.1
Q	Infiltration rate	LT^{-1}	3.1
$q_{0\infty}^{\otimes}$	Theoretical perturbed infiltration rate	LT^{-1}	3.2.2.2
	No. of points in a sub-complex	-	4.3.3.3
q	(SCE algorithm)		
$q_{0\infty}$	Steady flow rate	LT^{-1}	3.2.2.1

r	Number of trajectories (Morris design)		5.3.2
r_a	Practical range	L	3.2.3
Symbol	*Definition*	*Units*	*Paragraph*
r_d	Ring radius of a single-ring pressure infitrometer	L	3.2.2.1
$R_{i,obs}$	Observed (reference) daily hillslope runoff	L	7.4.2
$R_{i,sim}$	Simulated daily hillslope runoff.	L	7.4.2
S_{fx}	Friction slopes in x direction	-	4.2.1.3
S_{fy}	Friction slopes in y direction	-	4.2.1.3
t	Time	T	2.2.1
T	Test statistic in the Kolgomorov-Smirnov test		5.3.1
t_{ij}	duration of the *j*'th part of daily rainfall	T	
u	Flow velocities in x direction	LT^{-1}	4.2.1.3
v	Flow velocities in y direction	LT^{-1}	4.2.1.3
x	Horizontal coordinate (width)	L	3.2.1
X	Sample in the Kolgomorov-Smirnov test		5.3.1
x	Vector in the parameter space (Morris design)		5.3.2
X	Untransformed variable		6.3.1
x^*	Base value of x (Morris design)		5.3.2
X_1, X_2	Limits of X		6.3.1
x_i	Component of x (Morris design)		5.3.2
$x_{lower,i}$	Lower limit of x_i (Morris design)		5.3.2
$x_{upper,i}$	Upper limit of $x_{,}$ (Morris design)$_i$		5.3.2
y	Horizontal coordinate (length)	L	3.2.1
Y	Transformation of X		6.3.1
$y(x)$	Output as a result from simulation		5.3.2

	with x as input parameters (Morris design)		
z	Vertical coordinate	L	2.2.1
Z	Vector of standard normal variables		6.3.1

Symbol	*Definition*	*Units*	*Paragraph*
$z(x_i)$	Measured sample values at point x_i,		3.2.3
z_g	Ground surface level	L	4.2.1.3
$\hat{z}(x_i)$	Predicted (krigged) value at location x_i		3.2.3

Greek symbols

Symbol	*Definition*	*Units*	*Paragraph*
α	Empirical fitting parameter of van Genuchten-Mualem hydraulic functions	L^{-1}	2.2.1
α	No. of offsprings generated by each sub- complex (SCE algorithm)	-	4.3.3.3
α_m	Measure of the relative contributions of gravity and capillary forces to water movement in an unsaturated soil	L^{-1}	3.1
β	No. of evolution steps taken by each complex before shuffling (SCE algorithm)	-	4.3.3.3
γ	Estimated semivariance	-	3.2.3
δ	Dimensionless parameter in the Morris design	-	5.3.2
Δ	Dimensionless parameter in the Morris design	-	5.3.2
ε	Transformation constant	-	6.3.2
ϕ_m	Matric flux potential	L^2T^{-1}	3.1
θ	Volumetric water content	L^3L^{-3}	2.2.1

θ_F	Volumetric water content at field capacity	L^3L^{-3}	4.2.1.2
θ_{obs}	Mean observed daily moisture content	L^3L^{-3}	5.3

Symbol	*Definition*	*Units*	*Paragraph*
θ_r	Residual water content	L^3L^{-3}	2.2.1
θ_s	Saturated water content	L^3L^{-3}	2.2.1
θ_{sim}	Mean simulated daily moisture content	L^3L^{-3}	5.3
θ_W	Volumetric moisture content at wilting point	L^3L^{-3}	4.2.1.2
ω	Weighting factor	-	6.3.2
ψ	Soil potential	L	2.2.1

Mathematical and statistical symbols

Symbol	*Definition*	*Units*	*Paragraph*
CDF	Normal cumulative distribution function with sample mean and standard deviation taken from *Y(X)*		6.3.1
F(X)	Cumulative distribution functions of sample *X*		5.3.1
$g(F)$	Transformation function of *F*		6.3.2
$N_p(\mu, \Sigma)$	*p*-dimensional normal density		6.3.1
μ	Mean		
S	Lower triangular (Choleski) decomposition of Σ		6.3.1
S(Y)	Empirical cumulative distribution function of *Y(X)*		6.3.1
σ	Standard deviation		
U	Johnson Transformation		6.3.1
Σ	Variance-covariance matrix		6.3.1

$\lvert A \rvert$	Determinant of matrix A
$\overline{A}$	Mean of matrix A
Δx	Difference operator for variable *x*

Acronyms

Symbol	*Definition*	*Units*	*Paragraph*
CD	Coefficient of Determination		7.2
CI	Confidence Interval		2.2
GLUE	Generalized Likelihood Uncertainty Estimation		4.4.2.1
LAI	Leaf Area Index		4.2.1.2
MC	Monte Carlo		5.5.2.1
ME	Mean of the reduced Error vector		3.2.3
MRE	Mean squared Reduced Error		3.2.3
MSE	Mean Squared Error		6.3.3
RE	Reduced Error vector		3.2.3
res	residual		5.3
RMSE	Root Mean Squared Error		5.3
SA	Sensitivity analysis		4.3.1
SCE	Shuffled Complex Evolution		4.3.3.3
SSR	Sum of squared residuals		3.2.2.3
STD	Standard Deviation		5.3
UB	Uncertainty bound		6.4.3

Chapter 1

Introduction

ABSTRACT

In this Chapter, a general introduction to the parameter estimation problem in hydrological modelling is given. Based on the problems discussed in this introduction, the objectives of the PhD research are formulated and the structure of this document explained.

1.1. The parameter estimation problem in hydrological modelling

The increasing frequency of inundations all over the world (e.g. in Belgium in 1993, 1995, 1998, 1999 and 2002), has as effect that the society starts questioning about the effect of spatial ordering, land use and the warming up of the earth on hydrology, more in particular on the rainfall-runoff process. Not only concern about water quantity but also water quality, as a result of increasing industrial and agricultural activities, is increasing. In order to find adequate solutions, the government requires scientific grounded instruments that allow the set-up and implementation of sustainable and techno-economic feasible measures and policies.

Lumped hydrological models treat catchments and sub-catchments as uniform entities. This means that it is generally impossible to predict the effect of spatially non-uniform measures on the hydrology. The same is true if the effect of the spatially non-uniform precipitation distribution, especially during storms, on the runoff process is to be modelled. Since nowadays, more and more questions about the spatial ordering and its effects on catchment hydrology arise, one is obliged to use hydrological models that

treat input and area characteristics as spatially distributed. The amount of parameters in this context is generally a multiple of the amount of parameters needed by lumped models.

Empirical models are models based on empirically derived equations, i.e. relations established on the basis of experimental data. The best-known hydrological empirical 'model' is probably the Curve Number method, which divides the total amount of rainfall into runoff and infiltration on the basis of a curve number [*USDA, 1985*]. These curve numbers were empirically deducted from rainfall-runoff experiments on different hillslopes with different vegetation types, average slopes, soil types and antecedent soil moisture conditions. On the contrary, physically based models are based on mathematical representations of the physical processes taken place in the catchment. In general, physically based models need much more parameters than empirical models. Because these parameters have a physical meaning, in theory it should be possible to measure or estimate them using in-situ experiments or on representative samples in the laboratory.

From the above, it is obvious that physically based models that are capable of treating the total area in a distributed way, need a vast amount of parameters to describe all processes taking place at different locations within a catchment. Although in theory all parameters are measurable, in practice this is impossible. Impossible not only because of the huge amount of time and money it would cost to measure all parameters at all locations, but also because the effective parameter values needed by the model may differ from the measurements. The effective parameter values correspond to those parameter values that result in the most accurate model prediction. This difference can be due to the 'scaling' problem, i.e. the scale at which the measurements are made differs from the scale at which the hydrological processes are described by the model. A well-described example of this 'scaling' problem is the estimation of a hydraulic conductivity value for a larger area needed by the model. It is well known that hydraulic conductivity is a heterogeneous parameter and might differ between adjacent places as close as a few meters [*Mertens et al., 2002b*]. Not only is the hydraulic conductivity an extremely heterogeneous parameter but another important factor largely influencing hydraulic conductivity is sample size. Sample size here must been considered as the volume on which the hydraulic property is measured. By many authors it was found that

the hydraulic conductivity and its variability tends to increase as sample volumes decreases [*e.g. Lauren et al., 1988; Mallants et al., 1997a*]. Though using different measurement techniques even at the same scale (or sample size) can yield different conductivity estimates [e.g. *Reynolds et al., 2000; Herman et al., 2003*]. Two different 'strategies' can be thought of in an attempt to estimate effective parameters needed by the model.

The first 'strategy' is to try and measure parameters at the scale needed by the model. This can be done by improving existing measurement techniques and 'upscale' measured parameters or by the development of new techniques suited for the measurement of parameters at the scale needed by the model. The term 'upscaling' is used for research that focuses on finding area representative parameters based on local measurements performed at a smaller scale [*Bierkens et al., 2002*]. Although 'upscaling' research is nowadays a 'hot' issue, it remains an extremely difficult subject and generally accepted 'upscaling' techniques do not yet exist. In literature, research concerning the amelioration of existing measurement techniques or the development of new measurement techniques at different scales is scarce. A major drawback of this 'strategy' remains that even if a suitable measurement technique exists, be it either a direct measurement technique at the scale needed by the model or after upscaling of locally measured parameters, the measurement of parameters remains highly time- and money- consuming.

The second 'strategy' is called 'inverse modelling', 'autocalibration' or 'inverse optimisation' and has become more and more popular. Main reason for its success is the increase in computer power over the last decades. The objective of these techniques is finding one or more parameters sets (= effective parameters sets) that provide the best fit with one or more observation types over some period of time, e.g. river discharge or groundwater levels over a few years. All methods have in common that many model evaluations are needed. The result of each model evaluation (= parameter set) in terms of goodness-of-fit against the observations is saved. Thereafter, a new parameter set to be evaluated is selected based on the results of parameter sets already evaluated. Model evaluations stop if no improvement in the goodness-of-fit to the observations can be found, i.e. when an effective parameter set has been reached. In principle, parameter measurements are not required for these parameter estimation techniques. Only lower

and upper parameter bounds, in between which new parameter sets to be evaluated can be selected. These bounds can either be based on minima and maxima obtained from literature or from parameter measurements (in-situ or in laboratory). A major drawback of this second 'strategy' is that different parameter sets might yield a comparable goodness-of-fit making it impossible to choose the optimal one. This is called the parameter identifiability problem. In some cases, the effective parameter sets may even be situated at different locations in the parameter space. Since the value of the effective parameter set may be anywhere in parameter space, its value can be questioned in terms of its correspondence with measured parameter values (even at the same scale). In other words, since effective parameters can have very different values, it is possible that the link with their measured equivalent (if available from measurements in-situ or in the laboratory) does not exist.

It is well known that effective parameters depend on the quality and quantity of the calibration data used for the calculation of the objective function used by the inverse optimisation algorithm [*Freer et al., 1996*]. Not only the type and quality of the calibration data but also the informativeness of the time series used for calibration influences the effective parameters obtained from inverse modelling. Informativeness or the variability within a time series (e.g. presence of winter and summer periods, warm and cold, …) is found to be equally important than the length of the calibration data as such [*Gupta et al., 1998*]. It is generally accepted that a time series of 10-30 years is necessary to calibrate a rainfall-runoff model so that sufficient 'extreme' events are included in the calibration data. Very little research investigating the effect of using different input time series (e.g. rainfall and potential evapotranspiration) on effective model parameters has been carried out. In *Vazquez and Feyen (2003)* the effect of using different potential evapotranspiration calculation methods on effective parameter estimation is found to be significant. To our knowledge, no literature is available discussing the influence of the temporal resolution of rainfall or evapotranspiration on effective parameter estimation. Although no literature dealing with this problem can be found till now, we believe that it can play a dominant role in the inverse optimisation process and have a significant effect on the value of the estimated effective parameters.

1.2. Objectives of the study

The **overall objective** of this PhD research is to **gain new insights in the parameter identifiability problem in unsaturated zone modelling, more particular in soil moisture content modelling**.

In order to do so different steps can be distinguished. All steps aim at developing and comparing strategies to gain new insights in the parameter identifiability problem in unsaturated zone modelling and the robust estimation of effective parameter values:

i. *Collection of an experimental data set* containing soil hydraulic parameter estimates on the basis of laboratory and in-situ measurements as well as time series of the soil moisture content at different locations and depths on a hillslope. This data set forms the basis of the numerical analysis performed in this study.
ii. *Amelioration of the existing mathematical analysis* for the estimation of the field-saturated hydraulic conductivity on the basis of *in-situ single ring pressure infiltrometer measurements*.
iii. *Development of a 1-D unsaturated zone model* that allows the simulation of the soil moisture content over time at different depths at the local scale.
iv. *Identification of the soil hydraulic parameters dominating the simulation of soil moisture content* over time using different techniques (sensitivity analyses) and comparing them.
v. *Inverse optimisation of the dominating hydraulic parameters* to estimate their effective values that yield the best fit with the observed soil moisture content time series at the different depths and locations.
vi. *Investigation of the difference in goodness-of-fit* between a model run using the effective parameter sets and a model run using the parameter measurements (laboratory or in-situ) as model input and the examination of the difference between effective parameter values and their measured equivalents.
vii. *Development of methodologies that allow the incorporation of measured parameter values* in the two different parameter estimation strategies. Model fits as well as effective parameters are compared to the case where inverse optimisation is performed without the incorporation of parameter measurements.

The relation between the new obtained parameter sets and their measured equivalents can then be examined.

viii. *Investigation of the effect of the temporal resolution of rainfa***ll** on effective parameter estimates and the development of a procedure for the incorporation of rainfall intensity into daily rainfall records.

1.3. Outline of the study

In Chapter 2, the set-up of a rainfall-runoff experiment is described and recommendations for future similar experiments are given. For the measurement of the soil hydraulic parameters, a hillslope was selected in the sandy loam region of Belgium. Soil samples were taken from three profile pits along the hillslope. Using laboratory measurement techniques, the soil hydraulic parameters needed for unsaturated zone modelling were estimated. The description of the rainfall-runoff experiment set-up is consequently described.

Chapter 3 discusses the in-situ measurements of the field-saturated hydraulic conductivity using single ring pressure infiltrometer measurements prior to the start of the experiment. Since this technique is a relatively new technique [*Elrick et al., 1989*], its possibilities in the estimation of the field-saturated hydraulic conductivity using the classical mathematical approach were examined thoroughly. Additionally, the sensitivity of the estimated field-saturated hydraulic conductivity to small measurement errors was investigated. Based on these results, a new mathematical procedure was developed resulting in more robust estimates of the field-saturated hydraulic conductivity. Finally, the spatial correlation scale of the field-saturated hydraulic conductivity on the experimental hillslope was estimated.

Chapter 4 presents a brief literature review on the current state-of-the-art with respect to hydrological modelling in a general sense. In particular and in more detail, it focuses on the problem of the determination of effective parameters using inverse modelling techniques. A review of the most common optimisation algorithms (inverse modelling) applied in hydrology is presented. A detailed description of the Shuffled Complex Evolution (SCE) algorithm used throughout this research is thereafter given. Two

different approaches to the parameter identifiability problem are presented in detail because they are applied further in the research: the GLUE approach and the Pareto-Optimality approach. Finally the MIKE-SHE model set-up, as used in both Chapters 5 and 6, is described.

In Chapter 5, the importance of each of the soil hydraulic parameters when simulating water content profiles on the hillslope is evaluated. The suitability of the SCE algorithm as an efficient automatic calibration method for the estimation of effective parameter values is thereafter investigated. In this Chapter, no use is made of the prior measured (laboratory and in-situ) parameter values in the inverse modelling technique. Very wide upper and lower optimisation bounds were selected based on literature. The model fit using the prior measured parameters as input parameters is compared to the model fit with the effective parameters as input parameters. To conclude, the relation between effective parameter values and the prior measured parameter values is examined.

In Chapter 6, methodologies for the incorporation of prior parameter information in two different effective parameter estimation strategies, SCE and GLUE, are presented. Thereafter, the relevance of this prior information in the calibration of soil hydraulic parameters is examined. The combination of inverse modelling with prior parameter estimations is compared to the cases where both are applied individually, i.e. (i) inverse modelling without the incorporation of prior information, and (ii) the direct use of prior information in the model.

Chapter 7 investigates the effect of the temporal resolution of rainfall records on effective model parameters. Therefore, the importance of the temporal resolution of rainfall on model simulations is first investigated. The necessity of a procedure to incorporate rainfall intensity into daily rainfall records is examined. Thereafter, such a procedure is developed and tested. Using this procedure, the influence of the temporal resolution of rainfall on effective parameter estimation using the SCE algorithm is examined.

Chapter 8 summarises in short this research and formulates the general conclusions based on the conclusions of the different Chapters. It examines whether the conclusions are able to provide answers to the questions raised and fulfil the objectives stated in this

Chapter. In addition, it discusses the shortcomings and limitations of the approaches used throughout this doctoral research. After the discussion of the innovative aspects of this research, an opinion is formulated on the important aspects to be studied in future research.

Chapter 2

Rainfall runoff experiment on a hillslope

ABSTRACT

The purpose of this chapter is the explanation of the hypotheses, the design of a field experiment and the collection of field data within the objective to derive representative parameters for physically based distributed hydrologic models. The field experiment integrated measurement devices to record different hydrological variables (water content, soil water head, (sub)surface runoff, precipitation) on a field plot with a length of 80 m and a width of 20 m on a hill slope (mean slope of 6 %), situated in the sandy-loam region of Belgium. The system allowed the simultaneous measurement of water contents at 81 locations using an automated TDR-system and a continuous monitoring of precipitation and runoff using tipping buckets. Drains, installed at two depths, collected the subsurface runoff. Soil water heads at 54 locations were measured manually on a weekly basis. Soil hydraulic properties were measured in the laboratory on 115 soil samples taken from three soil profile pits along the hillslope. Additionally, single ring pressure infiltrometer measurements were carried out at 120 locations in the field using single ring pressure infiltrometers. The chapter concludes summarising the difficulties encountered, such as lack of (sub)surface runoff, problems with tensiometer measurements, electricity cuts and computer and datalogger failures. Recommendations for similar future experiments are consequently suggested.

2.1. Hypotheses and objectives

Nowadays, the simulation of different hydrological processes (e.g., infiltration and redistribution of precipitation into the soil, (sub)surface runoff, groundwater and river flow, …) relies more and more on spatially distributed mathematical models instead of

the lumped modelling approach. As a consequence, identification and quantification of essential variables and model parameters for such models are becoming more and more important. To proceed in this research topic, it is essential that experimental measurements are combined with a numerical analysis based on models [*Weiler et al (1998); Dunne and Leopold, 1983; Faeh et al., 1997*]. Otherwise, the danger exists, as clearly stated by *Grayson et al. (1992a, b)*, that the link with reality disappears when numerical techniques are applied without experimental verification.

With this in mind, a field experiment was designed to allow – in combination with a computer-based methodology - the characterisation of hydraulic catchment parameters on the level of a grid cell, taking into account the spatial and temporal variability of these properties. Based on the combination field experiment – computer-based methodology, it was the original objective to find the minimum required field measurements necessary for deducting representative information on the area (scale) of the gridcell. It had to be applicable on hillslopes with varying characteristics, and be applied in different time periods of the year. It had to offer the opportunity to measure in the field, in a relatively simple manner, properties which after being processed by inverse use of appropriate models result in representative grid information. These objectives actually coincide with the upscaling issue discussed in Chapter 4. In the next paragraphs, the underlying ideas for the experimental set-up and the subsequent steps in the data collection and interpretation are concisely described.

The experimental site was a hillslope in the sandy loam belt of Belgium. The field was divided in 27 grid cells (each 60m²). In each gridcell, the topography, infiltration characteristics, soil moisture retention functions, hydraulic conductivity functions and the moisture content and soil water head of the soil under natural climatologically conditions were measured. Hydraulic properties of the soil were determined on undisturbed ring samples taken from the different soil horizons in a soil profile. For the infiltration characteristics, single-ring pressure infiltrometers were used. To study the evolution of the moisture content, TDR-probes (Time Domain Reflectometry), inserted at many locations and depths, monitored automatically the soil moisture content. The surface and subsurface runoff was measured by an interception gutter and drains, respectively, all equipped with a measuring device at the bottom of the field.

The main expected experimental outcomes of this set-up were (1) a detailed spatial characterizing of relevant hydrological properties of the field and (2) input-output hydrographs of the precipitation system, respectively drainage system. The experimental set-up foresaw that more information was measured than necessary for the description of the rainfall-runoff process. This was done deliberately to be able to define step by step the minimum required number of measurements, out of the excess of measurements, necessary to reconstruct the process measured in the field adequately. The analysis and interpretation start with a 2-D or 3-D reconstruction of the geometry and the properties of the hillslope, based on the hill-slope characterisation. During the reconstruction, all available measured information was used e.g. the spatial distribution of the hydraulic properties. Via the model analysis, insight could be gained in how the spatial variability of the field properties could be described quantitatively. Simplifying this complex model would indicate the minimum number of measurements and procedures required to accurately up-scale the local measurements to representative field-scale (grid-scale).

However, as observation data became available and the quality of the data investigated, it became obvious that the experimental field set-up as described below (2.2 and 2.3) would have been successful in fulfilling the original objectives if fewer problems were encountered in the data acquisition. Because of the many difficulties encountered, the objectives of this PhD research were reformulated to those presented in Chapter 1. Recommendations for similar future experimental research are described in section 2.4.

2.2. Soil physical characterisation

2.2.1. Water movement in the unsaturated zone

The flow capacity Q [L^3T^{-1}] through a particular cross sectional area A [L^2] of a saturated soil is proportional to the potential gradient $\Delta\psi$ [L] occurring over the length of flow l [L]. The relation is given by the Darcy equation and the proportionality factor is generally defined as the saturated hydraulic conductivity K_s [LT^{-1}]:

$$Q = K_s A \frac{\Delta \psi}{l} \tag{2.1}$$

In unsaturated soils, water is less mobile because the matric forces strongly reduce the water flow. The magnitude of the soil water head h [L] exerted by the soil matrix depends on the water content θ [L^3/L^{-3}]. At low water contents, water is retained in only the smallest pores, and high suctions (soil water heads) hold the water in the soil. Largest pores are the last to be filled when a soil becomes saturated. These soil suctions and the fact that only the filled pore volume is available for water flow, lead to reduced conductivities for unsaturated flow. Therefore, the Darcy equation (Eq. 2.1) cannot describe unsaturated matrix flow, which plays an important role in soil-water-movement. It is possible to relate Q to the soil water head difference (Δh) for unsaturated soils as done in the Darcy equation but the proportional factor then becomes the unsaturated hydraulic conductivity $K(h)$ which is a function of the soil water head h. The equation is then called the Darcy-Buckingham equation. By combining the Darcy-Buckingham equation with a continuity criterion, an equation describing flows in terms of the soil water head (h) is obtained. The one-dimensional Richards' equation *Richards, 1931*] is written as:

$$C(h)\frac{\partial h}{\partial t} = \frac{\partial}{\partial z}\left(K(h)(\frac{\partial h}{\partial z}) \right) + \frac{\partial K(h)}{\partial z} \tag{2.2}$$

$$\text{with } C = \frac{\partial \theta}{\partial h} \tag{2.3}$$

where z is the distance along the flow path [L], t is time [T], $K(h)$ is the unsaturated hydraulic conductivity [LT^{-1}] and C is the soil water capacity [L^{-1}] and θ the volumetric water content [L^3L^{-3}].

The hydrodynamic properties of unsaturated soils, which define their hydraulic behaviour, are characterised by the soil hydraulic functions:

- the soil water retention curve $\theta(h)$ defines the volumetric water content θ as a function of the soil water head h; and

- the hydraulic conductivity curve $K(\theta)$ or $K(h)$ relates the hydraulic conductivity K to the soil water head h or water content θ.

The wetting and drying processes in soils are not identical, with the result that the soil water retention curve is usually hysteric, i.e. water contents at the same soil water head are higher during drying than during wetting. The hysteric effects are however small compared to the uncertainties associated with the estimated soil hydraulic functions. [*Faeh, 1997*]. Hysteresis is therefore neglected in this study. It is not necessary to have the soil hydraulic functions defined as analytical expressions for their implementation in numerical simulation models. It is equally easy to insert a series of points of $K(\theta)$ and $h(\theta)$ and let the model interpolate for values of θ in between. Though, analytical expressions are useful when an analytical solution of the Richards equation is desired or in inverse modelling. As this study deals with inverse modelling, the *van Genuchten (1980)* $\theta(h)$ model is used to describe the soil moisture retention curve:

$$\theta(h) = \left[(\theta_s - \theta_r) \left(\frac{1}{1 + (\alpha h)^n} \right)^m \right] + \theta_r \tag{2.4}$$

where θ_s and θ_r are, respectively, the saturated and residual water content [L^3L^{-3}], α [L^{-1}], n and m [-] are shape parameters. Assuming:

$$m = 1 - \frac{1}{n} \tag{2.5}$$

the water retention characteristic, Eq. 2.4, combined with the statistical pore-size distribution model for the hydraulic conductivity of *Mualem (1976)* results in following relative hydraulic conductivity curve:

$$K(S_e) = K_s S_e^{0.5} \left[1 - \left(1 - S_e^{\frac{1}{m}} \right)^m \right]^2 \tag{2.6}$$

with

$$S_e = \frac{\theta - \theta_r}{\theta_s - \theta_r} \tag{2.7}$$

Sand and clays represent two extremes for the soil water hydraulic functions. With sandy soils, soil water heads only increase (higher suctions) when water contents are substantially less than those at saturation. For clay soils on the other hand, a rapid increase in soil water head can be induced by a small water content change. However, as less water is lost for a specific water head increase in clay soils, their unsaturated conductivities show less rapid decrease than those of sandy soils in the region near saturation [*Faeh, 1997*].

2.2.2. Unsaturated zone parameter estimation

A total of 115 undisturbed soil samples (100-cm^3 rings with a length of 5.1 cm and a diameter of 5.0 cm) were taken horizontally and vertically in the different horizons of three profile pits (Fig. 2.1) along the hillslope. In each soil horizon, an average of 5 horizontal and 5 vertical undisturbed samples were taken. For each of the 115 undisturbed soil samples, the saturated hydraulic conductivity K_s [LT^{-1}] and the desorption branch of the water retention curve, $\theta(h)$, were determined. K_s was measured using a constant head permeameter [*Klute, 1986*] and $\theta(h)$ was measured in three consecutive steps [*Hillel, 1980*]: (1) desorption on a sand box apparatus for pF values of 0, 0.5, 1, 1.5, and 2 (pF = $\log_{10}(-h)$, h in cm), (2) desorption in a low pressure chamber (pF 2.3 and 2.8), and (3) desorption in a high pressure chamber (pF 3.4 and 4.2). The soil cores were undisturbed for step (1) and (2), and for step (3) the soil samples were turned into saturated homogenized paste and put in 3.5 cm diameter and 1 cm high rings.

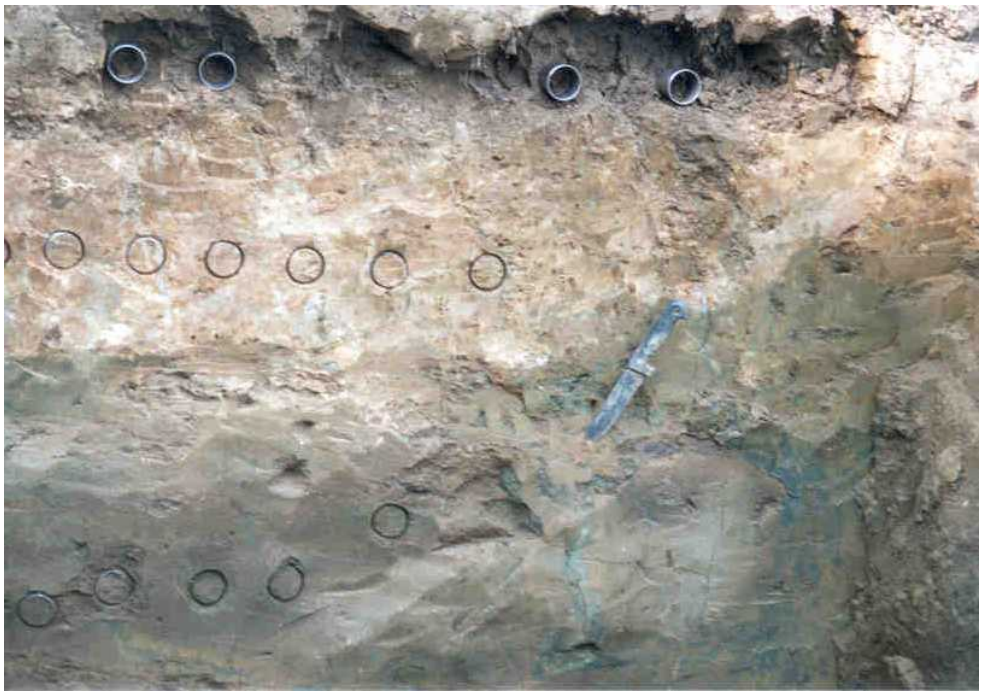

Figure 2.1 Taking of undisturbed soil samples in the profile pit at the very top of the hillslope

The measurements of the moisture retention curve (moisture content θ versus soil water head h) were subsequently used in a non-linear least squares optimisation context to obtain the *van Genuchten (1980)* parameters: θ_s, θ_r, α, n. Using the optimisation toolbox of MATLAB [*N.N., 1996*], a *Levenberg (1944)-Marquardt (1963)* optimisation algorithm was set-up with objective function (F):

$$F(x) = \sum_{i=1}^{9} \left(\theta(h_i)_{meas} - \theta_{pred}(h_i, x) \right)^2 \tag{2.8}$$

where i = 1,2…9 corresponds to the soil water head (h) or pF values (0, 0.5, 1, 1.5, 2, 2.3, 2.8, 3.4 and 4.2) at which moisture content was measured (θ_{meas}), θ_{pred} is the predicted water content using the *van Genuchten (1980)* equation (Eq. 2.5) and $x = \{\theta_s, \theta_r, \alpha, n\}$ the vector containing the unknown parameters. Optimisation boundaries were set between 0 and 1 for θ_s and θ_r [L^3L^{-3}], 0 and 10 for n [-], and 0 and 100 for the α [L^{-1}], parameter.

It is believed that global optima are found for each of the 115 optimisations because different initial parameter estimates resulted in the same best parameter sets. As shown in Fig. 2.2, a very good fit ($R^2 = 0.98$) is observed between the measured and predicted soil moisture content values over all 115 locations and all 9 measured applied heads. Fig. 2.2. shows that the *van Genuchten (1980)* equation has more problems getting a good fit close to saturation than near the dry end of the retention curve, i.e. more scatter at high moisture contents. This 'limitation' of the *van Genuchten (1980)* model has been well described in literature. Some authors therefore suggest to fit bimodal or even trimodal retention curves to the measured moisture contents in order to get a better fit near saturation [*Durner, 1994; Mallants et al., 1997b*].

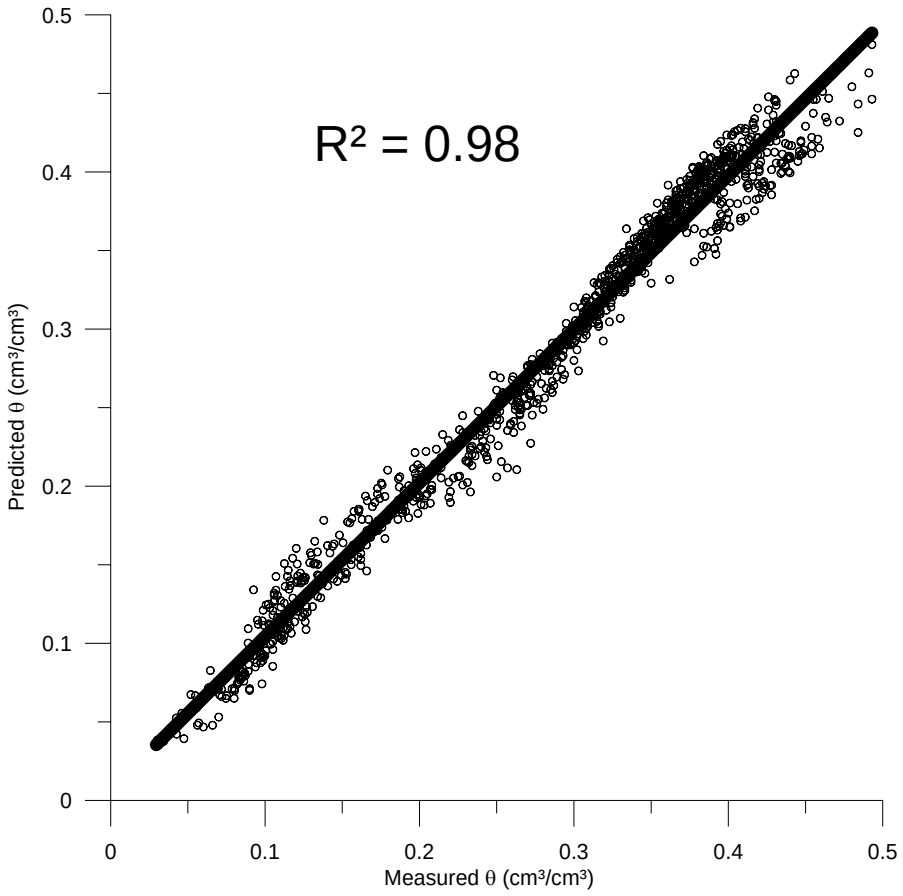

Figure 2.2 Measured against predicted moisture content for all soil cores

In order to get an idea about how well the *van Genuchten (1980)* equation is suited for the fitting a single water retention curve, a good and bad fit are shown in Fig. 2.3. The

bad fit still yields a R^2 value of 0.94. Though, the fit of the van Genuchten (1980) equation to the measured water retention curve for this particular soil core is not good, especially close to saturation. The good fit results in a value of R^2 of 0.99 and shows that for this soil core, the *van Genuchten (1980)* equation is able to predict the measured soil moistures content values from saturation to the dry end of the retention curve.

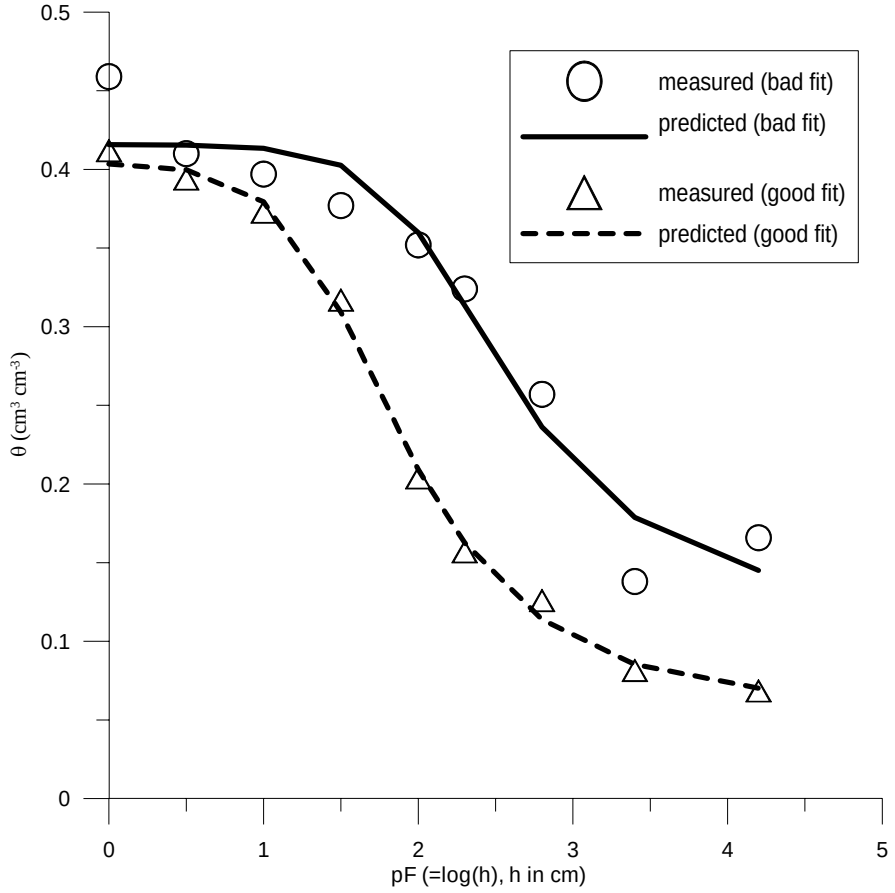

Figure 2.3 Comparison between a good and bad fit of the van Genuchten (1980) equation to the measured soil moisture contents at the applied soil moisture heads.

The difference in goodness-of-fit between the good and bad fit as illustrated in Fig. 2.3, is also reflected in the width of the 95% confidence intervals around the estimated *van Genuchten (1980)* parameters shown in Table 2.1. The confidence intervals were calculated using the RETC software [*van Genuchten et al., 1991*] and the calculation is based on the Jacobian matrix calculated in the optimum. Confidence intervals are rather small for the good fit while for the bad fit, they are wide for all of the parameters. The

lower 95% confidence interval for bad fit of the α and n parameter is even below zero, which is physically impossible. The wide confidence interval indicates that for this particular soil core, the uncertainty on the estimated *van Genuchten (1980)* parameters is large. Important to note is that for most of the 115 soil cores, the fit was observed to be rather good and this is reflected in the overall R^2 value of 0.98 as indicated on Fig. 2.2.

Table 2.1 Estimated van Genuchten (1980) parameters for the bad and good fit shown in Fig. 2.3 and their corresponding 95% confidence intervals

		95% Confidence Interval	
Variable	Estimated value	Lower	Upper
θ_s *(good fit)*	0.40	0.39	0.42
θ_s *(bad fit)*	0.42	0.37	0.46
θ_r *(good fit)*	0.06	0.03	0.09
θ_r *(bad fit)*	0.12	-0.06	0.30
α *(good fit)*	0.04	0.02	0.09
α *(bad fit)*	0.009	-0.009	0.03
n (good fit)	1.58	1.36	1.80
n (bad fit)	1.51	0.4	2.6

The hydraulic conductivity curve $K(\theta)$ is estimated following to *Mualem (1976)* model (Eq. 2.5 to Eq. 2.7) at each of the 9 measured moisture contents. The MIKE-SHE model [*Refsgaard and Storm, 1995*] used in this study uses the *Averjanov (1950)* $K(\theta)$ model to describe the hydraulic conductivity curve:

$$K(\theta) = K_s \left(\frac{\theta - \theta_r}{\theta_s - \theta_r} \right)^N \tag{2.9}$$

where N [-] is a shape parameter. This N parameter was estimated for each of the 115 soil samples through the use of a similar non-linear least squares optimisation method as described above and with objective function (F):

$$F = \sum_{i=1}^{9} \left(K(\theta_i)_{Mualem} - K(\theta_i, x)_{Averjanov} \right)^2 \quad (2.10)$$

where i = 1,2…9 corresponds to the 9 measured moisture content values, $K(\theta_i)_{mualem}$ the corresponding hydraulic conductivity value K of the *Mualem (1976)* model (Eq. 2.5 to 2.7) and $K(\theta_i, x)_{Averjanov}$ the predicted hydraulic conductivity value K using the Averjanov model (Eq. 2.9) and $\mathbf{x} = \{N\}$ the vector containing the unknown N parameter [-]. Optimisation boundaries for N were set between 0 and 100 and global optima were reached for each of the 115 soil samples.

After the deletion of outliers on the basis of visual scatter plots of the estimated parameters and only considering soil samples taken in the A or B-horizon, 84 estimated parameter sets were retained and divided in 35 A and 49 B-horizon parameter estimates according to the soil horizon they were taken from. Table 2.2 presents the mean, standard deviation, minimum and maximum of the estimated soil parameters from the laboratory measurements. A Kolgomorov-Smirnov test reveals that on a 5 % significance level θ_r, α, n and N significantly differ between the A- and B-horizon. From the visual observations in the three profiles pits as described in 2.3.1, a significant difference in saturated hydraulic conductivity between the colluvium A-horizon and the texture B-horizon was expected but is not observed. This might be due to different reasons: (i) the difference in hydraulic conductivity is indeed very small, (ii) the measurement error involved in estimating saturated hydraulic conductivity in the laboratory on small soil samples using a constant head permeameter, and (iii) the large variation in the measurements, i.e. large standard deviations may make it impossible to observe a significant statistical difference.

Table 2.2 Mean, standard deviation, minimum and maximum of the estimated soil parameters from laboratory measurements

Parameter	Mean	St. Dev.	Min	Max
K_s_A (ms^{-1})	9.74E-06	1.78E-05	4.56E-08	7.01E-05
θ_s_A (-)	0.40	0.02	0.35	0.45
θ_r_A (-)	0.02	0.03	2.19E-07	0.11
α_A(m^{-1})	1.95	1.19	0.29	5.77
n_A(-)	1.30	0.10	1.15	1.62
N_A(-)	12.59	3.32	6.68	21.58
K_s_B (ms^{-1})	1.57E-05	2.63E-05	4.37E-09	8.72E-05
θ_s_B (-)	0.39	0.03	0.33	0.45
θ_r_B (-)	0.05	0.03	1.80E-04	0.13
α_B(m^{-1})	1.87	1.54	0.26	5.79
n_B(-)	1.44	0.21	1.15	1.98
N_ B(-)	9.97	3.71	4.87	21.84

Figure 2.4 shows the 95 % confidence intervals of the soil water retention curves (Fig. 2.4(a)) and hydraulic conductivity curves (Fig. 2.4(b)) measured in the laboratory on the soil samples from the A- and B-horizon. From Fig. 2.4 it is not possible to classify the B-horizon as more clayey in terms of hydraulic properties than the A-horizon. Water retention curves of the B-horizon show more variability than the A-horizon water retention curves while hydraulic conductivity curves for both horizons are very similar. From the observations in all three profile pits larger differences between hydraulic properties of both horizons were expected. In situ-field hydraulic saturated hydraulic conductivity (K_{fs}) is also estimated in 120 locations on the field plot using a single ring pressure infiltrometer [*Reynolds and Elrick, 1990; Mertens et al., 2002*] and is described in detail in chapter 3.

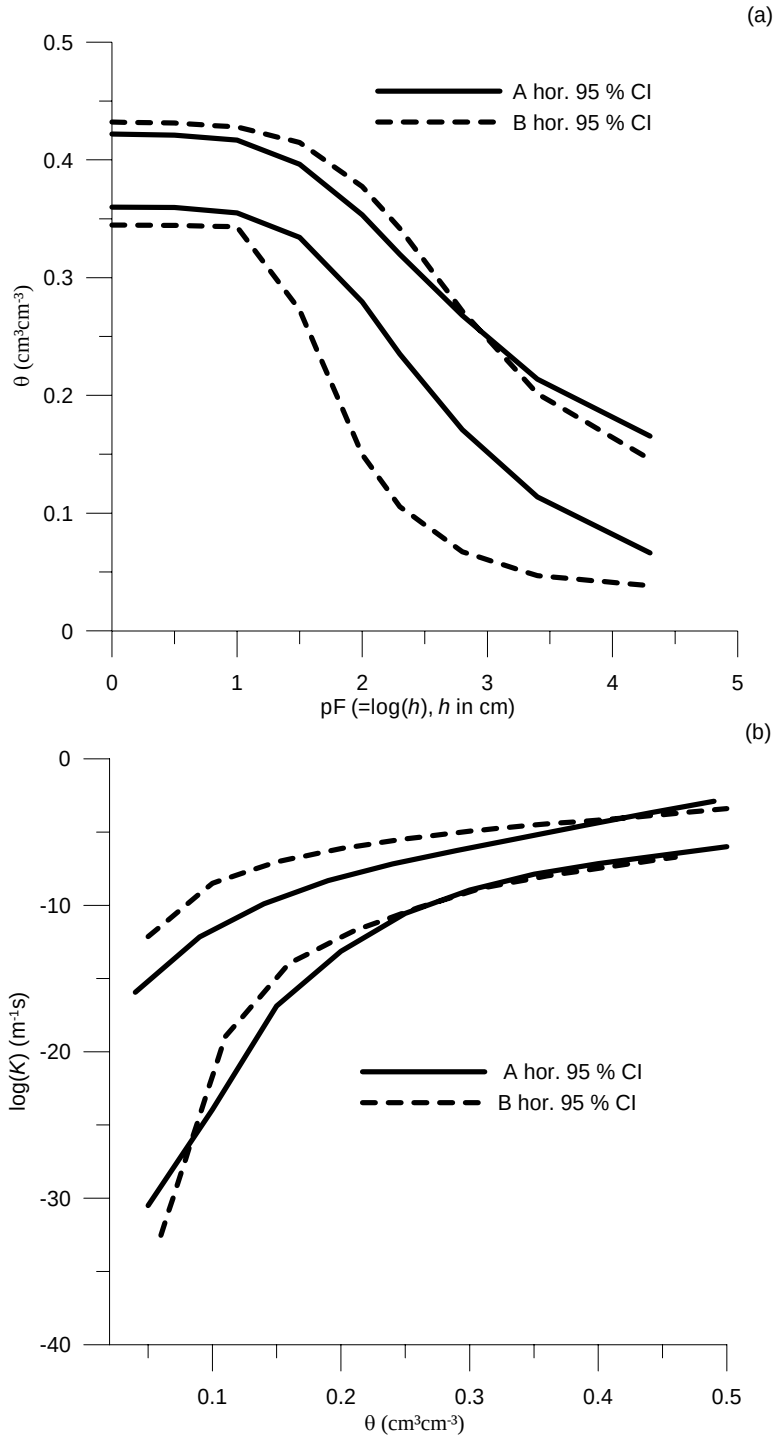

Figure 2.4 95 % confidence intervals of the soil water retention curves (a) and hydraulic conductivity curves (b) measured in the laboratory on soil samples from the A- and B-horizon

2.3. Experimental layout

2.3.1. Experimental hillslope

For the location of the experiment, a representative hillslope located in the Fruit Research Centre of the Katholieke Universiteit Leuven in Rillaar, Belgium (Fig. 2.5) was chosen. The entire hillslope has an area of 4000 m² and a mean slope of 10% (Fig 2.6) and is located in the sandy-loam belt (Luvisol) of Belgium. Before September 1999, it was covered with apple trees for fourteen years. In September 1999, the apple trees were removed. Augering was performed in order to get an idea of the depth to the B-horizon all over the hillslope. The location of an experimental field plot within the hillslope was chosen on the basis of these augerings. The depth to the B-horizon within the selected field plot varies between 0.12 and 2.24 meters. In most locations however, the B_t horizon was found within 1 meter from the surface while at some locations clear demarcation between the E and B_t horizon was difficult. Depth to the B-horizon decreases going uphill the experimental field though this should not be generalized: a lot of local exceptions exist. The experimental field plot has a mean slope of 6 % (Fig. 2.7), a width of 20 m and a length of 80 m. The plot was hydrologically isolated from the neighbouring area through the insertion of a plastic foil over a depth of 2 meters.

Before the start of the experiment, three profile pits were dug along the hillslope: one at the bottom of the hillslope, one in the middle and one at the top (Fig 2.1 and Fig. 2.6). In each of these pits, the different soil horizons were identified. The profile at the bottom of the hillslope shows a textural B-horizon (more clayey layer) at variable depth from 85 cm onwards. It is covered by colluvium. At the top of the profile, an A_p horizon rich in humus and containing the roots of the grass was observed. Below the textural B-horizon, a C or mother material is found which is tertiary sandy clay material, called Diestiaan.

On top of the textural B-horizon, some ‘pseudo’gley was observed. This ‘pseudo’gley is due to fluctuating groundwater levels. When groundwater level decreases, the iron oxidizes and precipitates resulting in a reddish colour. The profile pit in the dug in the

middle of the hillslope shows the textural B-horizon at a depth of about 65 cm. On top of it, an eluvial E horizon is observed. On top of this E horizon, colluvium is found underneath a thin A_p horizon. On top of the B-horizon some signs of 'stagnoggley' were found, i.e. this is gley due to a temporary hanging water table on top of the textural B-horizon. The profile pit at the very top of the hillslope showed in some places a truncated textural B-horizon at the top of the profile covered by only a very thin A_p horizon. Below the truncated textural B-horizon, a layer of glauconite was observed covering the tertiary Diestiaan material.

Figure 2.5 Location of the Fruit Tree Research Centre in Rillaar within Belgium

Figure 2.6 Experimental hillslope in sandy-loam soil belt of Belgium (area 4000 m², slope = 10%)

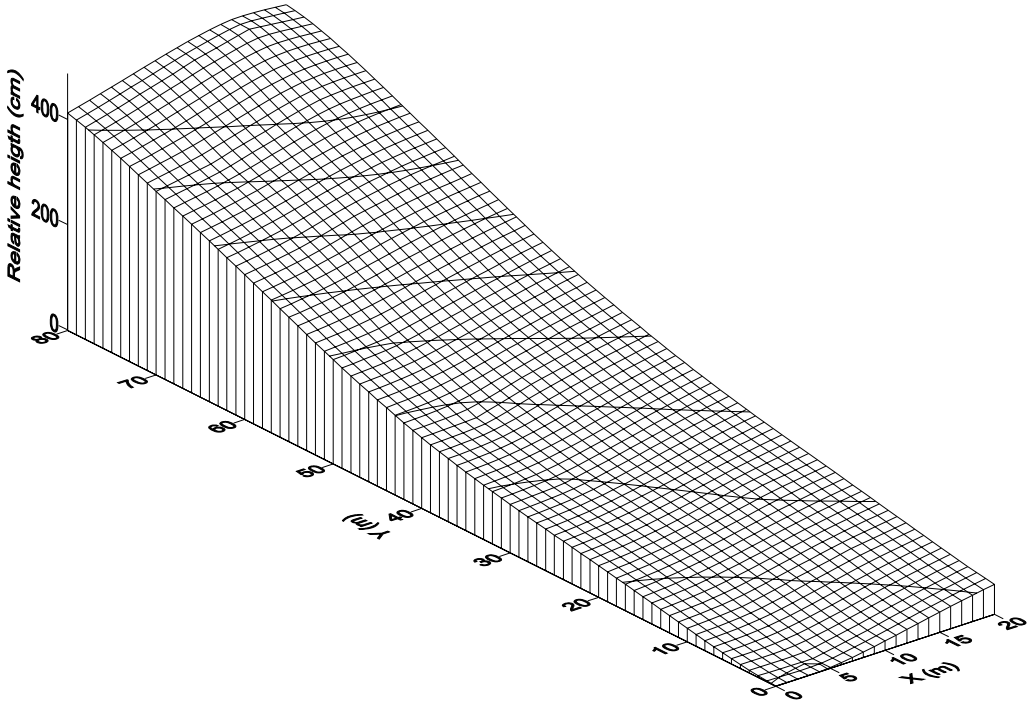

Figure 2.7 Relative height above the lowest point of the selected experimental field plot

2.3.2. Installing drains and surface gutter

At the bottom of the field, a trench of 2 m depth was dug and drains were installed at two different depths (Fig. 2.8). The first drain was installed on top of the texture B-horizon at approximately 85 cm depth in order to capture the lateral flow on top of this horizon downslope. It was believed that lateral subsurface runoff would occur as augerings during the winter period had shown a 'hanging' water table on top of this B-horizon. A second drain was installed at the top of the Tertiary 'Diestiaan' at a depth of 1.8 meter in order to capture possible lateral subsurface runoff downslope. Just underneath each drain a plastic foil was inserted horizontally to avoid the percolation of lateral subsurface runoff originating from the soil profile above the installed drain.

Figure 2.8 Installing drains in trench at bottom of experimental plot

After filling up the trench with sandy material, a gutter was installed over the whole width of the field (=20 m) to collect surface runoff. To avoid precipitation to fall directly in the gutter, the gutter was covered with a roof. The water from the two drains and surface gutter is guided to a deep pit of which the sides are made out of wood. The pit is covered with a plastic roof to prevent rain entering the pit. Inside the pit, the

discharge rate of drains and gutter are automatically registered by tipping buckets. In order to avoid mud and insects entering the tipping bucket, a reservoir was installed in front of the tipping bucket. The reservoir is filled with a constant level of water and is covered with a lid to prevent evaporation. Water entering this reservoir from the surface gutter makes the reservoir run over into the tipping bucket device while dirt remains in the reservoir.

2.3.3. Soil moisture content measurements

2.3.3.1. Time Domain Reflectometry

Time Domain Reflectometry (TDR) is a well-established method for measuring soil water content in both the laboratory and the field. [*Baker and Allmaras, 1990; Heimovaara and Bouten, 1990; Herkelrath et al., 1991; Topp and Davis, 1985; Heimovaara et al., 1995; Ferré et al., 1996*]. Like the neutron moderation and gamma density methods, TDR offers non-destructive, in-situ monitoring of water contents. Unlike these methods TDR does not use a radioactive source. TDR relies on the measurement of the propagation velocity of a guided electromagnetic wave through the soil. The propagation velocity is controlled by the dielectric permittivity of the medium. Due to the large relative dielectric permittivity of water (81) compared to that of air (1) and soil particles (3-5) [*Ferré et al., 1990*], the apparent relative dielectric conductivity of a soil is highly correlated with the volumetric water content.

Standard TDR probes are composed of two or three small diameter parallel rods. A high step voltage generator creates a fast rise time electromagnetic pulse. Shielded parallel cables or coaxial cables transmit the energy to the rods. At any point where the propagating step voltage encounters a change in impedance, caused by changes in the water content of the medium near the rods or in the configuration of the cable or rods, a portion of the energy is reflected back towards the source. The elapsed time between the partial reflection of the wave as it leaves the coax cables to enter the TDR probes and the total reflection from the end of the probe can be deduced from the measured reflected waveform. For a probe of known length, this travel time defines the average

velocity of propagation along the probes, which is used to calculate the average apparent relative dielectric permittivity over the length of the rods. An empirical relationship relates the measured apparent dielectric permittivity to the volumetric water content for a wide range of mineral soils [*Topp et al., 1980*]. As the wave travels along the coax cables, energy is reflected both from changes in the line impedance and dissipated through electrical conduction. The maximum useable cable length of TDR probes is often limited by excessive energy losses resulting in insufficient energy remaining to identify the reflection from the end of the probe. Reflections in the waveforms have smaller amplitudes and slopes and are therefore harder to detect. *Heimovaara (1993b)* concludes that the longer the TDR probe used, the longer cable length can be used. A maximum coax cable length of 33 m gave satisfying results for probes of 20 cm.

2.3.3.2. Field set-up of TDR system

On a grid of 10 by 10 meters (Fig. 2.9), a total 81 Time Domain Reflectometry (TDR) probes were installed. At each of the 27 locations, three TDR probes were installed very close to each other. Each probe was installed vertically into the soil and has a length of 25 cm. At each location, soil moisture content is measured at 3 depths: at the surface (between 0 and 25 cm), at a depth of 30 (between 30 and 55 cm) and 60 cm (between 60 and 85 cm). TDR probes were attached to coax cables that in their turn were attached to Campbell's SDMX50-Series Multiplexers (Fig. 2.10(a)).

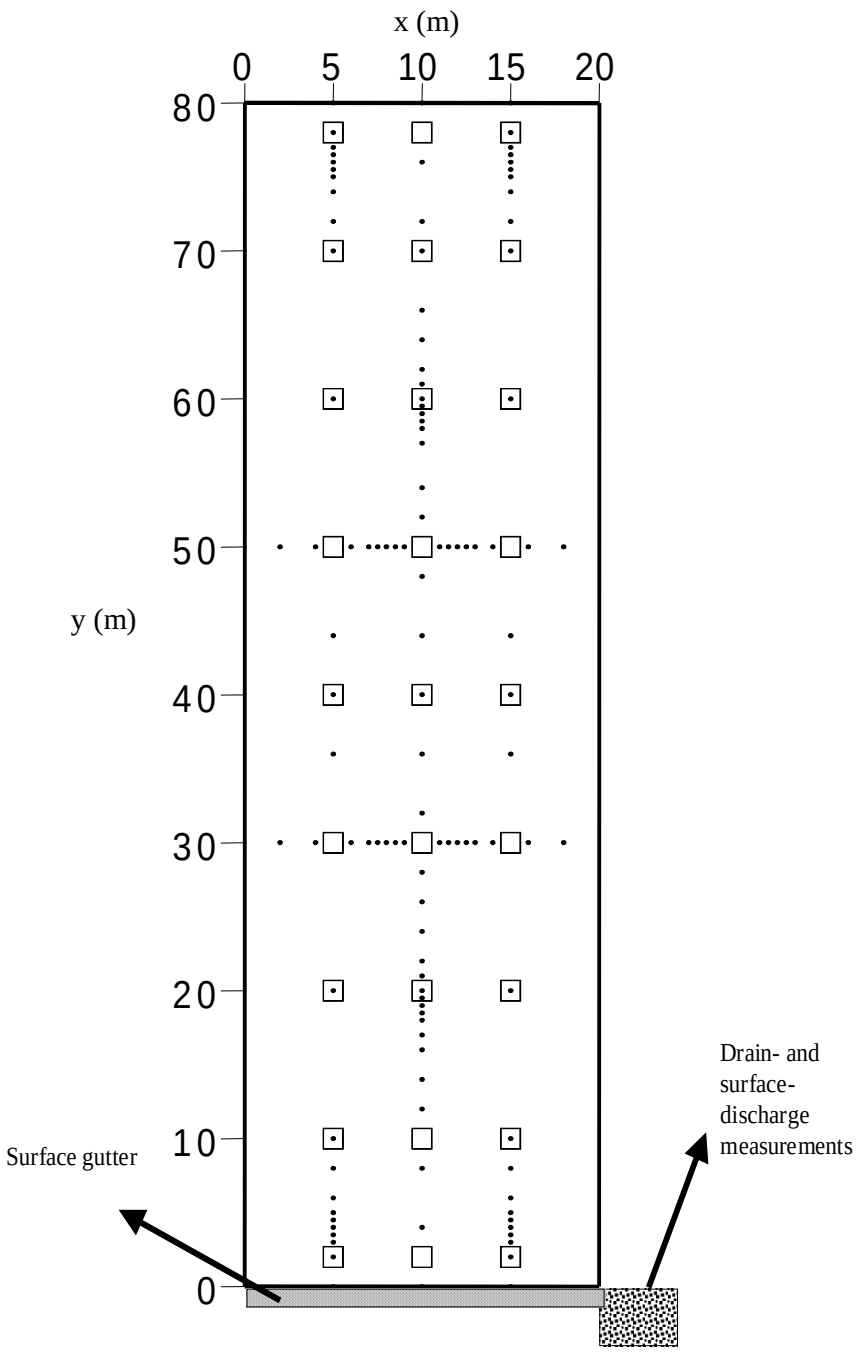

Figure 2.9 Field layout: location of TDR probes, tensiometers, surface gutter, drains and single-ring pressure infiltrometer measurements

The SDMX50-series multiplexers are eight-channel coaxial switching devices used in our TDR system. Three levels of switching allows up to 512-soil water content measurements. Because of the maximum cable length limit, two different and independent TDR systems had to be installed to cover the field. In this way, maximum cable length was limited to 33 m. In the first system, 6 multiplexers are controlled by a CR10 datalogger making automated measurements possible. The CR 10 datalogger controls multiplexers as well as the Tektronix 1502B cable tester (Fig. 2.10(b)) that is responsible for sending the electromagnetic signal and the capturing of the waveform. The 6 remaining multiplexers (total of 12) are controlled by a Campbell's CR10X datalogger that also controls a Campbell's TDR100 reflectometer (replaces the Tektronix 1502 B cable tester).


(a)

(b)

Figure 2.10 (a) Campbell's multiplexer, capable of multiplexing 8 TDR probes and (b) Campbell's CR10 datalogger and Tektronix 1502B cable tester

Both CR10 and CR10X dataloggers are capable using the incorporated Campbell's software for finding the travel time required for the electromagnetic wave to propagate a distance through the soil. From the travel time, the apparent relative dielectric conductivity is deduced and related to volumetric soil water content (θ) using Topps equation [*Topp et al., 1980*]. The problem encountered was that using cable lengths longer than 15 meter made it impossible for the internal Campbell's software to 'auto'detect reflections in the waveforms and hence resulted in unreliable soil moisture content measurements. Visually investigating the form of the waveform resulting from a 33 meters cables indeed revealed weakened reflection points. Though, in order to be

able to still detect these reflection points, the datalogger was programmed to convert each waveform to 251 points and save those to an ASCII file.

Six hourly soil moisture content measurements were performed at each location resulting in a large amount of data points to be stored inside the datalogger. As data storage inside the CR10 and CR10X dataloggers is limited, the dataloggers were programmed to send the data as soon as collected to a connected computer. As there were two systems, two computers were installed close to the field and on-line connected with each of the dataloggers. Weekly data was copied from these computers to diskettes.

A MATLAB code was developed which made it possible to detect 'weakened' reflection points from these ASCII files saved by the datalogger. The code was based on the description of the waveform analysis described by *Heimovaraa 1993b* with some minor modifications.

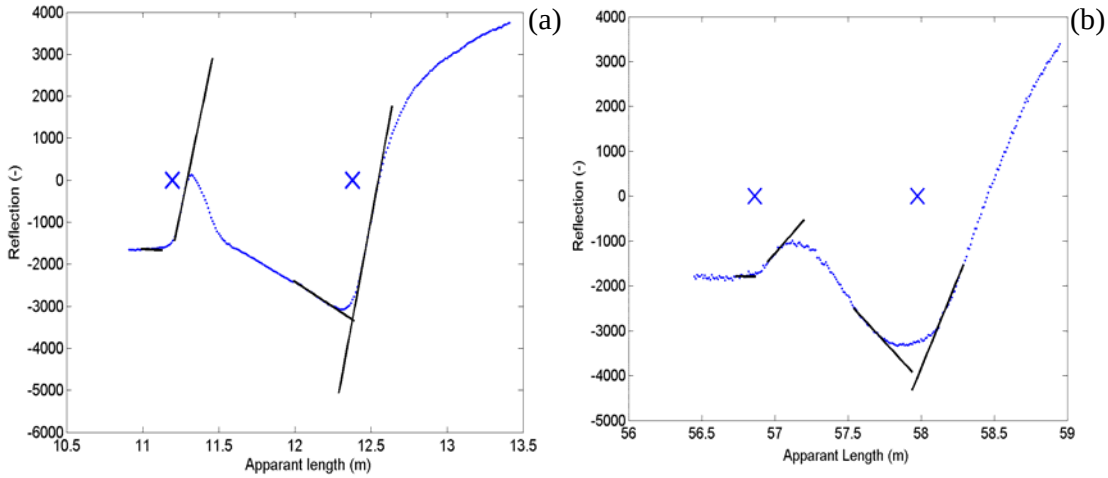

Figure 2.11 (a) Automated waveform analysis in MATLAB of a TDR probe with a cable length of 4 m and (b) automated waveform analysis in MATLAB of a TDR probe with a cable length of 33 m

Figure 2.11 compares the result of the analysis of the MATLAB code for a TDR waveform collected with a cable length of 4 m (a) and a cable length of 33 m (b). The waveform collected from a 33 m cable length has less distinct reflection points, i.e.

smaller amplitudes and slopes. Though as indicated by the tangent lines and crosses in Fig. 2.11, the MATLAB code still succeeds to detect these points while the intern software of the CR10 and CR10X could not.

2.3.4. Soil water head measurements

Next to the 3 TDR probes at each of the 27 locations (Fig 2.9 and Fig. 2.11(a)), two tensiometers were installed: one at 45 cm depth and one at 75 cm depth. The tensiometers are the 'Thies' type with an unglazed ceramic cup sealed to a frost-resistant transparent hollow tube (Fig. 2.12 (b)), with the upper end sealed by a rubber septum in a screw cap. Tensiometers were installed vertically, in a hand-augered hole, to the required depth. After insertion of the tensiometer in the hole, the hole was filled with a mix of soil and water to enhance the contact of the porous cup with the surrounding soil. The porous cup is filled with water that is in equilibrium with the soil matrix potential. Every week, the soil water head (*h*) was read using a pressure-transducer sensor, inserted through the septum by a needle (Fig. 2.12(b)). The suction in the tensiometer was displayed on a digital read-out on the sensor, which was recorded on a field sheet. Tensiometers were filled with a mix of water (75%) and ethanol (25%) in order to prevent freezing of the water during winter [*de Vos, 1997*].

(a) (b)

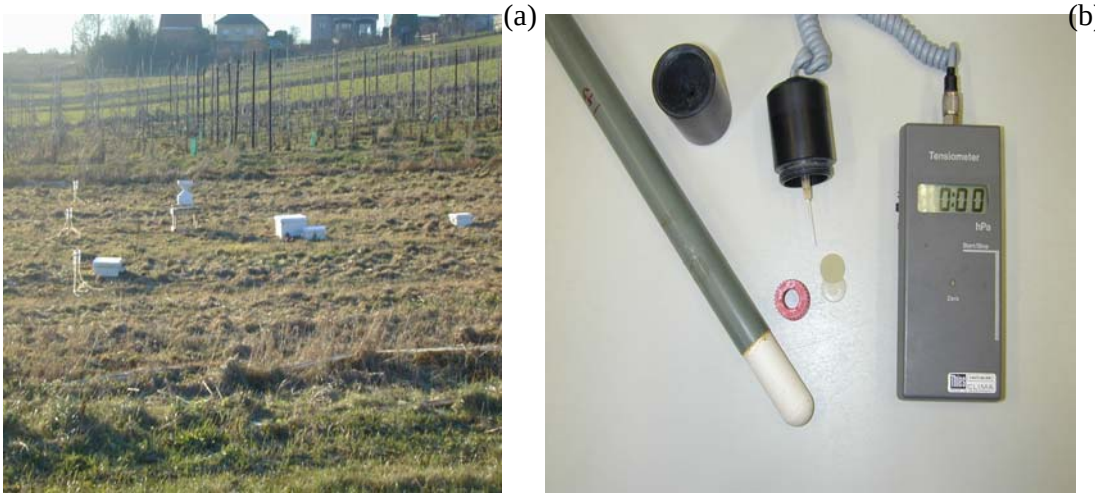

Figure 2.12 (a) Location of TDR multiplexers, tensiometers and tipping bucket (b) Tensiometer (porous cup, septa, lid) and tensiometer readout machine

2.3.5. Climatogical data

A tipping bucket is installed in the field at a height of 40 cm above ground level (Fig. 2.12(a)). It is attached to the CR10 datalogger that is programmed to accumulate rainfall data in 10 minutes and send it to the connected computer. Next to the field plot, at the top of the hillslope, a climatogical weather station of The Royal Meteorological Institute (Belgium) is located. Daily rainfall data and minimum and maximum temperature is measured. Comparing 10 minutes rainfall with the daily measured values reveals that they are within 10% of each other, which in terms of rainfall is considered as good. Daily potential evapotranspiration rates are calculated using the FAO Penman-Monteith method [*Allen et al., 1998*] from the daily minimum and maximum temperatures measured at the local meteorological station using the ET0 software [*Raes, 2002*].

2.4. Difficulties encountered and recommendation for future similar experimental research

At the beginning of the experiment, no surface runoff leaving the gutter was measured. Therefore, it was believed that spraying the grass dead and, thus leaving the soil bare all year through, would result in surface runoff as surface roughness decreased. Pitiful, this did not help in the generation of runoff. Only negligible amounts of runoff were registered making it impossible to distinguish whether it was actual runoff or just water entering the gutter between the small gaps in the wooden cover of the gutter. In general, rainfall intensities in Belgium are not high enough for the generation of vast amounts of runoff. In our experiment, on top of the low rainfall intensities, two other reasons for lacking surface runoff are: (i) the gentle slope of the hillslope and (ii) the high infiltration capacity of the topsoil.

Subsurface runoff was expected to occur on the experimental field from the visual observations of the textural B-horizon made in the profile pits as described above. Not only the visual observations in the profile pits but also augering after a long period of heavy rain revealed water ponding on top of this textural B-horizon. Therefore drains were installed to capture this lateral subsurface runoff. Yet, no subsurface runoff was

captured by the drains throughout the year. One could argue that the gentle slope of the experimental field or the bad installation of the drains could partly explain the lack of subsurface runoff. Though, it is believed that in contrast with the visual observations of the textural B-horizon and the augering observations, the textural B-horizon is more permeable than visually observed. As elaborated in 2.2.2, a significant difference in saturated hydraulic conductivity between the colluvium A-horizon and the texture B-horizon was not observed from the laboratory measurements on the Kopecky rings.

The lack of surface and subsurface runoff measurements is an essential gap when aiming to fulfil the original objectives stated above in 2.1. Therefore, a reformulation of the objectives was necessary and is presented in Chapter 1. Another major problem encountered were the tensiometer measurements. Drying out of the tensiometers and fracturing of the porous cups were the largest difficulties encountered. The tensiometer system needs constant care and weekly visits were not sufficient to prevent drying out and breaking down of the tensiometers. The installation of tensiometers needs lots of experience because the tensiometer has to be properly embedded so that it is in full contact with the soil. Therefore a mix of water and mud was used to fill up the hole after the insertion of the tensiometer. Still, some tensiometers were not working properly directly after installation. It is believed that the tensiometer system could work properly under laboratory conditions where constant care and follow up can be guaranteed. Last but less crucial problem is the existence of gaps in the soil moisture content data and the 10 minutes rainfall measurements. These gaps exist due to power cuts, computer crashes and lightning. Strong lightning broke down the communication port of the computers necessary for the reception of data from the dataloggers; even though the system was earthed.

From the poor perceptions made and problems encountered in this study, some recommendations for future experimental research are suggested. The most important recommendation deals with the selection of the experimental field plot. A steeper hillslope than the 6 % hillslope used in this study is recommendable under natural Belgian climatological conditions. Artificial precipitation through the use of a sprinkler irrigation system could compensate the need for a steeper hillslope. The installation of such an irrigation system is expensive and time-consuming. Additional problem is that water has to be available in vast quantities (e.g. lake, river or well) in the direct

neighbourhood. Finally, a good overlap of the different sprinklers so that even spreading of the artificial precipitation over the entire field plot is guaranteed is not straightforward. If subsurface runoff is desired, detailed laboratory and preferably in-situ measurements of the saturated hydraulic conductivity of both A- and B-horizons is necessary before the installation of drains. Not only visual observations of the B-horizon on top of which subsurface runoff is expected are needed but a significant difference in measured saturated hydraulic conductivity is a must. Proper installation of the drains also needs experience but it is believed that the installation of drains at the bottom of the experimental field plot as described in 2.3.1, was successful.

The TDR system presented in 2.3.2 worked more than satisfactory. If possible of course, shorter cable lengths are always advisable so that the internal software in the CD10 and CD10X dataloggers can detect inflection points itself. If so, there is no need for a constant connection with computers because soil moisture content data can directly be stored in the datalogger. Data gaps due to computer crashes and lightning can hence be avoided. On top, power cuts can also be avoided as datalogger and Tektronix 1502B or TDR100 work on 12 Volt and hence can be powered by a battery. The tensiometer system used in this study was found to be unsuitable for weekly measurements of soil water head for a long period. Tensiometers will perform acceptable when more attention can be given to its maintenance, e.g. in short duration experiments when maintenance can be done on a daily basis. If interested in weekly soil water head measurements, a different system is advisable, e.g. a mobile system which can be taken along after the weekly measurements.

Chapter 3

Characterisation of the field-saturated hydraulic conductivity on a hillslope: in-situ single ring pressure infiltrometer measurements*

ABSTRACT

Spatial variability of surface hydraulic properties is an important factor for infiltration and runoff processes. At 120 locations in an experimental plot on a hillslope, steady-state infiltration rates were measured at two applied pressure heads with a single-ring infiltrometer. The solution of two steady-state infiltration equations for each location (the simultaneous-equation approach, SEA) yielded 41 negative α_m-values, 79 positive α_m values and 120 positive K_{fs}-values. The sensitivity of K_{fs} and α_m to small measurement errors was estimated using Monte-Carlo simulation (MC). Results of this MC simulation showed that the uncertainty on α_m is extremely high while the uncertainty on K_{fs} is fairly small. Hence, although the pressure infiltrometer technique as applied here is useful to estimate K_{fs} at each measurement location, it is not suited for the estimation of an α_m-value at each measurement location. A new procedure is proposed for the simultaneous estimation of one overall 'field α_m' and the 79 K_{fs} values of measurement locations having a positively calculated α_m using SEA. Using this 'field α_m', K_{fs} values for the other locations with a negative α_m are hence determined. Finally, the spatial correlation of K_{fs} on the hillslope is examined. Ranges of ln(K_{fs}) between 2.85 and 3.8 m were observed, respectively, for the omnidirectional case and the y direction along the hillslope. Comparing in-situ K_{fs} estimates with the laboratory K_s

---

* Adapted from Mertens, J., Jacques, D., Vanderborght, J. and J. Feyen , 2002. Characterisation of the field-saturated hydraulic conductivity on a hillslope: in situ single ring pressure infiltrometer measurements. *Journal of Hydrology*, 263, 217-229

estimates reveals that they are significantly different. Although a robust method for the determination of K_{fs} is presented in this chapter, care must always be taken interpreting K estimates at different (model)scales.

3.1. Introduction

Field investigations of the hydraulic properties of the unsaturated (vadose) zone are becoming increasingly important elements in hydrogeological and geotechnical studies. The properties of the unsaturated zone control the generally slow downward seepage of potential groundwater contaminants as well as the amount of direct runoff [*Elrick et al., 1989*]. A number of field techniques have been used to measure the hydraulic properties of soils in the unsaturated zone [*Angulo-Jaramillo et al., 2000*]. Infiltration based methods are recognised as valuable tools to investigate hydraulic and transport soil properties. In particular, three complementary methods appear to be interesting in the study of unsaturated and-near saturated hydrological soil behaviour. They are the confined one-dimensional pressure double ring infiltrometer, the unconfined three-dimensional single ring pressure infiltrometer and the unconfined three-dimensional tension disc infiltrometer.

In this chapter, we examine infiltration data measured with a constant head single-ring pressure infiltrometer method. This technique is useful in the estimation of the in-situ K_{fs} $[LT^{-1}]$ ("field saturated" hydraulic conductivity) and ϕ_m $[L^2T^{-1}]$ (matric flux potential). The term "field saturated" is used because, under field conditions, a certain amount of air is usually entrapped in the soil during the infiltration process [*Reynolds et al., 1983; Elrick et al., 1989*]. This can result in lower estimates of the "saturated" hydraulic conductivity compared to measurements in completely saturated soils [*Stephens et al., 1987*]. The flux potential, ϕ_m, is defined as [*Gardner, 1958*]:

$$\phi_m = \int_{h_i}^{0} K(h)dh \tag{3.1}$$

where h is the soil water head and h_i the initial soil water head [L]. Equation. 3.1 shows that ϕ_m is function of the initial soil water head. ϕ_m is the surface below the *K(h)* curve and *K(h)* values very small for very negative h. Therefore, the surface under the *K(h)* from $h_{-\infty}$ to h_i is negligible if h_i is very negative or in other words if the initial soil is dry. Hence, when starting the single-ring pressure infiltrometer measurements on an initially dry soil, ϕ_m can be considered constant and not a function of the initial soil water head. It is for this reason that the single-ring pressure infiltrometer measurements in this study, were carried out in summer during a long dry period. *Bagarello and Provenza (1996)* showed that if the initial soil condition is not dry, the estimation of K_{fs} is influenced by the initial soil water head. ϕ_m is independent of the applied head for the pressure infiltrometer method and is related to α_m [L^{-1}]:

$$\alpha_m = \frac{K_{fs}}{\phi_m} \tag{3.2}$$

The α_m parameter is a measure of the relative contributions of gravity and capillary forces to water movement in an unsaturated soil. The smaller the α_m value, the larger the capillary forces relative to gravity. The value of α_m measured in the field using ponded infiltration techniques is determined primarily by soil structure, particularly when macropores are present [*Elrick et al., 1989; Elrick et al., 1995*].

Constant head conditions have traditionally been used because constant head devices are easy to maintain experimentally and because the analysis is relatively simple. A difficulty with this approach is that insufficient information is obtained from the measurement of steady-state flow under one constant head to evaluate both K_{fs} and ϕ_m [*Elrick et al., 1995*]. Either one of the two parameters (or the α_m-value), must be measured or estimated independently [*Elrick et al., 1989*] or steady-state flow measurements are needed for two or more ponded heads. If α_m is estimated independently however, some error can result. If steady-state measurements are taken at two or more heads, soil heterogeneity can cause a large percentage of invalid (i.e. negative) and unrealistic K_{fs} and ϕ_m values [*Elrick et al., 1995*].

The fixed α_m value approach as suggested by *Elrick et al. (1989)*, requires only one flow rate measurement. However, individual α_m-values for soils are generally not available. Based on structural and textural information, *Elrick et al. (1989)* classified soils into four categories and suggested choices of α_m for each category. They proposed values of α_m ranging between 0.01 cm^{-1} (compacted clays, e.g. landfill caps and liners, lacustrine or marine sediments, etc.) and 0.36 cm^{-1} (coarse and gravely sands; may also include some highly structured soils with large cracks and macropores).

In this study, only constant head infiltration measurements were performed for two heads at each measurement location. This was done because of the simplicity of measuring the infiltration and because of the belief that the procedure presented in this study allows the achievement of good estimates of K_{fs}. K_{fs} and α_m are calculated from the observed infiltration rates (Q_1 and Q_2 [LT^{-1}]) corresponding to the applied heads (H_1 and H_2 [L]) using the classical constant head approach (or Simultaneous Equations Approach, SEA) [*Reynolds and Elrick, 1990*]. *Philip (1985)* concluded that negative values of K_{fs} and α_m imply that solutions for K_{fs} and α_m are too strongly dependent on the ratio of the observed infiltration rates (Q_2/Q_1). He gave two numerical examples how a random measurement error and some mild heterogeneity could cause negative K_{fs} or α_m estimates. *Elrick et al. (1989)* report three error sources that could cause negative K_{fs} or α_m when using the Guelph permeameter method: (i) non-attainment of true steady-state flow; (ii) errors in the experimental measurements of Q_1 and Q_2 because of air bubble size and reading errors in the permeameter; and (iii) entrapment of air in the soil due to water redistribution during filling of the permeameters and restarting of infiltration. These three error sources exist also for the single-ring pressure infiltrometer measurements since the only difference is the borehole and its preparation. We minimised these error sources during measurements by (i) increasing measurement time, (ii) using small air inlet tubing and (iii) making the reservoir large enough to make measurements at two heads possible without refilling [*Ankeny et al., 1988*]. Nevertheless K_{fs} and α_m are very sensitive to the Q_2/Q_1 ratio [*Wu et al., 1993*]. Preferential flow in macropores (vertical and lateral cylindrical pores, cracks) not activated in one infiltration measurement at a specific head becomes activated in the other infiltration measurement with the second applied head, can change the Q_2/Q_1 ratio, depending on the geometry and locations of the macropores. The activation or not of

macropore flow depending on the potential is well known in the unsaturated domain [*Elrick and Reynolds, 1992*]. In the ideal case where macropores would be homogeneously spread out over the soil volume, no artefacts can be encountered. When the saturated bulb is so small that no macropores are within the bulb for the smaller pressure head but are in the saturated bulb for the subsequently applied pressure head, the flow may increase dramatically due to the expansion of the bulb and the activation of macropores.

The objectives of this chapter were to: (i) examine the possibilities of the single-ring pressure infiltrometer measurements in estimating K_{fs} and α_m using the classical constant head approach for two heads at each measurement location, (ii) analyse the sensitivity of K_{fs} and α_m to small measurement errors, (iii) develop a procedure for the estimation of one overall 'field α_m' using an inverse optimisation technique and (iv) estimate the spatial correlation scale of K_{fs} measured on the experimental hillslope.

3.2. Materials and Methods

Infiltration was measured using single ring pressure infiltrometers at 120 locations on the 80 by 20 m field plot located on the hillslope described in detail in Chapter 2. The single ring pressure infiltrometer measurements were conducted in August 2000 before the start of the rainfall-runoff experiment.

3.2.1. Measurements

To estimate field-saturated conductivity (K_{fs}), we measured the steady-state infiltration rate from a ring under a constant positive pressure head (H) using a single ring pressure infiltrometer (Fig. 3.1). Water is supplied to the soil surface at a positive head through a sealed top lid by a Mariotte bottle with a moveable air tube allowing a wide range of H. The set-up is similar to the Guelph Permeameter reservoir [*Reynolds et al., 1985; Reynolds and Elrick, 1990; Vauclin et al., 1994; Angulo-Jaramillo et al., 2000*]. The ring (Fig. 3.1) has a diameter of 95 mm and can be driven into the ground to a maximum depth of 57 mm. The ring was carefully driven into the ground without

removing the short grass; no special surface preparation was needed. The grass was not removed as we were interested in the in-situ natural infiltration characteristics.

At each location, steady-state infiltration rates were measured manually at two different pressure heads applied in a sequence at a single location. The supplied pressure heads were slightly different for each location, but in all cases, the measurements started at the smallest value. The supplied pressure heads ranged from +6 cm to a maximum of +25 cm. Steady-state was reached after an average of 90 minutes per head. The criterion used for attaining steady-state infiltration was that the 5 minutes infiltration volume during a 30 minutes record remained constant. All measurements were done during a long dry period since, as also explained above, the initial water content of the soil may influence the estimation of K_{fs} [*Bagarello and Provenza, 1996*]. The measurement campaign was limited in time thereby minimising the risk of temporal changes in soil structure that may affect the saturated conductivity [*Russo et al., 1997*]. In this case, no prior rainfall-runoff experiments were performed and the measurement campaign was two weeks long. No precipitation was recorded during that period.

Figure 3.1 Single ring pressure infiltrometer set-up

The total number of measurement locations was 120 and the measurement scheme is shown in Fig. 3.2. The scheme layout was designed in order to obtain enough pairs for the estimation of semi-variograms at different lag distances in both the x- and y-direction. An accurate estimation of the semi-variograms requires a minimum of 30-50 pairs [*Journal and Huijbregts, 1978*]. To estimate directional variograms, measurements were done on lines parallel and perpendicular to the hillslope. The testing of the layout was performed using the GSLIB program [*Deutsch et al., 1992*].

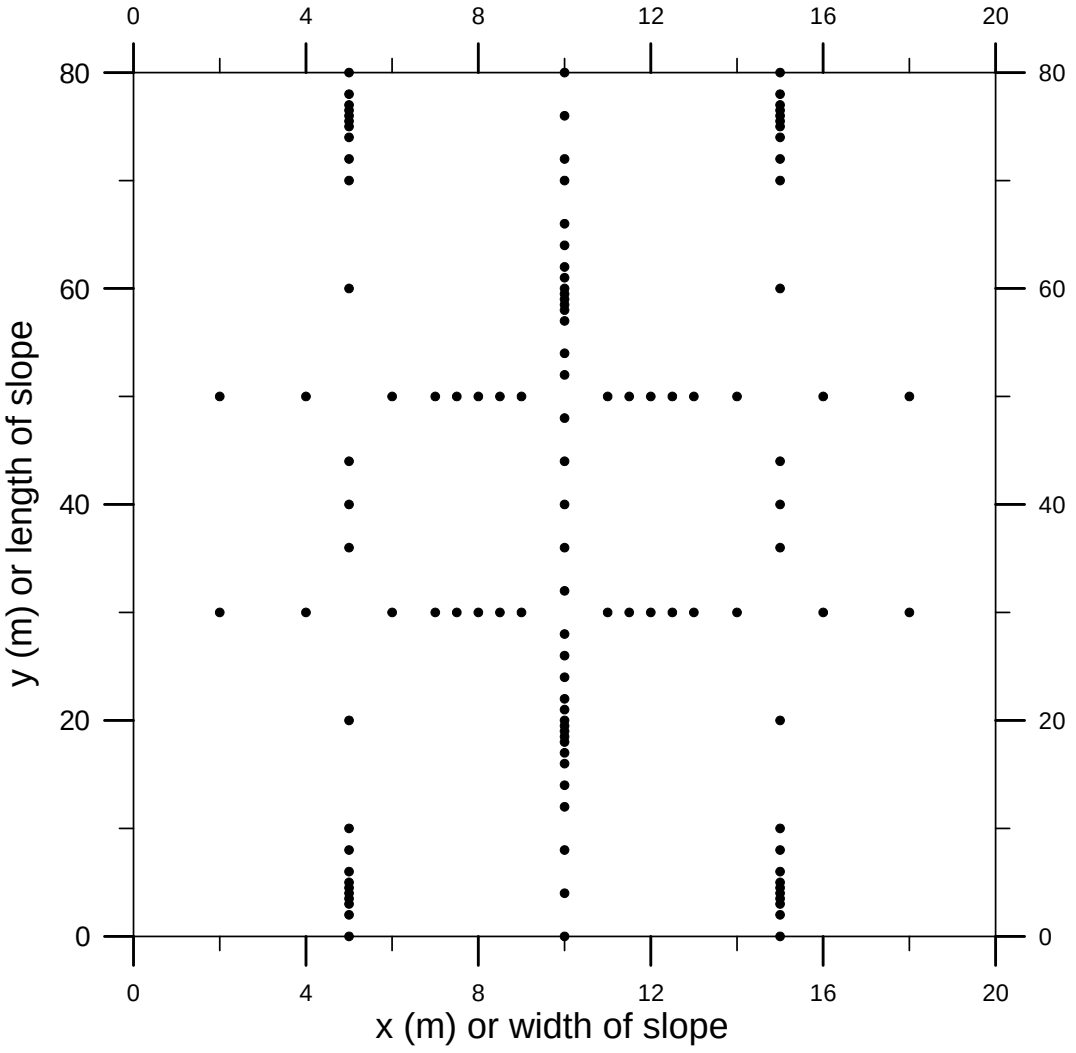

Figure 3.2 A scheme of the hillslope showing the 120 measurement locations

3.2.2. Derivation of K_{fs} and α_m

3.2.2.1. Simultaneous-Equations Approach (SEA)

An analysis of steady, ponded infiltration from a single ring which takes into account the soil hydraulic parameters, ring radius, depth of ring insertions, and depth of ponding was published by *Reynolds and Elrick (1990)*. The following equation for three-dimensional steady flow of water from the ring was given:

$$q_{0\infty} = K_{fs}(1 + \frac{H}{\pi r_d G}) + \frac{\phi_m}{\pi r_d G} \tag{3.3}$$

where $q_{0\infty}$ [LT^{-1}] is the steady flow rate, K_{fs} [LT^{-1}] is the field saturated hydraulic conductivity, H [L] is the height of the ponded head, r_d [L] is the ring radius, ϕ_m [L^2T^{-1}] the matric flux potential and G [-] a dimensionless parameter:

$$G = 0.316\frac{d_r}{r_d} + 0.184 \tag{3.4}$$

where d_r [L] is the depth of insertion of the ring in the soil. The first term of the right-hand side of Eq. 3.3 represents the gravitational effect, the second one corresponds to the influence of the ponded head, H, and the third term represents the contribution of the capillary forces to the soil water flow [*Angulo-Jaramillo et al., 2000*]. When the steady-state infiltration rates are measured at two positive hydraulic heads H_1 and H_2 at the same location, K_{fs} and ϕ_m are obtained by solving the resulting two equations Eq. 3.3, (Simultaneous-Equations Approach). On each measurement location, two hydraulic heads were applied and the corresponding steady-state infiltration rate measured. This allows the simultaneous solving of two equations for K_{fs} and ϕ_m (or α_m) per measurement location.

3.2.2.2. Sensitivity analysis

A rigorous analysis of the uncertainties of the single-ring pressure infiltrometer measurements is beyond the scope of this study. Instead, a simple error analysis using Monte Carlo simulations (MC-simulations) was performed here to assess the propagation of uncertainties in measured inflow rates on the values of K_{fs} and α_m. A random error on the steady-state infiltration rate is assumed. The error is assumed equivalent to a possible reading-off error of mean 0 mm and standard deviation 0.5 mm (normal distribution) on the value read-off the reservoir. The error is randomly added to read-off values for both applied pressure heads. Inflow rates (Q_1 and Q_2) are calculated and the assumed error in this experiment results in a standard deviation on Q_1 and Q_2 of 0.0034 cm min^{-1}. Mean of Q_1 and Q_2 over all measurements is 0.2 cm min^{-1}so the mean error on the inflow rates is about 1.7 %. Consequently K_{fs} and α_m values are calculated using the SEA for each random error. 1000 simulations per measurement location or 120000 simulations were performed and the statistical properties derived.

A second sensitivity analysis is performed in order to examine the effect of an increase of the number of pressure head levels per location on the uncertainty of K_{fs} and α_m. This analysis is done for three pressure heads and corresponding infiltration rate per measurement location. Monte-Carlo simulations were performed using the same probability distribution on the inflow rate as described above, but assuming three pressure head levels. Three K_{fs} values (0.005, 0.03 and 0.09 cm min^{-1}) and six α_m values (0.01, 0.02, 0.05, 0.1, 0.2, and 0.5 cm^{-1}) are arbitrarily chosen though keeping in mind the range of α_m proposed by *Elrick et al. (1989)*. For each pair of K_{fs} and α_m, three $q_{0\infty}$ values were calculated for three different H's (10, 20 and 30 cm) using Eq. 3.3. Then a measurement error is added to $q_{0\infty}$ and a regression through the new $(H, q_{0\infty}^{\otimes})$ is performed ($q_{0\infty}^{\otimes}$ = theoretical perturbed infiltration rate). Three pressure head levels require regression through the three pairs $(H, q_{0\infty}^{\otimes})$ while when using only two levels, simultaneously solving of Eq. 3.3 for both pairs was sufficient. Three pairs are hence expected to result in smaller standard deviations of K_{fs} and α_m but are more time consuming when taking the field measurements.

3.2.2.3. Inverse optimisation technique

The calculation of best fit parameters (e.g. K_{fs} and α_m) in general requires minimisation of the following objective function [*Bard, 1974*]:

$$SSR = \sum_{i=1}^{n_o} [M(p) - O_i]^2 \tag{3.5}$$

where *SSR* is the sum of squared residuals, *M(p)* is the model function with a set of parameters *p*, and *O* is a vector of n_o data points (observed).

We propose here a new procedure using an optimisation technique. The procedure optimises simultaneously one overall 'field' α_m and n K_{fs} values (one at each measurement location). The optimum is reached when the *SSR* is minimal, i.e. when the sum of squared differences between observed Q and simulated $q_{0\infty}$ values for each location is minimal. Considering only one α_m, Eq. 3.3 can be rewritten as:

$$\begin{bmatrix} Q_{1,1} \\ Q_{1,2} \\ Q_{2,1} \\ Q_{2,2} \\ . \\ . \\ Q_{n,1} \\ Q_{n,2} \end{bmatrix} = \begin{bmatrix} H_{1,1}00.....0 \\ H_{1,2}00.....0 \\ 0H_{2,1}00...0 \\ 0H_{2,1}00...0 \\ ..... \\ ..... \\ 00.....H_{n,1} \\ 00.....H_{n,2} \end{bmatrix} * \begin{bmatrix} a_1 \\ a_1 \\ a_2 \\ a_2 \\ . \\ . \\ a_n \\ a_n \end{bmatrix} + \begin{bmatrix} 100.....0 \\ 100.....0 \\ 0100...0 \\ 0100...0 \\ ..... \\ ..... \\ 00.....1 \\ 00.....1 \end{bmatrix} * \begin{bmatrix} a_1 \\ a_1 \\ a_2 \\ a_2 \\ . \\ . \\ a_n \\ a_n \end{bmatrix} * b \tag{3.6}$$

where $a_i = \frac{K_i}{\pi r_d G}$, $b = \frac{1}{\alpha_m} + \pi r_d G$, $Q_{i,1}$, $Q_{i,2}$ and $H_{i,1}$, $H_{i,2}$ correspond respectively to the first and second measured steady-state infiltration rate ($Q_{0\infty}$) and head (H) at each measurement location i.

Equation 3.6 is the model with parameter a_i and b. Note that Eq. 3.6 is in fact a non-linear model because of the second term. Lower limits for K_{fs} and α_m were set to 0 while

upper limits were set to infinity for all parameters. The initial estimates of K_{fs} were arbitrarily set at 0.25 cm min^{-1} and the initial estimate α_m was set at 0.01 cm^{-1}.

3.2.3. Statistical and geostatistical methods

Since only one field α_m value is considered in this study, only K_{fs} is considered in the geostatistical analysis. Prior to the spatial analysis of K_{fs}, it is convenient to examine the data of K_{fs} by means of simple conventional statistical methods. The Lilliefors test [*Conover, 1980*] is used as normality check of ln K_{fs}. The Lilliefors test is similar to the Kolmogorov-Smirnov test, but adjusts for the fact that the parameters of the normal distribution are estimated from the K_{fs} values rather than specified in advance. Using the theory of the regionalized variables [*Cressie, 1993*], the spatial correlation structure of K_{fs} is investigated. The semivariance is defined as:

$$\gamma(h_l) = \frac{1}{2n(h_l)} \sum_{i=1}^{n(h_l)} [z(x_i) - z(x_i + h_l)]^2 \tag{3.7}$$

where $\gamma(h_l)$ is the estimated semivariance for lag distances class h_l, $z(x_i)$ and $z(x_i+h_l)$ are the measured sample values at point x_i and $x_i + h_l$ respectively, and $n(h_l)$ is the total number of sample pairs for the interval h_l. The omnidirectional and directional variograms along x and y axis are calculated using the GSLIB program [*Deutsch et al., 1992*]. An exponential model was visually fitted to the variograms:

$$\gamma(h_l) = C_0 + C_s * \left[1 - e^{\frac{-3h_l}{r_a}} \right] \tag{3.8}$$

where C_0 is the nugget variance and C_s is the (co)variance contribution or sill value, h_l the lag distance [L] and r_a is the practical range, that is the distance at which the variogram value is 95% of the sill. The model was checked by cross-validation, testing for the absence of systematic errors and the consistency of the kriging variance and error. In particular, following *Jury et al. (1987)* and *Russo and Jury (1987)*, we checked the following criteria:

$$ME = \frac{1}{n}\sum_{i=1}^{n} RE(x_i) \cong 0 \tag{3.9}$$

where

$$RE = \frac{\hat{z}(x_i) - z(x_i)}{\{\mathrm{var}[\hat{z}(x_i) - z(x_i)]\}^{1/2}} \tag{3.10}$$

and

$$MRE = \left[\frac{1}{n}\sum_{i=1}^{n} RE(x_i)^2\right]^{1/2} \cong 1 \tag{3.11}$$

where *ME* is the mean of the reduced error vector *RE*, *MRE* is the mean square reduced error, *n* is the sample size, $z(x_i)$ and $\hat{z}(x_i)$ are the measured and predicted (krigged) values at location x_i, where *i* varies from 1 to *n*.

3.3. Results and Discussion

3.3.1. Simultaneous-Equations Approach

As discussed above, an important limitation of the single ring pressure infiltrometer measurements is the potential for negative values of the estimated K_{fs} and/or α_m [*Heinen and Raats, 1990; Elrick and Reynolds, 1992; Wu et al., 1993; Russo et al., 1997*]. The SEA approach (Eq. 3.3 and Eq 3.4) can only yield positive values for K_{fs} if $Q_2 > Q_1$, but can yield both positive and negative values for α_m. That is why all 120 calculated K_{fs} values of our data set were found to be positive. Table 3.1 shows the basic statistical properties of the calculated K_{fs} and α_m values using the SEA procedure. 79 out of 120 calculated α_m values were positive. A negative value of α_m is physically impossible since this would mean that either K_{fs} or ϕ_m is negative. The 41 negative α_m values make

that the overall average α_m of all positive and negative α_m values was negative. Values of α_m down to -10 cm^{-1} were obtained. The mean K_{fs} for locations where $\alpha_m > 0$ is half (0.032 cm/min) of the mean K_{fs} for all locations (0.073 cm/min) and only one fifth of the mean K_{fs} where $\alpha_m < 0$ (0.152 cm/min). Standard deviation on K_{fs} when taking only negative values into account is 8 times larger than the one of K_{fs} where only positive α_m values are considered. Table 3.1 suggests that negative α_m values generally correspond to higher K_{fs} values. Examining the single measurements reveals that this is not true for all since distributions of K_{fs} values for positive α_m and for negative α_m overlap partly, although the overlap is minor.

Table 3.1 Descriptive statistics of K_{fs} (cm min^{-1}) and α (cm^{-1}) calculated using the SEA and in comparison with the statistics of the 'optimised' values

	N.	Avg.	Min.	Max.	Std.Dev.
All measurements (SEA)					
K_{fs}	120	0.0734	0.0010	1.4544	0.1555
α_m	120	-0.0126	-9.5796	8.2911	1.1739
Location of positive α_m values (SEA)					
K_{fs}	79	0.0324	0.0010	0.1320	0.0350
α_m	79	0.1864	0.0006	8.2911	0.9298
Location of negative α_m values (SEA)					
K_{fs}	41	0.1526	0.0051	1.4544	0.2445
α_m	41	-0.3958	-9.5796	-0.0249	1.4784
All measurements (optimisation)					
K_{fs}	120	0.0293	0.0020	0.1516	0.0292
$\alpha_{m,\,opt}$	1	0.0300	/	/	/

As studied by *Wu et al. (1993)* preferential flow in macropores changes the Q_2/Q_1 ratio which may lead to negative α_m values. Since macropore flow is only gravity driven and barely influenced by capillary forces, the third term in Eq. 3.3 is very small (i.e. due to its large positive α_m). Therefore measurement errors which are propagated in the intercept of the q versus H relation (sum of first and third term), may result in a negative third term in Eq. 3.3 (i.e. negative α_m). This matches the finding of this study that

locations where α_m is calculated negative, generally have high K_{fs} values. Preferential flow indeed increases hydraulic conductivity values [*Bouma, 1981; Beven and Germann, 1982; Edwards et al., 1988; Logsdon et al. 1990*]. However, we will demonstrate in the next section that measurement errors result in erroneous and uncertain estimates of α_m values for all types of soils.

3.3.2. Sensitivity analysis

The aim of this part of the study is to examine the effect of small fluctuations in 'measured' inflow rate on K_{fs} and α_m. Only those observations where α_m was found positive using the SEA (79 locations) were used in the sensitivity analysis in order to avoid the effect of negative α_m values. Monte Carlo simulations (1000 simulations for each of the 79 locations) result in model output statistics for K_{fs} and α_m. Figure 3.3 shows the simulated mean value and standard deviation for K_{fs} (a) and α_m (b). The standard deviation of α_m is very high (notice the log scale) for all measurement locations and a trend of increasing standard deviation with increasing α_m values is observed. The sensitivity of α_m to small variations in inflow rate is extremely high and small input fluctuations in measured infiltration rates result in a large range of α_m values: from –1000 cm^{-1} up to +2000 cm^{-1}. This exercise reveals that the α_m value calculated using the SEA from single-ring pressure infiltrometer measurements with only two pressure head levels is meaningless. This conclusion must at this stage be restricted to our conditions (e.g. initial soil moisture content and soil type,…). As stated above, negative α_m values do not necessarily imply high K_{fs} values (or preferential macropore flow) but as shown in the Monte Carlo simulations, negative α_m values could also be the result of small variations in the measured infiltration rate due to e.g. measurement errors. The standard deviation of K_{fs} is nearly constant for all measurement locations i.e. no trend of increasing standard deviation with increasing K_{fs} values can be noticed, and standard deviations remain reasonably small for all measurement locations. K_{fs} is not very sensitive to these infiltration rate measurement errors. In conclusion, single-ring pressure infiltrometer measurements using only two pressure head levels at each location is a suitable method for the in-situ derivation of K_{fs} but unsuitable for estimating α_m.

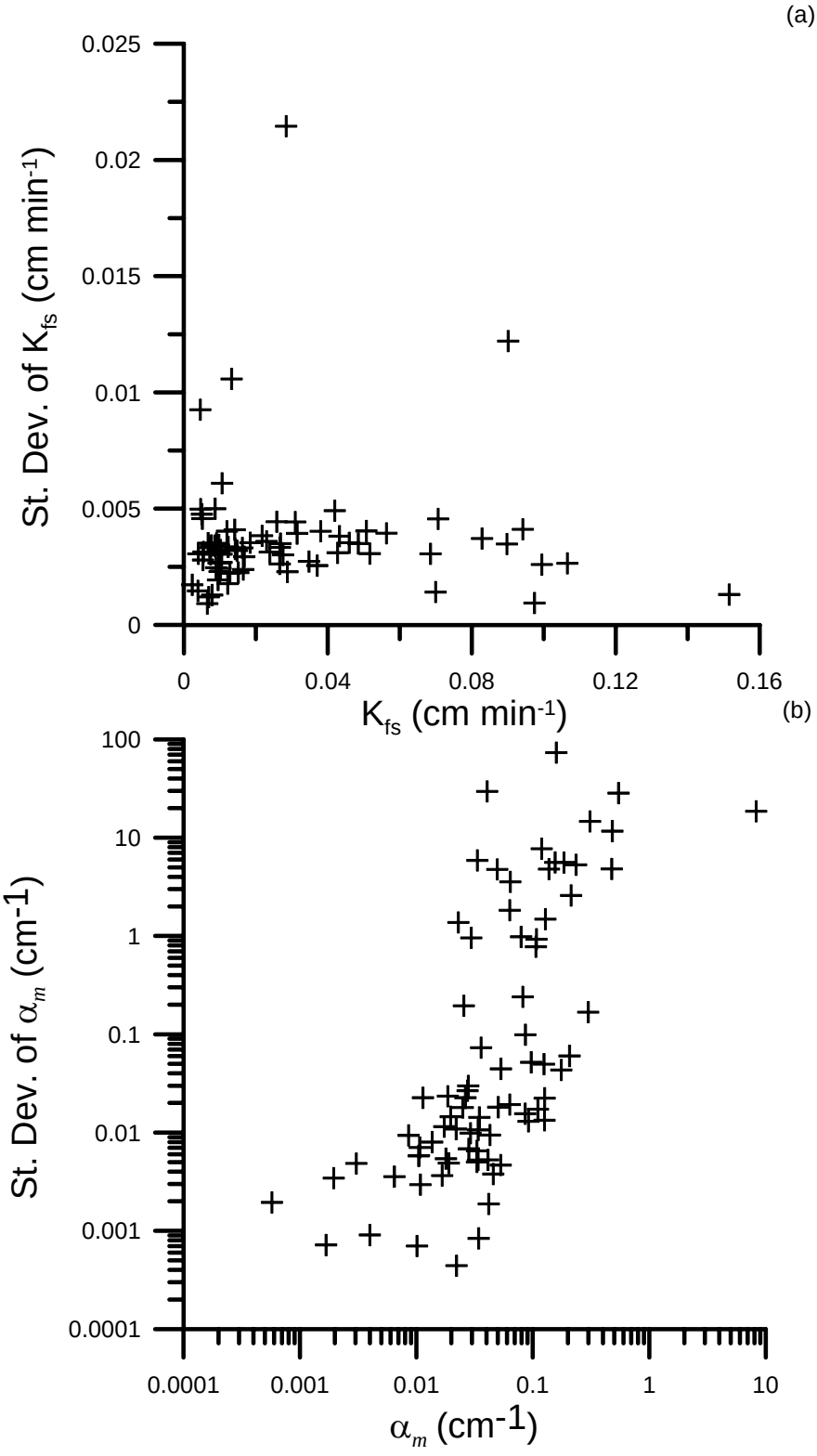

Figure 3.3 Result of the Monte Carlo simulations with two applied pressure heads. (a) K_{fs} and standard deviation of K_{fs} (b) α_m and standard deviation of α_m

The result of the second sensitivity analysis (3 theoretical heads applied) in which three K_{fs} values (0.005, 0.03 and 0.09 cm min^{-1}) and six α_m values (0.01, 0.02, 0.05, 0.1, 0.2, and 0.5 cm^{-1}) are arbitrarily chosen and Monte Carlo simulations performed as explained above, is presented in Fig. 3.4. As shown in Fig. 3.4(a), standard deviations of K_{fs} again remain quite constant and reasonably small over the range of K_{fs} for all considered α_m values. Six Monte-Carlo simulations (1000 runs each) were performed for each of the three considered K_{fs} levels, i.e. one simulation for each value of α_m. Fluctuations in infiltration rate over the considered range of α_m and K_{fs} values do not influence standard deviation of K_{fs}. Figure 3.4(b) reveals that even when considering three pressure head levels, the estimated α_m values remain very sensitive to measurement errors in the infiltration rate over the considered range of α_m.

A trend of increasing standard deviation with increasing values of α_m can again be observed. This trend can be explained physically: low α_m values correspond to soils in which capillary forces are relatively important compared to gravity forces. This means that in these soils, the third term in Eq. 3.3 is relatively large and hence α_m or ϕ_m has a large influence on the value of $q_{0\infty}$. In other words, $q_{0\infty}$ is sensitive to the value of α_m or α_m can be determined quite well. On the other hand, when α_m increases (gravity forces more important than capillary forces), the third term becomes very small compared to the first two terms of Eq. 3.3, which implies that α_m does not contribute a lot to the value of $q_{0\infty}$ (or $q_{0\infty}$ is insensitive to the value of α_m) and can hence not be determined with great certainty.

It is obvious from Fig. 3.4(b), that single-ring pressure infiltrometer measurements, is not a suitable method to estimate α_m, even when using three pressure head levels. Here, the conclusion that calculated α_m values using SEA are meaningless can be extended to a large number of other soils having a wide range of α_m and K_{fs} values. Since small infiltration variations (or measurement errors) do not have a large effect on the estimation of K_{fs}, it is a stable method for the in-situ estimation of K_{fs}.

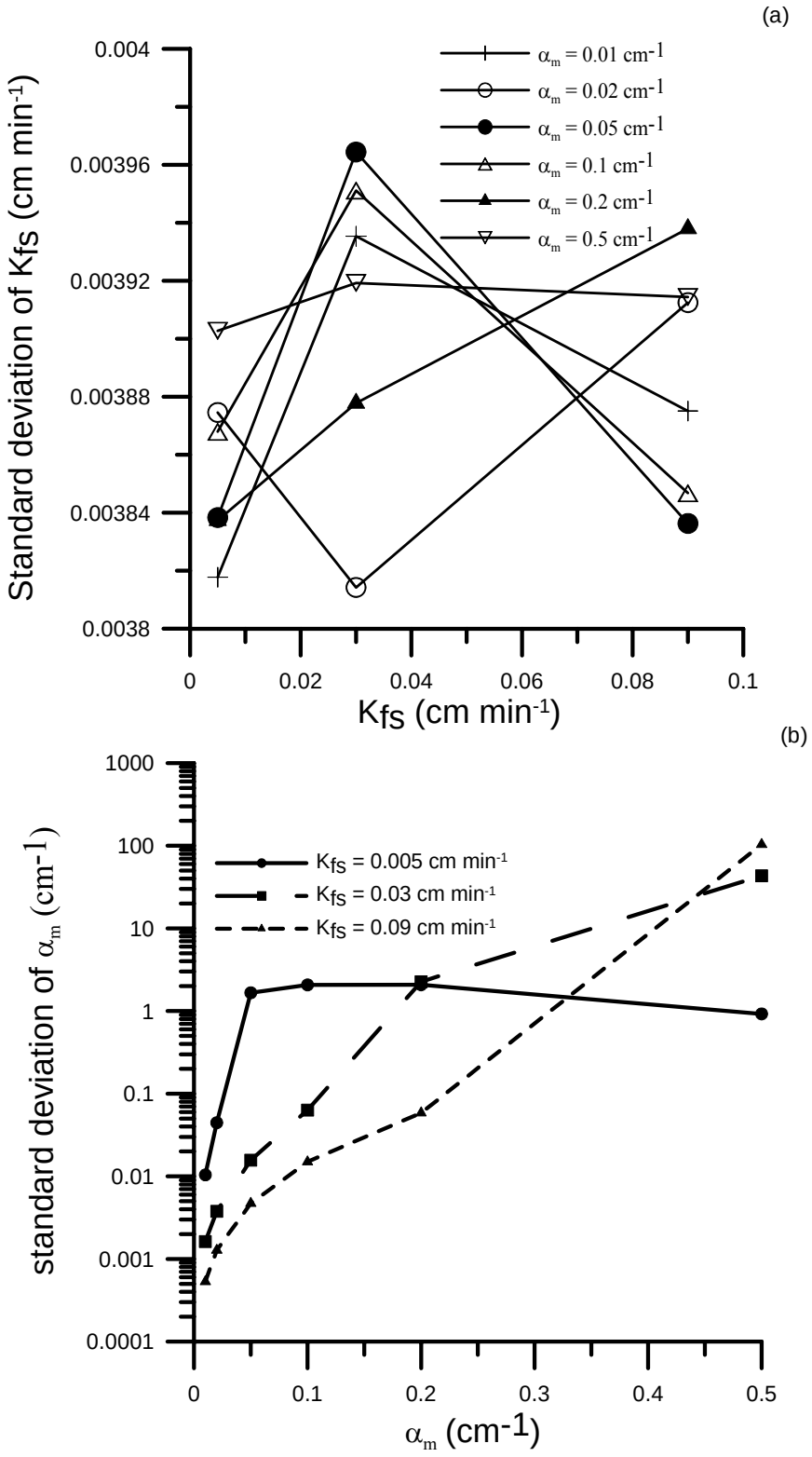

Figure 3.4 Result of the Monte Carlo simulations of fictive pressure head infiltrometer data using three pressure head levels (a) K_{fs} and standard deviation of K_{fs} (b) α_m and standard deviation of α_m

3.3.3. Inverse optimisation technique

As discussed above, a single-ring pressure infiltrometer measurement is a good tool for the estimation of K_{fs} in-situ. A problem remains that the estimation of K_{fs} is a function of α_m. However, the sensitivity analysis showed that it is impossible to obtain a meaningful estimation of α_m from the steady-state infiltration rate measurements. As stated above, *Elrick et al. (1989)* suggested a fixed α_m value method. However, individual α_m values for soils are generally not available.

One solution for the choice of the α_m value could be to consider the average of the 79 positive α values as the 'overall' α_m. Following this, an overall α_m of 0.19 cm^{-1} can be calculated. Recalculating all K_{fs} values with the overall α_m value would finally result in two K_{fs} values per measurement location (or 240 K_{fs}) and one overall α_m. Finally, the average of both K_{fs} values at each measurement location can be considered as the best estimate. Another and statistically more sound solution is to take the average of all α values as the 'overall' α_m. Statistically speaking, including all α values (including the negative ones) is expected to middle out the individual errors associated with each α estimate so the mean is close to the 'real' α value as its error is close to zero. Though in our case, due to a few outliers this results in a negative value of – 0.0126 which is physically impossible.

An alternative, more robust way of estimating the 'overall' α_m value is proposed in this study. In the sensitivity analysis, it was proven to be impossible to get an accurate estimate of local α_m values using the SEA. It also revealed that K_{fs} is less sensitive to measurement errors and also to an erroneous α_m estimate or that α_m can be completely out of the normal range while the estimate of K_{fs} is still acceptable. That's why the authors believe that it makes sense to suggest a fixed α_m for all measurement locations. Using this fixed α_m value, an error is made due to the fact that the local α_m might differ from the optimised one but this error only has a very small impact on the estimation of the local K_{fs}.

Again, only locations where α_m was positive (SEA) are taken into consideration. The optimisation of Eq. 3.6 aims at finding 79 *a* values (equivalent to 79 K_{fs} values) and 1 overall *b* value (related to α_m) by minimising the sum of the squared residuals. Several sets of initial parameters were used; all leading to the same optimised parameter set. This means that the optimised parameter set does not correspond to a local minimum in the objective function but corresponds to the overall minimum or optimum. Compared to the case in which the average of the positive α_m values is taken as the overall α_m, this optimisation procedure results in a value of α_m which is based on all measurements where α_m is positive simultaneously.

The sensitivity analysis learned that negative α_m values can be the result of measurement errors. Though positive α_m values do not imply that measurement errors are negligible, negative α_m values are for sure an indication of 'large' uncertainty; hence it makes sense (first reason) to exclude these negative α_m locations. It must be stressed that the actual α_m value using SEA is meaningless, though in this study, its sign decides whether it is to be used in the optimisation procedure or not.

When the Levenberg-Marquardt optimisation procedure was applied for all locations, including the negative α_m sites, the optimised α_m value always reached the top of the upper bound set in the optimisation procedure, even when this bound reached extreme values of 100 cm^{-1}. This is because the optimising procedure looks for one overall α_m which is negative but α_m is not allowed to become negative by its lower bounds (set to 0). Therefore, the optimising procedure increases the value of α_m in order to decrease the third term of Eq. 3.3 in the same way a negative α_m does. Hence, (second reason) the optimisation procedure was limited to the locations having a positive α_m value.

Figure 3.5 shows the result of the optimising procedure: simulated ('optimised') and measured infiltration rates are very close (R^2 = 0.9961) and no trend was found in the residuals. The overall α_m or $\alpha_{m,,opt}$ was 0.03 cm^{-1} and the optimised K_{fs} values are shown in Fig 3.6. The large difference between average positive α_m's using SEA (0.18 cm^{-1}) and the optimised α_m (0.03 cm^{-1}) is due to a few outliers (e.g. one α_m of 8.29 cm^{-1}) in the result of the SEA calculation and the large uncertainty on α_m as shown in the sensitivity

analysis. Comparing this $\alpha_{m,,opt}$ of 0.03 cm^{-1} with the values proposed by *Elrick et al. (1989)* indicates that this value lies within the range of the 'unstructured fine textured soils', in which the soil found at the measurement site can be classified. Optimised K_{fs} values are generally not as high as the originally calculated K_{fs} values using the SEA, although this is certainly not true for all measurement locations.

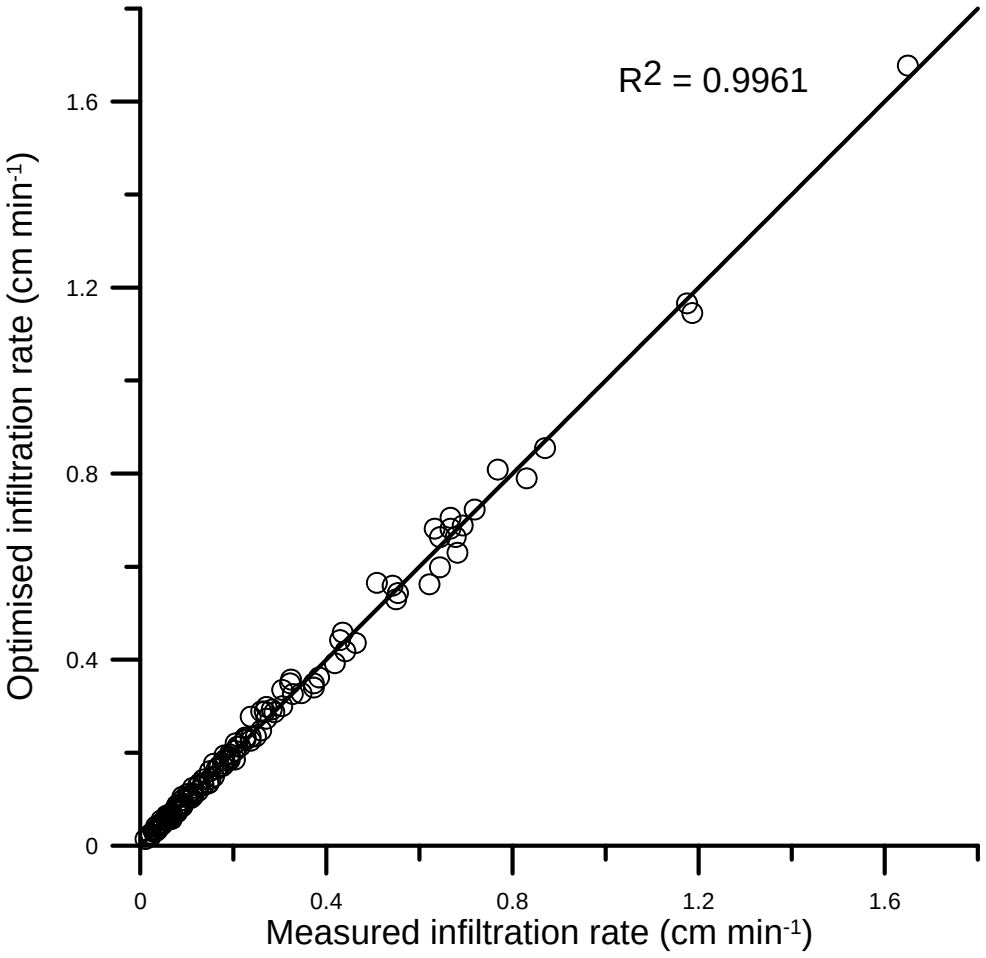

Figure 3.5 Result of inverse optimisation: measured infiltration rate compared to optimised (simulated) infiltration rate

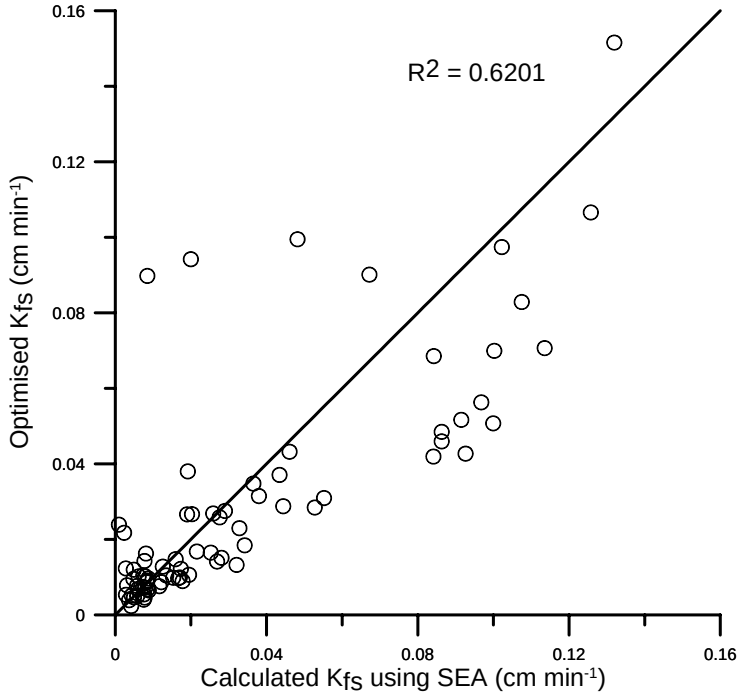

Figure 3.6 Optimised K_{fs} values at locations with an originally calculated positive α compared to originally calculated K_{fs} using the SEA method

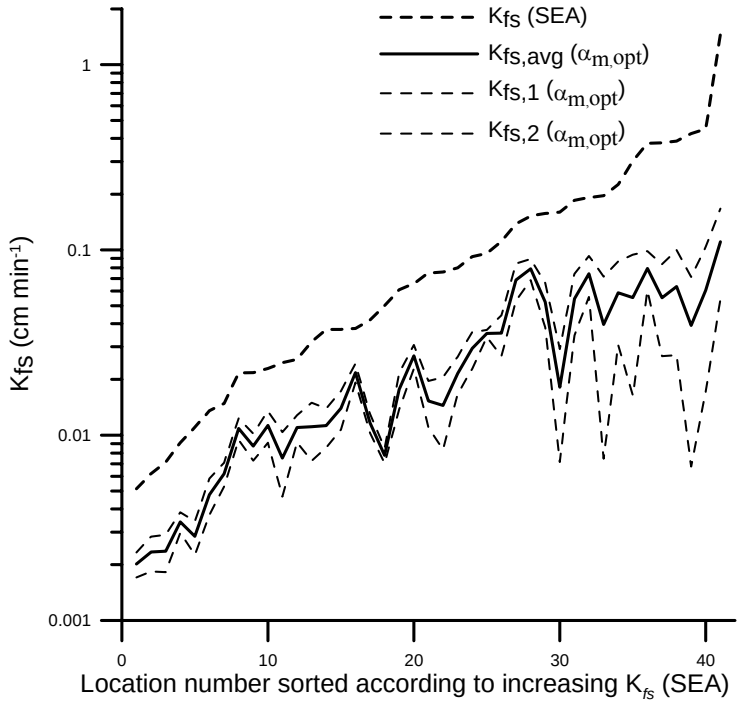

Figure 3.7 K_{fs} values based on $\alpha_{m,opt}$ at locations with an originally calculated negative α_m

At locations where α_m was found negative, we solved Eq. 3.3 for K_{fs} using $\alpha_{m,,opt}$ and obtained two K_{fs} estimates at each location, one for each applied pressure. The average of these two estimators (= $K_{fs,avg}$) is considered to be the in-situ measured K_{fs} for that location. Fig. 3.7 shows the originally calculated K_{fs} values using the negative α_m, the K values from Eq. 3.3 for each H (using $\alpha_{m,,opt}$) and the averaged K_{fs}, which is considered to be the in-situ estimated K_{fs} for that location. Furthermore, Fig. 3.7 reveals that the $K_{fs,avg}$ is again lower than the originally calculated K_{fs} using negative α_m values, and that for all measurement locations. This is quite obvious because an increase in the third term of Eq. 3.3 (α_m from a negative to a positive value) has to be compensated by a decrease in K_{fs} for equal q values.

Advantage of the optimising technique compared to calculating K_{fs} according to SEA is that in this technique, all measurements (at least where α_m was found to be positive with the SEA) are involved in finding the optimum 79 K_{fs} values and the overall α_m value simultaneously. No posterior averaging (except for the negative α_m values) of K_{fs} values compared to the method proposed by *Elrick et al. (1998)* is needed. The statistics of the K_{fs} for all locations using the overall α_m value are shown and compared with the K_{fs} values calculated using the SEA in Table 3.1.

3.3.4. Comparison K_{fs} and K_s measured in laboratory

The value of K_{fs} is the result of the hydraulic soil properties of the A-horizon as well as of the B-horizon. The influence of the B-horizon will be larger at locations where the B-horizon is closer to the surface. Figure 3.8 compares the cumulative distributions of the K_s values measured in the laboratory on the soil samples (after deletion of outliers) taken from the profile pits (A- and B-horizon) and the K_{fs} values measured by the single ring pressure infiltrometer measurements (for both the SEA approach and the inverse optimisation approach as discussed in this chapter). In addition, Fig. 3.8 reveals that the range of K_{fs} is significantly smaller than the ranges of K_s for both the A- and B-horizon (even after the deletion of outliers, cfr. Chapter 2). A Kolgomorov-Smirnov test shows that on a 5 % significance level, the distributions of K_{fs} (for both approaches) are significantly different from both the A- and B-horizon K_s distributions. This test is based

on the maximum difference between the distributions and because the standard deviation of K_s is much larger than for K_{fs}, the test reveals a significant difference. Average values of both K_s and K_{fs} are comparable: mean K_{fs} value is slightly lower than the mean of K_s for both horizons while the mean is slightly higher. A larger difference between mean K_s and K_{fs} was to be expected since under field conditions, a certain amount of air is usually entrapped in the soil during the infiltration process. Lower estimates of the 'saturated' hydraulic conductivity compared to measurements in completely saturated soils (e.g. lab estimates) can hence be expected [*Stephens et al., 1987*].

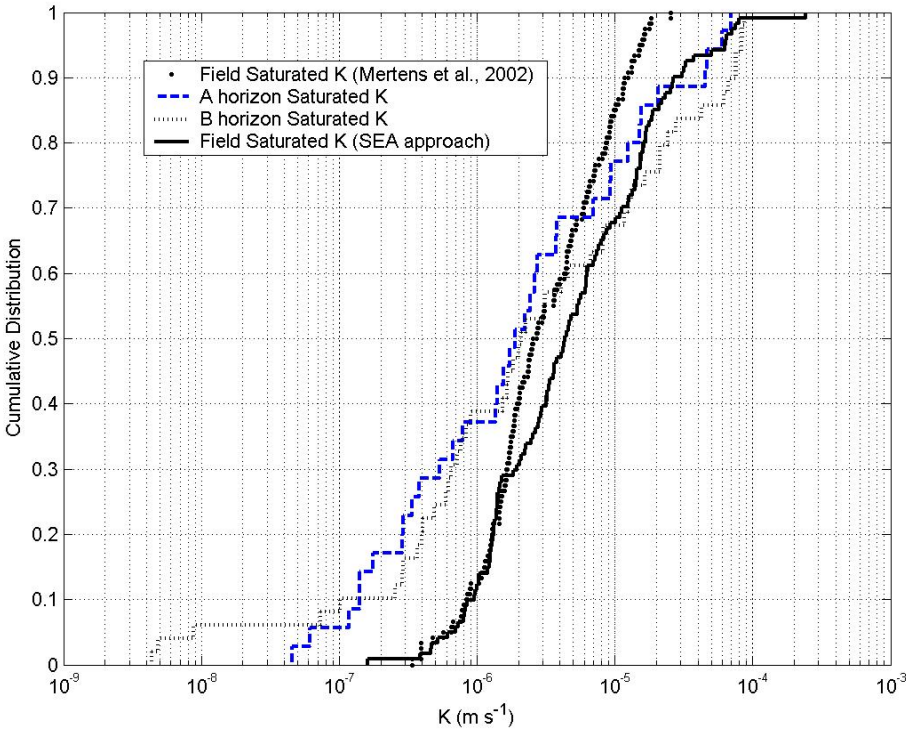

Figure 3.8 Comparison between field saturated hydraulic conductivity from single ring pressure infiltrometer measurements and A- and B-horizon soil core hydraulic conductivity estimates in the laboratory

From literature, it is known that different measurement techniques at different scales and even at the same scale, can result in different parameter estimates. In *Reynolds et al. (2000)* a comparison is made between tension infiltrometer, pressure infiltrometer, and soil core estimates of saturated hydraulic conductivity. It is concluded that parameters

from the different measurement techniques are significantly different even though they were measured at similar scales. In the summer of 2002, in-situ tension-infiltrometer measurements followed by in-situ single ring pressure infiltrometer measurement at the same location and same scale were carried out for a transect along the hillslope [*Herman et al., 2003*]. Thereafter, soil core were taken with similar dimensions and K_s estimated in the laboratory. Same conclusions can be drawn: K_s estimates are significantly different between different measurement techniques even when measured at similar scales.

3.3.5. Statistical and geostatistical results

The normal probability of the $\ln(K_{fs})$ values calculated based on $\alpha_{m,opt}$ is visualised in Fig. 3.9. The Lilliefors test did not reject the null (normal) hypothesis at the 0.05 level of significance, meaning that K_{fs} is log-normally distributed as shown in several other studies [*Jury, 1985; Russo et al., 1997; Zavattaro et al., 1999; Mohanty et al., 1994; Jacques, 2000*]. Figure 3.10(a) shows the omnidirectional variogram of $\ln(K_{fs})$, Fig. 3.10(b) the directional variogram in the x-direction or orthogonal to the hillslope and Fig. 3.10(c) the directional variogram in the y-direction or along the hillslope. In addition, the fitted exponential model through each variogram is shown in Fig. 3.10.

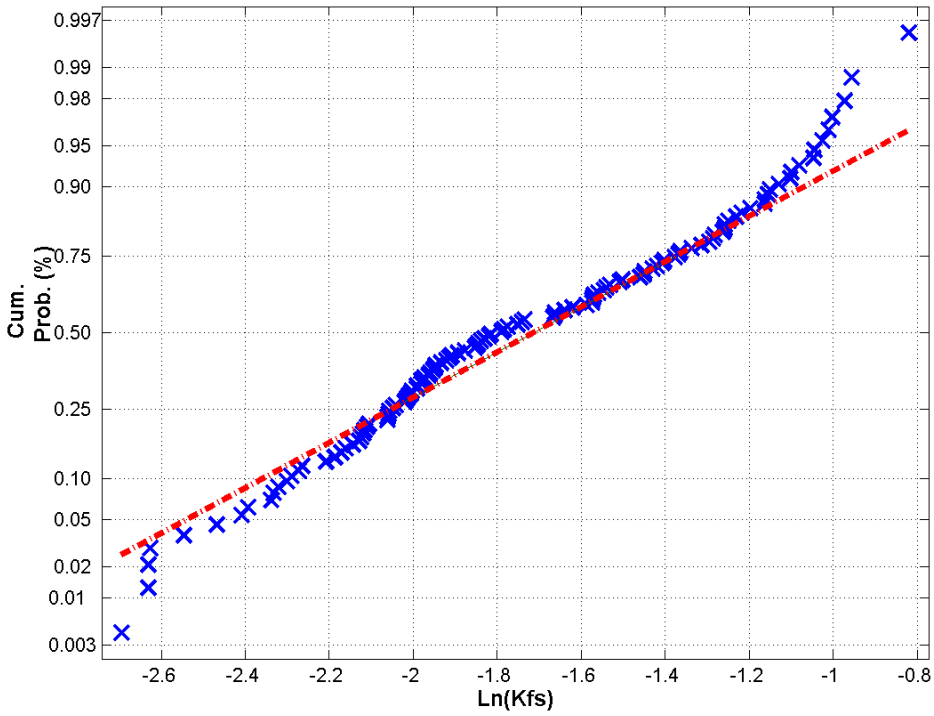

Figure 3.9 Normal probability plot of ln(K_{fs}). Straight line represents the theoretical cumulative normal probability function

The three parameters of the exponential model (Eq. 3.7) were estimated by visual fitting and are shown in Table 3.2. Cross validation using the model parameters fitted to the omnidirectional variogram, resulted in a mean of the reduced error vector (*ME*) of –0.045 a mean square reduced error (*MRE*) of 1.056. As these values are ideally 0 and 1 respectively, the fitted model was found to be suitable.

Table 3.2 Estimated parameters of the exponential semivariogram models

	Nugget (C_0)	Sill (C_s)	Range in m (r_a)
Omnidirectional	0.4	0.65	2.85
Directional (x)	0.2	0.7	3.2
Directional (y)	0.7	0.5	3.8

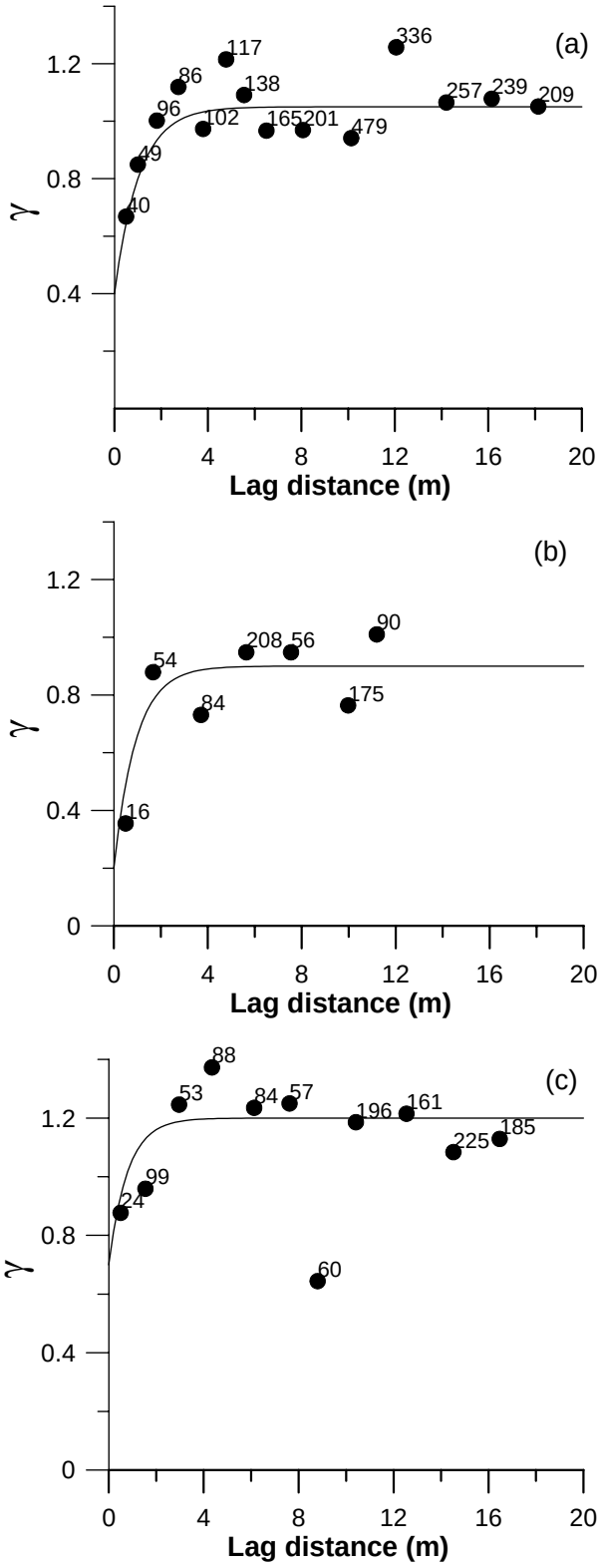

Figure 3.10 Experimental semi-variograms (circles) and fitted models of ln(K_{fs}) (a) omnidirectional semivariogram (b) directional semivariogram along x axis and (c) directional semivariogram along y axis.

Examining the semi-variograms reveals that some spatial pattern is present in all three semi-variograms. A range of ln(K_{fs}) of 2.85 m (omnidirectional) to 3.8 m (along the hillslope) is observed. *Russo et al. (1997)* found a range of ln(K_{fs}) between 0.6 m and 2.5 m which is in the same order of magnitude as the values found here. The quite high nugget values also suggest that the local variation between adjacent locations is high. As shown above, the uncertainty of measurement errors on the K_{fs} is reasonably small so this rather short correlation distance or range could be caused by several other factors. The field plot used to be an orchard of which the roots have created preferential flow pathways resulting in the shortening of the range. Worm- or moleholes can be another factor resulting in big differences between adjacent measurements.

3.4. Conclusions

In situ measurements of discharge-head (Q,H) pairs were used to estimate the field saturated hydraulic conductivity K_{fs}, and the parameter α_m [*Gardner, 1958*] at 120 locations on a hillslope (80 meters long, 20 meters wide) by means of a single-ring pressure infiltrometer. Only the steady-state infiltration rate was used for further analysis and using the classical SEA approach, seventy-nine of these (Q,H) pairs yielded positive α_m while all pairs resulted in positive K_{fs} values. The SEA approach showed that locations where α_m was negative, generally have high K_{fs} values. The negative α_m values might be the result of the domination of macropore flow in the infiltration process at that location. Negative α_m values do not imply that preferential macropore flow (or higher K_{fs}) is the case as shown in the sensitivity analysis. This MC analysis reveals that the sensitivity of α_m on measurement errors using the constant head SEA with two or three pressure head levels is enormous. Therefore, negative α_m values can be the result of a small measurement error instead of macropore flow. Sensitivity of K_{fs} to measurement errors is very low and constant over the range of K_{fs} and α_m. Based on this sensitivity analysis, it is believed that single-ring pressure infiltrometer measurements using two or three pressure head levels at each location is a suitable method for the in-situ derivation of K_{fs} but unsuitable for the estimation of α_m. A new technique using the inverse optimising of 120 K_{fs} values and only 1 α_m value using all infiltration measurements was proposed. The technique allows a robust method for the

derivation of that α_m value which is generally not known for a given location. The inverse optimising converged successfully and optimised and measured infiltration rates are very close. The spatial analysis revealed ranges of ln(K_{fs}) between 2.85 and 3.8 m omnidirectional and along the hillslope (y-axis), respectively. Though a robust method for the derivation of field saturated hydraulic conductivity is presented in this chapter, care must be taken interpreting the measured K_{fs} values. Lots of different methods for estimating hydraulic conductivity exist, all having their specific advantages and disadvantages at different scales. For the same soil and even at the same scale, different techniques might yield different K_s estimates [*Reynolds et al., 2000*, *Herman et al., 2003*]. Hence, it is impossible to know the 'real' conductivity. It can be doubted whether 'real' conductivity exists, as it is most likely that conductivity is a function of the scale. In most studies, one is not even interested in the 'real' conductivity but in an 'effective conductivity' for the (model)scale one is working with. It is hence doubtful that measured *K*, independent from the technique and scale it was measured at, coincide with the 'effective' *K* needed by the model used. In the next chapters, it is investigated how much different the *K* estimates (laboratory and in-situ) are from the 'effective' ones needed by the MIKE-SHE model. In Chapter 5, the difference between 'effective' and 'measured' parameters is not only investigated for *K* but for all other unsaturated zone parameters. In chapter 6, the relevance of measuring a priori laboratory of in-situ parameter estimates for the estimation of effective parameters is questioned.

Chapter 4

Hydrological modelling: model selection, parameterisation and calibration

ABSTRACT

This Chapter presents a brief literature review with respect to hydrological modelling. In particular the chapter focuses on the problem of the determination of effective parameters using inverse modelling techniques. After a general introduction, a discussion on the model selection and the scaling issue is elaborated. Consequently, the difference between local and global sensitivity analyses is discussed and their relevance in the effective parameter estimation issue shown. After the discussion of the advantages and disadvantages of manual and automatic calibration of hydrological models, the history of the most common optimisation algorithms (inverse modelling) as used in hydrology is presented. Optimisation algorithms are divided in global and local search methods. A detailed description of the Shuffled Complex Evolution algorithm as used in Chapter 5, 6 and 7 is thereafter given. Problems of inversed modelling are discussed in detail and divided in two main categories: (i) problems related to the quantity and quality of the calibration data and (ii) problems related to the parameter identifiability. Two different approaches to the parameter identifiability problem are presented in detail because they are applied further in this research: the GLUE approach and the Pareto-Optimality approach. Differences in philosophies and methods between both are only briefly discussed because their applications in Chapter 6 provide more details. Finally, The MIKE-SHE model set-up as used in Chapters 5 and 6 is described.

4.1. Introduction

The reliance on models as hydrological tools is increasing as hydrologists examine emerging problems and exploit new data sources [*Sooroshian and Gupta, 1995*]. Models enable us to study very complex problems and to synthesize different kinds of information. However, model results are only as reliable as the model assumptions, inputs, and parameter estimates. Therefore, two problems are faced: (i) the selection of a suitable model to represent the study site and (ii) the selection of values for the model parameters (= 'effective' model parameter values) so that the model closely simulates the behaviour of the study site. The process by which the parameters are selected is called model 'calibration'. A brief literature review on both problems is presented below, though the review focuses on the calibration problem. The SCE algorithm [*Duan et al., 1992*] is discussed in more detail because it is this inverse modelling technique that is used as automatic calibration strategy throughout this research. The SCE set-up and parameters used throughout this research are also discussed. At the end of the Chapter, the unsaturated zone, evapotranspiration and overland flow modules of the MIKE-SHE hydrological model [*Refsgaard and Storm, 1995*] are highlighted because these components are applied throughout this study.

4.2. Model selection and scaling issue

Lots of hydrological models exist, all having different conceptual backgrounds and types of application. Generally speaking, there are two main model categories; empirical models and physically based models. A third category, conceptual models describes those that are somewhere between the two, i.e. they contain some parts that are empirically derived and some that are based on mathematical representations of the physical processes. The two main types of models have distinct advantages and disadvantages inherent to the structure of those models. Empirical models, due to their simplistic nature, require only a few input parameters. However, the data sets for each of the parameters need to be recorded over long periods to reliably calibrate the model. Physically based models require maybe less input data for calibration, but generally have a much larger range of parameters. Distinction between lumped and spatially

distributed models is based on the way they treat hydrological catchments. Lumped models treat catchments and sub-catchments as uniform entities; this means that it is generally impossible to predict the effect of spatially non-uniform measures on the hydrology. Spatially distributed models divide the study area usually in smaller entities using uniform (rectangular grid cells) or non-uniform (grid cells with variable geometry) units [*Abbott and Refsgaard, 1996*]. The advantages of the spatially distributed models are in practice to a certain extent overshadowed by a number of important disadvantages, as there are: (i) the lack of required area characteristics and model input on the level of the gridcell in which the area is divided, (ii) the lacking of standardised measuring techniques to measure area characteristics on the level of the gridcell, and (iii) the available limited knowledge and experience concerning upscaling techniques which should in principle allow to extrapolate properties measured in points to gridcell representative information [*Wood et al., 1998*]. It is evident that the smaller the area of the gridcells in which the catchment is divided, the easier it is to take point measurements as representative for the gridcell. As the area of the grid increases, the uncertainty concerning the extrapolation increases exponentially. On the other hand, calculation time increases exponentially if the area of the grid decreases [*Refsgaard and Butts, 1999*].

There has been a strong increase in the use of distributed modelling over the last decade. This has partly been because the increase in computer power, programming tools and digital databases has made the development and use of such models so much easier. There are also very good scientific reasons underlying the increased use of these models. One is the need for distributed predictions of flow pathways as a basis for other types of modelling, such as the transport of sediments or contaminants. Another is the need for prediction of the impacts of land use and other changes, as argued above, only possible using physically based, distributed models [*Beven, 2002*]. On the other hand, their complexity, requirement of huge amount of resources, (e.g. measurements with high temporal and spatial resolution), computer capacity and the vast parameter set involved, has lead to a large amount of reviews and discussions of the advantages, limitations and potentials of physically based distributed models [e.g. *Beven, 1989; Grayson et al., 1992; Smith et al., 1994; Beven, 1996; Refsgaard, 1997; Franks et al., 1998; Beven, 2002; Christiaens and Feyen, 2002*]. The hydrological scientific community nowadays focuses on two big issues in the use of physically based models:

(i) they are only representative for the original scales and conditions at the time of the derivation of the equations and (ii) a relatively large parameter unidentifiability problem compared to conceptual or empirical models due to the excess of model parameters. The scaling issue is elaborated below. For a discussion on the parameter unidentifiability problem, the reader is referred to 4.4.2.

The 'scaling issue' has gained increasing attention in the hydrological scientific community during the last ten years [*Blösch and Sivapalan, 1995*; *Christensen, 1997; Boulet et al., 1999; Bierkens et al., 2000*]. A nice review is published by *Bierkens et al. (2000).* An attempt is made to classify the wealth of different upscaling and downscaling methods in a number of limited categories and for each category, examples are provided. Decision rules as to which method to use for a specific problem facilitate in the choice of the up- or downscaling method. The reason a problem of scale transfer exists is 'heterogeneity'. It is stated that if the parameters modelled and observed were homogenous, i.e. would not vary in space and time, they would be scale invariant. It is accepted that the physically based equations used in physically based models are representative for the original scales and conditions at the time of derivation of the equations [*Beven, 1989; Grayson et al., 1992; Refsgaard and Butts, 1999; Christiaens and Feyen, 2002*]. Hydraulic property upscaling is a process that incorporates a mesh of hydraulic properties defined at the measurement scale into a coarser mesh of "effective/average hydraulic property" that can be used in large scale (e.g. basin scale, watershed scale) modelling of hydrological processes [*Zhu and Mohanty, 2002*]. The need for hydraulic property upscaling results from the disparity between the scales at which measurements are made and the scales more appropriate to the numerical simulations of hydrological processes. Soil hydraulic properties have been studied extensively at the core scale (measurement scale) but applications to large heterogeneous fields are scarce. As discussed in Chapter 2, the main original objectives of the field experiment were on the 'upscaling' issue. After reorientation of the study, the 'scaling' issue remains important in this PhD study (cfr. chapter 3, 5,6 and 7) though is no longer the dominant research topic of the research.

The hydrological model used throughout this research is the spatially distributed physically based MIKE-SHE model [*Refsgaard and Storm, 1995*]. Therefore, it is described in more detail below.

4.2.1. MIKE-SHE model

The MIKE-SHE model incorporates the different components of the hydrological cycle on a catchment scale (Fig. 4.1). The modelling code can be classified as a deterministic model using a continuous time scale and with a finite difference numerical solution. The code is not only capable of simulating water transport but also accommodates solute transport and transformation. Different options are offered to allow for simple model approaches in case the data is insufficient to apply the physically based equations or the highest level of detail is not desirable. This model was selected because it was readily available at the laboratory and it incorporates the processes encountered in this study, i.e. 1D unsaturated zone flow (Chapters 5, 6 and 7), evapotranspiration (Chapters 5, 6 and 7), and overland flow (Chapter 7). The way MIKE-SHE incorporates these three processes is described below.

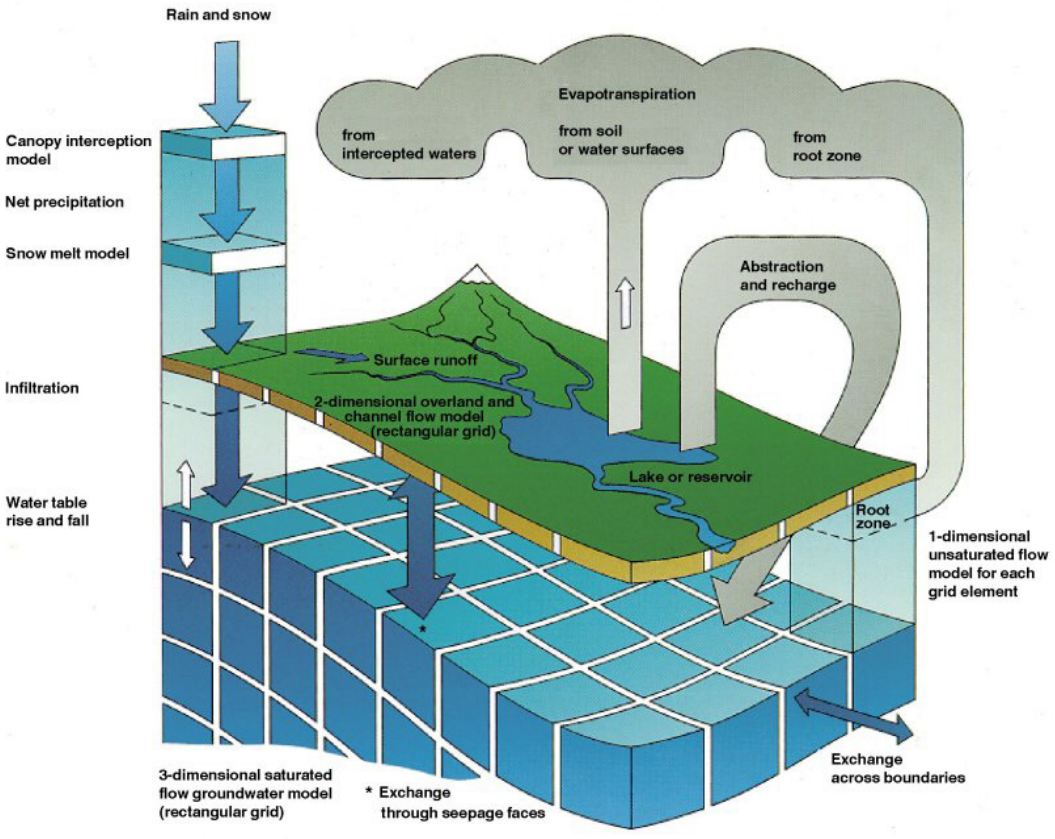

Figure 4.1 Schematic representation of the MIKE-SHE model (after DHI Water and Environment)

4.2.1.1. Unsaturated zone component

This component plays a key role in the water movement of MIKE-SHE because all other components depend on the boundary data from the UZ component. Water flow is considered to be one-dimensional (vertical flow in a soil column bordered by the grid), a simplification that is based on the assumption that horizontal subsurface flow is negligible to vertical flow in the unsaturated zone. The Richards' equation for one-dimensional vertical flow is implemented [*Richards, 1931*]:

$$C\frac{\partial h}{\partial t} = \frac{\partial}{\partial z}\left(K\frac{\partial h}{\partial z}\right) + \frac{\partial K}{\partial z} + Q_{uz} \tag{4.1}$$

$$\text{with } C = \frac{\partial \theta}{\partial h} \tag{4.2}$$

where h is the soil water pressure head [L], t is time [T], z is the soil depth [L], K is the hydraulic conductivity [LT^{-1}], Q_{uz} is the source/sink term (i.e. root extraction) [$L^{-3}T^{-1}$], and C is the soil water capacity [L^{-1}] approximated by the slope ($d\theta/dh$) of the soil water retention curve (Eq. 4.2) and θ the volumetric water content [L^3L^{-3}]. The only type of source/sink used in MIKE-SHE is a term describing water extraction by roots and soil evaporation. More details can be found in *Refsgaard and Storm (1995)*. Two hydraulic functions are required as input in order to simulate water flow in the soil profile. These functions are the moisture retention curve $\theta(h)$, and the hydraulic conductivity curve $K(\theta)$. In this study the *van Genuchten (1980)* $\theta(h)$ model for the soil water retention and the *Averjanov (1950)* $K(\theta)$ model for the hydraulic conductivity is used. Both models and their parameters are discussed in 2.2.2. Knowledge about the soil physical properties in terms of the moisture retention and hydraulic conductivity curve is subject to research in this study.

4.2.1.2. Evapotranspiration

A part of the precipitation will be subject to interception by vegetation and subsequent loss to the atmosphere by evaporation. The remainder of the precipitation will reach the

soil surface, resulting in surface runoff (to another grid cell) or infiltrate to the unsaturated zone. Some of the infiltrating water is evaporated from the upper part of the root zone or transpired by the plants. The evapotranspiration component is based on the empirical *Kristensen and Jensen (1975)* model and interacts with the overland and channel flow component and the unsaturated zone component. In this way, it provides net rainfall and evapotranspiration loss rates based on soil water conditions in the root zone. As in this research only bare soils are encountered, plant transpiration must not be modelled. Therefore only the soil evaporation part of the *Kristensen and Jensen (1975)* model is discussed below, more details can be found in *Refsgaard and Storm (1995)*.

Soil evaporation (E_s) occurs from the upper part of the unsaturated zone and consists of a basic amount of evaporation, $E_p \cdot f_1(\theta)$, plus additional evaporation from excess soil water as the soil saturation reaches field capacity. This can be described by the following function:

$$E_s = E_p\, f_2(\theta) + \left(E_p - E_{at} - E_p\, f_2(\theta)\right) f_3(\theta)\left(1 - f_1(LAI)\right) \tag{4.3}$$

where E_p is the potential evapotranspiration, E_{at} is the actual transpiration (= 0 in this research) and the function $f_1(LAI)$ expresses the dependency of the transpiration on leaf area index of the plant by:

$$f_1(LAI) = C_2 + C_1 LAI \tag{4.4}$$

where C_1 and C_2 are empirical parameters [-]. C_1 is a plant dependent parameter. For agricultural crops and grass, C_1 has been estimated to be about 0.3. C_1 influences the ration between soil evaporation to transpiration. For smaller C_1 values, the soil evaporation becomes larger relative to the transpiration. For higher C_1 values, the ratio approaches the basic ration determined by C_1 and the input value of *LAI*. For agricultural crops and grass, grown on clayey loamy soils, C_2 has been estimated to about 0.2. Similar to C_1, C_2 influences the distribution between soil evaporation and transpiration. In this research the C_1 and C_2 have been set to the recommended values. Actually, the value of C_1 is not important at all in this study as $LAI = 0$.

The functions $f_2(\theta)$ and $f_3(\theta)$ are given by:

$$f_2(\theta) = \begin{cases} C_2 \dfrac{\theta}{\theta_W} & for \quad \theta_M \le \theta \le \theta_W \\ C_2 & for \quad \theta \ge \theta_W \\ 0 & for \quad \theta \le \theta_r \end{cases} \tag{4.5}$$

$$f_3(\theta) = \begin{cases} \dfrac{\theta - \dfrac{(\theta_W + \theta_F)}{2}}{\theta_F - \dfrac{(\theta_W + \theta_F)}{2}} & for\ \theta \ge \dfrac{(\theta_W + \theta_F)}{2} \\ 0 & for\ \theta < \dfrac{(\theta_W + \theta_F)}{2} \end{cases} \tag{4.6}$$

where θ_F is the volumetric moisture content at field capacity [L^3L^{-3}], θ_W is the volumetric moisture content at wilting point [L^3L^{-3}], θ_r is the residual volumetric moisture content [L^3L^{-3}] and θ is the volumetric moisture content [L^3L^{-3}]. In the absence of vegetation as is the case in this research, $f_1(LAI)$ and E_{at} can be set to zero in Eq. 4.3.

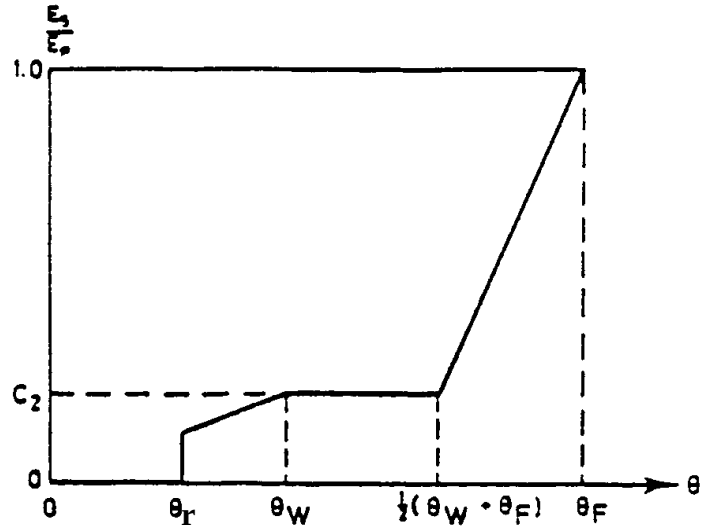

Figure 4.2 Soil evaporation E_s in relation to E_p as a function of soil moisture content, θ, in upper layers in the case of $LAI = 0$.

This allows us to see how E_s varies in relation to E_p for different values of θ. In this case, Eq. 4.3 can be simplified to:

$$\frac{E_s}{E_p} = f_2(\theta) + f_3(\theta) - f_2(\theta) f_3(\theta) \tag{4.7}$$

and is plotted in Fig. 4.2. In the MIKE-SHE model, soil evaporation is restricted to the upper node in the unsaturated zone, which should generally be less than 10 centimetres deep.

4.2.1.3. Overland and channel flow component

In case runoff is generated due to high intensity rainfall or when the groundwater table rises above the ground surface, water will start flowing over the land across grid boundaries. The topography governs flow routing. Flow quantity is determined by flow resistance, corrected for losses due to evaporation and infiltration along the flow path. The overland flow process is described by a diffusion wave approximation of the Saint-Venant equation (conservation of mass, Eq. 4.8, and conservation of momentum Eq. 4.9) in the two horizontal directions, whereby the Manning/Strickler equation (Eq. 4.10) is used to evaluate the friction slope:

$$\frac{\partial h}{\partial t} + \frac{\partial}{\partial x}(u h_g) + \frac{\partial}{\partial y}(v h_g) = 0 \tag{4.8}$$

$$S_{fx} + \frac{\partial}{\partial x}(z_g + h_g) = 0 \qquad \text{and } S_{fy} + \frac{\partial}{\partial y}(z_g + h_g) = 0 \tag{4.9}$$

$$S_{fx} = \frac{u^2}{K_x^2 h_g^{\frac{4}{3}}} \qquad \text{and } S_{fy} = \frac{v^2}{K_y^2 h_g^{\frac{4}{3}}} \tag{4.10}$$

where h_g is the flow depth above the ground surface [L], z_g the ground surface level [L], u and v the flow velocities in the two directions [LT^{-1}], S_{fx} and S_{fy} the friction slopes in

the two directions [-] and K_x and K_y- the Strickler coefficients [$L^{-3}T^{-1}$] in the two directions

4.3. Calibration framework

During calibration, parameters are adjusted for optimisation of certain calibration criteria (objective functions). The process is repeated until a specified criterion is satisfied. For a manual calibration, this criterion is usually linked with a rather subjective acceptable goodness of fit of the model to the observations. In automatic calibration, this criterion may be a maximum number of evaluations, convergence of the objective function or convergence of the parameter set. Formulation of a proper framework for (automatic) calibration involves following key elements [*Madsen, 2003*]:

- Model parameterisation and choice of calibration parameters,
- Specification of calibration criteria, and
- Choice of optimisation algorithm.

4.3.1. Model parameterisation, sensitivity analyis and choice of calibration parameters

The challenge is to formulate a relatively simple model parameterisation in order to provide a well-posed calibration problem but at the same time keep it sufficiently distributed in order to capture the spatial variability of key model parameters. In the initial model parameterisation process, sensitivity analysis can be conducted to investigate the sensitivity of model responses to its parameters, and hence to identify those which should be further refined via calibration.

A definition of sensitivity analysis (SA) is given by *Saltelli et al., (2000)*: “SA is the study of how the variation in the output of a model (numerical or other) can be apportioned, qualitatively or quantitatively, to different sources of variation, and of how the given model depends upon the information fed into it.” SA is used to increase the

confidence in the model and its predictions, by providing an understanding on how the model response variables respond to changes in the inputs i.e. calibration data, model structures or parameters. In this study, SA is applied prior to the calibration exercise to investigate the importance of each parameter, i.e. to identify a candidate set of important parameters for calibration. This is important since the difficulty of calibrating models against field or laboratory data increases with the number of processes to be modelled and hence the number of parameters to be estimated. It allows for a dimensionality reduction of the parameter space in which the calibration/optimisation is performed. Different SA techniques suited for this objective exist, each having their strengths and weaknesses. Local SA concentrates on the local impact of the parameters of the model and is usually carried out by computing partial derivatives of the output functions with respect to a given parameter set. Global SA apportions the output uncertainty to the uncertainty in the parameters, described typically by probability functions that cover the parameters' ranges of existence. In Chapter 5, two different global SA are used with as objective the characterisation of the parameters that the MIKE-SHE model as set up in this study is sensitive to. In other words, of the most and least important parameters are characterised with respect to changes in the output of the MIKE-SHE model set-up as a result of changes in their parameter value (input).

4.3.2. Specification of calibration criteria

The way calibration criteria are specified is different between a manual and an automatic calibration. Therefore, they are discussed individually.

4.3.2.1. Manual calibration

To manually calibrate a model, some aspect of the hydrological behaviour to which the model must be matched is to be selected. In this study daily soil moisture content values are selected. In manual calibration, a trial and error procedure of parameter adjustments is used. After each parameter adjustment is made, the simulated and observed output variables (e.g. hydrographs, piezometric data, soil moisture content, …) are visually compared to see if the match has improved. With training and a good deal of

experience, it is possible to obtain very good model calibrations using the manual approach [*Madsen, 2003*]. Though even for the experienced user, manual calibration can be a rather frustrating and time-consuming exercise. This is mainly because the logic by which parameters should be adjusted to improve the match is difficult to determine due to compensating effects that the model parameters generally have in the model output. The main weakness of manual calibration is that the absence of generally accepted objective measures of comparison makes it difficult to know when the process should be terminated, i.e. whether the best possible fit has been obtained. Different persons may also obtain very different parameter values because manual calibration involves a great deal of subjective judgment [*Sorooshian and Gupta, 1995*].

4.3.2.2. Automatic calibration: inversed modelling

The inverse problem is concerned with the estimation of variable model 'parameters' which do not have a physical significance or have a physical significance but are difficult to measure. The development of computer based methods for automatic calibration of hydrological models has been motivated by *Sorooshian and Gupta (1995)*:

- the need to speed up calibration. This is not always the case as most automatic calibration techniques are time-consuming because lots of model evaluations are generally needed. Though because it is automated, one is not obliged to a trial and error procedure, i.e. time becomes available while the computer does the job,
- the fact that there are few model calibration experts available, and
- the need to assign some measure of objectivity to the parameter estimates and model predictions.

Early attempts to develop automatic calibration methods were reported by *Dawdy and O'Donnell* (*1965), Nash and Sutcliffe (1970)* and *Ibbitt (1970)* amongst others. These researchers set the stage by bringing the vast body of research on statistical regression and model fitting techniques to bear on the calibration problem. Since these beginnings, a great deal of progress has been made. In 1995, *Sorooshian and Gupta (1995)* stated

that automatic calibration methods had not yet matured to the point that they can entirely replace manual methods. Though, recent papers that compare manual and automatic procedures show that automatic calibration performs at a level of skill comparable to manual procedures [*Gupta et al., 1999; Madsen et al., 2002; Madsen, 2003*]. Though, care should always be taken when interpreting the estimated effective parameters. *Boyle et al. (2000)* state that parameter estimates resulting from automatic calibrations can be unacceptable and present a hybrid approach that combines the strengths of both manual and automatic calibration. Inverse problems are likely to occur whenever mathematical models are used to explain or enhance observations [*McLaughin and Townley, 1996*]. Examples can be found in fields as diverse as astronomy, medicine, meteorology, quantum mechanics and hydrology.

The automatic calibration scheme involves optimisation of numerical measures (objective functions) that compare observations of the state of the system with corresponding simulated values. In a multi-objective context, model calibration can, in general, be performed on the basis of [*Madsen, 2003*]:

- Multi variable measurements, i.e. groundwater level, river runoff and water content in the unsaturated zone.
- Multi site measurements, i.e. several measurements of the same variable distributed within the catchment.
- Multi response modes, i.e. objective functions that measure various responses of the hydrological processes such as e.g. the general water balance, peak flows and low flows.

When using multiple objectives, the calibration problem can be stated as follows:

$$\min\left\{F_1(p), F_2(p), \ldots F_{n_p}(p)\right\},\ p \in P \tag{4.11}$$

where $F_i(p)$, $i = 1, 2 \ldots n_p$ are the objective functions. The optimisation problem is constrained in the sense that p is restricted to the feasible parameter space P. These limits are chosen according to physical and mathematical constraints, information about physical characteristics of the system, and from modelling experiences. Most important

decisions to be made in an automatic calibration routine are the choice of the objective function(s) and the optimisation algorithm (cfr. 4.4).

Objective function(s)

Generally, the objective function is a measure for the difference between the model-simulated and the observed hydrological state variable (e.g. soil moisture content, hydrograph, piezometric data, ..). Hence the purpose of an automatic calibration is therefore to find those values of the model parameters that optimise (minimise or maximise) the numerical value of the objective function. In general the choice of the objective function measure can be divided in two categories: least squares measures or maximum likelihood measures. Least squares measures only account for the difference between observed and measured data and in general squares and sums this difference in the calculation of the measure. Least squares measures cannot account for autocorrelation (non-independence) or changing variance in data errors as they implicitly assume that the joint probability of the errors over the available data record is Gaussian with mean zero and that the errors are independent of each other. If these assumptions do not hold, a maximum likelihood measure is necessary (only independent events required). For more details about both categories and different possible measures within each category, the reader is referred to *Sorooshian and Gupta (1995)*.

In Chapter 5, the Root Mean Squared Error, RMSE, is selected as goodness-of-fit measure. Since only soil moisture measurements are available, we are dealing with a single-objective optimisation. In Chapter 6, a penalty term is included in the objective function next to the goodness-of-fit measure. This term penalises deviations between model parameters and prior measured parameters. This is not the traditional way of incorporating prior information in an optimisation problem. The most common way is by setting the lower and upper bounds of the feasible parameter space to the minimum and the maximum of measured or estimated parameters. The feasible parameter space can also be defined as a hyperellipsoid by using the prior knowledge about the distribution of the different parameters and their correlation. New in this research is the incorporation of prior information directly in the objective function. In this way, some kind of multi-objective calibration problem is faced. Traditionally, the objectives are

either different variables, variables measured at different sites or different responses. In this study, the second objective is related to the prior parameter information.

4.3.3. Choice of optimisation algorithm

The surface described by the objective function in the parameter space is called the 'response' surface. An optimisation algorithm is a logical procedure that is used to search the response surface, constrained to the allowable parameter ranges, to find the 'optimum' (minimum or maximum) of the objective function value. In the following, a brief overview of the different optimisation strategies is elaborated and it is assumed that the objective function must be minimized. They have in common that they begin with an initial guess of the solution and then iteratively try to improve that guess according to their corresponding strategy scheme. In the following, they are categorised into 'local' and 'global' search methods.

4.3.3.1. Local Search Methods

Local search methods are designed to efficiently find the minimum of 'unimodal' functions. These are functions for which any strategy that seeks to continuously proceed downhill (improving function value) must eventually arrive at the location of the function, irrespective of where in the parameter space the search procedure is started. Therefore, a local search procedure involves thee main decisions: (i) which direction to move, (ii) how far to move in that direction, and (iii) how to decide that no further improvement is possible. The different local strategies differ in the methods by which these decisions are made and can be further classified as 'direct search' methods and 'gradient' based methods.

Direct search methods

A direct search optimisation strategy uses only function value information in the decision process. Typically these methods start at an initial point and select some direction and step size and evaluate the function at the new point. Based on the differences in function values, a prediction is made of which is the best direction to

move to improve the function and how large a step should be taken in that direction. If the new point has a lower function value that the previous point, it replaces the old one and the procedure is repeated. If the new point turns out to be worse than the previous point, the step size is reduced and another try is made at a new location. The search stops when the strategy is unable to find a direction in which improvement is possible. According to *Sorooshian and Gupta (1995)* most popular methods used in the calibration of hydrological models have been the "Rosenbrock method" [*Rosenbrock, 1960*], the Pattern Search method [*Hooke and Jeeves, 1961*], and the "Simplex method" [*Nelder and Mead, 1965*]. This latter is used in the global Shuffled Complex Evolution optimisation method used in this study, which is briefly explained in section 4.3.3.3.

Gradient based methods

The only difference with the direct search methods is that a gradient based search optimisation strategy uses information about both the function value and function gradient in the decision process. At the end point of the optimisation, the gradient value will be numerically very close to zero. Gradient-based techniques have been widely applied in groundwater modelling. These methods have the advantage that they are able to estimate the uncertainty of the parameters making some statistical assumptions. This is done through a quadratic approximation of the response surface in the region of the best parameter values. It is questionable whether the statistical assumptions are ever fulfilled, probably assumptions hold in the case of steady state groundwater modelling. Few gradient-based search strategies have been tested for their effectiveness and efficiency in calibrating hydrological models. The ones tested were found not to be effective for highly non-linear models such as conceptual Rainfall-Runoff models and the unsaturated zone model used throughout this research.

4.3.3.2. Limitations of local search methods

The reason that local search methods have not generally given satisfactory results is that in most practical problems involving calibration of non-linear hydrological models have response surfaces that are multi-modal, i.e. there are several locations of the parameter space where the value of the function is a 'local' minimum. In such cases, the points where a local search algorithm terminates will depend on the location where it is started.

Therefore, it is impossible to know with certainty if the procedure has located the actual global optimum of the function. Typically, several different starting points were tried, and each search attempt terminated in a different location. There local search optimisation strategies are inappropriate for calibration of hydrological models (except for groundwater modelling), instead strategies designed for "global" search of the parameter space must be employed.

4.3.3.3. Global Search Methods

These are designed to efficiently discover the minimum of multi-modal functions. Such strategies fall in three categories: deterministic, stochastic or a combination of both. Deterministic strategies require that certain criteria related to the continuity of the function and its derivatives be satisfied to guarantee convergence to the global solution. These conditions are usually not met in the case of calibration of non-linear hydrological models [*Sorooshian dan Gupta, 1995*].

Random search methods

Random (stochastic) search methods use random number generators to randomly sample the parameter space in search of points with improved function values. The samples are generated according to some probability distribution applied to the feasible parameter space. In 'pure' random search, the sampling is done using a uniform distribution. This assumes no prior knowledge of where in the feasible space the best parameter set exists. However, because pure random search does not make use of the function value obtained during optimisation to guide the search, it is not very efficient. Therefore, other random search methods have been developed. These methods adaptively adjust the probability distribution used for the sampling based on the function value information obtained during the search. One such strategy is the Adaptive Random Search (ARS) proposed by *Masri et al. (1978)* and modified by *Pronzato et al. (1984)*. More details can be found in *Sorooshian and Gupta (1995).*

Multi-start algorithms

In these methods, several trials of local search (deterministic) optimisation methods from randomly selected starting points in the feasible parameter space are performed

[*Johnston and Pilgrim, 1976*]. In *Duan et al. (1992)* it was demonstrated that a multi-start procedure based on the non-linear simplex method (Multi Start Simplex, MSX) worked well on a simple hydrological watershed model.

Shuffled Complex algorithms: Shuffled Complex Evolution algorithm

The Multi Start Simplex (MSX) strategy has certain desirable properties that enable it to overcome some of the difficulties encountered in the calibration of hydrological models. However, a source of inefficiency in the method is that each simplex search operates completely independently, with no sharing of information. The Shuffled Complex Evolution algorithm (SCE) [*Duan et al., 1992*] is based on the notion of sharing information and on the concepts (genetic algorithm) drawn from natural biological evolution [*Wang, 1991*]. The genetic algorithm is a search procedure based on the mechanics of natural selection and natural genetics, which combines an artificial survival of the fittest with genetic operators abstracted from nature [*Holland, 1975; Wang, 1991*]. The SCE strategy combines the strengths of the simplex procedure [*Nelder and Mead, 1965*] with the concepts of controlled random search [*Price, 1987*], competitive evolution [*Holland, 1975*] and the developed concept of complex shuffling by *Duan et al. (1992).*

In this study, the Shuffled Complex Evolution (SCE) algorithm is adopted for the optimisation of the UZ soil parameters in the MIKE-SHE model [*Madsen, 2002*]. In the following, a description of the steps used in the SCE algorithm is given. For a detailed description of the SCE algorithm, the reader is referred to *Duan et al. (1992)*.

The SCE algorithm comprises 4 steps [*Madsen, 2002*]:

(1) Initialisation: an initial sample of parameters sets is randomly generated from the feasible parameters space. For each parameter set, the objective function (F) is calculated. The initial sample has the size $s = p \times m$ where p is the number of complexes (= group of a number of parameter sets) and m is the number of points in each complex.

(2) Partitioning into complexes: the s points are ranked in order of increasing objective function value ($F_1 \leq F_2 \leq \ldots \leq F_s$). The s points are then partitioned into p complexes, such that points corresponding to function values $\{F_1, F_{p+1}, \ldots, F_{(s-1)p+1}\}$ form the first

complex, points corresponding to function value $\{F_2, F_{p+2}, \ldots, F_{(s-1)p+2}\}$ form the second complex, etc.

An example taken from *Duan et al. (1994)* is presented in Fig. 4.3 and Fig. 4.4. Figure 4.3a shows how a sample population containing s = 10 points is divided in p = 2 complexes. Each complex contains m = 5 points which are marked by (•) and (*), respectively. The contour lines in Fig. 4.3 and Fig. 4.4 represent a function surface that has a global optimum located at (4,2) and a local optimum located at (1,2).

(3) Evolution: A sub-complex of size q is formed from the complex by randomly choosing q points from the m points in the complex. A triangular probability distribution is used for assigning the probability of a point to be included in the sub-complex (i.e., larger probability for points with smaller objective function value). The sub-complex is evolved (offspring generation) according to the simplex algorithm [*Nelder and Mead, 1965*] and β evolution steps are taken by each complex.

In Fig. 4.4, the black dots (•) indicate the locations of the points in a complex before the evolution step is taken. A sub-complex containing q = 3 points (i.e., forms a triangle in this case) is selected according to the prespecified triangular probability distribution to initiate the evolution step. The symbol (*) represents the new points generated by the evolution steps. There are three types of evolution steps: reflection, contraction and mutation. Figures 4.4a, 4.4b and 4.4d illustrate the "reflection" step, which is implemented by reflecting the worst point in a sub-complex through the centroid of the other points. Since the reflected point has a lower criterion value than the worst point, the worst point is discarded and replaced by the new point. Thus an evolution step is completed. In Fig. 4.4c, the new point is generated by a "contraction" step (the new point lies half-way between the worst point and the centroid of the other points), after rejecting a reflection step for not improving the criterion value.

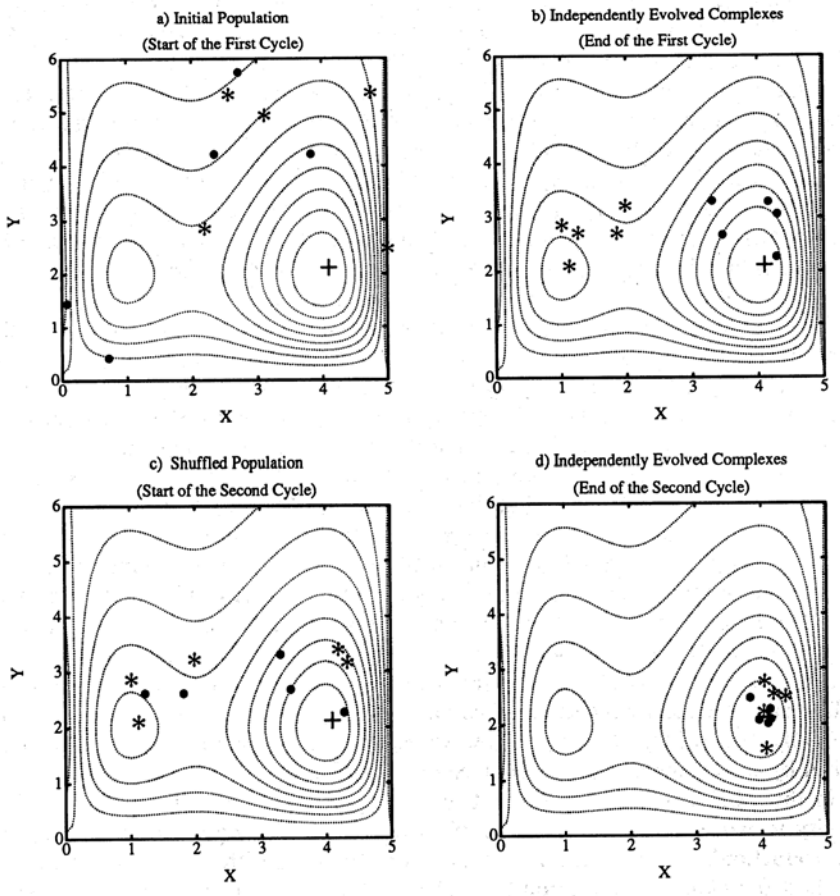

Figure 4.3 Illustration of the Shuffled Complex Evolution (SCE) Method with s = 10 points and p = 2 complexes after Duan et al.(1994)

In Fig. 4.4e, a "mutation" step is taken by randomly selecting a point in the feasible parameter space to replace the worst point of the sub-complex. This is done after a reflection step is attempted, but results in a point outside of the feasible parameter space. Another scenario in which a mutation step is taken is when both the reflection step and the contraction step do not improve the criterion value. Figure 4.4f shows the final complex after $\beta = 5$ evolution steps.

Figure 4.3b shows the locations of the points in the two independently evolved complexes at the end of the first cycle of evolution. It can be seen that one complex (*) is converging toward the local optimum, while the other (•) is converging toward the global optimum.

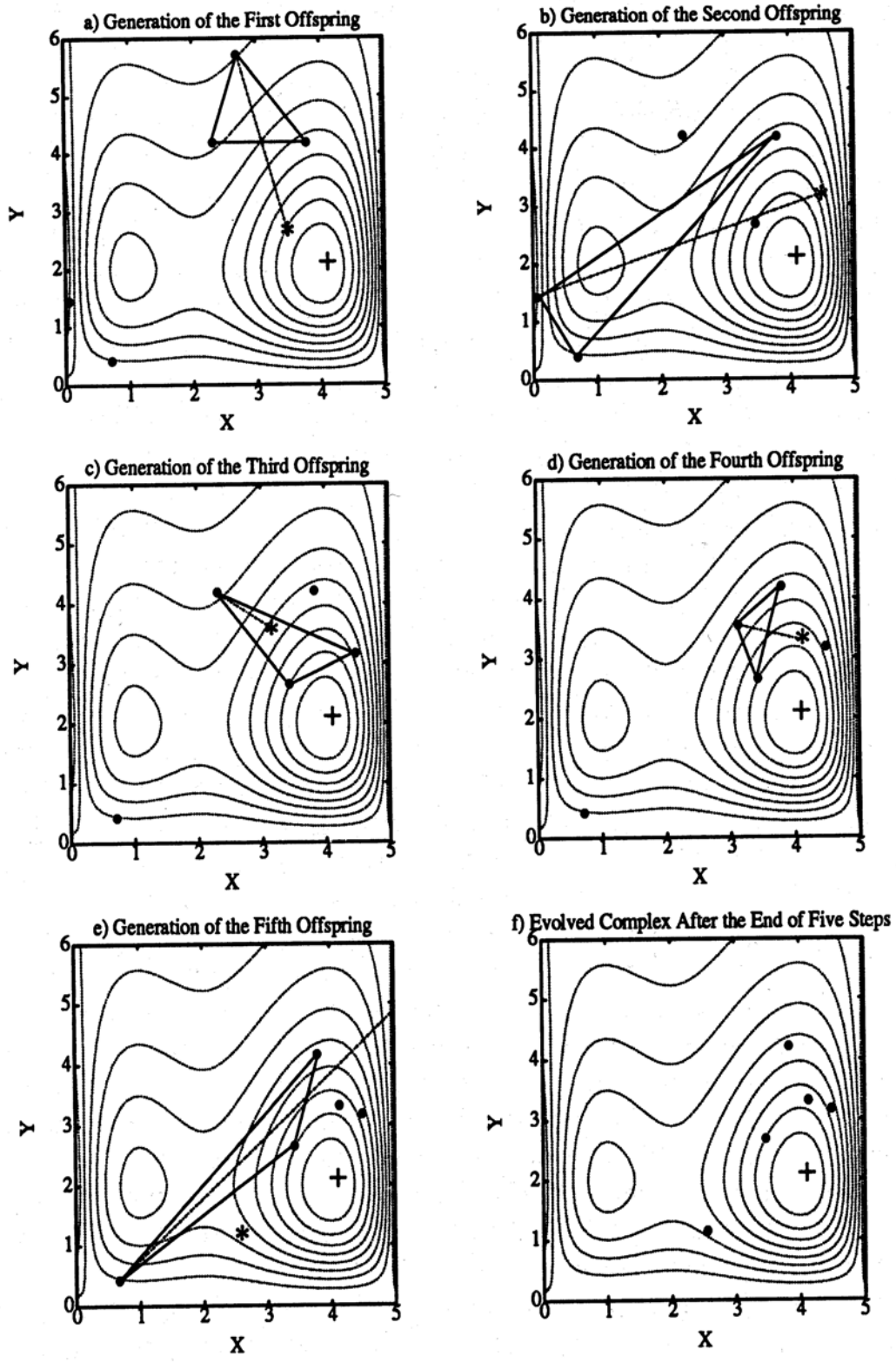

Figure 4.4 Illustration of the Evolution steps taken by each Complex after Duan et al. (1994)

(4) Complex shuffling: the new sample of *s* points is shuffled and new complexes are formed as specified in step (2).

Figure 4.3c displays the new membership of the two evolved complexes after shuffling and Fig. 4.3d exhibits the two complexes at the end of the second cycle of evolution. It is clear that both complexes are converging to the global optimum at the end of the second cycle.

Steps (2) – (4) are repeated until a stopping criterion is met. In general, three stopping criteria can be defined [*Madsen and Kristensen, 2003*]:

- Maximum number of model evaluations,
- Convergence in the objective function space. In this case the optimisation terminates if the objective function of the best parameter set has not changed more than a defined minimum value in a given number of shuffling loops, and
- Convergence in parameter space. In this case the optimisation terminates if the range of parameter values of the entire population in the parameter space is less than a given value.

The algorithmic parameters of the SCE algorithm to be specified by the user are presented in Table 4.1. The most important algorithmic parameter is the number of complexes *p*. Sensitivity tests have shown that the number of parameters compromised in the optimisation procedure, is the primary factor determining the proper choice of *p*. In general, the larger the value of *p*, the higher the probability of converging into the global optimum but at the expense of a larger number of model simulations. *Kuczera (1997)* suggested setting *p* equal to the number of parameters included in the optimisation to avoid premature convergence of the SCE algorithm. This may, however, require a large number of model evaluations, and hence imply an unacceptable computational burden. In practical applications, one should choose *p* to balance the trade-off between the robustness of the algorithm and the computing time [*Madsen and Kristensen, 2003*].

Table 4.1 Algorithmic parameters for the SCE algorithm (n = no. of calibration parameters) and recommended values given by Duan et al. (1994) and Kuczera (1997).

Parameter	Description	Range	Recommended value
p	No. of complexes	$p \geq 1$	n
m	No. of points in each complex	$m \geq 2$	$2n+1$
q	No. of points in a sub-complex	$2 \leq q \leq m$	$n+1$
α	No. of offsprings generated by each sub-Complex	$\alpha \geq 1$	1
β	No. of evolution steps taken by each complex before shuffling	$\beta \geq 1$	$2n+1$
p_{min}	Minimum No. of complexes required as the search proceeds	$1 \leq p_{min} \leq p$	p

In this study, the SCE algorithm is adopted for calibration of the MIKE-SHE integrated modelling system. p was set to 5 on the basis of preliminary optimisation runs having different number of complexes (2, 5, 8 and 13). This revealed that more than 5 complexes did not result in different optimum solutions and more simulations were needed to reach the optimum. In the case of only 2 complexes, a local optimum was found which was only slightly worse than the global optimum. Other SCE control parameters were set to the ones recommended by *Duan et al. (1992) and Kuczera (1997)* as presented in Table 4.1. The stopping criteria for the optimisation routine were either (i) change of the best objective function less than 0.1% within 5 loops, or (ii) a maximum number of model evaluations of 2000.

4.4. Problems of inverse modelling

This paragraph discusses the main problems encountered with inverse modelling. They can be divided in three classes: (i) the observed calibration data, (ii) optimisation algorithms and (iii) the equifinality problem.

4.4.1. Observed Calibration data

It is generally accepted that proper choice of the calibration data can do much to reduce the difficulties encountered during calibration of a hydrological model. The critical issues here are (i) how much data are necessary and sufficient for calibration and (ii) what kind of data will give the best results, i.e. the most precisely specified parameter estimates [*Sooroshian and Gupta, 1995*].

4.4.1.1. Quantity of data

It has been common practice to use as much data as available for the calibration, after setting aside part of the data set for verification. Verification of the model is to test the performance of the calibrated model on a selected portion of the data that were not used for the calibration. This is often referred to as a 'split sample' test, i.e. part of the data record is used for calibration and the remaining part for verification. It is common for the calibrated model to fit the calibration data very well, but then be found not performing well on the validation data period. When such behaviour is observed, it may be necessary to critically examine the entire calibration procedure to determine if certain assumptions are appropriate or valid and if necessary to revise the procedure.

4.4.1.2. Quality of data

The quality of the data is dependent on the information contained in the data and the noise (errors) in the data. It is hoped that the information content is as large and the noise as small as possible. An informative data set is one that contains or represents enough variability in watershed behaviour that the different modes of operation of the hydrological processes are properly represented. For example, if the data selected are from a relatively dry year, certain runoff processes may not be activated. Therefore the model response will be insensitive to some of the model parameters that determine the partitioning of water between the various subsurface and overland flow components. In this research, observed daily moisture content for the year 2001 is incorporated in the inverse modelling. Hence, a winter and summer period are included suggesting that the

dataset has enough 'hydrological variability'. Research into data requirements has led to the understanding that the informativeness of the data is equally important than the amount used for model calibration [e.g. *Kuczera, 1982; Sooroshian et al., 1983; Gupta and Sorooshian, 1985; Yapo et al., 1996 and Gupta et al., 1998*]. Though, when the model is used for predicting extremes, the amount of data used for calibration becomes important, as the occurrence of these events in the data has to be sufficient.

The presence of measurement and logging errors causes the data quality to deteriorate, thereby resulting in less confidence in the parameters estimated. In this research data errors in the observed soil moisture content may originate from freezing, datalogger and computer failures and transfer of data problems. It is believed that the data errors on the soil moisture content do not contain biases and are in the order of ± 0.01 cm^3/cm^3. Biases are generally accepted in the case of precipitation data measurements that tend to underestimate the actual amount of rainfall. Before incorporating the observations in the optimisation algorithm, the observed data, were analysed for obvious measurement errors (numerical impossible values of soil moisture contents) and outliers were deleted. Chapter 7 briefly describes the quality of calibration data and its influence on the calibration process. In particular, the influence of the temporal resolution of rainfall data on (i) model fit and (ii) effective parameter estimations are investigated.

4.4.2. Parameter identifiability

In *Duan et al. (1992),* a detailed study was conducted on a simple six-parameter conceptual model (SIXPAR) using synthetic data to identify clearly the nature of the difficulties encountered in conceptual model calibration. The study found that, despite the simple model structure and the absence of model structural error or input data error, the parameter estimation problems are not trivial. *Duan et al. (1992)* summarized these problems as a list of five features (see Table 4.2). The primary conclusion of *Duan et al. (1992)* was that the optimisation techniques commonly used before are not powerful enough to deal with the response surface conditions encountered in model calibration. They were designed to solve single-optimum problems and were not able to deal effectively with all of the problems listed in Table 4.2. The SCE method presented was found to be both effective and efficient compared with other existing global methods,

including the ARS method and the multi-start Simplex method [*Duan et al., 1992; Sorooshian et al., 1993*]. A comparison of SCE and simulated annealing also shows the superiority of the SCE algorithm [*Thyer et al., 1999*]. Numerous case studies have demonstrated that the SCE algorithm is consistent, effective and efficient in location the optimal model parameters of a hydrological model [*Duan et al., 1992, 1993; Sorooshian et al., 1993; Luce and Cundy, 1994; Gan and Biftu, 1996; Kuczera, 1997; Boyle et al., 2000*]

Table 4.2 Summary of the five major characteristics complicating the optimisation problem in conceptual Rainfall Runoff model calibration [*Duan et al., 1992*]

1.	Regions of attraction	More than one main convergence region
2.	Minor local optima	Many small 'pits' in each region
3.	Roughness	Rough response surface with discontinuous derivatives
4.	Sensitivity	Poor and varying sensitivity of response surface in region of optimum and non-linear parameter interaction
5.	Shape	Non-convex response surface with long curved ridges

While considerable attention has been given to the development of automatic calibration methods, much less attention has been given to a realistic assessment of parameter uncertainty in hydrological models. Estimates of hydrological model parameters are generally speaking subject to errors because the observed data contain measurement errors and because the model never perfectly represents the system or exactly fits the data. Although the SCE optimisation algorithm can reliably find the global minimum in parameter space, it remains difficult, if not impossible to find a unique best parameter set whose performance measure differs significantly from other feasible parameter sets. Such poor identifiability may result in considerable uncertainty in the model output and, makes it virtually impossible to relate these parameter values to easily measurable soil or land-surface characteristics [*Vrught et al., 2002; Mertens et al., 2003*]. Two approaches are currently dealing with this problem of unidentifiability of parameters. One approach is the concept of the 'equifinality' of parameter sets within the Generalized Likelihood Uncertainty Estimation (GLUE) first described by *Beven and Binley (1992).* This is different from the concept of Pareto-optimality, which refers to the multi objective equivalence of parameters sets [*Gupta et al., 1998; Yapo et al.,*

1998; Madsen et al, 2003]. Concepts of both approaches are briefly described below and both strategies are applied in Chapter 6.

4.4.2.1. Equifinality: GLUE approach

Beven and Binley (1992) reject the idea of an optimum parameter set in favour of the idea of 'equifinality' of parameter sets (models). This equifinality arises due to effects of error and uncertainty in the modelling process, resulting from error in the model representation of hydrological processes and catchment characteristics and error in the boundary conditions of the simulation, which can never be known perfectly [*Freer et al., 1996*]. It also appears that the good simulations may be distributed across a wide range of parameter values, leading to the conclusion that it is the combined set of parameters that is important.

The GLUE (Generalised Likelihood Uncertainty Estimation) methodology ranks the parameter sets according to some likelihood value. Some models can certainly be rejected as 'non-behavioural'. One model will give the best result to some period of calibration data, but there will be many other that will be almost equally good. Many of these will be in very different parts of the parameter space. It is also very likely [*Freer et al., 1996*] that if a second period of data is considered, that the rankings of these possible models will change and the best model found for the first period will not necessarily be the best of the second. Calibration is hence no longer a search for the best parameter set, but targets the demarcation of parameters resulting in an acceptable description of the system to be modelled. Consequently, the acceptable or behavioural models result in a range of possible behaviours of model predictions. In the GLUE approach these are weighted according to their calculated likelihood's from the calibration period and the weights used to formulate a cumulative distribution of predictions from which uncertainty quartiles can be calculated. GLUE requires considerable computing resources. Thousands of model realization are generally necessary to characterise the parameter space adequately, while the results of each retained simulation must be stored to calculate the uncertainty bounds. It has been applied to both fully distributed physically based models [*Beven and Binley, 1992; Christiaens and Feyen, 2002*] and other more conceptual models [*Freer et al., 1996;*

Lamb et al., 1998; Beven and Freer, 2001; Bashford et al., 2002]. In general, the GLUE procedure has three requirements: (i) specification of a sampling range for each parameter considered, (ii) specification of a sampling methodology and (iii) a definition of a likelihood measure and the criteria for acceptance and rejection of models. This last requirement is a subjective choice and GLUE results in terms of the amount and identity of 'behavioural' parameters sets as well as the width of uncertainty bounds are very sensitivity to this choice [*Freer et al., 1996*].

Another GLUE shortcoming is the fact that only parameter uncertainty is taken into account in the estimation of the uncertainty bounds. Uncertainty in the simulated time series is not only a result of parameter uncertainty but comprises also model structure uncertainty and input uncertainty (e.g. uncertainty in rainfall and evapotranspiration). It is shown that for conceptual rainfall runoff models, input uncertainty of rainfall can take up to 40 or 50 % of the total uncertainty on the model results [*Willems, 2000*]. *Willems (2000)* also found that for lumped conceptual rainfall-runoff models, the parameter uncertainty will be small in comparison with the model-structure uncertainty. It is expected that the reverse will be valid for a distributed physically-based rainfall-runoff model as used in this study: model-structure uncertainties will be much smaller than the parameter uncertainties. Parameter uncertainties will indeed largely increase as a result of the increasing number of parameters and the corresponding parameter identifiability problem. In Chapter 6, the GLUE procedure is applied with and without the incorporation of prior information in the sampling procedure. This made it possible to evaluate the relevance of prior measured information in the estimation of the amount and identity of the behavioural parameter sets as well as on the width of the uncertainty bounds.

4.4.2.2. Pareto-optimality: Multi-Objective calibration

Gupta et al. (*1998)* state that the GLUE approach has still weaknesses that need to be addressed (e.g. the selection of prior parameter distributions, the likelihood criterion and the cutoff thresholds). They state that such approaches represent a bold attempt to introduce some much-needed new thinking into a field that is in grave danger of becoming intellectually sterile. Only recently, an automated procedure for multi-

objective calibration has been introduced by *Gupta et al.* (*1998).* The ideas presented in *Gupta et al.* (*1998)* have similarities and notable differences from the GLUE approach. The major difference is the focus on the inherent multi-objective nature of the model calibration problem. Application of automatic procedures has mainly been based on a single overall objective measure of comparison (e.g. Root Mean Squared Error between observed and simulated values). The use of a single measure is often inadequate to properly measure all the important characteristics of the system that are reflected in the observations which are used by the hydrologist to evaluate the quality of the calibrated model for the specific model application being considered [*Madsen, 2000*]. In a multi objective context, parameter combinations exist that are "equally good" due to trade-offs between the different objectives. For instance, one may find a set of parameters that provide a very good simulation of high flows but a poor simulation of low flows and vice versa. Points having the smallest value of both objectives are unique called 'Pareto' optimal points and are said to be situated on the Pareto' front. Moving along the Pareto front results in smaller values of one objective (better fit) but at the expense of the value of the second objective. The trade-off between both objectives is very informative: a significant trade-off between the two objectives means that a very good calibration of one objective provides a bad fit to the other objective and vice versa.

It must be noted that this rationale for multi-objective equivalence of several parameter sets is different from the rationale of what *Beven and Binley (1992)* call 'equifinality' of parameter sets. The arguments used here are based on the multiple ways in which the best fit of a model to the data can be defined and not on the probabilistic representation of parameter uncertainty as in the GLUE methodology. Pareto-optimal parameter sets may overlap with the behavioural parameter sets defined in a GLUE procedure but will in general not be equivalent. It is important to emphasise the difference here. The GLUE concept assesses the parameter uncertainty from a statistical point of view, according to some likelihood measure which is in general based on a single aggregate objective measure. Multi-objective equivalence is related to the trade-off between the different objectives which are related to model structural problems, i.e. if the model was perfect one would find a unique optimum no matter which objective function was defined. As explained above, some kind of multi-objective calibration is performed in Chapter 6. One objective is the classical root RMSE while the second objective is the distance of the evaluated parameter set from the measured parameter distributions on the soil cores.

As shown in Chapter 6, a trade-off (Pareto front) between the goodness of fit to the observations and the coincidence with prior measured parameter distributions is encountered.

Chapter 5

Sensitivity of soil parameters in unsaturated zone modelling and the relation between effective, laboratory and in-situ estimates*

ABSTRACT

The soil moisture content at 27 locations and three different depths (at the surface, at 30 and 60 cm depth) were measured on a 80 by 20 m plot on a hillslope during the year 2001. Soil hydraulic functions were estimated in the laboratory on 100 cm^3 undisturbed soil cores. These soil cores were collected at 115 locations situated in two horizons in three profile pits along the hillslope. In-situ field saturated hydraulic conductivity was estimated at 120 locations making use of single-ring pressure infiltrometer measurements. Sensitivity of the 6 parameters per horizon plus the depth (d) from the surface to the B-horizon or a total number 13 soil physical parameters (Saturated hydraulic conductivity (K_s), saturated moisture content (θ_s), residual moisture content (θ_r), inverse of the air-entry value (α), van Genuchten shape parameter (n), Averjanov shape parameter (N) for both horizons and depth (d) from surface to B-horizon) in a two-layer single column 1-D MIKE-SHE model based on Richards' equation was investigated. A Monte Carlo based sensitivity analysis was compared with Morris' One-At-a-Time design sensitivity analysis. In both analyses, N of both horizons were found to be the least sensitive parameters, so 11 out of the 13 parameters were withheld and incorporated into an inverse optimisation using the Shuffled Complex Evolution algorithm. K_s of both horizons, θ_s of the A-horizon and d were found to be the most

---

* Adapted from Mertens, J., Madsen H., Kristensen M., Jacques, D., and J. Feyen, 2003. Sensitivity of soil parameters in unsaturated zone modelling and the relation between effective, laboratory and in-situ estimates. *Submitted to Hydr. Proc.*

sensitive parameters. At each location, 11 effective parameters were estimated. Distributions over all locations of these 11 effective parameters were compared with the estimated soil physical parameters from the undisturbed soil samples and the single-ring pressure infiltrometer estimates. All distributions were found to be significantly different at a 5 % level except for the inverse of the air-entry value of the A-horizon and the saturated hydraulic conductivity and saturated moisture content of the B-horizon. These differences are due to scale effects, problems with the measurement techniques, model errors and uncertainty in the observations.

5.1. Introduction

Soil moisture is of fundamental importance in hydrological processes. How much water infiltrates, is lost by evapotranspiration, and recharges the subsurface depends on the soil moisture content [*Rodriguez-Iturbe, 2000, Bashford et al., 2002*]. Given the importance of soil moisture to earth system processes, the quantification of its spatial and temporal behaviour is receiving increased attention from the hydrological scientific community (from the hill slope and small watershed scale to the global scale [*Grayson et al., 1997; Famiglietti et al., 1998*]). However, this task is not trivial since soil moisture exhibits a high degree of variability, in both time and space. This study investigates which parameters dominate the modelling of in-situ 1-D water flow and focuses on how to estimate them.

Simulation of soil moisture content profiles requires ‘effective’ soil hydraulic parameters which yield the best fit with observations. As explained in de detail in Chapter 4, this is usually done through manual or automatic calibration (inverse modelling) of soil hydraulic parameters which are impossible or too difficult to measure in-situ or in the laboratory. Before calibration, it is useful to conduct a sensitivity analysis (SA) to determine which parameters the model response is sensitive to, and to which parameters the model response is not sensitive. Different SA techniques exist, each having their strengths and weaknesses. Local SA concentrates on the local impact of the parameters of the model and is usually carried out by computing partial derivatives of the output functions with respect to a given parameter set. Global SA apportions the output uncertainty to the uncertainty in the parameters, described

typically by probability functions that cover the parameters' ranges of existence [*Saltelli et al., 2000*]. In this chapter, two different SA are carried out and compared. Both are global SA: the first one is based on a Monte-Carlo analysis (MC) [*Spear and Hornberger, 1980*], while the second one is a One-At-a-Time (OAT) design or screening method [*Morris, 1991*].

Based on the SA, the most important parameters can subsequently be incorporated in the inverse optimisation or calibration process. Traditionally, calibration of hydrological models has been performed manually using a trial-an-error parameter adjustment procedure. The process of manual calibration, however, may be very tedious and time consuming, depending on the number of model parameters and their interaction. Furthermore, due to the subjectivity involved, it is difficult to explicitly assess the confidence of the model simulations. As presented in Chapter 4, a great deal of research has been directed to the development of more efficient and more objective automatic calibration procedures. A large number of studies have been conducted that compare different optimisation algorithms [*e.g. Duan et al., 1992; Gan and Biftu, 1996; Cooper et al., 1997; Kuczera, 1997; Franchini et al., 1998, Thyer et al., 1999, Madsen et al., 2002*]. The main conclusion from these studies is that the global population-evolution based algorithms are more effective than multi-start local search procedures, which in turn perform better than pure local search methods. This study uses the SCE (Shuffled Complex Evolution) algorithm [*Duan et al., 1992*] explained in detail in chapter 4 which is a population-evolution-based global optimisation method.

In this chapter, the soil moisture content profiles measured on an experimental hillslope plot are used as observations. Using the MIKE-SHE hydrological modelling system [*Refsgaard and Storm, 1995*], numerical 1-D soil columns are set-up at each measurement location. The objectives of this chapter are: (i) to present two complementary sensitivity analyses for the evaluation of important soil hydraulic parameters for simulating water content profiles on a hillslope; (ii) to investigate the use of an efficient automatic calibration method for estimation of their 'effective' values; and (iii) to analyse the relation between 'effective' parameter values and parameter values estimated in the laboratory and in-situ.

5.2. Field Layout, observations and numerical modelling

The site description, field layout and observations are presented in detail in Chapter 2. The spatially distributed physically based MIKE-SHE model [*Refsgaard and Storm, 1995*] is briefly described in Chapter 4. The processes encountered in this chapter i.e. 1D unsaturated zone flow and evapotranspiration are described in more detail in Chapter 4. The particular model set-up used in this chapter is explained below.

For each of the 27 measurement locations where soil moisture and matrix head were measured, an UZ model was built up consisting of a single-column (1 m^2). The lower boundary condition was considered to be a constant watertable at 6 m depth, i.e. a groundwater independent model. Based on the observations of the auger measurements, two soil layers (referred to as A and B hereafter) are incorporated. The entire soil column is discretised into 86 calculation nodes over the 6 m. Nodes are not evenly spaced, closer spacing was set near the surface (first 65 nodes spaced only 2 cm apart) and spacing increases with depth. As the depth (d) between the A- and B-horizon is also considered as a parameter, d should be an even number and can vary between 0 and 1 m as explained below. Rainfall and potential evapotranspiration measurements for the year 2001 are given as daily time series.

In this chapter, daily time series of the soil moisture content between 0 and 25 cm, 30 and 55 cm and 60 and 85 cm depth at 27 locations are studied as output variables. The soil moisture output of the MIKE-SHE model over the TDR probe (25 cm) is considered to be the average of the output moisture content of all calculation nodes within the respective 25 cm. As the depth between A- and B-horizon (d) is allowed to vary between 0 and 1 meter, simulated soil moisture content at each of the three depths might refer to either the A- or B-horizon or a combination of both.

5.3. Parameter sensitivity analysis

The classical statistical approach for assessing parameter uncertainty is based on a multinormal approximation of the probability density function of the model parameters

around the estimated optimum. However, as shown by *Duan et al. (1992)* the multinormal approximation is often insufficient to describe the standard deviations and correlation structure of the estimated model parameters. Therefore, two sensitivity analyses are performed in this study, a sampling based (Monte Carlo) sensitivity analysis [*Spear and Hornberger, 1980*] and a screening method or a One-At-a-Time design [*Morris, 1991*].

For each of the two soil layers A and B, the sensitivity of the MIKE-SHE model to 6 UZ parameters is evaluated: K_s, θ_s, θ_r, α, n and N. The depth d [L] to the B-horizon is also considered in the analysis and hence the sensitivity of in total 13 parameters is evaluated. Upper and lower limits (taken as the 95 % confidence interval) of the recommended distributions by *Meyer et al. (1997)* of the Sandy Loam soil type (A-horizon) and of the Silty Clay type (B-horizon) are calculated. In the SA as well as in the optimisation procedure described below, it was chosen to use the same upper and lower bounds for the A- and B-horizon parameters as the bounds have a very large overlap and no prior information was to be included. The minima and maxima from both soil types were chosen as respective lower and upper bounds for both horizons and are presented in Table 5.1.

Table 5.1 Lower and upper bounds used in the sensitivity analysis and in the parameter optimisation

Parameter	Lower Bound	Upper Bound
K_s ($m\ s^{-1}$)	7.1e-10	7.8e-5
θ_s (-)	0.23	0.59
θ_r(-)	0.0173	0.102
α(m^{-1})	0.11	20.20
n(-)	1.06	2.21
N(-)	6	15
d(m)	0.1	1

For a particular parameter set, the soil moisture content at the three depths is extracted from the simulation results. Thereafter, Root Mean Squared Error (RMSE) and Standard Deviation (STD) is calculated against the observed moisture content for the year 2001:

$$RMSE = \sqrt{\frac{\sum_{i=1}^{n}\left(\theta_{i,obs} - \theta_{i,sim}\right)^2}{n}} \tag{5.1}$$

$$STD = \sqrt{\frac{\sum_{i=1}^{n}\left(res_i - \overline{res}\right)^2}{n-1}}, \quad \overline{res} = \frac{\sum_{i=1}^{n} res_i}{n} \tag{5.2}$$

where n = 365 is the number of days, $\theta_{i,obs}$ is the mean observed daily moisture content, $\theta_{i,sim}$ is the mean simulated daily moisture content, and $res_i = \theta_{i,obs} - \theta_{i,sim.}$ is the residual. The RMSE is a measure of the overall goodness-of-fit which can be divided into a bias term and a term that measures the goodness-of-fit of the dynamics (STD). Therefore in addition to RMSE, STD was also calculated for each parameter combination to evaluate which parameters have an important influence on the dynamics (STD) as well as on the overall fit (RMSE).

5.3.1. Monte Carlo based sensitivity analysis

The first method is based on Monte Carlo (MC) sampling where a number of parameter sets are randomly generated (uniform distribution) within their respective feasible regions and the corresponding model output evaluated [*Spear and Hornberger, 1980; Madsen, 2000*]. In this study, 20000 parameter sets are randomly generated and the corresponding model evaluated. The parameter sets are thereafter sorted with respect to the objective function value and two subsets are formed consisting of the best and worst parameters sets. The distributions of the two samples (X_1 and X_2) are compared using the two-sample Kolgomorov-Smirnov test. The test statistic (T) is given by:

$$\mathrm{T} = \max\left(\left|F(\mathrm{X}_1) - F(\mathrm{X}_2)\right|\right) \tag{5.3}$$

where $F(X_1)$ and $F(X_2)$ are the sample cumulative distribution functions of X_1 and X_2, respectively. The larger the test statistic, the higher the probability that the two samples have different distributions. The test statistic can be associated with a particular

probability level (*P*) (significance level) for a proper assessment of the significance of the sensitivity of the parameter [*Conover, 1980*].

5.3.2. Morris's One-At-a-Time design

The One-At-a-Time (OAT) design proposed by *Morris (1991)* can be called a global sensitivity experiment, because it covers the entire space over which the parameters vary [*Saltelli et al., 2000*]. The method estimates the main effect of a parameter by computing a number (*r*) of local sensitivities, at different points x_1, x_2 …x_r in the parameter space and then takes their averages. This reduces the dependence on the specific point that a local experiment has. In addition, the variability of the local sensitivities provides a measure of the interaction between the parameters and the existence of non-linear effects. The *r* values are selected in such a way that each parameter is varied over its feasible interval. The method is particularly suited for use with expensive (in computer time/power) computational models or models which have a large number of parameters. The number of computer runs needed by this design is proportional to the number of parameters (*k*). The method is used to determine which parameters have (a) negligible effects, (b) linear and additive effects, or (c) non-linear or interaction effects. The design is composed of individual randomized Once-At-a-Time designs, in which the impact of changing the value of each of the parameters is evaluated in turn. The key idea of the Morris design is the following:

1. A 'base' value x^* is randomly chosen for the vector *x*, each component x_i being sampled from the set $x_{lower,i} + [0, 1/(a_{int} -1), \ldots, 1-\Delta]*[x_{upper,i} - x_{lower,i}]$ where a_{int} is a chosen integer, $\Delta = a_{int} /[2 * (a_{int}-1)]$, $x_{lower,i}$ is the lower limit of x_i, *and* $x_{upper,i}$ is the upper limit of $x_{,i}$.

2. One of the *k* components (or parameters) is randomly selected (component *i* of x^*) and is increased or decreased by $\delta_i = \Delta * [x_{upper,i} - x_{lower,i}]$ such that a vector $x^{(1)}$ results that is still in the parameter space,

3. The estimated elementary effect ($d(x_i)$) of the ith component of $x^{(1)}$ is:

$$d_i(x^{(1)}) = \frac{y(x^{(1)}) - y(x^*)}{\Delta} \text{ if } x^{(1)} \text{ has been increased by } \delta_i, \text{ or}$$

$$d_i(x^{(1)}) = \frac{y(x^*) - y(x^{(1)})}{\Delta} \text{ if } x^{(1)} \text{ has been decreased by } \delta_i, \quad (5.4)$$

where y is the output (in this case either RMSE or STD).

4. Randomly choose a new component j different from i and form a new vector $x^{(2)}$ which differs from $x^{(1)}$ for component j with $\delta_j = \Delta * [x_{upper,j} - x_{lower,j}]$, i.e. either $x_j^{(2)} = x_j^{(1)} - \delta_j$ or $x_j^{(2)} = x_j^{(1)} + \delta_j$. The elementary effect of parameter j is then calculated from Eq. 5.4.

Step 4 is repeated in such a way that a succession of $k+1$ (k = number of parameters) input vectors x^*, $x^{(1)}$, $x^{(2)}$, …, $x^{(k)}$ is produced with two consecutive vectors differing in only one component. Furthermore, any component (i) of the base vector x^* is selected exactly once to be changed by δ_i to estimate one elementary effect for each parameter. Steps 1-4 are repeated r times, each with a different randomly generated base vector. Hence the number of runs needed for the Morris sensitivity analysis is equal to $r * (k+1)$.

The mean (μ) and standard deviation (σ) of the distribution of elementary effects for the ith input parameter provides information about the influence of the ith parameter on the output. A high mean indicates that the ith parameter has an overall influence on the output while a high standard deviation indicates either a parameter interacting with other parameters or parameters whose effect is non-linear. In this study, the Morris method was implemented in MATLAB and r was selected to be 14 and $k + 1 = 14$ (k = 13 parameters considered in the sensitivity analysis), so in total 336 MIKE-SHE runs were needed. a_{int} was chosen to be 4 which results in $\Delta = 2/3$. The choice of Δ and r was based on the examples presented in *Saltelli et al. (2000)* and *Morris (1991)*.

5.4. Automatic calibration procedure

In this study, the Shuffled Complex Evolution (SCE) algorithm (Chapter 4) is adopted for the optimisation of the Unsaturated Zone (UZ) soil parameters in the MIKE-SHE model [*Madsen, 2003*]. The SCE control parameters used are presented in Chapter 4. At each location; the same upper and lower bounds as the ones used in the sensitivity analysis are set in the SCE algorithm (Table 5.1). Two out of 27 locations were not considered in the optimisation since the TDR probes at those locations broke down after some time. Preliminary optimisation runs were performed using different objective functions, e.g. total RMSE or STD (sum of the RMSE or STD for the 3 depths), and combinations of both. Effective parameter sets obtained using different objective functions differ but the overall goodness of fit was found to differ only slightly between different objective functions. Differences in the number of evaluations necessary to reach the optima were also very small for the different objective functions. Hence, total RMSE was used as objective function used for the optimisation. Preliminary optimisation runs were also performed to see whether putting more weight on the surface RMSE (because there are more dynamics at the surface) resulted in a better overall match. These test runs showed some improvement in the surface match of observed and simulated moisture content but introduced bias in the 30 and 60 cm observations, and hence it was decided to put equal weights on the three RMSE measures. The stopping criteria for the optimisation routine were either (i) change of the best objective function less than 0.1% within 5 loops, or (ii) a maximum number of model evaluations of 2000.

5.5. RESULTS AND DISCUSSION

5.5.1. Laboratory and in-situ parameter estimates

The left part of Table 5.2 shows the mean, standard deviation, minimum and maximum of the UZ soil parameters as estimated from the lab and in-situ measurements (cfr. Table 2.1).

Table 5.2 Mean, standard deviation, minimum and maximum of the considered UZ soil parameters as measured in laboratory and K_{fs} as measured by the single-ring pressure infiltrometer in-situ compared with the optimised or 'effective' parameters obtained from the automatic calibration

	Parameters from lab. and in-situ K_{fs}				Optimised or effective parameters			
Parameter	Mean	St. Dev.	Min	Max	Mean	St. Dev.	Min	Max
$K_s\_A\ (ms^{-1})$	9.74E-06	1.78E-05	4.56E-08	7.01E-05	9.24E-08	2.78E-07	7.10E-10	1.37E-06
$\theta_s\_A\ (-)$	0.40	0.02	0.35	0.45	0.36	0.03	0.32	0.43
$\theta_r\_A\ (-)$	0.02	0.03	2.19E-07	0.11	0.07	0.02	0.04	0.10
$\alpha\_A\ (m^{-1})$	1.95	1.19	0.29	5.77	2.60	2.06	0.11	8.35
$n\_A(-)$	1.30	0.10	1.15	1.62	1.20	0.14	1.06	1.56
$N\_A(-)$	12.59	3.32	6.68	21.58	-	-	-	-
$K_s\_B\ (ms^{-1})$	1.57E-05	2.63E-05	4.37E-09	8.72E-05	1.26E-05	2.09E-05	8.94E-09	7.80E-05
$\theta_s\_B\ (-)$	0.39	0.03	0.33	0.45	0.41	0.08	0.31	0.56
$\theta_r\_B\ (-)$	0.05	0.03	1.80E-04	0.13	0.09	0.04	4.24E-03	0.14
$\alpha\_A\ (m^{-1})$	1.87	1.54	0.26	5.79	3.93	3.90	0.11	14.00
$n\_B(-)$	1.44	0.21	1.15	1.98	1.67	0.29	1.17	2.17
$N\_B(-)$	9.97	3.71	4.87	21.84	-	-	-	-
$K_{fs}\ (m\ s^{-1})$	4.88E-06	4.87E-06	3.33E-07	2.53E-05	-	-	-	-
d	0.76	0.48	0.12	2.24	0.79	0.21	0.26	1

When measuring soil physical properties on small-undisturbed soil samples, cracks near the borders of the ring or wormholes can affect parameter estimation and therefore outliers were deleted from the lab estimates. Outliers were defined as soil cores showing very large apparent conductivities indicating the presence of preferential pathways (i.e. cracks or worm or root holes) all the way through the soil core. In general, it shows that wide ranges were measured for all parameters. Comparing measured ranges with the ranges set in sensitivity analysis and the optimisation from literature [*Meyer et al., 1997*] reveals that measured ranges are comparable to the ranges set in the optimisation (see Table 5.1 and 5.2). In most cases, the measured range is within the bound sets in the optimisation or if not, very close to the upper or lower limit.

5.5.2. Parameter sensitivity analysis

5.5.2.1. Monte Carlo based sensitivity analysis

The Monte Carlo analysis was performed for one of the locations (x = 10, y = 2). The Kolmogorov-Smirnov test was performed for 8 different cases i.e. comparing best (X_1) and worst (X_2) parameter sets for the surface RMSE and surface STD, 30 cm RMSE and 30 cm STD, 60 cm RMSE and 60 cm STD and total RMSE and total STD. Different sample lengths of X_1 and X_2, varying between 50 and 1000 (50, 100, 250 and 1000) were analysed. Only minor differences were found between the Kolmogorov-Smirnov tests using different sample lengths. Hence, the sample length did not seem crucial in the decision whether or not the distributions are significantly different. The cumulative distributions of the 250 best and worst parameter sets when ranked according to the total RMSE for the A- and B-horizon are shown in Fig. 5.1a and 5.1b, respectively. A clear conclusion from these figures is that the distributions of the best and worst parameter sets for *N* coincide for both horizons. The Kolgomorov-Smirnov test shows indeed that the distribution of the best and worst parameter sets do not significantly differ for *N* at a 5% significance level. For all other parameters, the test showed that the best and worst parameter distributions differ at least in one of the considered depths. All of this indicates that the model output is not 'sensitive' to the absolute value of *N*. However, care must be taken here when interpreting the results, theoretically speaking, we can only state that it is equally likely to get a good or bad simulation with a certain value for *N* when all other parameters are allowed to vary. Interpreting the results becomes more difficult when high correlations amongst parameters exist. In this study, correlations amongst the best parameter sets were found to be rather low, between 0 and 0.6, the same is true for correlations amongst the worst parameters sets.

In Table 5.3, parameters are ranked according to their significance level (= probability that the two samples have the same distributions) with total RMSE and total STD as objective function. Differences in ranking are observed when parameter sets are ranked according to the overall RMSE or overall STD. Although, these differences are rather small and most and least sensitive parameters coincide for both analyses.

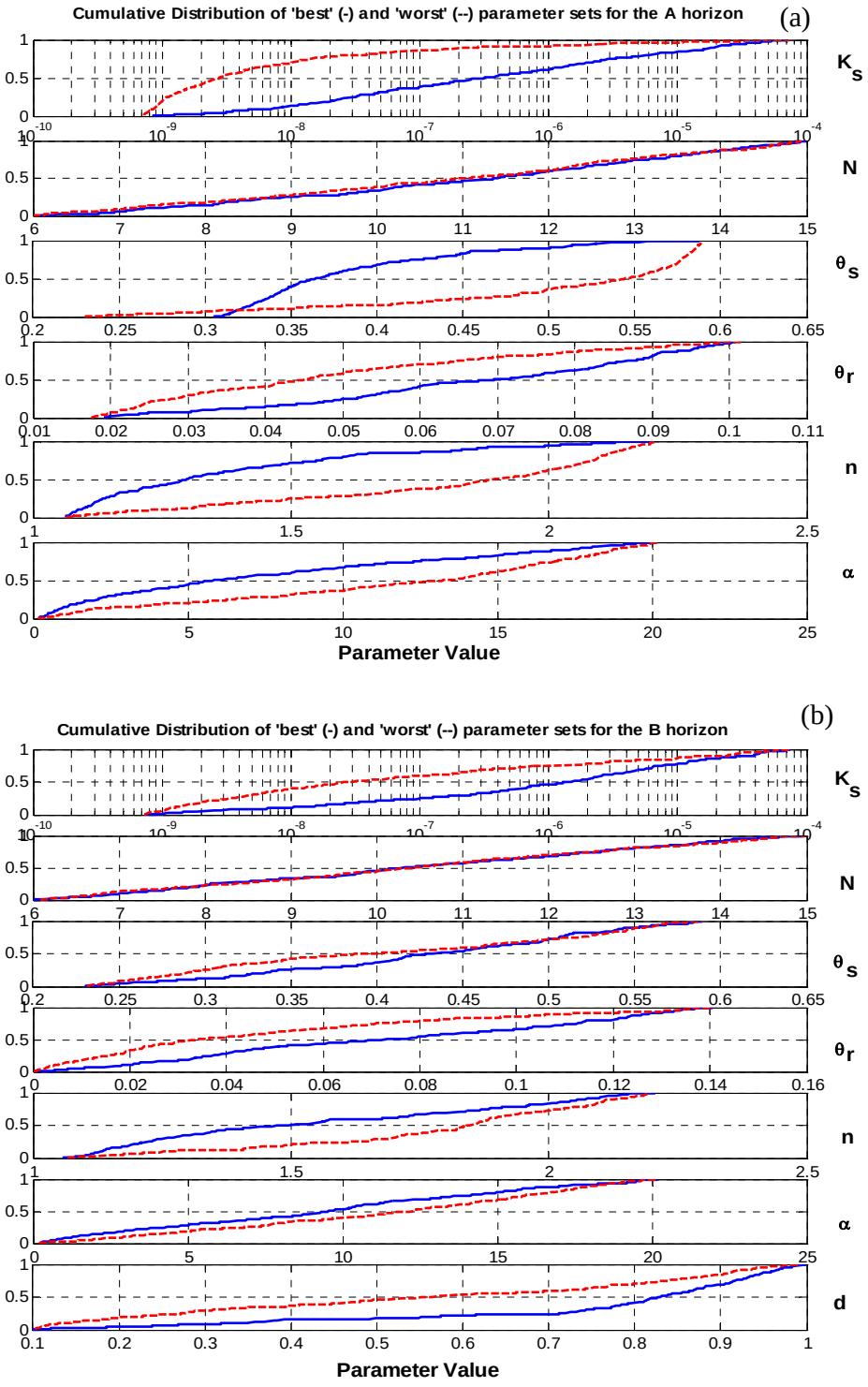

Figure 5.1 Cumulative distribution of the 250 'best' (-) and 'worst' (--) parameter sets for the Monte Carlo SA sorted according to total RMSE (a) parameters of the A-horizon and (b) parameters of the B-horizon and d = depth to B-horizon

Table 5.3 Comparison between the ranking of parameters according to their sensitivity level (high to low sensitivity) or significance level as a result of the Monte Carlo sensitivity analysis (MC) and the Morris design with both total RMSE or STD as objective functions (T statistic not significant at a 5 % significance level)*

MC RMSE	MC STD	Morris RMSE	Morris STD
θ_s_A (-)	θ_s_A (-)	K_s_A (ms^{-1})	K_s_A (ms^{-1})
K_s_A (ms^{-1})	α_A(m^{-1})	θ_s_A (-)	n_A(-)
n_A(-)	n_A(-)	θ_r_A (-)	α_A (m^{-1})
θ_r_A(-)	K_s_A (ms^{-1})	α_A (m^{-1})	θ_s_A (-)
K_s_B (ms^{-1})	θ_s_B (-)	d(m)	K_s_B (ms^{-1})
n_B(-)	K_s_B (ms^{-1})	K_s_B (ms^{-1})	α_B (m^{-1})
d(m)	d(m)	θ_s_B (-)	d(m)
α_A (m^{-1})	n_B(-)	n_A(-)	n_B(-)
θ_r_B (-)	θ_r_A (-)	α_B (m^{-1})	θ_s_B (-)
α_B(m^{-1})	α_B (m^{-1})	N_A(-)	θ_r_A (-)
θ_s_B (-)	θ_r_B (-)	θ_r_B (-)	N_A(-)
N_A(-)*	N_A(-)	N_B(-)	θ_r_B (-)
N_B(-)*	N_B(-)*	n_B(-)	N_B(-)

Comparing significance levels in both analyses shows that the most sensitive parameters are: K_s, θ_s, and n of the A-horizon, K_s, and n of the B-horizon and depth (d) from the surface to the B-horizon. However, parameters become more sensitive when other objective functions than the total RMSE or STD are used, e.g. the surface, at a depth of 30 or 60 cm RMSE/STD. In general, the B-horizon parameters are less sensitive when considering the surface RMSE/STD and the A-horizon parameters less sensitive when considering the 30 and 60 cm RMSE/STD. However, for the 30 and 60 cm RMSE/STD, surface parameters still seem to be quite sensitive as they control how much water infiltrates to the B-horizon.

Since N of the A- and B-horizon are found to be insensitive parameters (with respect to all 8 objective functions considered) and are not correlated with any of the other

parameters, it can be concluded from this analysis that *N* should not be considered in the automatic calibration.

5.5.2.2. Morris's One-At-a-Time design

Estimated means (μ) and standard deviations (σ) of the distribution of the elementary effect of each parameter against the total RMSE are shown in Fig. 5.2. Absolute values of μ ($|\mu|$) are plotted in Fig. 5.2 making it easier to visualize overall sensitivity of the parameters. Plotting the distribution of the elementary effect of each parameter against the total RMSE yields comparable but not the same results as shown in Table 5.3. The sensitivity of parameters in the Morris method cannot be quantified, only a qualitative ranking of importance of parameters with respect to overall importance and interaction with other parameters or non-linear effects can be performed. Objective ranking can be performed against μ or σ yielding an idea about which parameters have the largest overall effect (μ) or which parameters have high interaction with other parameters and non-linear effects (σ).

The ranking in Table 5.3 is based on a combination of both μ and σ and hence is rather subjective (from high to low sensitivity). As in the Monte Carlo SA, this sensitivity analysis shows that *N* of both horizons have a very small overall important influence on the output (small μ) and that neither seem to have important interactions with other parameters or significant non-linear effects (small σ). Other graphs which show the elementary effects against surface, 30 and 60 cm RMSE or STD all reveal that *N* of both horizons have small μ and σ, generally smaller than μ and σ of all other parameters.

Differences exist between the exact position of parameter ranking with respect to RMSE or STD as objective function as shown in Table 5.3. However, in general both rankings give the same overall picture of parameter sensitivity. Most sensitive parameters are: K_s, θ_s, θ_r, and α of the A-horizon, K_s of the B-horizon and the depth *d* to the B-horizon since they have high overall importance on the output and/or important interactions with other parameters or significant non-linear effects.

In general, B-horizon parameters have smaller elementary effects on the surface RMSE/STD and A-horizon parameters smaller elementary effects on the lower RMSE/STD. However, as observed in the Monte Carlo SA, A-horizon parameters have relatively high elementary effects even when plotted against 30 or 60 cm RMSE/STD. Again from this sensitivity analysis, it can be concluded that *N* should not be included in the automatic calibration because its overall importance and interactions with other parameters or non-linear effects are negligible.

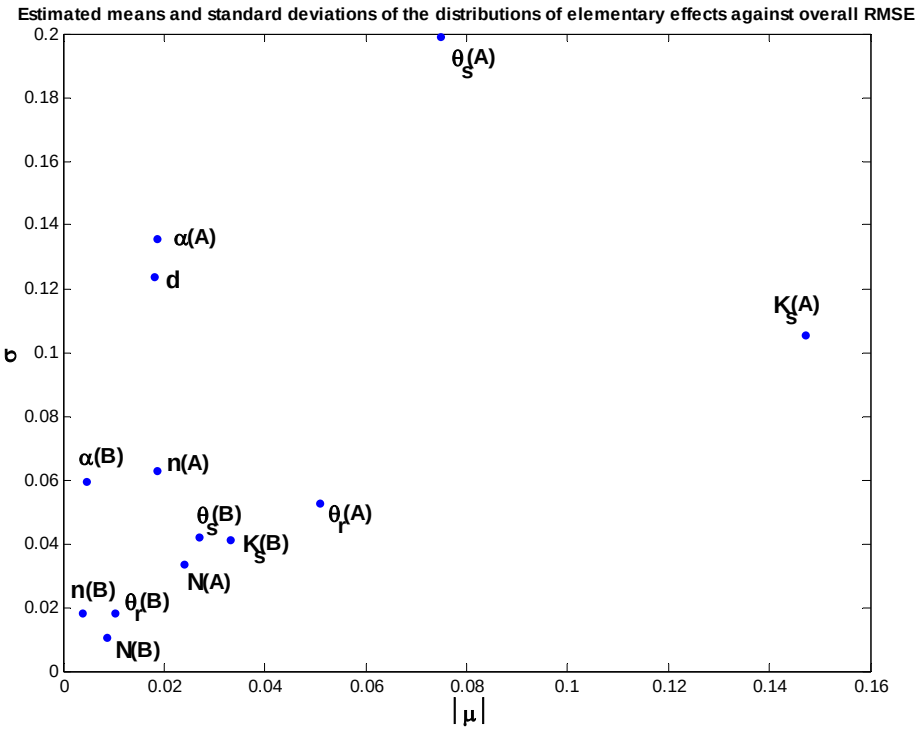

Figure 5.2 Estimated means $|\mu|$ and standard deviations (σ) of the distributions of elementary effects of all parameters against overall RMSE for the Morris SA

5.5.2.3. Comparison of Sensitivity Analyses

Exact ranking positions of importance of parameters between both sensitivity analyses differ but most and least sensitive parameters coincide as shown in Table 5.3. General conclusions and implications for the incorporation of parameters in the automatic

calibration are the same for both analyses. Hence it is decided that in the optimisation procedure presented below, *N* of A- and B-horizon are fixed to an initial value of 9. In both analyses the B-horizon parameters have smaller impact on the surface RMSE/STD and A-horizon parameters have smaller impact on lower RMSE/STD. However, the A-horizon parameters have, in general, higher impact on the 30 and 60 cm RMSE than the B-horizons have on the surface RMSE. Overall importance of the A-horizon parameters with respect to total RMSE or STD compared to the B-horizon parameters is also obvious from both analyses. The reasons for this is that A-horizon parameters dominate how much water infiltrates (to the B-horizon) and that the observed moisture content near the surface is much more dynamic and hence total RMSE/STD is quite dominated by the surface RMSE/STD.

The main advantage of the Morris method is the relatively low computational cost compared to the Monte Carlo SA. The Morris design requires a total number of runs that is a linear function of the number of examined parameters. Another advantage of the Morris method is that it gives a 'qualitative' idea about the individual interactions amongst parameters, i.e. parameters can be ranked according to their degree of interaction or non-linear effects, although this cannot be quantified. The Monte Carlo based technique requires much more computer time but has the advantage that sensitivity can be quantified. On the other hand, the Monte Carlo statistics are univariate statistics that do not properly account for parameter correlations. It is believed that both techniques are complementary and on the basis of both, sound conclusions concerning the parameter sensitivity can be drawn.

As reported by *Radwan (2002)*, the possibility exists that parameter ranking depends on the chosen range between which the parameters are allowed to vary. It is important that the parameter ranges are comparable amongst the parameters i.e. when wide parameter ranges are chosen for one parameter, one should try to estimate corresponding ranges for all other parameters in the SA. If for one parameter a large range while for the second parameter only a small range is chosen, it is obvious that the parameter having the large range will show most important (as long as the sensitivity is not that different for both parameters). This problem can be expected to be particularly important in the Morris design SA as Δ (or the amount a parameter is increased or decreased) is a

function of the parameter range. It is believed that in our study, comparable ranges are chosen for each parameter as upper and lower limits are taken as the 95 % confidence interval of the recommended distributions by *Meyer et al. (1997)*.

5.5.3. Automatic calibration

At most locations, the optimisation was stopped after 2000 simulations and in these cases the objective function was not improved in at least the last two loops. At some locations, optimisation stopped before because the objective function value had not changed in 5 loops. The mean, standard deviation, minimum and maximum of the optimised parameters are shown in Table 5.2.

Comparing minima and maxima of optimised parameters (over the 25 locations) with the upper and lower bounds set [*Meyer et al., 1997*] in the optimisation, reveals that in very few locations the upper and lower bounds were 'hit' in the optimisation procedure. Mean of the optimised parameters is for all parameters well within the prior range. 'Effective' or optimised parameter ranges are found to be much smaller than the prior ranges suggesting that the 'effective' parameter range over the field is quite well delineated within the prior bounds. Examples of observed and simulated soil moisture content at the three considered depths, after optimisation of the 11 parameters, are shown in Fig. 5.3. Figure 5.3a shows the best correspondence (smallest total RMSE) between simulated and observed soil moisture content (x = 10, y = 2) and Fig. 5.3b the worst (x = 5, y = 78). As explained in Chapter 2, gaps in the observed soil moisture measurements are due to power cuts, lightning (break down of the communication port of the computers) and frost periods (bad functioning of the TDR probes). The SCE algorithm succeeded in finding parameters for the MIKE-SHE model that simulate the soil moisture at the different depths at each location quite well. Water balance errors were also checked and found in all cases to be less than 1 %. Total optimisation time for each location equivalent to 2000 MIKE-SHE runs was about 25 hours on a 2 Ghz processor.

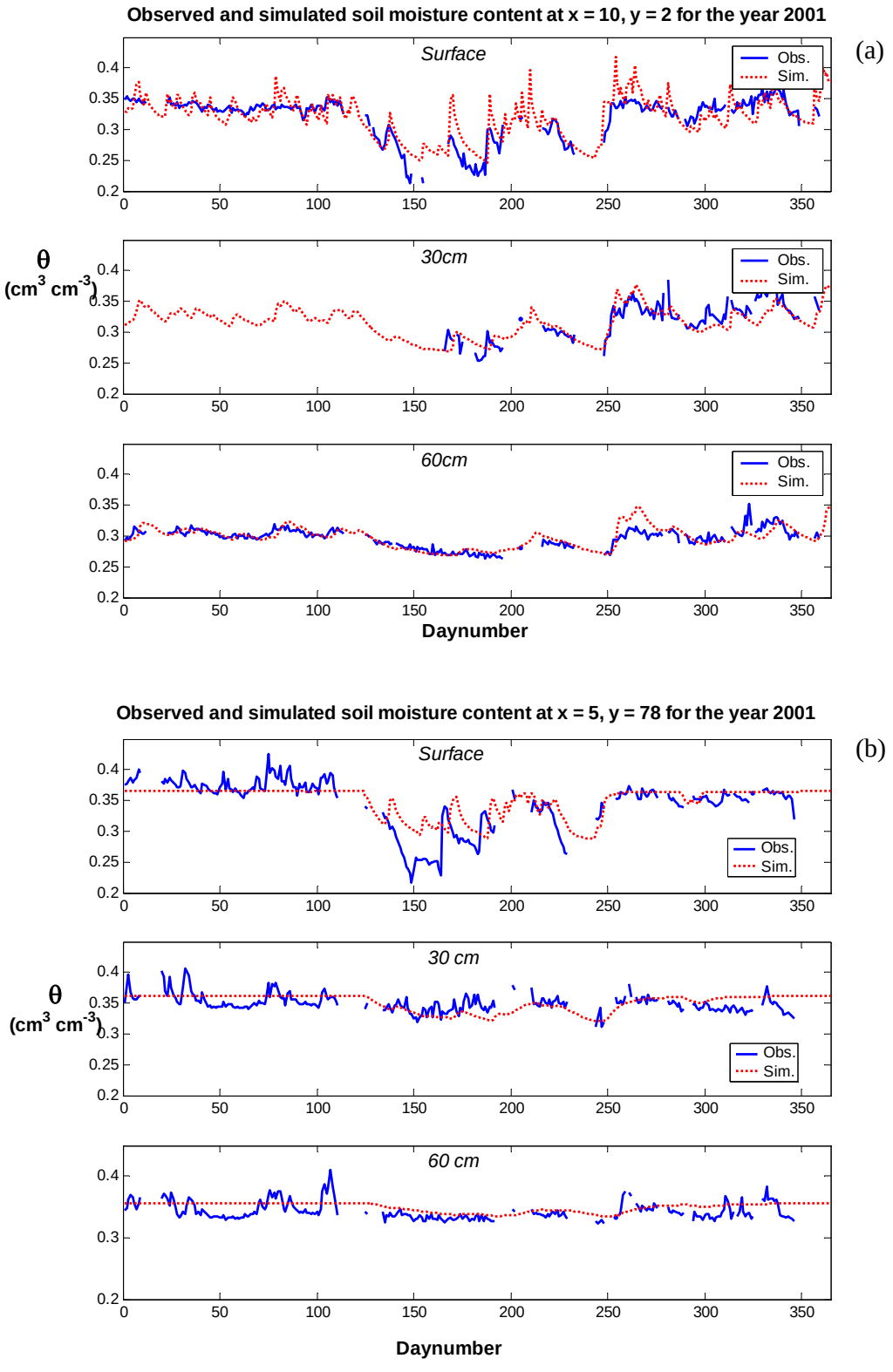

Figure 5.3 Observed and simulated soil moisture content at different depths for the year 2001 at (a) location with the best fit (x = 10 and y = 2 and (b) location with the worst fit (x = 5 and y = 78)

5.5.4. Comparison between 'effective' and in-situ and laboratory estimates

Figure 5.4 shows a comparison between the cumulative distributions of the 'effective' or optimised parameter sets, the parameters estimated in the laboratory and in-situ estimated K_{fs} [cfr. Chapter 3 and *Mertens et al. (2002)*]. A Kolgomorov-Smirnov test was applied and distributions compared. All distributions were found significantly different at the 5 % significance level except for α of the A-horizon and K_s and θ_s of the B-horizon. From this figure and the comparison presented also in Table 5.2, it is concluded that, in general, optimised or 'effective' parameters do not correspond to the ones estimated in the laboratory or in-situ.

The effect of this significant difference between most measured and effective parameters on the soil water retention curve and the hydraulic conductivity curve of the A-horizon is shown in Fig. 5.5. 95 % confidence intervals of the measured soil water retention curves (Fig. 5.5a) and hydraulic conductivity curves (Fig 5.5b) in the laboratory are compared to the 95 % confidence intervals of the effective soil water retention curves (Fig. 5.5a) and hydraulic conductivity curves (Fig 5.5b). The effective soil water retention curves at low potentials are comparable to the measured ones but as the potential rises, they show more variability than the measured ones.

Effective hydraulic conductivity curves are lower over the whole range of soil moisture content values. This was to be expected as shown in Fig. 5.4, where the effective K_s is significantly lower than the measured K_s of the A-horizon. Effective retention curves for the B-horizon show even more variability than the measured ones whereas the effective hydraulic conductivity curves are comparable to the measured ones. It is well known that even small differences in retention and hydraulic conductivity curves yield large variability in soil moisture content simulations [*Durner, 1994*].

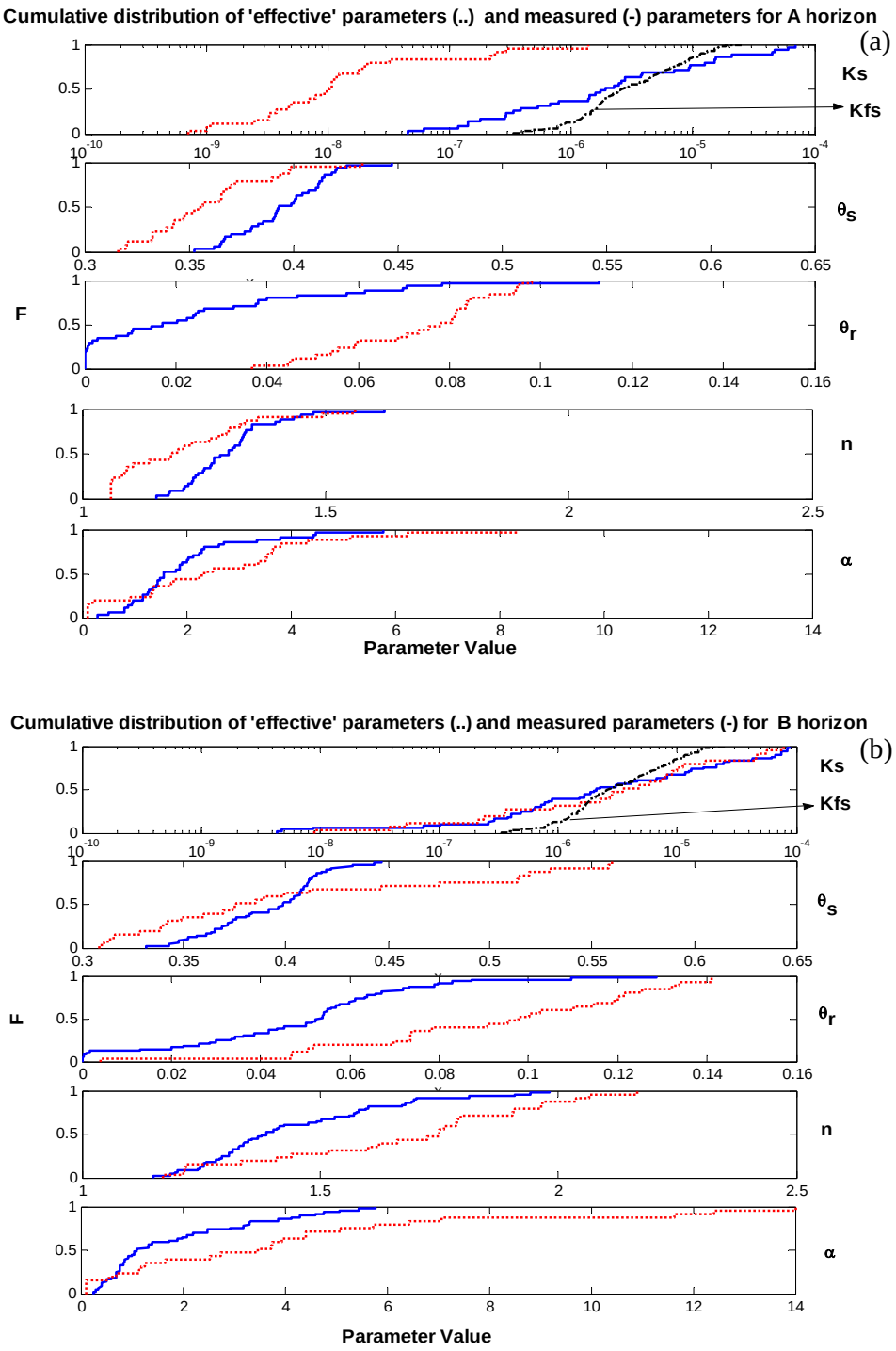

Figure 5.4 Cumulative distribution of the measured (-) and 'effective' (--) parameter sets sorted for the (a) A-horizon and (b) B-horizon. Cumulative distribution of field saturated hydraulic conductivity (K_{fs}) is also shown in (a) and (b)

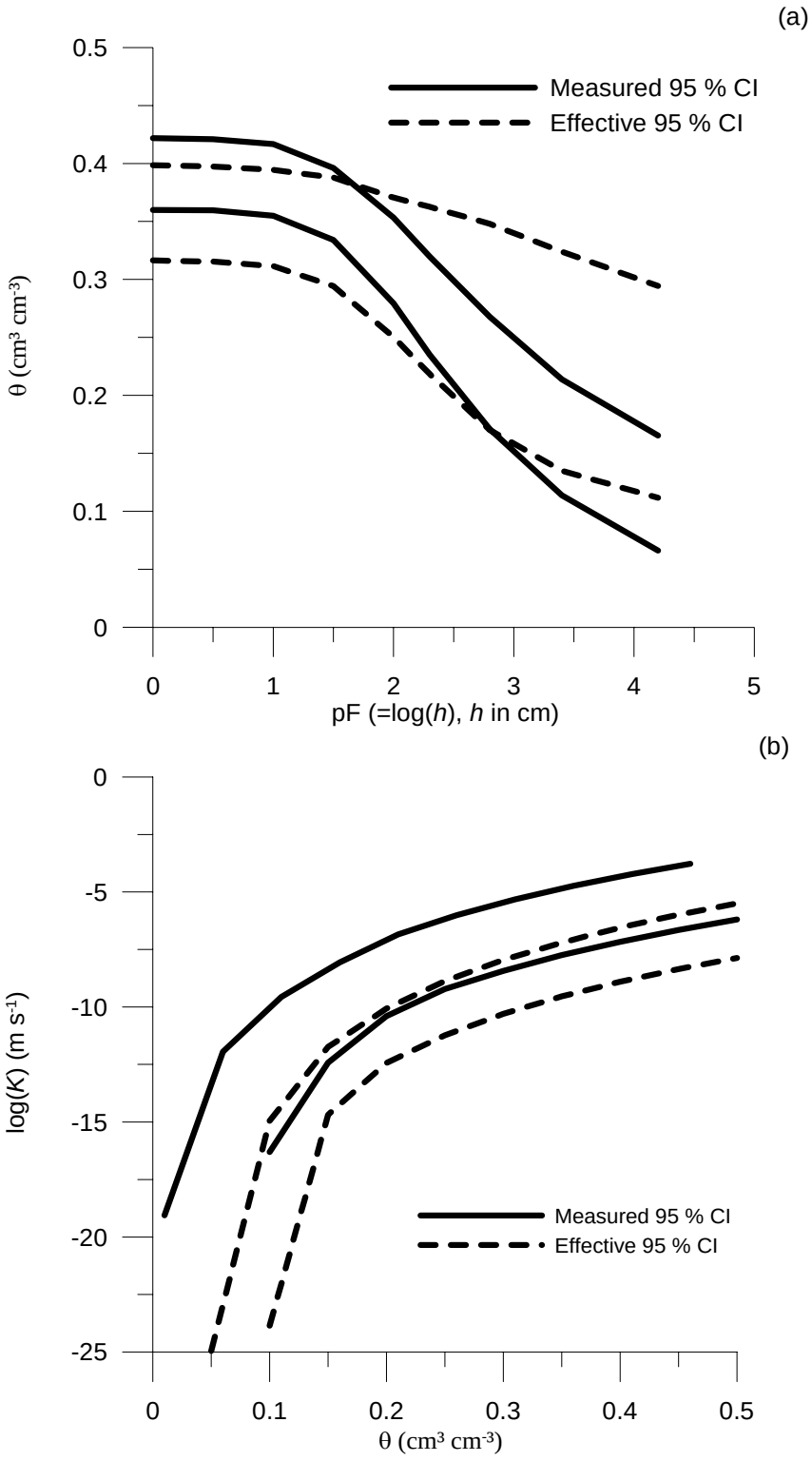

Figure 5.5 95 % confidence intervals of the measured soil water retention curves (a) and hydraulic conductivity curves (b) in the laboratory compared to the 95 % confidence intervals of the effective soil water retention curves (a) and hydraulic conductivity curves (b)

Knowing that effective parameters differ from their measured equivalents, it was investigated how much poorer model fits are obtained when using the measured parameter values rather than their effective equivalents. First of all, 350 combinations of measured parameters on soil samples from the A-horizon with parameters measured on soil samples from the B-horizon were randomly selected. After simulation of all 350 parameter combinations, 95 % confidence intervals (CI) on the simulated moisture content were calculated. For comparison, mean and 95 % confidence intervals (CI) of the observed moisture content over the 25 locations were calculated.

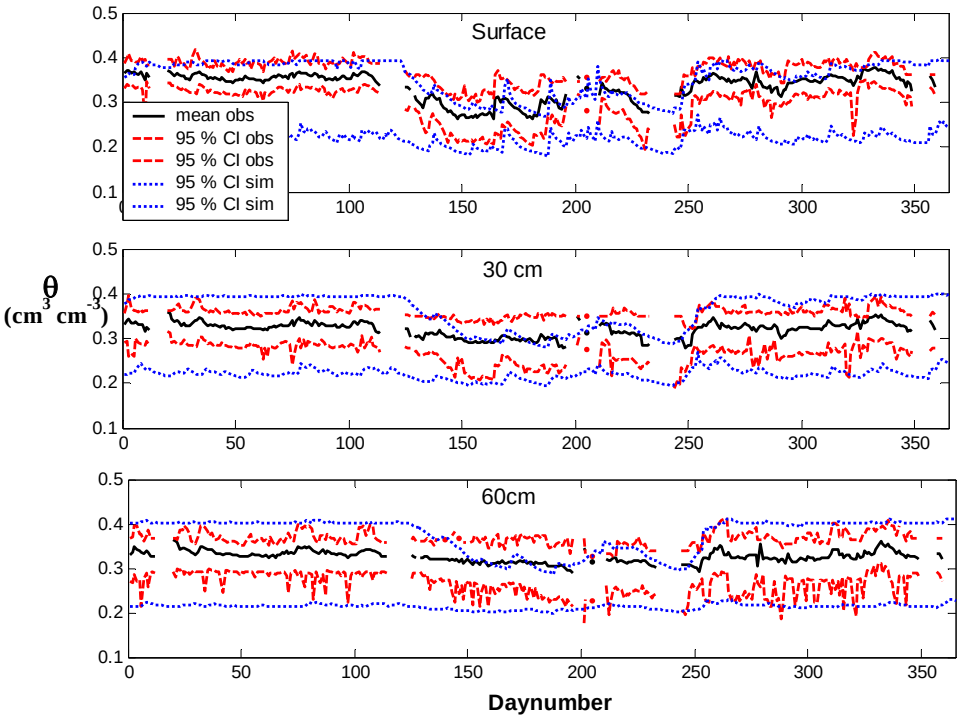

Figure 5.6 Mean observed moisture content over all 25 locations, 95% confidence interval of the observed moisture content over these 25 locations and 95 % confidence interval of simulated moisture content using parameters measured in the laboratory at the different depths

In Fig. 5.6 the CI for all three depths are compared. The simulations show larger variability at all three depths than the observations. However, although the simulated CI are wider, they do not always include the measured CI, especially during the dry summer period. Again this indicates that the measured laboratory parameters are not

capable of simulating a reasonable fit to observed moisture content observations in the field.

In general, different reasons can be thought of to explain these differences between 'effective' and measured parameters. The first and probably most important is the 'scaling problem'. In the last two decades, a vast amount of literature about upscaling and downscaling studies emerged [*e.g. Blöschl and Sivapalan, 1995; Finke et al., 1998; Heuvelink and Pebesma, 1999; Bierkens et al., 2000*]. The reason that the problem of scale transfer exists is the heterogeneity of soil properties. If the modelled and observed parameters or variables were homogenous (in space and time), they would be scale invariant [*Bierkens et al., 2000*]. In this study, heterogeneity in space and time is present in all parameters used for the description of the soil moisture content. Heterogeneity of hydraulic conductivity in space and time is probably the most studied [e.g. *Russo and Jury, 1987; Vauclin et. al., 1994; Russo et. al., 1997*]. Hence, ideally, physical properties should be measured at the same scale as characterized by the processes described by the model. Scale differences in this study are obvious: laboratory measurements are carried out on undisturbed soil samples which have a volume of 100-cm^3, single ring pressure infiltrometer measurements on a surface of 25 cm^2. Parameters from both measurement techniques are compared to effective parameters estimated using a model domain with a surface of 1 m^2 and a depth 6 m.

In this respect, studies that compare hydraulic conductivity values measured at different scales are important to mention [eg. *Lauren et al., 1988 and Mallants et al., 1997a*]. It is known that values of hydraulic conductivity measured in the laboratory on open-ended columns, decrease with increasing column size. Not only the value of the hydraulic conductivity decreases but also the Coefficient of Variation (CV) decreases with increasing column size. In *Mallants et al., 1997a*, it is shown average hydraulic conductivity decreases from 13.9 cm/h for measurements on 5 cm long and 5 cm diameter columns, to 5.28 for measurements on 20 cm long and 20 cm diameter columns to 0.49 cm/h for measurements on 100 cm long and 30 cm diameter columns. Coefficient of Variation decreases correspondingly from 619 % to 217% to 105%. In this research, it is observed that mean effective K_s of the A horizon, is 100 times smaller than the corresponding measured K_s on the 100 cm^3 undisturbed soil samples (cfr. Table 5.2). The reason for the increase in K_s values and variability with decreasing size is most

likely the presence of open-ended macropores (i.e. macropore from top till bottom through the soil column) in combination with a small sampling volume. The same is true for this study: effective parameters of the A horizon are estimated on 1 m² surfaces with variable depth and compared to parameters measured on 100-cm³ undisturbed soil samples. Hence, the 'scaling issue' is probably the dominating reason causing the big gap between effective and measured parameters.

A second possible reason responsible for the large gap between effective and measured parameters may have to do with the different measurement techniques used in this study. *Reynolds et al., 2000* and *Herman et al., 2003* found that using different measurement techniques even at the same scale (or sample size) can yield different K_s estimates. These authors show that K_s estimated from tension-infiltrometer measurements, single-ring pressure infiltrometer measurements and laboratory measurements on undisturbed soil samples all at the same scale, may well be significantly different. There is not only uncertainty involved in the parameter values estimated using different techniques but also in the observed time series. In this study, time series of daily soil moisture content values, measured using the TDR system described in 2.3.3, are used in the inverse modeling exercise. Therefore, any uncertainty in the observed time series is propagated in the estimation of the effective parameters.

A third possible reason for the big gap is the question whether the global optimum of the objective function has been reached by the autocalibration algorithm. In this study, the risk of missing the global optimum has been minimised by the use of a global optimisation method, i.e. the Shuffled Complex Evolution algorithm. Therefore, we have confidence that the SCE algorithm discovered the global optima for all locations.

A last possible reason that can help explain differences between effective and measured parameters has to do with the uncertainty inherent to any kind of modeling exercise. This uncertainty can be further divided in three main categories of uncertainty: (a) parameter uncertainty, which is the main topic of this PhD research, (b) model structure uncertainty and (c) input uncertainty (e.g. uncertainty in rainfall and evapotranspiration). As already briefly discussed in Chapter 4, it is shown that for conceptual rainfall runoff models, input uncertainty of rainfall can take up to 40 or 50 % of the total uncertainty on the model results [*Willems, 2000*]. In this study, similar

rainfall data have been used as in the work of *Willems (2000)*. Therefore, it can be expected that the order of magnitude of the rainfall-input uncertainty will be comparable when interested in runoff volumes or peak flows. In this study, daily soil moisture content values are simulated and as shown in Chapter 7, the temporal resolution of rainfall used for the simulation of daily soil moisture values is not important. Therefore, it is believed that in this study, input uncertainty of the rainfall will be much smaller than 40 or 50% of the total uncertainty.

Willems (2000) also found that for lumped conceptual rainfall-runoff models, the parameter uncertainty will be small in comparison with the model-structure uncertainty. It is expected that the reverse will be valid for the physically-based MIKE SHE model used in this study: model-structure uncertainties will be much smaller than the parameter uncertainties. Parameter uncertainty increases with the increasing number of parameters generally needed by physically-based models because of the parameter identifiability problem. Two main possible model structure uncertainties for the MIKE SHE model setup in this study can be thought of: (a) hysteresis in the pressure head, water content and hydraulic conductivity relationships during wetting and drying cycles is not taken into account and (b) preferential flow is not incorporated. It is not easy to estimate the importance of both processes on our experimental hillslope. The possibility exists that decayed fruit tree roots (the site used to be a fruit tree orchard) have created macroporosity in the soil. Though, preferential flow only becomes important under saturated conditions or during heavy rains after a long dry period. These conditions are rarely encountered in natural circumstances i.e. no ponding nor surface runoff observed on the hillslope. Additionally also surface roughness and constrictions (e.g. partial filling of pores) will reduce flow rates in macropores under natural conditions [*White, 1985*]. Therefore, it is believed that preferential flow is not dominating the infiltration process on the hillslope and can hence be excluded from the model structure. On top of that, no data is available from the field experiment to estimate parameters for both the hysteresis and the preferential flow process. Therefore, incorporating these processes in our model structure would have increased the parameter identifiability problem and corresponding parameter uncertainty even more.

Under different physical (soil type, slope, etc.) and climatic conditions, by using other observation types (e.g. runoff, soil water heads), and by applying other numerical

models, it is possible that differences between measured and effective parameters are smaller or larger than observed in this study. Though, as argued above, we believe that a difference between measured and effective parameters is likely to exist in any hydrological model to a smaller or larger extent.

5.6. Conclusions

Measured soil moisture content for the year 2001 in 25 locations at three different depths on a hillslope were used as observations for the inverse optimisation of soil hydraulic parameters for the *Richards'* equation. Prior Monte Carlo SA of the 1-D model revealed that soil moisture content is not sensitive to the *Averjanov N* parameter. A One-At-a-Time (OAT) SA (Morris' design) showed comparable conclusions to the Monte Carlo SA and hence *N*, for both horizons, was excluded from the inverse optimisation. Both SA show that K_s and θ_s of the A-horizon, K_s of the B-horizon and the depth *d* between the A- and B-horizon are the most important parameters in this study. The main advantage of the Morris method is the relatively low computational cost compared to the Monte Carlo SA and its ability to generate a 'qualitative' idea about the individual parameter interactions (or non-linear effects). Both techniques are complementary and on the basis of both, sound conclusions concerning the parameter sensitivity can be drawn.

The Shuffled Complex Evolution (SCE) algorithm was adopted for the optimisation of the UZ soil parameters in the MIKE-SHE model. The SCE algorithm succeeded in finding optimal parameter sets for the MIKE-SHE model which simulate the soil moisture time series at the different depths at each location quite well. Effective or optimised parameter sets are compared to their measured equivalents and all parameter distributions were found significantly different at the 5 % significance level except for α of the A-horizon and K_s and θ_s of the B-horizon. Knowing that effective parameters differ from their measured equivalents, it was investigated how much poorer model fits are obtained when using the measured parameter values rather than their effective equivalents. First of all, 350 combinations of measured parameters on soil samples from the A-horizon with parameters measured on soil samples from the B-horizon were

randomly selected. After simulation of all 350 parameter combinations, 95 % confidence intervals (CI) on the simulated moisture content were calculated. For comparison, mean and 95 % confidence intervals (CI) of the observed moisture content over the 25 locations were calculated.

Four different possible reasons were discussed that help explain the big gap between the effective parameters and the measured parameters: (a) probably most important reason is the 'scaling problem'; (b) uncertainty in estimated parameters using different measurement techniques (even at the same scale) as well as uncertainty involved in the measurement of the observed time series; (c) has the global optimum of the objective function been reached by the autocalibration algorithm? and (d) uncertainty inherent to any kind of modelling exercise (parameter uncertainty, model structure uncertainty and input uncertainty). Under different physical and climatic conditions, by using other observation time series, and by applying other numerical models, differences between effective and estimated (measured) parameters may be smaller or larger than observed in this study. Though, we believe that a difference between measured and effective parameters is likely to exist in any kind of hydrological model.

From this Chapter, one could question why measure parameters (in-situ or in laboratory) if they differ from the 'effective' parameters needed by our models? It could be argued that measuring parameters is useless and we better use the available computer power to autocalibrate the parameters within wide literature ranges. In the next chapter, an answer to this question is searched for and the usefulness of the estimated parameters as prior information in effective parameter estimation is investigated. Next to the SCE approach, the GLUE approach is also applied [*Beven and Binley, 1992; Beven, 2001; Christiaens and Feyen, 2002*] in which the algorithm is not looking for the 'best' parameter set but targets the demarcation of parameters resulting in an acceptable description of the system to be modelled. The relevance of including prior measured parameters in both (SCE and GLUE) parameter estimation strategies is investigated.

Chapter 6

Including prior information in the estimation of effective soil parameters in unsaturated zone modelling*

ABSTRACT

The soil moisture content was measured at 25 locations along three transects and at three different depths (surface, 30 and 60 cm) on an 80 × 20 m hillslope for the year 2001. Soil cores were collected in 84 locations situated in three profile pits along the hillslope. Moisture retention curve and hydraulic conductivity curve parameters were estimated after measurements in the laboratory on undisturbed soil cores. A joint probability distribution of these estimated parameters is here used as prior information combined with soil moisture measurements for the estimation of effective soil hydraulic parameters. A two-horizon single column 1-D MIKE-SHE model, based on the *Richards' (1931)* equation, was set-up for 9 soil moisture measurement locations along the middle transect of the hillslope. At each of these 9 locations, the Shuffled Complex Evolution (SCE) algorithm was applied to estimate 'effective' model parameters using wide parameter ranges. Effective parameters from a SCE optimisation without prior information were found significantly different from the prior parameters. A SCE optimisation where prior information is incorporated produces a comparable (only slightly worse) goodness-of-fit to the SCE where no prior information is incorporated but the effective parameter estimates are much more realistic in terms of prior parameter estimates. A Generalized Likelihood Uncertainty Estimation procedure (GLUE) was

---

* Adapted from Mertens, J., H. Madsen, L. Feyen, D. Jacques, and J. Feyen, 2003. Including prior information and its relevance in the estimation of effective soil parameters in unsaturated zone modelling. *Submitted to Journal of Hydrology*

subsequently performed for the estimation of uncertainty bounds on the model output. GLUE with the incorporation of prior information resulted in more and more realistic (closer to prior estimates) behavioural parameter sets available for the estimation of the uncertainty bounds. On top of that, uncertainty bounds better comprised the observations. Incorporating prior information in GLUE reduces the amount of model evaluations needed for the same amount of behavioural parameter sets. It is concluded that prior information is useful information in both SCE and GLUE parameter estimation strategies.

6.1. Introduction

Manual or automatic calibration (inverse modelling) aims at finding a parameter set ('effective' parameter set) that yields the best fit with the observations with respect to some goodness-of-fit criteria. This chapter presents two methods of incorporating soil hydraulic parameter estimates based on the soil core measurements from the laboratory as prior information in the estimation of effective parameters needed by the model. The relevance of including the prior information in the calibration is investigated.

As discussed in detail in Chapter 4, traditional methods of calibration of hydrological models have aimed at finding an optimal set of parameter values within some particular model structure. The limitations of the optimal parameter set concept have been discussed by *Beven and Binley (1992)* and *Beven (1993; 2001)*, who suggest that there may be many parameter sets that are equally acceptable in simulating the system, and that these may often come from very different regions in the parameter space. On top of that, different acceptable model structures may exist. Within these model structures, again different parameters sets exist that are equally acceptable. Given the observations available, there may be no rigorous basis for differentiating between these parameter sets. *Beven and Binley (1992)* introduce the term 'equifinality' to address the problem of existence of different parameter sets that result in a comparable model output. The most important implication of the 'equifinality' problem is hence the non-uniqueness of the solution found by the inverse modelling or calibration process.

One response to equifinality has been to seek and develop more robust optimisation algorithms. A large number of studies have been conducted that compare different optimisation algorithms for calibration of hydrological models [*e.g. Duan et al., 1992; Gan and Biftu, 1996; Cooper et al., 1997; Kuczera, 1997; Franchini et al., 1998; Thyer et al., 1999; Madsen et al., 2002*]. The main conclusion from these studies is that the global population-evolution based algorithms are more effective than multi-start local search procedures, which in turn perform better than pure local search methods. This study uses the SCE (Shuffled Complex Evolution) algorithm [*Duan et al., 1992*], described in detail in Chapter 4.

Another response to the equifinality problem is the GLUE (Generalized Likelihood Uncertainty Estimation) approach, discussed also briefly in Chapter 4. GLUE accepts that it may not be possible to distinguish between different parameter sets and aims at ranking the parameter sets based on some likelihood scale. In the GLUE approach it is believed that many parameter sets will be almost equally good. These parameter sets are classified as the so-called 'behavioural' parameter sets. Simulation results based on the 'behavioural' parameter sets are weighted according to their respective calculated likelihood values to form a cumulative distribution of predictions from which uncertainty quantiles can be calculated. The likelihood values correspond to a goodness-of-fit measure between the model output and the observations. Thousands of model realizations are generally necessary to characterize the parameter space adequately, while the results of each retained simulation must be stored to calculate the uncertainty bounds. GLUE hence requires considerable computing resources.

In this chapter, the measured soil moisture content profiles are again used as observed data. Using the MIKE-SHE hydrological modelling system [*Refsgaard and Storm, 1995*], numerical 1-D soil columns were set-up at 9 measurement locations along the middle hillslope transect (x = 10, cfr. Fig. 2.7). In the previous chapter, sensitivity analyses were carried out to identify the most important parameters that were subsequently incorporated in an inverse optimisation algorithm. At each location, a set of 11 'effective' parameters that yielded the best fit with the local soil moisture content observation was computed. Distributions of these 11 'effective' parameters over all locations were compared with the corresponding measured soil hydraulic parameters from undisturbed soil samples and in-situ single-ring pressure infiltrometer estimates.

Eight out of the 11 considered distributions of 'effective' and 'measured' parameters were found to be significantly different at a 5 % level and the study concluded that estimated parameters from soil cores or in-situ measurements does not correspond to the 'effective' parameter values resulting from model calibration. The objectives of this chapter are based on the conclusion of Chapter 5 [*Mertens et al, 2003a*]: (i) develop methodologies for incorporating prior information in two different effective parameter estimation strategies: SCE and GLUE, and (ii) investigate the relevance of this prior information in the calibration of soil hydraulic parameters.

6.2. Field layout, observations, numerical modelling and sensitivity analysis

The site description, field layout, observations as well as the MIKE-SHE model [*Refsgaard and Storm, 1995*] are presented in detail in Chapter 2. The same particular model set-up and studied output variables as described in Chapter 5 are used in this Chapter. As described in Chapter 5, a Monte Carlo based sensitivity analysis [*Spear and Hornberger, 1980; Madsen, 2000*] and a Morris's One-At-a-Time [*Morris, 1991*] design produced similar results and consequences for the incorporation of parameters in the SCE automatic calibration procedure. K_s, θ_s, θ_r, α and n of both horizons, and the depth d from the surface to the B-horizon were found to be important parameters, while model results were found to be insensitive to the value of N in the A- and B-horizon. Hence, the value of N in the A- and B-horizon was fixed to a value of 9.

6.3. Parameter estimation strategies: SCE and GLUE

Two methods for the incorporation of prior information in two different parameter estimation strategies (SCE and GLUE) are presented below. Both methods incorporate the same kind of prior information through the use of a joint probability distribution of the parameter estimates from the laboratory, marginal distributions as well as the measured correlation between them are incorporated. In the SCE algorithm, prior information is incorporated through the use of a penalty term in the objective function penalising deviations from the prior joint probability distribution. In the GLUE

algorithm, the measured joint probability distribution is used to generate the parameter sets evaluated.

6.3.1. Prior joint probability distribution

The first step in the development of a joint probability distribution [*Carsel and Parrish, 1988]* for the soil hydraulic parameters was to obtain the set of best fitting distributions that would adequately approximate the estimated distributions of the individual parameters of the laboratory measurements. For each parameter, a mathematical transformation was sought that would produce a normally distributed variable. The transformations applied to each of the measured parameter distributions were: $Y= X$, $Y = ln(X)$, $Y = 1/X$, $Y = X^2$, $Y =X^{0.5}$, $Y = X^{0.33}$. Additionally, the Johnson transformations [*Johnson and Kotz, 1970; Johnson, 1987; Carsel and Parrish, 1988*] were also applied: $Y = ln[(X- X_1) /(X_2-X)]$, $Y = sinh^{-1}[U]$, where $U = (X- X_1)/(X_2- X_1)$, *ln* denotes natural log, and X denotes an untransformed variable with limits of variation from X_1 to X_2 ($X_1<X< X_2$). In this study, X corresponds to K_s_A , θ_s_A, θ_r_A, α_A, n_A, K_s_B, θ_s_B, θ_r_B, α_B, n_B, and d as estimated from the laboratory and in-situ augering. For each parameter, all transformations were tested for their normality using a single sample two-sided Lilliefors hypothesis test of normality [*Conover, 1980*]. Let $S(Y)$ be the empirical cumulative distribution function (c.d.f.) estimated from the transformed measured parameter distributions $Y(X)$ and CDF be a normal c.d.f. with sample mean and standard deviation taken from $Y(X)$. The Kolgomorov-Smirnov test statistic (T) is:

$$T = max|S(Y) - CDF| \tag{6.1}$$

The transformations resulting in the smallest T-statistic were selected for all parameters and are shown in Table 6.1. Normal probability plots were also made to visually check the normality of the transformations. All selected transformations resulted in an acceptance of the null hypothesis that $Y(X)$ is normally distributed at a significance level of 0.05. After transformation, a normal distribution was fitted to the transformed distribution and the mean and variance were estimated (Table 6.1). Table 6.2 shows the correlations between the transformed parameters that were estimated from the undisturbed soil samples. Comparing the absolute values of correlations observed in this

study with values found in the literature reveals that they are similar [*Meyer et al., 1997; Mallants et al., 1996*].

The multivariate normal distribution is characterized in terms of marginal distribution means and variances and pair-wise covariances in the form of a covariance matrix. For more details about multivariate normal distributions, the reader is referred to Appendix A and the statistical handbook 'Applied Multivariate Statistical Analysis' by *Johnson and Wichern, 1992*. The *p*-dimensional normal density $N_p(\mu, \Sigma)$ for the random vector $Y = [y_1, y_2, \ldots, y_p]'$ can be written as:

$$f(Y) = \frac{1}{(2\pi)^{p/2}|\Sigma|^{1/2}} \exp\left[-(Y-\mu)^T \Sigma^{-1}(Y-\mu)/2\right] \qquad (6.2)$$

where p is the number of variables and the elements of Y ($-\infty < y_i < +\infty$) are random variables with mean μ and variance-covariance matrix Σ; $|\Sigma|$ denotes the determinant of the variance-covariance matrix Σ.

Table 6.1 Mean and standard deviation of the considered soil hydraulic parameters as estimated from laboratory measurements, the transformation applied and the corresponding normal distribution $N(\mu,\sigma)$ after transformation

Parameter	Estimated Mean	Estimated St. Dev.	Transformation Type	Transformation Normal Distribution after Transformation
K_s_A (ms^{-1})	9.74E-06	1.78E-05	Y = ln(X)	N(-13.17, 2.03)
θ_s_A (-)	0.4	0.02	Y= X	N(0.40, 0.02)
θ_r_A (-)	0.02	0.03	$Y = X^{0.33}$	N(0.23,0.14)
α_A (m^{-1})	1.95	1.19	Y = ln(X)	N(0.49,0.61)
n_A(-)	1.3	0.1	Y = 1/X	N(0.77,0.05)
K_s_B (ms^{-1})	1.57E-05	2.63E-05	Y = ln(X)	N(-12.95, 2.94)
θ_s_B (-)	0.39	0.03	Y= X	N(0.39, 0.03)
θ_r_B (-)	0.05	0.03	Y= X	N(0.05, 0.03)
α_B (m^{-1})	1.87	1.54	Y = ln(X)	N(0.28,0.86)
n_B(-)	1.44	0.21	Y = 1/X	N(0.70,0.09)
d(m)	0.76	0.48	Y = ln(X)	N(-4.69,6.43)

It is assumed that A- and B-horizon parameters are independent and that *d* is independent of both the A- and B-horizon parameters. Random deviates from a correlated multivariate normal distribution are obtained by first generating a vector *Z* of independent standard normal deviates and then applying a linear transformation of the form:

$$Y = \mu + S^T Z \tag{6.3}$$

where μ represents the vector of means, *Z* is a vector of standard normal variables and *S* is the lower triangular (Choleski) decomposition of Σ, such that $\Sigma = S^T S$. This joint probability distribution is considered as prior information in both the GLUE and the SCE algorithms.

Table 6.2 Correlations between the transformed parameters (i.e. to normal distribution) estimated from the undisturbed soil samples

	K_s_A (ms^{-1})	θ_s_A (-)	θ_r_A (-)	α_A (m^{-1})	n_A(-)
K_s_A (ms^{-1})	1.00				
θ_s_A (-)	0.37	1.00			
θ_r_A (-)	-0.41	-0.47	1.00		
α_A (m^{-1})	0.21	0.52	-0.49	1.00	
n_A(-)	0.26	0.05	-0.36	0.59	1.00
	K_s_B (ms^{-1})	θ_s_B (-)	θ_r_B (-)	α_B (m^{-1})	n_B(-)
K_s_B (ms^{-1})	1.00				
θ_s_B (-)	0.61	1.00			
θ_r_B (-)	-0.19	-0.11	1.00		
α_B (m^{-1})	0.68	0.45	-0.46	1.00	
n_B(-)	-0.29	0.10	-0.36	-0.03	1.00

6.3.2. SCE optimisation algorithm

For a detailed description of the SCE algorithm, the reader is referred to Chapter 4. The SCE algorithm was applied for 9 locations along the x = 10 transect (cfr. Fig. 2.7), with

and without the incorporation of the prior information. In addition, SCE optimisations were carried out using the mean daily-observed moisture content over all 25 locations in the calculation of the objective function. The stopping criteria for the SCE optimisation routine were either (i) improvement of the objective function less than 0.1% within 5 loops, or (ii) a maximum number of model evaluations of 2000.

In case no prior information is incorporated, the objective function (F_1) is chosen to be equal to the total RMSE and the parameter optimisation bounds are taken from literature for a sandy loam [*Meyer et al., 1997*] for both A- and B-horizon parameters. As shown in Table 6.3, these parameter bounds from literature are very wide, and for almost all parameters much wider than the estimated lower and upper parameter values from the laboratory measurements (after deletion of outliers). For the *d*-parameter, the bounds are estimated from the in-situ measurements and are allowed to vary only between 0 and 1 meter (most of measurements within this range, except for few outliers). The same parameter bounds are used when prior information is included. The prior information is incorporated by including a penalty term in the objective function:

$$F_2 = \sqrt{(P-\mu)\Sigma^{-1}(P-\mu)^T} \tag{6.4}$$

where P is a vector containing the evaluated transformed parameters. This function penalises deviations from the average measured (transformed) parameters and weights this penalty by the measured transformed covariance matrix. The weighting using this covariance matrix relates the difference between the evaluated and the prior parameter to the variance of that parameter as well as the covariance (correlation) with other parameters.

Since the objective function is now made up of two objectives (F_1 and F_2), we are dealing with a multi-objective calibration problem. In this case, objective F_1 evaluates the goodness-of-fit of the model and the other objective F_2 evaluates the deviations of the evaluated parameter set from the prior information. The result of a multi-objective calibration is not a single unique set of parameters but will consist of the so-called 'Pareto set' of solutions [*Gupta et al., 1998; Madsen, 2003*]. In the simplest case of two objectives as is the case here, points on the Pareto front have the characteristic that no

other points have both a smaller value of F_1 and a smaller value of F_2. This Pareto front corresponds to the trade-offs between the different objectives, i.e. a point on the Pareto front having a better fit to the observations (lower RMSE) will have relative large deviations from the prior information.

Table 6.3 Lower and upper bounds from literature [Meyer et al. 1997] and bounds estimated from laboratory measurements after deletion of outliers (= estimated parameter value outside literature range)*

	Meyer et al. 1997		Laboratory estimates			
Parameter	Lower bound	Upper bound	Lower bound (A)	Upper bound (A)	Lower bound (B)	Upper bound (B)
K_s (ms^{-1})	7.10E-10	7.80E-05	6.97E-08	5.85E-05	3.79E-08	0.0001465*
θ_s (-)	0.23	0.59	0.3599	0.4315	0.3458	0.4375
θ_r (-)	0.0173	0.102	0.0001132*	0.1034*	0.01041*	0.09482
α (m^{-1})	0.11	20.2	0.597	4.445	0.3263	5.384
d(m)					0.12	2.24

The multi-objective calibration problem is solved by aggregation of the two objectives into one measure. To compensate for differences in magnitude between the RMSE term and the penalty term, the two objectives are transformed to a common distance scale [*Madsen, 2003*]. From the initial population in the SCE algorithm, the transformation functions are deducted. Both objective functions are first normalised and then transformed to having the same distance from the origin to the optimum of the initial sample. The transformation function is given by:

$$g_i(F_i) = \frac{F_i}{\sigma_i} + \varepsilon_i \qquad , i = 1, 2 \tag{6.5}$$

where F_i is the objective function of the i-th objective, σ_i is the standard deviation of the i-th objective function of the initial sample, and ε_i is a transformation constant given by:

$$\varepsilon_i = \max\left\{\min\left\{\frac{F_j}{\sigma_j}\right\}, j = 1,2\right\} - \min\left\{\frac{F_i}{\sigma_i}\right\} \tag{6.6}$$

The aggregated objective function is given by:

$$F_{agg} = \omega g_1(F_1) + (1-\omega) g_2(F_2) \tag{6.7}$$

where ω is a weighting factor. If ω = 0.5 both objectives are given the same weight and the SCE optimisation provides a balanced optimum [*Madsen, 2003*]. In this study, the Pareto front is calculated by performing several individual SCE optimisations using different weights ($0 \leq \omega \leq 1$).

6.3.3. GLUE analysis

The GLUE procedure basically has three requirements: a sampling range must be specified for each parameter considered, a sampling methodology for the parameter space must be developed, and a likelihood measure has to be defined such that a better model response results in a higher value for the likelihood measure. In this study, the GLUE methodology is performed using two different sampling strategies. The first strategy is a GLUE analysis without prior information that uses a Monte Carlo analysis with uniform random sampling using the lower and upper parameter bounds for a sandy loam soil type from literature. In the second strategy the GLUE analysis incorporates the laboratory measurements as prior information in the Monte Carlo analysis by sampling the parameter sets to be evaluated from their joint probability distribution. Hence, not only the marginal distributions of the measured parameters are incorporated, but also the correlation between the measured parameters is taken into account. In both GLUE analyses, the average of the daily-observed moisture content over all 25 locations for each respective depth is used in the calculation of the objective function. To be consistent with the SCE analysis, the total RMSE is also taken as objective function in both GLUE analyses.

As likelihood measure (L), the inverse of the Mean Squared Error (MSE) is chosen:

$$L = \frac{1}{MSE} = \frac{1}{RMSE^2} \tag{6.8}$$

Choosing the inverse of the MSE and not the inverse of the RMSE gives relatively more weight to the best parameter sets. The likelihood measure is assigned to the behavioural parameter sets with RMSE smaller than a certain defined cut-off value. The likelihoods are rescaled so their sum equals one, and these rescaled likelihoods are then multiplied with their corresponding daily-simulated water content to form a cumulative distribution of daily soil moisture contents from which uncertainty quantiles can be calculated.

6.4. Results and Discussion

6.4.1. Direct use of prior information

As discussed in Chapter 5, effective parameters differ from their measured equivalents (cfr. Fig. 5.6). It was also investigated how much worse model fits are obtained when using the measured parameter values rather than their effective equivalents. Conclusion was that the measured laboratory parameters are not capable of simulating a reasonable fit to observed moisture content observations in the field and hence the measured laboratory parameters are useless as direct information in the model. The following paragraphs investigate how and whether it is relevant to incorporate this prior information in parameter estimation.

6.4.2. Including prior information in the SCE optimisation algorithm

The estimated Pareto front for the location x = 10, y = 2 is presented in Fig. 6.1. In the multi-objective framework as it is applied within this study, three 'key' points on the Pareto front can be easily deducted. The first point is the result of the SCE optimisation without prior information corresponding to using a weight of zero to the penalty term (or $\omega = 1$) in the objective function Eq. 6.7. The second point or the balanced optimum is the result of the SCE optimisation with the incorporation of prior information and using equal weights (or $\omega = 0.5$) for both objective terms. The third point is the result

of a model run with the prior mean transformed parameters as input parameters. This model run results in a penalty function of zero. These three Pareto key points are indicated on Fig. 6.1 as triangles. The other points of the Pareto front are shown on Fig. 6.1 as circles were the result of SCE optimisations using different weights for both objective functions. Four additional SCE optimisation were carried out with ω = 0.2, 0.33, 0.66, and 0.8. Hence, for the estimation of the Full Pareto front a total of 6 SCE optimisations or a 12000 model evaluations are performed.

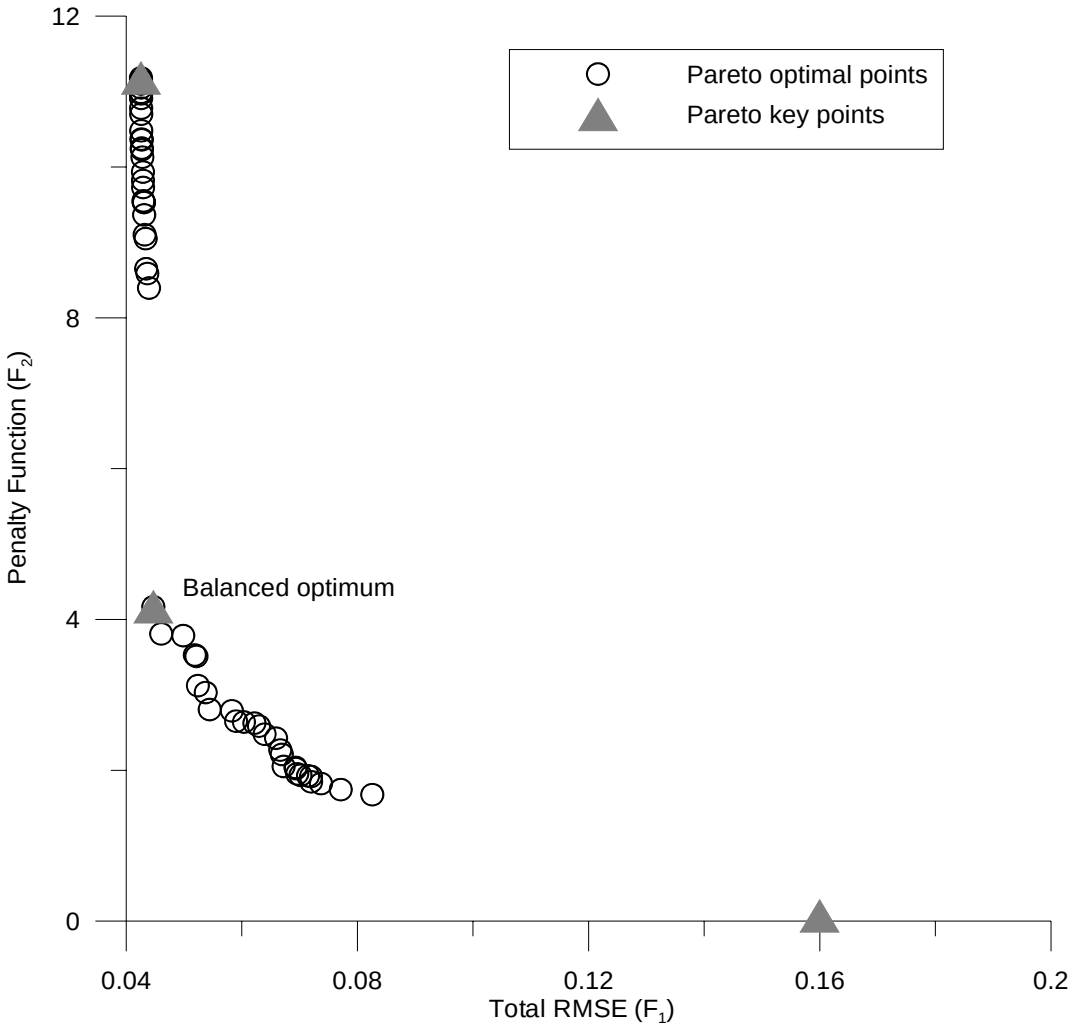

Figure 6.1 Estimated Pareto front for the location x = 10, y = 2 indicating the trade-off between goodness-of-fit to the observations (Total RMSE) and deviations from the prior measured parameters (Penalty Function)

The three key points are important because they determine the shape of the Pareto front. Therefore, they were calculated for all 9 locations along the transect and are shown in Fig. 6.2. It is the shape of the Pareto front that reveals the importance of the trade-off between the goodness-of-fit to the observations and the deviations from the prior information. The sharp Pareto front observed for all locations, indicates a significant trade-off between goodness-of-fit to the observations and deviations from the prior information. However, the sharp structure of the front reveals that including prior information provides only a minor decrease of the goodness-of-fit to the observations and an effective parameter set much closer to the prior parameters.

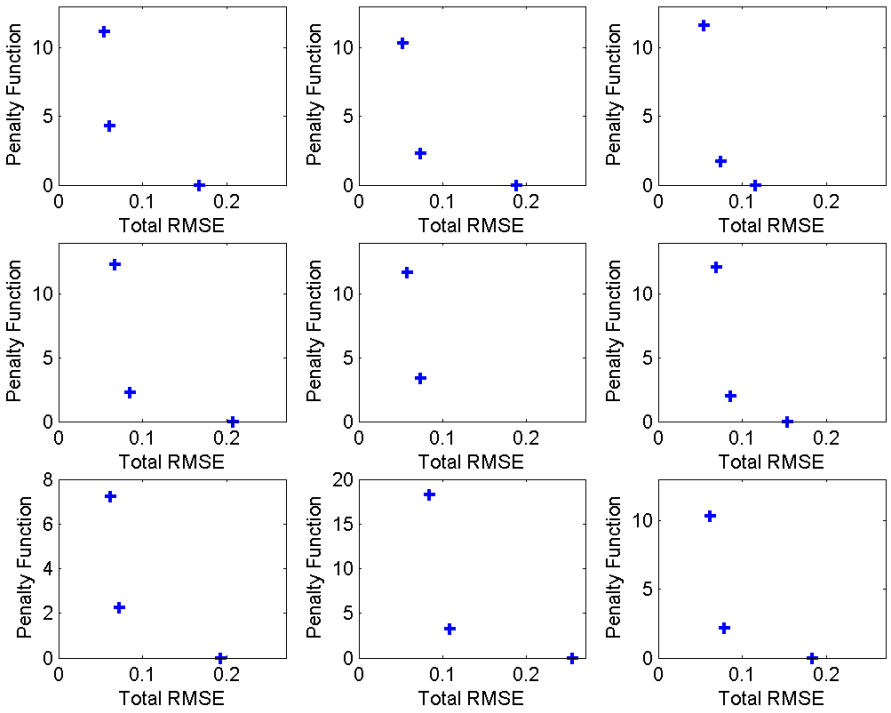

Figure 6.2 Estimated Pareto key points for all 9 locations along the transect $x = 10$

Figure 6.3 presents the cumulative distributions of the A-horizon parameters of the 9 'effective' parameter sets (along the transect) obtained from the SCE optimisations with (balanced optimum) and without incorporating prior information and the cumulative distribution of the prior information. As was expected, incorporating prior information through the use of a penalty term is successful in narrowing the gap between effective

parameters and prior information (except for α_A). Effective distributions from a SCE with the incorporation of prior information show a much smaller parameter range or variance than effective parameters resulting from SCE without prior information. Same conclusions hold for the B-horizon parameters.

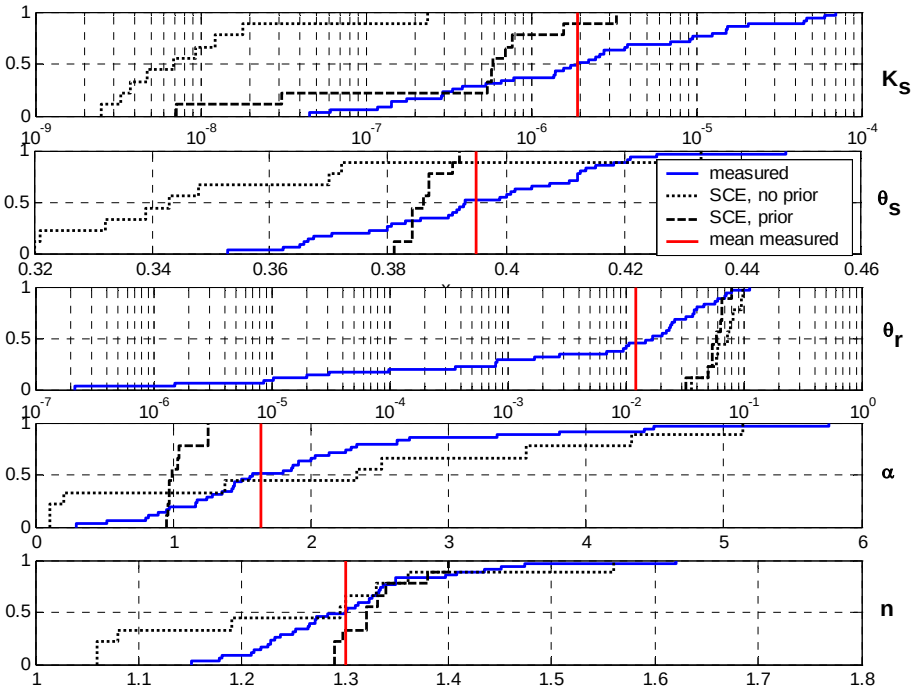

Figure 6.3 Cumulative distributions of the 9 'effective' parameter sets (along the transect) obtained from the SCE optimizations with and without incorporating prior information and the cumulative distribution of the prior information for the A-horizon

Figure 6.4 shows the simulated moisture content as a result from SCE with and without prior information and the measured moisture content at the location x = 10, y = 2 for the year 2001 at all depths. Although a slightly higher RMSE is calculated for the SCE optimisation with the prior information incorporated, differences in simulated moisture content as a result from SCE optimisation with and without prior information are small. Small differences in simulated moisture content are observed over all 9 locations.

From this, it can be concluded that including prior information in the SCE algorithm is useful: effective parameter sets are obtained close to the measured prior information

which have a comparable goodness-of-fit to the observations than the effective parameter sets resulting from a SCE optimisation without prior information (very sharp Pareto front). These parameter sets are believed to be more realistic as they are the result of an inverse modelling that combines in-situ soil moisture content observations and measured parameters in the laboratory.

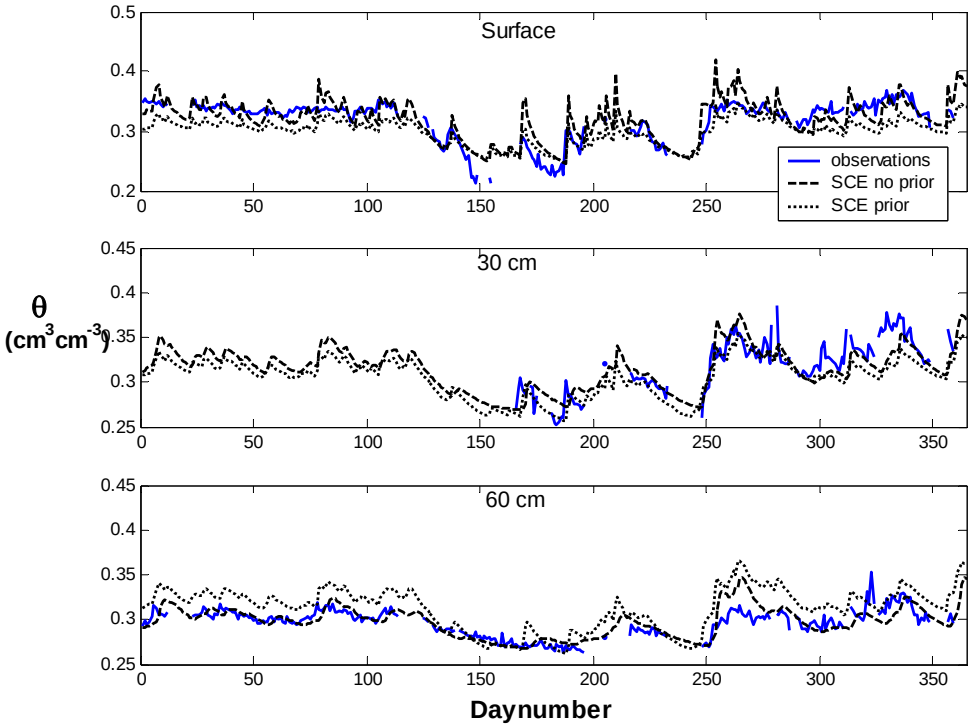

Figure 6.4 Simulated moisture content as a result from SCE with and without prior information and the measured moisture content at the location x = 10, y = 2 for the year 2001 at all depths

6.4.3. Model validation

As discussed in Chapter 4, it has been common practice to use as much data as available for the calibration, after setting aside part of the data set for verification. This is often referred to as a 'split sample' test. In this calibration, only soil moisture measurements of the year 2001 were used. Hence, the soil moisture measurements from 1 January till 29 July 2002 are available for our verification or validation of the model. The model verification was only performed for the 9 locations along the middle transect (x = 10).

Simulated moisture content using the effective parameters from the SCE with and without prior information is shown in Fig. 6.5 for both the calibration and the validation period at the location x = 10, y = 10. The same figures for each of the 9 locations along the x = 10 transect, are shown in Appendix B. Figure 6.6 shows the Pareto key points for all 9 locations for the calibration, validation and the total period (calibration + validation).

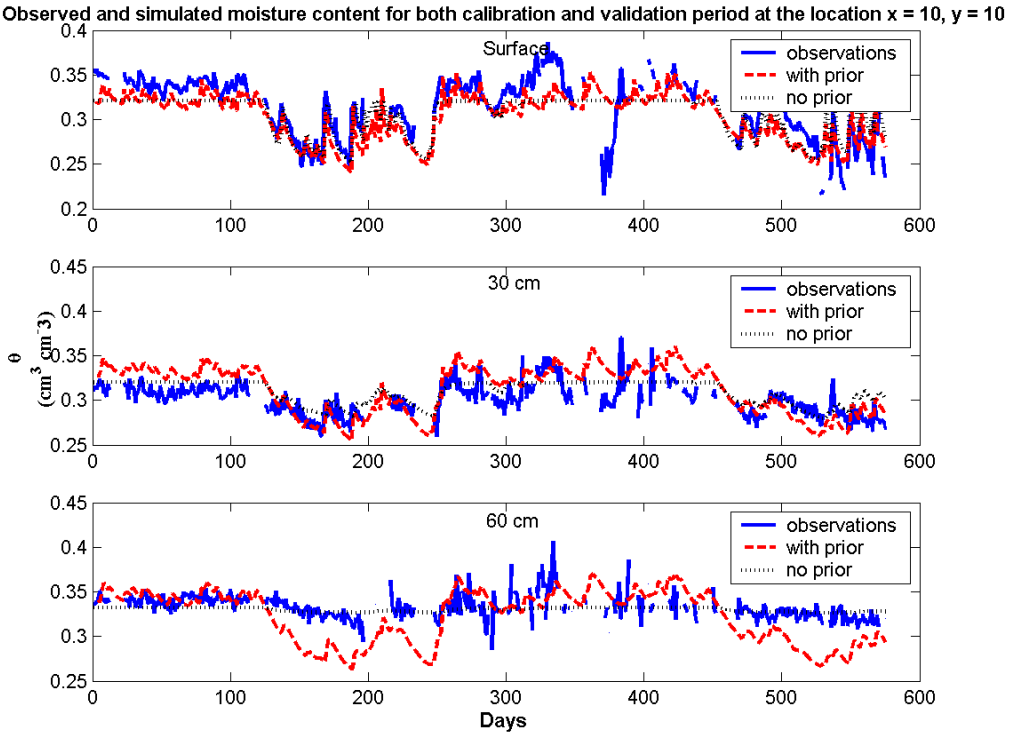

Figure 6.5 Simulated moisture content at three different depths using the effective parameters from the SCE with and without prior information for both the calibration and the validation period at the location x = 10, y = 10

As shown in Fig. 6.6, differences between RMSE of the calibration and the validation period are very small. Therefore, it can be concluded that the model behaves well during the validation period (cfr. figures in Appendix B). As expected, RMSE values of the validation period are higher that the RMSE values obtained for the calibration period, though only slightly. The RMSE values of the total period are hence found in between the RMSE of the calibration and validation for all locations. This is true both for model

simulations using the effective parameters obtained with and without the prior information.

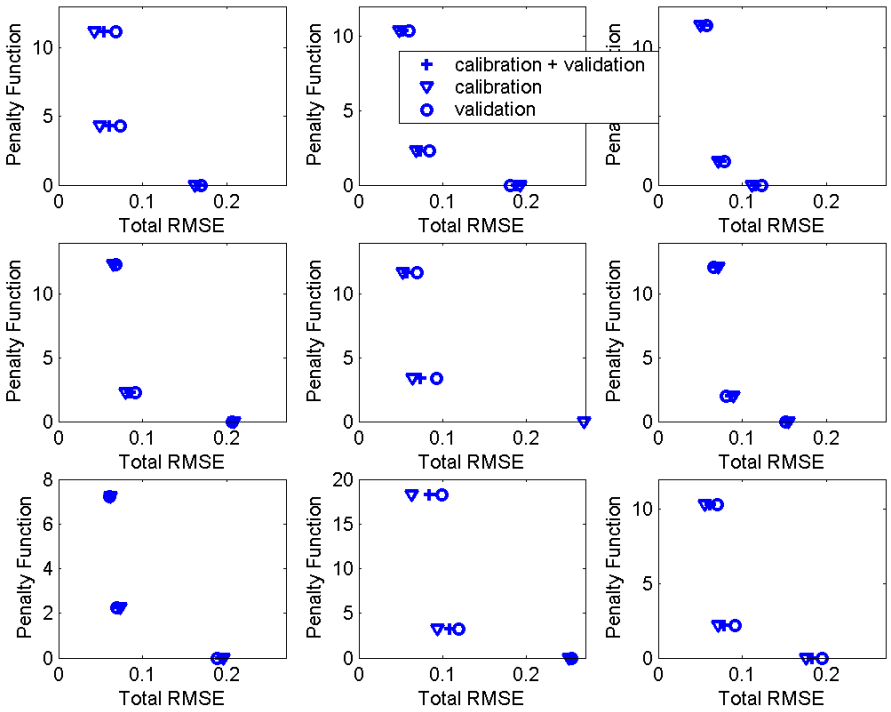

Figure 6.6 Pareto key points for all 9 locations for the calibration, validation and the total period (calibration + validation).

During the calibration period (Fig. 6.2), the effective parameters with the incorporation of the prior information resulted in slightly higher RMSE values than the model simulations using the effective parameters obtained without the incorporation of prior information. As shown in Fig. 6.6, the same is true for the validation period. Although slightly higher RMSE values are found using the effective parameters with the prior, the dynamics of the model simulations for most locations seem better (cfr. Appendix B). For example, the dynamics of the soil moisture content at all depths for the location x = 10, y = 10 shown in Fig. 6.5 are represented better with the prior than without the prior information. In the case without the prior information, no dynamics at all are observed during the winter period. During winter, moisture content is fixed at field capacity and no dynamic variability is simulated. This is also reflected in Fig. 6.7 where simulated

versus observed moisture content is plotted for surface simulation at the location x = 10, y = 10. A straight line is observed at θ_{sim} = 0.34 for the case with the prior. The increase in dynamics is a result of the higher effective conductivities obtained when incorporating prior information in the objective function.

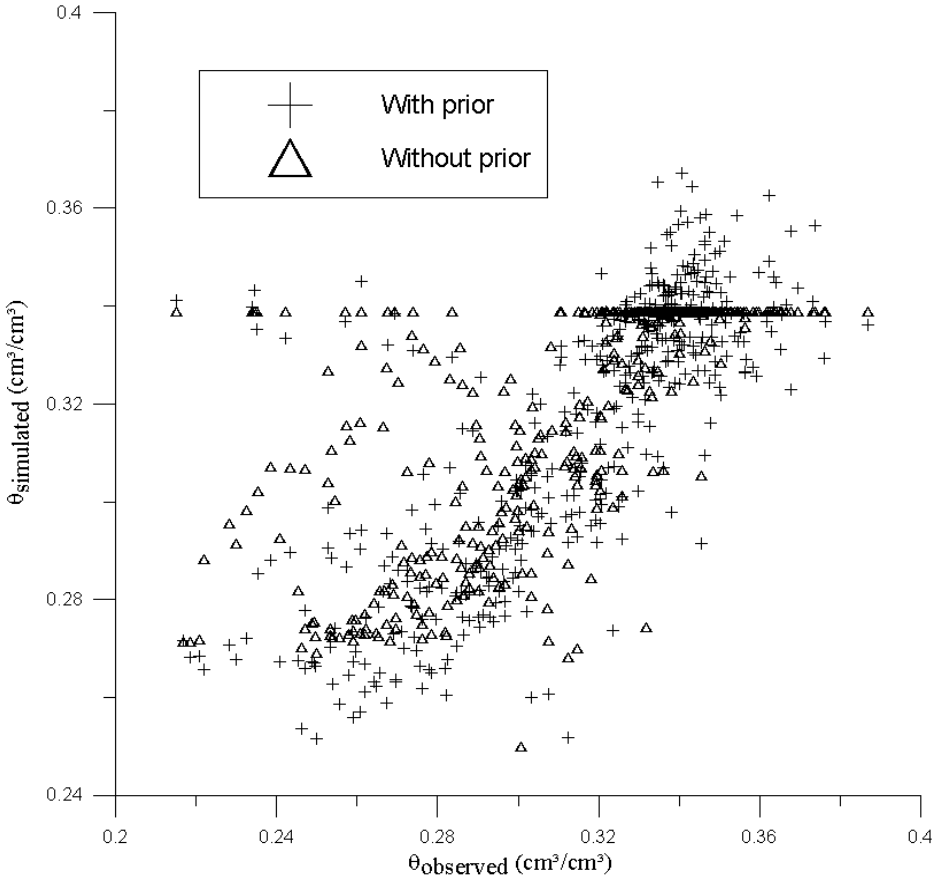

Figure 6.7 Simulated versus observed moisture content for the surface simulation using both effective parameters obtained with and without prior information at x = 10, y = 10

6.4.4. GLUE analysis

In the Generalized Likelihood Uncertainty Estimation (GLUE) analysis, 20000 parameter sets were generated. The parameter sets were ranked according to their objective function (total RMSE). The most difficult and important choice to be made in the GLUE approach is the 'cut-off-value'. This is the value that separates the parameter

sets into' behavioural' and 'non-behavioural'. As explained below, the choice of this value has a significant impact on the calculated uncertainty bounds. Although no rules exist for the choice of this value, it was chosen with respect to the goodness-of-fit of the 'worst' behavioural parameter set. Simulated moisture content using the worst 'behavioural' parameter set was plotted against the mean measured moisture content. On the basis of this graph, acceptable goodness-of-fit was decided on and resulted in a cut-off value of 0.05 (i.e. behavioural parameter set if total RMSE < 0.05). In interpreting results from a GLUE analysis, one should always be aware of the sampling issue: it is hard to find out whether the parameter space has been sampled sufficiently.

Table 6.4 Minimum total RMSE and amount of behavioural parameter sets of the GLUE analysis with and without prior information; minimum total RMSE of an SCE optimisation without prior information and the balanced optimum RMSE value of the SCE with prior information (both against average moisture content)

	GLUE with prior	GLUE without prior	SCE with prior (Bal.Opt.)	SCE without prior
Minimal total RMSE	0.039	0.041	0.047	0.038
# Behavioural parameter sets	68	17	/	/

In Table 6.4, the total RMSE of the best parameter set of the GLUE with and without prior information are presented as well as the minimum total RMSE of an SCE optimisation without prior information and the balanced optimum RMSE value of the SCE with prior information (both against average moisture content). The total RMSE of the behavioural GLUE parameter sets (total RMSE < 0.05) is close to the total RMSE of the SCE optima. This may be an indication that the parameter space was sufficiently sampled by the GLUE analysis but it is no guarantee at all. Rather than to investigate if the parameter space has been sampled sufficiently, the study aims at comparing the results of the GLUE analyses with and without prior information for the same number of model evaluations. Table 6.4 shows that including prior information in the GLUE analysis increases the amount of behavioural parameter sets from 17 to 68 using the same cut-off value in both analyses. Minimum RMSE is also lower in the GLUE analysis with prior.

Cumulative distributions of the behavioural parameter sets from the GLUE with and without prior information and the cumulative distribution of the prior information for the A-horizon parameters are compared in Fig. 6.8. As expected, the behavioural parameter sets obtained as a result of a GLUE with prior information, are much closer to the measured prior information. The same is true for the B-horizon parameters.

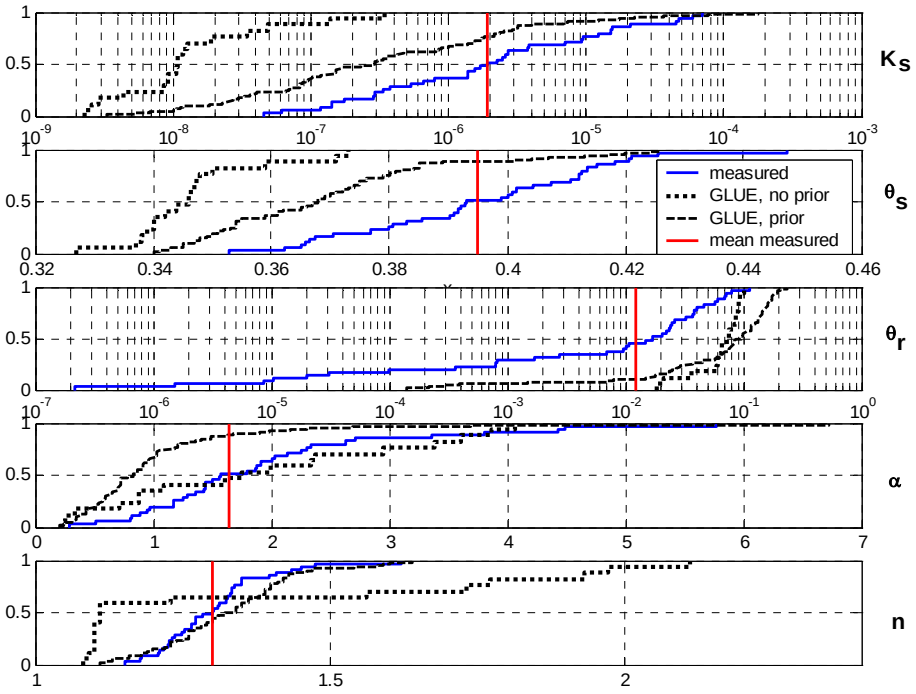

Figure 6.8 Cumulative distributions of the behavioural parameter sets obtained in the GLUE analysis with and without incorporating prior information and the cumulative distribution of the prior information for the A-horizon

Figure 6.9 shows the goodness-of-fit to the observations (Total RMSE) and deviations from the prior measured parameters (Penalty Function) of the behavioural parameter sets from the GLUE analysis with and without prior information. The Pareto key points and the balanced optimum of the SCE optimisations against mean observed moisture content are also shown in Fig. 6.9. As expected, it shows that the penalty calculated for the behavioural parameters in the GLUE analysis with prior information is smaller than without the prior information. The SCE balanced optimum has a lower penalty term and a slightly higher RMSE value than the behavioural parameter sets from both GLUE analyses. SCE without the penalty results succeeds in finding the best model fit.

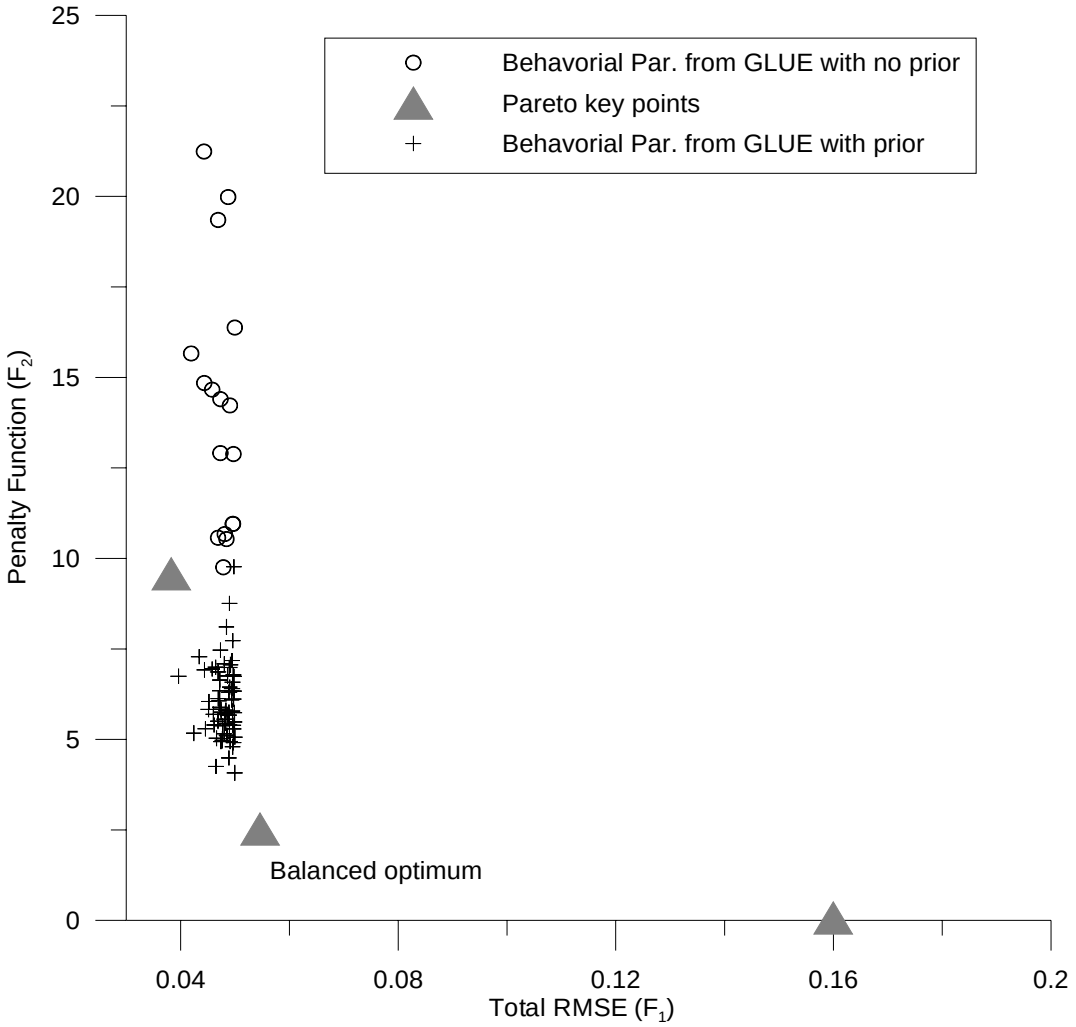

Figure 6.9 Goodness-of-fit to the observations (Total RMSE) and deviations from the prior measured parameters (Penalty Function) of the behavioural parameter sets from the GLUE analysis with and without prior information for the average moisture content, Pareto key points and balanced optimum of the SCE optimisations against mean observed moisture content are also indicated

In Fig. 6.10, the mean observed moisture content over all 25 locations and the 95 % uncertainty bounds (UB) of the GLUE with and without prior information are plotted. Important to remark is that these uncertainty bounds are very sensitivity to the choice of the cut-off value. Allowing more behavioural parameters, i.e. increasing the cut-off RMSE value, results in wider uncertainty bounds and vice versa. Also the choice of the likelihood measure has an influence on the width of these bounds but its effect in this case was found to be less pronounced than the choice of the cut-off value. Since it is our objective to investigate the relevance of incorporating prior information in the GLUE

analysis, the absolute widths of these UB are of less importance than the difference between the UB resulting from GLUE with and without prior information. Uncertainty bounds for the soil moisture content at the surface when no prior information is incorporated do not always include the mean observations during the first half of the year and for short periods at the end of the year. Including prior information widens the UB all over the year so that it includes the mean observed soil moisture content. On the other hand, including prior information narrows the UB for the soil moisture content at 30 and 60 cm depth, although they still contain the mean moisture content over the year. Hence, incorporating prior information through the use of a joint probability distribution in a GLUE analysis is useful as it (i) increases the amount of behavioural parameter sets the UB are estimated from and (ii) the UB better comprise the observed data.

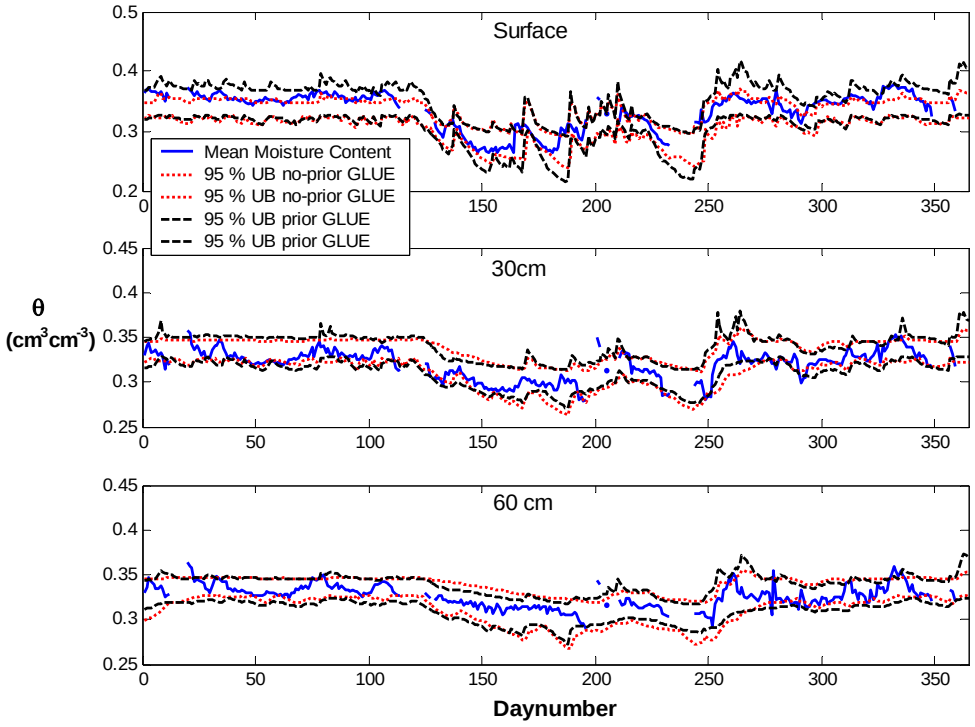

Figure 6.10 Mean observed moisture content over all 25 locations, 95% uncertainty bounds corresponding to a GLUE analyses with and without prior information at the different depths

The prior joint probability density distribution incorporates the correlation between the parameters. To investigate the importance of correlation, a GLUE analysis was

performed in which the measured parameter distributions were incorporated but correlation between parameters was not taken into account. This analysis resulted in 25 behavioural parameter sets and a minimum RMSE of 0.0424. The amount of behavioural parameter sets in this analysis is hence between the GLUE analysis with and without prior information (Table 6.4) while the minimum RMSE is slightly higher than the GLUE without prior information. The UB resulting from this GLUE analysis comprise the observed data in the beginning of the year 2001 only partly. Hence, correlations between the parameters seem to be valuable information when incorporating prior information into a GLUE analysis. As explained in chapter 4, only parameter uncertainty is taken into account in the estimation of the uncertainty bounds. In *Willems (2000),* it is found that input uncertainty of rainfall can take up to 40 or 50 % of the total uncertainty on the amount of runoff simulated using a conceptual rainfall-runoff model. In Chapter 7, it is shown that the temporal resolution of rainfall used for the simulation of daily moisture content as done in this study, is not very important (cfr. 7.4.5). Therefore, it is believed that in this study, input uncertainty of rainfall will be much smaller than 40 or 50 % of the total uncertainty on the daily moisture content simulations.

It is shown that a GLUE analysis sampling from a prior joint probability distribution has two major advantages: (i) it increases the amount of behavioural parameter sets the uncertainty bounds are estimated from and (ii) the uncertainty bounds better comprise the observed data. Both advantages refer to the sampling issue. If more model evaluations were performed for the GLUE analysis without prior information, similar results would be obtained In this case, the interesting question is how many more model runs would be needed by the GLUE without prior information to provide similar results? This would give us an idea about the gain of using prior information. If computer time would be free, incorporating prior information in a GLUE analysis would not seem beneficial because a large number of model evaluations could be performed. Although computer time has become cheaper and cheaper over the years, a GLUE analysis is still very expensive with respect to computer time. Hence, incorporating prior information in a GLUE analysis is worthwhile as more behavioural parameter sets are achieved with the same number of model evaluations. On top of that, behavioural parameter sets are more realistic in terms of measured parameters.

6.5. Conclusions

Measured soil moisture contents for the year 2001 at three different depths (surface, 30 and 60 cm) on a hillslope were used as observations for the estimation of effective soil hydraulic parameters for the *Richards' (1931)* equation. Prior parameter estimations available from laboratory measurements were used in the development of a joint probability distribution. The study presented the incorporation of this joint probability distribution as prior information in an SCE optimisation and a GLUE analysis.

The SCE algorithm was adopted for the optimisation of the UZ soil parameters in the MIKE-SHE model. At 9 locations along the middle transect of the hillslope, the SCE algorithm was applied with and without the incorporation of prior information. Including prior information in the SCE algorithm was realized by including a penalty term as a second objective function that accounts for the deviation of an evaluated parameter set from the measured prior parameters. A very sharp Pareto front was found for all locations. This means that incorporating prior information in the SCE algorithm can be achieved by relaxing only slightly on the goodness-of-fit to the observations. Effective parameter sets resulting from the SCE with prior information, are more reliable with respect to the prior information and hence may be more physically feasible to the field conditions than effective parameter sets from a SCE optimisation without prior information. An SCE optimisation with the incorporation of prior information as outlined in this work, efficiently utilizes all relevant information from different measurements, i.e. soil moisture content observations and parameter measurements.

The validation of the model was proven successful as differences between RMSE of the calibration and the validation period are very small. This is true both for model simulations using the effective parameters obtained with and without the prior information. Similar to the calibration period, the effective parameters with the incorporation of the prior information resulted in only slightly higher RMSE values than the model simulations using the effective parameters obtained without the incorporation of prior information. Although slightly higher RMSE values are found using the effective parameters with the prior, the dynamics of the soil moisture content at all depths are represented better with the prior than without the prior information. The

increase in dynamics is a result of the higher effective conductivities obtained when incorporating prior information in the objective function.

A GLUE analysis using a uniform random sampling strategy across the specified parameter range from literature and a GLUE analysis using the joint probability distribution of the measured laboratory parameters were compared. Including prior information into a GLUE analysis was found to be useful because (i) more parameters sets are classified as behavioural and hence are available for the estimation of the uncertainty bounds and (ii) the uncertainty bounds comprise the observed data better. On top of that, behavioural parameter sets are more physically feasible as they are much closer to measured parameters. Both, the prior measured parameter distributions as well as the correlation amongst parameters were found to be useful and beneficial to include in the GLUE analysis. The main advantage of including prior information in a GLUE analysis is a question about sampling. If computer time was not an issue, a GLUE analysis without prior information would be able to give comparable results to a GLUE with prior information in terms of uncertainty bounds and model predictions. Incorporating prior information in a GLUE analysis can reduce the amount of model evaluations needed for the same amount of behavioural parameter sets.

From the previous chapter, it could be questioned why measure parameters if they differ from the ‘effective’ parameters anyway? It showed that effective parameters differ from the measured ones when doing a ‘blind’ optimisation, i.e. an inverse modelling with wide literature parameter bounds. This Chapter reveals that although the measured parameters are different from the effective ones resulting from a ‘blind’ optimisation, they are still useful as prior information in both an SCE and GLUE analyses as explained above.

Chapter 7

The effect of the rainfall time scale on effective soil parameters*

Abstract

Hydrological modelling often implies the use of rainfall data. Its quality and resolution directly affect the accuracy of the simulation results. This Chapter illustrates how a simple approach of incorporating rainfall intensity information in daily rainfall records significantly improves the simulation of surface runoff. The procedure is developed using a frequency analysis on rainfall data of the Royal Meteorological Institute of Belgium, collected with a resolution of 10-minutes and for a consecutive period of 61 years. The frequency analysis of the data allowed the incorporation of rainfall intensity information into daily rainfall records. A hillslope rainfall-runoff model was set-up and daily runoff simulated for the year 1988 using different temporal rainfall resolutions: 10 minutes observed rainfall data, daily observed rainfall data and disaggregated daily rainfall data. The daily rainfall data were disaggregated to minute rainfall data using a procedure based on a frequency analysis. Hydraulic soil parameters were randomly selected and daily runoff was simulated using the 10-minute observed rainfall data (= reference runoff). The use of daily rainfall data resulted in an annual runoff close to zero because the rainfall is spread out uniformly over 24 hours. Cumulative daily runoff using disaggregated rainfall data closely follows the reference runoff throughout the year. A Morris sensitivity analysis showed that the generation of runoff on a hillslope is highly sensitive to the value of the saturated hydraulic conductivity (K_s). Effective K_s was estimated using the Shuffled Complex Evolution optimisation algorithm with as

---

*Adapted from Mertens, J., Raes, D., Feyen, J., 2002. Incorporating rainfall intensity into daily rainfall records for simulating runoff and infiltration into soil profiles. *Hydrological Processes*, 16, 731-739

objective the closest possible fit to the reference runoff. Effective K_s using daily rainfall is only 2/3 of the K_s used for the generation of the reference runoff while effective K_s using disaggregated rainfall coincides with the reference K_s. The disaggregation procedure results in higher model efficiencies and more realistic effective parameters than the case where daily rainfall records are used.

7.1. Introduction

In the previous Chapters, research was focused on the estimation of effective soil hydraulic parameters and its effect on model results. No attention was given to the importance of the quality of the climatological input data (in our case: rain and potential evapotranspiration series). These input data determine the accuracy with which processes can be simulated. A large number of studies have been carried out to quantify the difference in simulation results by using different potential evapotranspiration calculation methods [*Choisnel et al., 1992; Xu and Singh, 1998; Beyazgül et al., 2000; Xu and Singh, 2000; Kite and Droogers, 2000; Xu and Singh, 2001*]. From all these studies it can be concluded that large differences exist between the different potential evapotranspiration estimation strategies. Since the evapotranspiration process plays a dominant role in infiltration and runoff, the choice of the potential evapotranspiration strategy is likely to have a significant effect on model simulation results. Very little research has been carried out trying to estimate the effect of different potential evapotranspiration methods on effective model parameters [*Vazquez and Feyen, 2003*]. In this study, only daily minimum and maximum temperatures were measured and used to estimate potential evapotranspiration [*Allen et al., 1998*]. It is hence impossible to investigate the effect of different potential evapotranspiration estimation strategies since they generally require more data as wind speed, sunshine duration, humidity, etc. Therefore this study is limited to the effect of the temporal resolution of rainfall records on model simulations and effective parameters.

In this respect, models that disaggregate input rainfall data into a sequence of individual storms of a finer time scale are very useful [*Gyasi-Agyei, 1999*]. Former research on this subject [*Richardson and Wright, 1984; Hersenhorn and Woolhiser, 1987; Econopouly, 1987; Kihupi, 1990; de Lima and Grasman, 1999; Gyasi-Agyei, 1999*] has in common

that sophisticated statistical techniques are used in the disaggregation procedure. Since these authors are interested in the characterisation of hydrological processes on a small temporal scale, the outlined procedures aim at disaggregating rainfall into storms that resemble the natural rainfall as closely as possible. This Chapter presents a simple procedure that is useful for simulating the effect of rainfall upon related hydrological processes over long time periods when only rainfall data on a daily basis are available and when a precise reconstruction of rain events is not required. Such processes could be the leaching of soil-applied pesticides into groundwater over several years or the prediction of the monthly or yearly volume of surface runoff in a catchment.

When using daily rainfall records as input in a soil water flow model, no information on rainfall intensity is available. A hydrological model based on the Richards equation (i.e. physically based) will be unable to simulate surface runoff in a correct way because it will distribute the rainfall amount over the 24 hours of the day. When 10-minute rainfall data are provided as input, precise information on rainfall intensity becomes available and surface runoff can be estimated in a robust way. In the previous Chapters, daily rainfall was used for the simulation of daily soil moisture content. At the end of this Chapter, it is shown that the effect of the temporal resolution of rainfall on daily soil moisture content values is minimal. This is contradictory to its crucial importance in the simulation of surface runoff [*Mertens et al., 2002*].

In cases where only daily rainfall is available, methods for predicting runoff such as the Soil Conservation Service (SCS) runoff curve-number approach [*USDA, 1985*] are often used. Although the SCS runoff equation can properly produce the direct runoff to the streamflow [*Steenhuis et al., 1995*], the approach will not always give satisfactory results because infiltration and surface runoff are processes that are very sensitive to rainfall intensity. Since rainfall intensity is not included in the SCS runoff curve-number approach the daily input data can hide some important features of the rainfall that can only be revealed when using more detailed data [*Vanderborght et al., 2000*]. *Mertens et al. (2002)* show that disaggregating the daily rainfall as proposed in this study is preferable to the SCS runoff curve-number method when rainfall characteristics are known for the area or can be quickly obtained from a measuring campaign. The procedure presented in this Chapter shows how additional information concerning rainfall intensity can be integrated in the daily rainfall records. Since temporal

resolution of rainfall has a large impact on the simulation of runoff, it can be expected that effective parameters, as a result from an optimisation against runoff, will be different and function of the temporal resolution of the used rainfall data.

The objectives of this Chapter can be summarised as: (i) to study the importance of the temporal resolution of rainfall on simulated daily runoff using a physically based model; (ii) to develop and test a procedure for incorporating rainfall intensity into daily rainfall records with as objective a more robust simulation of the cumulative daily runoff over a year and (iii) to investigate the effect of the temporal resolution of rainfall records on effective model parameters.

7.2. Analysis of rainfall intensity

In this analysis, a precipitation dataset was used that was collected in the climatological park of the Royal Meteorological Institute (RMI) in Uccle (50°47' N, 04°21'E, 100 m above sea level) near Brussels (Belgium). The precipitation was recorded by a Hellmann-Fuess recorder at a 10-minutes time interval, starting from May 1898 till present [*Demarée et al., 1998*]. The resolution of the rainfall data is 0.1 mm. Hence a very large and complete precipitation data set is available at the RMI. In this research, the 10-minute interval precipitation data between 1934 and 1994 were analysed.

The mean annual rainfall observed over those 61 years is 801 mm. Total rainfall volumes are almost equally distributed throughout the year without any significant difference between the rainfall in any of the months. From the 61 years, i.e. 61 * 365.25 (days) * 24 (hours) * 6 (10-minutes) = 3,208,356 observations, about 94% of all measurements were zeros [*Demarée et al., 1998*]. The non-zero measurements were divided into three intensity classes of 10-minute rainfall data: between 0.1 and 1 mm, between 1.1 and 2 mm and larger than 2.1 mm of rain per 10-minutes. The frequency of occurrence of rainfall in each intensity class was calculated for each month.

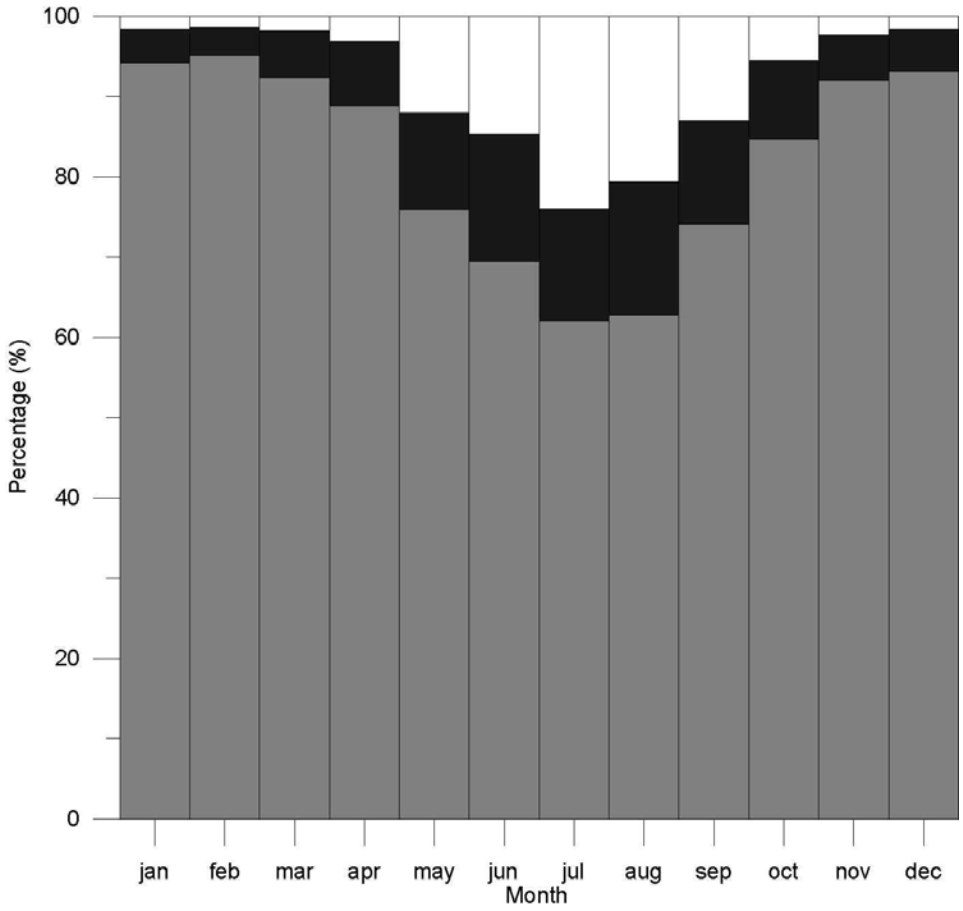

Figure 7.1 The percentage of monthly rainfall in different intensity classes (grey, between 0.1 and 1 mm/10min; black, between 1.1 and 2 mm/10 min and white, larger than 2.1 mm/10 min)

The percentage of monthly rainfall that falls in each intensity class is presented in Fig. 7.1. Although total monthly rainfall amounts were found to be the same throughout the year, it is observed that the rainfall intensities in summer (June – August) are higher than in winter (November – February). In January only 1.6 % of the monthly precipitation falls in showers with intensities larger than 2.1 mm per 10-minutes while in July 24 % of the monthly precipitation falls on average with such intensity. For the 61 years of observations, it was calculated in how may storms rainfall came down during a rainy day. Table 7.1 shows the average number of storms per rainy day for each month. The end of a storm is defined as a rainfall amount of zero mm during a period of ten minutes. The number of storms on a rainy day in August is only half of the amount of storms on a rainy day in January. Although total amount of monthly rainfall

is similar all over the year, it is clear that in summer rain falls in fewer storms with higher intensities.

Table 7.1 Average number of storms per rainy day for each month

Month	Number of storms
January	6
February, March, April	5
May, June, July	4
August	3
September	4
October	5
November, December	6

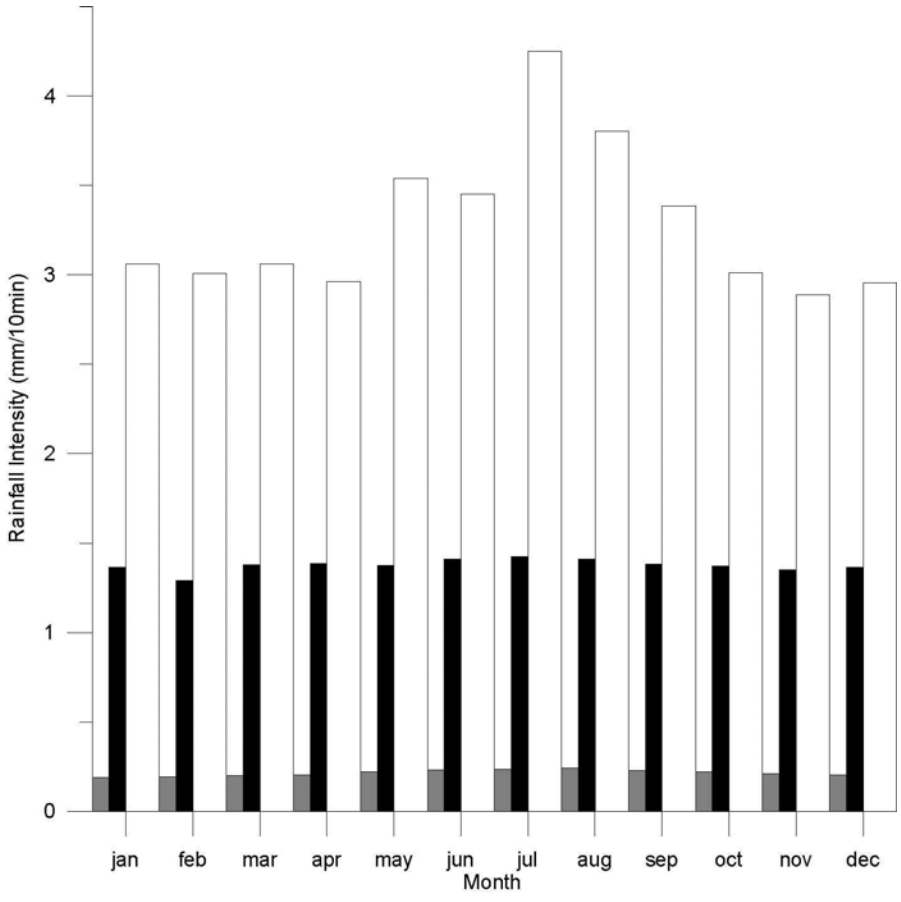

Figure 7.2 Mean rainfall amount for each of the three considered intensity classes (grey, between 0.1 and 1 mm/10min; black, between 1.1 and 2 mm/10 min and white, larger than 2.1 mm/10 min)

The mean monthly rainfall intensities for each intensity class are plotted in Fig. 7.2. There is no clear difference over the year between the average values for the lower and middle intensity classes. Mean monthly rainfall intensity of the highest class is only about 3 mm/10 min in the winter months but 3.5 to 4.2 mm/10 min in the summer months. Hence, not only a higher percentage of the summer rainfall is found in the highest intensity class but also the mean intensity is higher in summer. The cumulative distribution of the rainfall intensity within each of the three intensity classes is presented in Fig. 7.3.

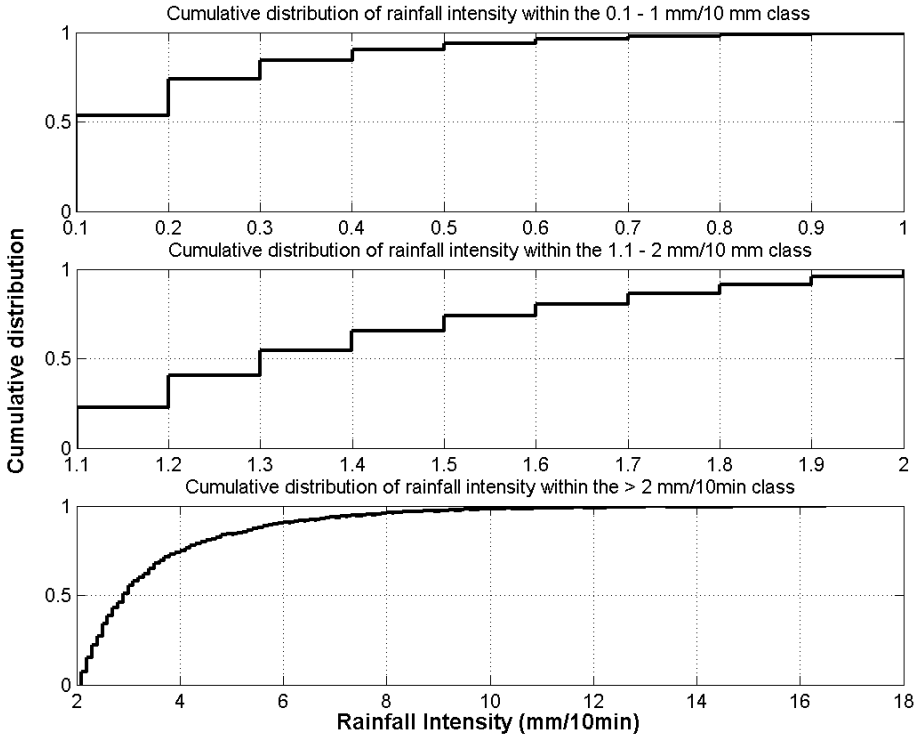

Figure 7.3 Cumulative distribution of the rainfall intensity (mm/10min) within each of the three intensity classes

Figure 7.3 shows that the distribution within the lowest intensity class (between 0.1 and 1 mm/10min) is not even close to a normal distribution. More than half of the rainfall (53%) in this class fell with an intensity of 0.1 mm/10 min (= median) though the mean of the rainfall intensity within this class is 0.3 mm/10 min (cfr. Fig. 7.2). For the two higher intensity classes, differences between mean and median of the distributions are

small. Figures 7.1, 7.2 and 7.3 form the basis for the procedure described below. They are based on the analysis of 61 years of 10-minute rainfall observations. It is obvious that such a long and complete data set is often not available. Therefore, a sampling exercise was carried out to investigate the effect of a shorter observation period (2 and 5 years randomly selected from the 61 years) on the monthly percentage of rainfall within each intensity class.

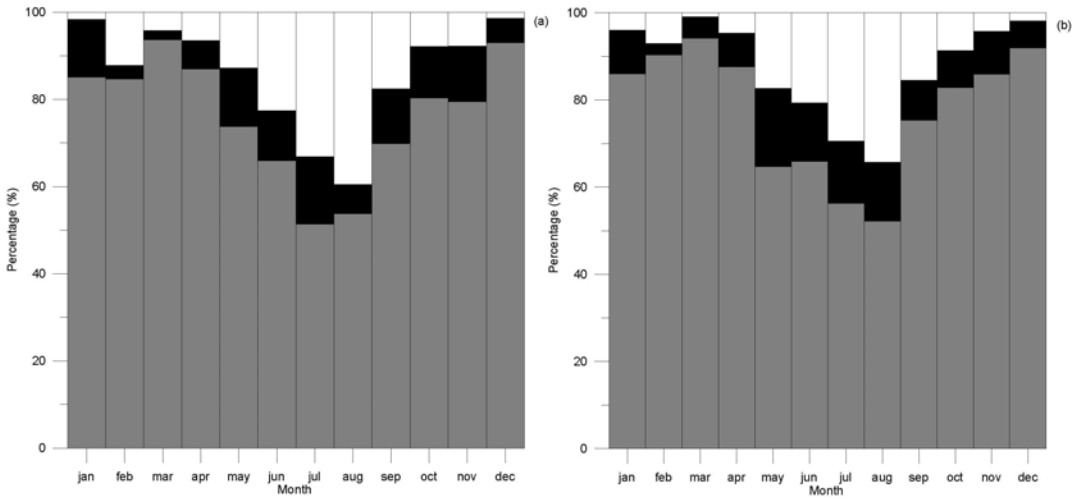

Figure 7.4 The percentage of monthly rainfall that falls in the different intensity classes (grey, between 0.1 and 1 mm/10min; black, between 1.1 and 2 mm/10 min and white, larger than 2.1 mm/10 min) when only (a) a 2-year period (1990-1991) and (b) a 5-year period (1990-1994) out of the 61 years observations was analysed

Figure 7.4 presents the distribution of rainfall intensities over the three classes when only 2 (a) or 5 years (b) were randomly selected from the 61 years of rainfall and used in the analysis. Comparing Fig 7.1 and 7.4 indicates that relatively short measuring campaigns already reveal the general trend of the difference in rainfall intensities between the summer and winter months. Table 7.2 shows the correlation between the frequency distributions for each intensity interval between 2, 5 and 61 years of observation. High correlations are observed (> 90%) between each of the observed years and each intensity interval, except for the correlation between the 2 and 61 years period for the intensity class between 1 and 2 mm/10 min. The variances in each intensity interval are comparable over the years and no clear trend of decreasing

variances with increasing observation period can be noticed. Calculating the Coefficient of Determination (CD) between the 61-observation period values and the 2 and 5 years observation values results in CD values of 0.98 to 0.99.

Table 7.2 Correlation between rainfall intensity distributions for the three considered classes (0-1mm/10min, 1-2 mm/10min and > 2mm/10min) for rainfall data from 2 years(1990-1991), 5 years (1990-1994) and 61 years of observation. Variance over the months for each year and intensity class is also shown

Rainfall intensity distributions	Years of observation	Years of observation		
		2 years	5 years	61 years
Between 0 and 1 mm/10min				
	2 years	1	0.72	0.95
	5 years	0.96	1	0.96
	61 years	0.95	0.96	1
	variance	195.38	210.2	157.23
Between 1.1 and 2 mm/10min				
	2 years	1	0.72	0.4
	5 years	0.72	1	0.74
	61 years	0.4	0.74	1
	variance	19.96	18.93	22.01
Greater than 2 mm/10min				
	2 years	1	0.97	0.93
	5 years	0.97	1	0.97
	61 years	0.93	0.97	1
	variance	150.02	122.94	65.66

This suggests that a two or five years observation period already suffices the needs of the presented procedure making it very powerful and practical applicable as a relatively short measuring campaign is easily set up. It is obvious that the longer the measuring campaign the better the rainfall characteristics can be described. As the rainfall pattern in other regions might differ from the Belgian conditions, the number of observed years

that will be needed to get a representative image of the frequency distribution of the rain intensity might differ as well.

7.3. Incorporating rainfall intensity into daily rainfall records

The procedure mainly consists in splitting up the rainfall record P_i observed on day i into as many parts as intensity classes (j) are considered. The duration t_{ij} of the j'th part of daily rainfall, that has an intensity of m_j, is given by:

$$t_{ij} = \frac{P_i * (I_j / 100)}{m_j} * 10 \min \qquad (7.1)$$

The subscript i refers to the day number (from 1 to 365 or 366) and j refers to the rainfall intensity class (in this case from 1 to 3). To clarify the procedure, a diagram of the procedure for a rainy day is presented in Fig. 7.5. I_j is the percentage of the monthly rainfall that has an intensity corresponding with the one of class j. Hence, the value I_j varies throughout the year and was obtained from Fig. 7.1. The value of m_j is not allowed to vary throughout the year for the low and middle intensity classes (m_1 and m_2) because it was observed from Fig. 7.2, that mean intensities for both intensity classes do not vary throughout the year. Though the mean for those two classes does not vary over the year, Fig. 7.3 shows that the distributions of the rainfall within the two lower intensity classes are very particular (especially true for the lowest intensity class). Therefore the distributions within both classes were incorporated in the procedure. To do so, a random number between 0 and 1 is generated on each rainy day and for each of the two intensity classes. To each random number a corresponding rainfall intensity is taken from the cumulative distribution shown in Fig. 7.3, and is applied as m_j with j = 1 or 2. The value of m_3 corresponding to the highest intensity class is allowed to vary over the year and is set equal to the mean monthly rainfall intensity (cfr. Fig. 7.2) within this highest intensity class. For the highest intensity class, the distribution within the intensity class was not incorporated to keep the procedure simple, i.e. no need for the fitting of a distribution to the continuous distribution shown in Fig. 7.3.

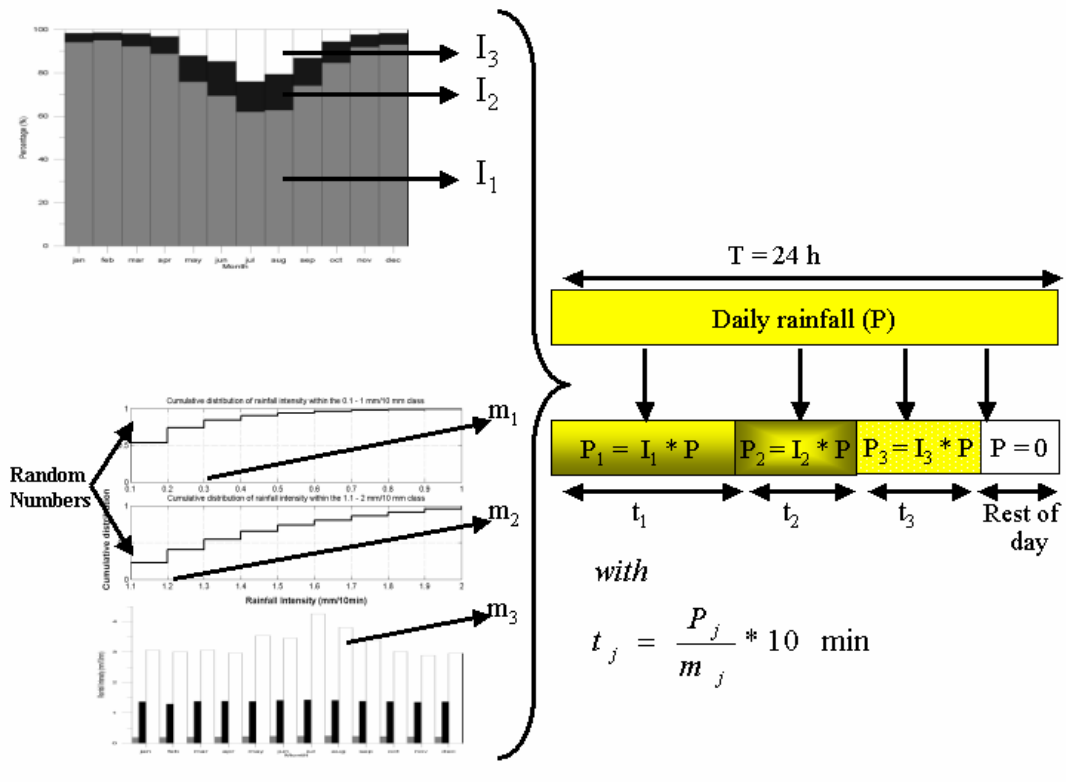

Figure 7.5 Diagram of the procedure for a rainy day in August

The number of intensity classes and their upper and lower bounds to be considered for the procedure depends on the variation of rainfall intensity one can expect in the region. For our region, the procedure was also tested using 4 and 5 intensity intervals with different lower and upper bounds but they did not result in more precise simulation results [*Mertens et al., 2002*]. It can be expected that for regions having rainy and dry seasons and regions where rainfall shows larger variations throughout the year, more intensity classes might be needed. In order to keep the procedure simple, some additional assumptions are made when the daily rainfall records are split up into minute input data. Although rainfall often comes in several showers (Table 7.1) at different moments of the day, it is assumed that all precipitation measured on a day falls in one single storm at the beginning of the day. The simplification is justified by the fact that the objective of the procedure is not to mimic daily rainfall, but to integrate information on the rainfall intensity in the daily rainfall records. The possible combinations of how the three rainfall intensities can succeed each other (scenarios) are listed in Table 7.3. Each time rain occurs, one of the six scenarios was selected randomly in the simulation

runs. Although, in general, a cold weather front produces a storm of an advanced type (High, Middle, Low), and the warm weather front a uniform or an intermediate pattern [*Schwab et al., 1996*], no preference was given to a particular scenario since the aim of the procedure is not to mimic single storms.

Table 7.3 Succession of rainfall intensities for each scenario

Scenario Number	Succession of rainfall intensities (low = 0.1 to 1 mm/10 min., middle = 1.1 to 2.1 mm/10 min. and high = greater than 2.1 mm/10min		
1	Low	Middle	High
2	High	Middle	Low
3	Middle	High	Low
4	Middle	Low	High
5	High	Low	Middle
6	Low	High	Middle

In *Mertens et al. (2002)*, this procedure is tested on 1D soil columns for three years: 1947 (dry year), 1982 (normal year) and 1988 (wet year) and three soil types (clay loam, silt and sandy loam). The reference runoff – simulated surface runoff obtained by using the observed 10-minute rainfall records as input – is compared with the simulations whereby the daily rainfall records are split up into minute data according to the procedure presented above. It is concluded that the procedure performs very well and the simulated amount of water that infiltrates during a year deviated maximum 1.19 % from the reference value. In this Chapter, the procedure is tested using a 2-D-artificial rainfall runoff model based on the hillslope described in Chapter 2.

7.4. Effect of temporal rainfall resolution on simulated hillslope runoff and effective parameters

7.4.1. Model set-up

A hillslope MIKE SHE model [*Refsgaard and Storm, 1995*] was set up including the unsaturated zone, evapotranspiration and overland flow component described in Chapter 4. As explained in this chapter, the MIKE SHE model is capable of describing 1-D subsurface water flow combined with 2-D surface (overland) water flow. The dimensions (80 m by 20 m or 1600 m²) and topography (Fig. 2.7) correspond to the experimental field described in Chapter 2. The lower boundary condition was considered to be a constant watertable at 6 m depth, which means that the model is groundwater independent. To simplify the model, only 1 soil horizon is considered. Hence only 6 UZ zone parameters are needed to describe the UZ soil parameters: K_s, θ_s, θ_r, α, n and N. The entire soil column is discretised into 86 calculation nodes over the profile depth of 6 m. Nodes are not evenly spaced, closer spacing was set near the surface (first 65 nodes spaced only 2 cm apart) and spacing increases with depth. Potential evapotranspiration for the year 1988 is given as daily time series. The model was 'hotstarted', i.e. a similar model run was executed using the daily rainfall and evapotranspiration of 1987. The initial conditions for the model used in this study were set to the conditions simulated on the 31st of December 1987. Total cumulative runoff from the hillslope for the year 1988 is studied as output variable.

7.4.2. Effect of temporal rainfall resolution on simulated hillslope runoff

In order to simulate runoff on the rather flat hillslope, the detention storage (= water depth at which overland flow occurs) was set to 0 while the Strickler-Manning coefficient (cfr. Eq. 4.10) was chosen to be 10 $m^{1/3}s^{-1}$. A reference parameter set of the 6 UZ soil parameters was chosen in between the ranges for a clayey soil from *Meyer et al. (1997)* and are presented in Table 7.4.

Table 7.4 Reference parameter values

Parameter	Reference value
K_s (ms^{-1})	1.00E-07
θ_s (-)	0.46
θ_r (-)	0.034
α (m^{-1})	1.6
n(-)	1.37
N(-)	9

Model simulations are performed using this reference parameter set and three different temporal resolutions of rainfall for the year 1988: (i) real 10-minute observed rainfall data obtained from the RMI; (ii) daily rainfall (= daily sum of the observed 10-minute data); and (iii) disaggregated rainfall according to the procedure described above. The simulation using the reference soil hydraulic parameters and the real observed 10-minute rainfall data is called the reference simulation resulting in the reference runoff. The model efficiency (E) of the daily and disaggregated rainfall simulated runoff against the reference runoff is also calculated as:

$$E = 1 - \frac{\sum_{i=1}^{n} (R_{\mathrm{i,obs}} - R_{\mathrm{i,sim}})^2}{\sum_{i=1}^{n} (R_{\mathrm{i,obs}} - \overline{R}_{\mathrm{i,obs}})^2} \tag{7.2}$$

with n = 365 is the number of days, $R_{i,obs}$ is the observed (in this case reference) daily hillslope runoff, $\overline{R}_{\mathrm{i,obs}}$ the mean observed daily hillslope runoff over the year 1988 and $R_{i,sim}$ the simulated daily hillslope runoff. Simulated reference runoff instead of real observed runoff had to be used in this study because as explained in Chapter 2, no surface runoff was observed on the experimental hillslope.

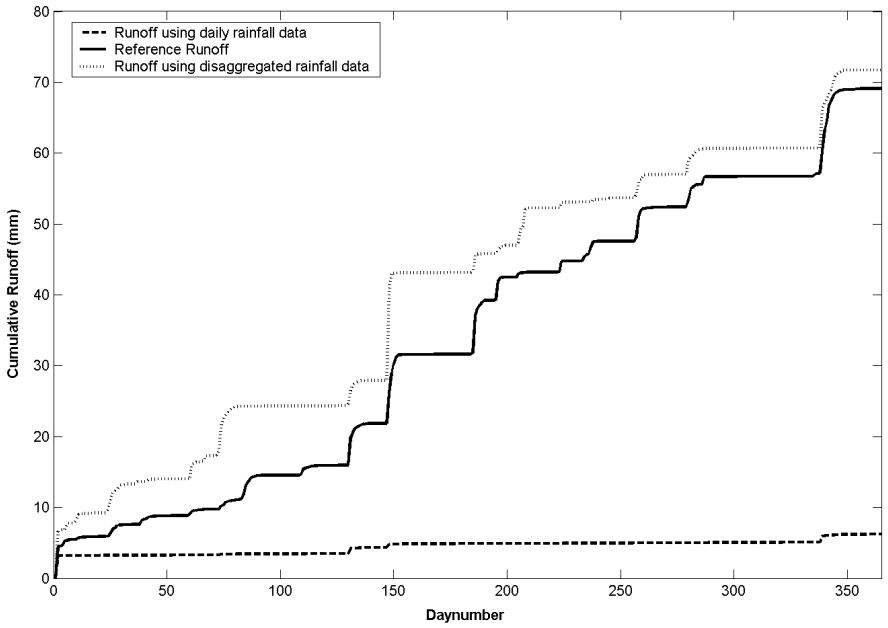

Figure 7.6 Simulated hillslope runoff as a result from a model run with daily and disaggregated rainfall data compared to the reference runoff

Figure 7.6 shows the cumulative daily runoff over the year 1988 as a result of the three different rainfall inputs. The reference runoff can be considered as the closest to reality, i.e. the observed 10-minute rainfall data are used which is the closest to the real rainfall. As also shown for 1-D soil columns in *Mertens et al. (2002)*, the simulated cumulative runoff using the daily rainfall (and the reference soil parameters) is close to zero and hence far from the reference runoff. Actually the model efficiency is negative, E = -2.02, suggesting that the model performs worse than when the average reference runoff is taken as simulated runoff throughout the year (in this case, E = 0). The reason for this is the fact that the model code distributes rainfall uniformly over the day, i.e. a low intensity rainfall lasting all day. This can be expected to generate very little or no surface runoff because the resulting modelled rainfall intensity is generally lower than the saturated hydraulic conductivity. Figure 7.6 shows that disaggregating the daily rainfall values according to the procedure described above results in a cumulative runoff close to the reference runoff (E = 0.88). As explained above, it was not the procedure's aim to mimic single storm events but to improve cumulative daily runoff simulations over longer time periods when only daily rainfall data are available. The procedure is

successful in its aim because the difference between the reference runoff and the runoff as a result from the procedure is small. Concluding, it can be stated that the procedure succeeded in the disaggregation of daily rainfall so that simulated daily runoff is close to reality. This is only true in terms of cumulative volumes for which the procedure was developed, and will certainly not be the case when interested in extreme events.

7.4.3. Sensitivity Analysis

In this Chapter, the One-At-a-Time design [*Morris, 1991*] sensitivity analysis described in detail in Chapter 5 is carried out. The sensitivity of the MIKE-SHE model, more in particular, the sensitivity of runoff simulations to all 6 UZ parameters was evaluated: K_s, θ_s, θ_r, α, n and N. Upper and lower limits are taken as the 95 % confidence interval of the recommended distributions by *Meyer et al. (1997)* and were presented in Table 5.1. For a particular parameter set, the Root Mean Squared Error (RMSE) of the simulated runoff against the reference runoff for the year 1988 is calculated as:

$$RMSE = \sqrt{\frac{\sum_{i=1}^{n}\left(R_{i,obs} - R_{i,sim}\right)^2}{n}} \tag{7.3}$$

where n = 365 is the number of days, $R_{i,obs}$ is the observed (= reference) and $R_{i,sim}$ the simulated daily hillslope runoff.

In this Chapter, the number of trajectories r was selected to be 48 (more than the 14 suggested in Chapter 5 because of short simulation time) and $k + 1 = 7$ (k = 6 parameters considered in the sensitivity analysis), so in total 336 MIKE-SHE runs were needed. As in Chapter 5, a_{int} was again chosen to be 4 which results in $\Delta = 2/3$. Estimated means (μ) and standard deviations (σ) of the distribution of the elementary effect of each of the 6 UZ parameters against RMSE are shown in Fig. 7.7. Absolute values of μ ($|\mu|$) are plotted in Fig. 7.7 making it easier to visualize the overall sensitivity of the parameters. As explained in Chapter 5, the sensitivity of parameters in the Morris method cannot be quantified. Only a qualitative ranking of importance of

parameters with respect to overall importance and interaction with other parameters or non-linear effects can be performed. Objective ranking can be performed against μ or σ yielding an idea on which parameters have the largest overall effect (μ) or which parameters have high interaction with other parameters and non-linear effects (σ).

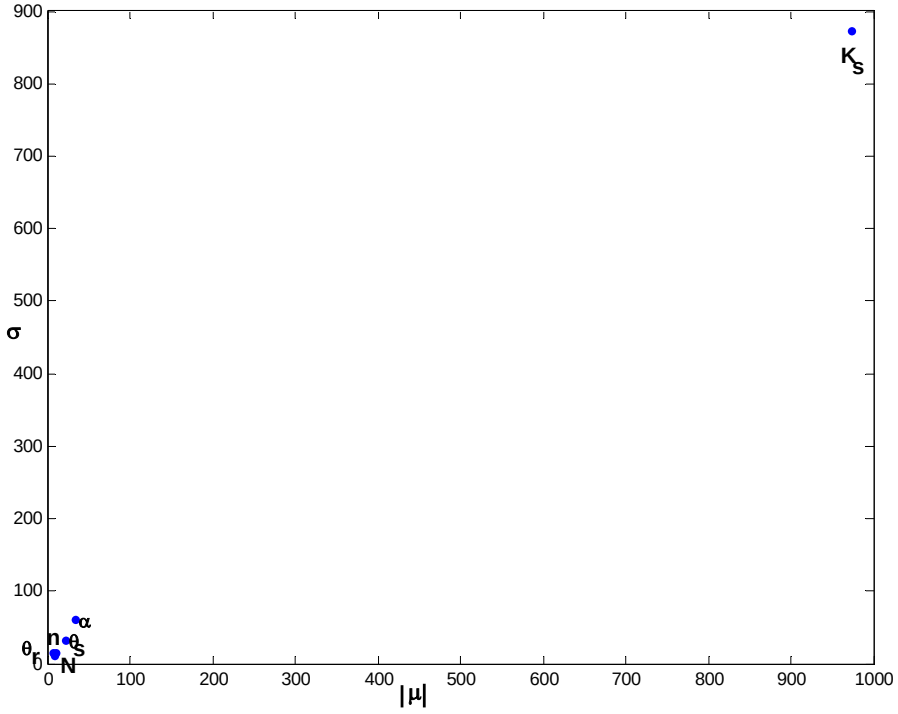

Figure 7.7 Estimated means $|\mu|$ and standard deviations (σ) of the distributions of elementary effects of all parameters against overall RMSE for the Morris SA

The SA shows that only saturated hydraulic conductivity (K_s) seems to be an important parameter in the runoff generation. The other parameters have a minimal overall importance ($|\mu|$) as well as very small interactions with other parameters or very small non-linear effects (σ). Since K_s determines the maximal infiltration capacity of a soil near saturation, it was to be expected that runoff would be highly sensitive to the value of this parameter. Although α and θ_s seem to be relatively more important in the generation of runoff than θ_r, n and N, their importance is negligible compared to K_s. The same is true for the estimated interactions or non-linear effects α and θ_s have. Therefore,

it was decided not to incorporate other parameters but K_s in the SCE optimisation algorithm presented below.

As a test, an SCE optimisation algorithm incorporating all 6 UZ parameters was carried out. It was observed that significantly different 'effective' water retention and hydraulic conductivity curves resulted in similar runoff patterns throughout the year. Though, this was only true if their saturated hydraulic conductivity values were close. This finding confirmed the result of the Morris SA: simulated runoff is only sensitive to the saturated hydraulic conductivity (K_s) and the values of the other parameters (θ_s, θ_r, α, n and N) are not important in the runoff generation.

7.4.4. Effect of temporal rainfall resolution on effective soil parameters

The Shuffled Complex Evolution (SCE) algorithm is adopted for the optimisation of the UZ soil parameters in the hillslope MIKE-SHE model described above. The SCE control parameters presented in Chapter 4 are also used here, with the exception of the number of complexes that was set equal to two. Because only K_s is incorporated in the algorithm, the recommended value for the number of complexes is one (= equal to the number of parameters). However using only one complex, corresponding to a local search, would probably not have been very efficient for our purposes. The other parameter values were fixed to their reference value presented in Table 7.4. The optimisation bounds for the K_s parameter were set to [1e-9, 1e-5] with the reference K_s value (1e-7) within the optimisation bounds. The reference runoff shown in Fig. 7.6 was considered as being the observed runoff data in the inverse optimisation. The same objective function as in the sensitivity analysis was used (Eq. 7.3). The stopping criteria for the optimisation routine were either (i) change of the best objective function less than 0.1% within 5 loops; or (ii) a maximum number of model evaluations of 2000.

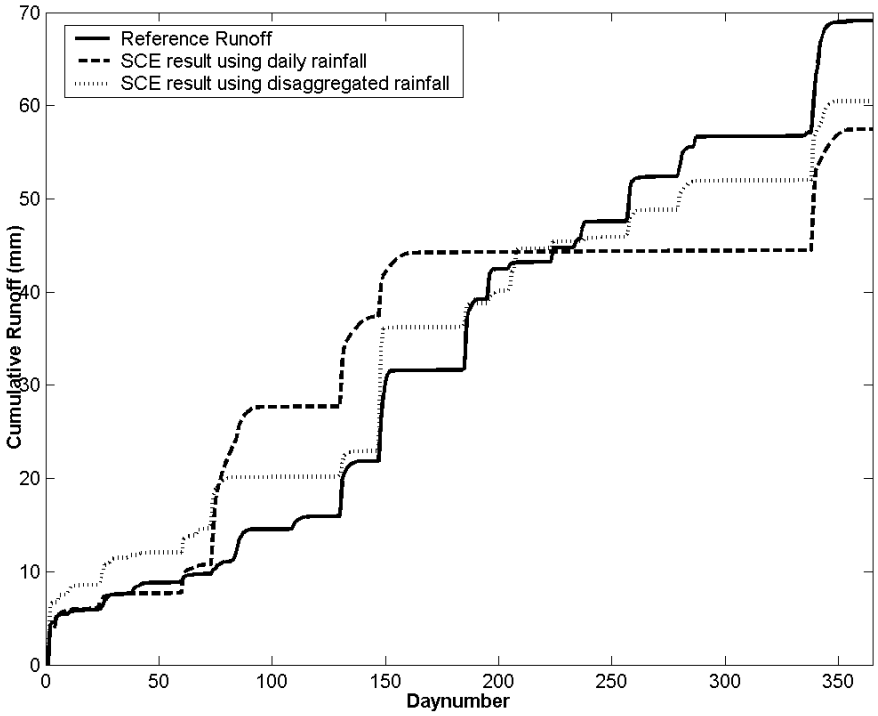

Figure 7.8 Simulated hillslope runoff as a result from the SCE algorithm using daily and disaggregated rainfall data compared to the reference runoff

Figure 7.8 shows the result of the SCE algorithm for the daily rainfall and the disaggregated rainfall input compared to the reference runoff. The SCE algorithm succeeded in finding a K_s value that results in a total runoff of 58 mm per year using daily rainfall data where as the reference parameters simulated nearly no runoff at all (cfr. Fig. 7.6). A smaller effective K_s value than the reference one was to be expected as the optimisation algorithm had to increase runoff and was only allowed to do so by decreasing K_s. Effective K_s was found to be 6.47e-8 and hence about 2/3 of the reference K_s which was equal to 1.00 e-7. Inverse optimisation of the daily rainfall model resulted in a model efficiency (E) of 0.79. Although, simulated annual runoff is only 15 % lower than the reference annual runoff (69 mm) and a relatively high model efficiency is observed, the dynamics of the cumulative runoff throughout the year are far away from the dynamics of the reference simulation. In particular, the dynamics of the second half of the year are extremely poor, i.e. no dynamics at all are observed between day 160 and 330.

Inverse optimisation of K_s using the disaggregated rainfall improves the model efficiency from 0.88 to 0.95. This improvement is rather small and this is also reflected in the value of the effective K_s that was found to be 1.07e-7 and thus very close to the reference K_s value of 1.00e-7. The dynamics of the cumulative runoff throughout the year still correspond very well to the reference runoff. The fact that only a slight model improvement is observed, shows that disaggregating the rainfall results in a realistic (close to reference) cumulative runoff without the need for optimisation. Additionally, a comparable effective K_s to the reference K_s is observed suggesting that effective parameters obtained using disaggregated rainfall are much more realistic (close to the reference) compared to the effective parameters estimated using daily rainfall input.

As a conclusion, it can be stated that incorporating rainfall intensity into daily rainfall records improves simulation results before calibration and reduces the need for calibration. Additionally, if calibration is performed, higher model efficiencies can be expected than when daily rainfall records are used. Probably the largest contribution of the procedure is that effective parameters estimated using disaggregated rainfall are much closer to reality than when daily rainfall records are used.

7.4.5. Effect of temporal rainfall resolution on simulated soil moisture content

In Chapters 5 and 6, daily rainfall is used in the MIKE SHE model and daily moisture content at three different depths as output variable. Effective parameters are estimated using daily rainfall records. Hence, the possibility exists that estimated effective parameters are a function of the temporal resolution of the rainfall as shown above for the case runoff is studied as output variable. Figure 7.9 shows the simulated soil moisture content at three depths at the location x = 10, y = 2 using the effective soil parameters estimated in Chapter 5 for that location. The model is run using three different temporal resolutions of rainfall: observed 10-minute rainfall, observed daily rainfall and disaggregated rainfall for the year 1988. Only very small differences in simulated moisture content at all depths between the different temporal rainfall

resolutions exist. This is in contrast with Fig. 7.6 where big differences in simulated runoff are observed for different temporal rainfall resolutions.

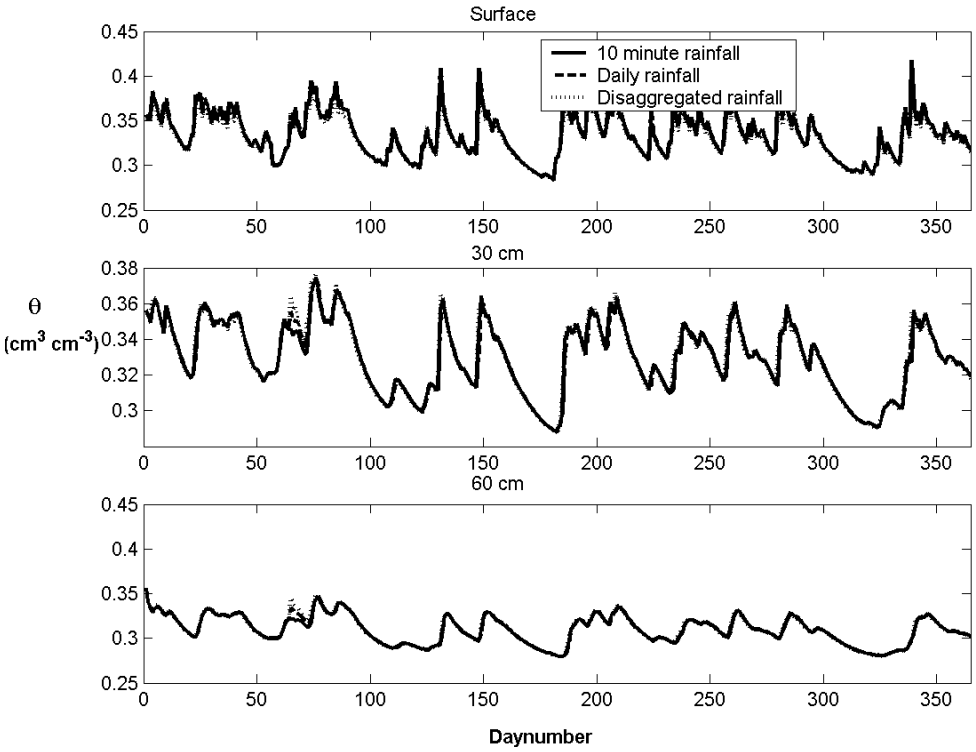

Figure 7.9 Simulated soil moisture content at the location x = 10, y = 2 for the year 1988 using three different temporal resolutions of rainfall: observed 10-minute rainfall, observed daily rainfall and disaggregated daily rainfall

The large difference in the effect temporal rainfall resolution has on runoff and soil moisture content can be explained as follows. In a field saturated soil, if rainfall exceeds the infiltration capacity (K_s) the additional rainfall is considered to be runoff while soil moisture content stays constant, i.e. somewhere between saturation and field capacity. This means that for soil moisture content, the temporal resolution of the rainfall is not important because soil moisture content is close to saturation and does not change much. On the other hand, runoff generation is a function of rainfall intensity and thus of the temporal resolution of rainfall records. This also means that one would not expect the effective soil parameters obtained in Chapters 5 and 6 using daily rainfall records to

be significantly different if rainfall records of a finer temporal resolution would have been used.

7.5. Conclusions

The procedure described in this Chapter is an easy-to-use and powerful tool for hydrological studies trying to estimate infiltration and/or runoff volumes over long time periods when only daily precipitation data is available. An analysis of 10-minute data forms the basis of the precipitation frequency distribution into different interval classes. If one does not dispose of such data a measuring campaign for fine temporal resolution precipitation data of some years is required.

A hillslope rainfall-runoff model was set-up using the MIKE-SHE software. Cumulative daily runoff over a year was simulated using rainfall with different temporal resolutions. Infiltration and runoff that were simulated using the disaggregation procedure on daily rainfall records were very similar to the reference with a model efficiency of 0.88. The reference consisted of a simulation whereby the observed 10-minute rainfall data were used as input. Simulated runoff using daily rainfall records was close to zero; a model efficiency of –2.02 was observed. The procedure described in this Chapter has the advantage that it is easily understandable and very easy to apply compared to disaggregation techniques that use very sophisticated statistical techniques. This study shows that such techniques are not required when one is interested in the simulation of cumulative hydrological variables over months/years.

A sensitivity analysis showed that runoff is highly sensitive to the value of the saturated hydraulic conductivity K_s. Therefore, an SCE optimisation algorithm was set up for the estimation of K_s using different temporal rainfall resolutions. Root Mean Squared Error between simulated and reference runoff was used as objective function. The SCE succeeded in finding an effective K_s value that resulted in a model efficiency of 0.79 using daily rainfall records (cfr. E = -2.02 before optimisation). Even though the relatively high model efficiency, the dynamics of the daily rainfall model are poorly mimicked with respect to the reference runoff. On the other hand, optimisation of the disaggregated rainfall model did not improve the model efficiency a lot (E from 0.88 to 0.95) and dynamics closely matched the reference. Effective K_s is hence a function of

the temporal rainfall resolution. In particular, effective K_s using daily rainfall input records was found to be only 2/3 of the K_s used in the reference model. Disaggregation of the daily rainfall records resulted in an effective K_s very close to the reference K_s.

It is believed that for catchment models with many parameters, an autocalibration using daily rainfall records can find an effective parameter set that produces an acceptable fit. Contrary to our simple model, for these models the dynamics might also be acceptable due to the large amount of parameters these models have. Since all these parameters have different effects on the simulated runoff, the masking of the effect daily rainfall records have on the simulated runoff, becomes easy. Still, it is believed that disaggregating the daily rainfall according to the procedure presented in this Chapter, will increase the efficiency of the (auto)calibrated model. To be able to prove this for catchment models, and to get some idea about the significance of the increase in model efficiency, more research is needed. Maybe more important is that effective parameters of the autocalibrated model using daily rainfall records can for sure be called less 'realistic' than effective parameters resulting from the disaggregated rainfall model. This is true because effective parameters using the disaggregated model are optimised on the basis of rainfall closer to reality than daily rainfall records. No need for the masking of the effect daily rainfall records on the runoff have, e.g. no need for decreasing the saturated hydraulic conductivity needed to increase the amount of surface runoff. Although more research is needed, it is dared to state that the disaggregation procedure can provide higher model efficiencies and more realistic effective parameters than the case where daily rainfall records are used.

Chapter 8

Summary, conclusions and recommendations for future research

With the growing popularity of complex physically based distributed watershed models, the need to better define the magnitude of model parameters is increasing. Therefore, more and better field and laboratory measurements for the estimation of these parameters are being developed. Still, research dedicated to the development of more and better measurement techniques is limited and, according to our feeling, not proportional to the increase in the importance of parameter estimation. Though, even if suitable techniques would exist for the estimation of all model parameters at the scale required in the model, it would remain practically impossible (highly time- and money-consuming) to measure the vast amount of parameters needed by these physically based distributed watershed models. Even if money and time would be unlimited, uncertainty remains whether the measured parameters would be suitable as model input.

An alternative to measuring parameters is offered by automated parameter estimation techniques (i.e. inverse modelling) that mainly developed due to continuously increasing power of computers. They are becoming more and more popular because: (i) the lack of suitable parameter measurement techniques at scales required by our models, (ii) the enormous time- and money-consuming character of parameter measurements and (iii) the uncertainty of their suitability as direct model input parameters. In contradiction to the limited amount of literature discussing new measurement techniques, lots of recent literature deals with the development of new and better automated parameter estimation techniques.

This PhD research focused on the possibilities and limitations of both direct parameter measurements and inverse modelling applied individually and presented a methodology that combines both. It is shown that the developed methodology combining both

strategies is capable of estimating effective parameters in a more robust way than when the strategies are applied individually.

8.1. Summary and conclusions

Lots of problems were encountered during and after the experimental set-up on the hillslope. Most crucial problem was the lack of surface and subsurface runoff measurements. Three reasons possibly explain the lack of surface runoff: (i) low rainfall intensities, (ii) the gentle slope and (iii) the high infiltration capacity of the topsoil. It is believed that the lack of subsurface runoff can be explained by the high permeability of the textural B horizon. This was in contrast with the visual observations during the augering prior to the start of the experiment. The original objectives the experiment was designed for are presented in Chapter 2. Because of the lack of surface and subsurface runoff, original objectives had to be reformulated and are presented in Chapter 1. On the other hand, the soil moisture measurement system worked better than satisfactory; though longer cables than generally accepted in literature were used. This was made possible due to the methodology of saving the total waveform and its subsequent analysis using the developed MATLAB code.

The field saturated hydraulic conductivity K_{fs}, and the parameter α_m were estimated at 120 locations on a hillslope by means of a single-ring pressure infiltrometer. A Monte Carlo analysis showed that the sensitivity of α_m on measurement errors using the classical analysis is large. On the other hand, the sensitivity of K_{fs} to measurement errors is very low and constant over the range of K_{fs} and α_m. A new technique was developed that consists of the inverse optimisation of 120 K_{fs} values and only 1 α_m value using all infiltration measurements. The spatial analysis revealed ranges of ln(K_{fs}) between 2.85 and 3.8 m omnidirectional and along the hillslope (y-axis), respectively. Though a robust method for the derivation of field saturated hydraulic conductivity was presented, care must be taken interpreting the measured K_{fs} values. Lots of different methods for estimating hydraulic conductivity exist, all having their specific advantages and disadvantages at different scales. For the same soil and even at the same scale, different techniques might yield different K_s estimates [*Reynolds et al., 2000, Herman et al.,*

2003]. As shown later in the study, it is hence well possible that the measured K_s, independent from the technique used and the scale it was measured at, does not coincide with the effective K_s needed by the model.

Time series of the soil moisture content for the year 2001 in 25 locations at three different depths on the hillslope were used as observed data time series. The sum of the Root Mean Squared Error (RMSE) of the simulated moisture content at the three depths against the observed time series was considered as objective function in two Sensitivity Analyses (SA). A Monte Carlo Sensitivity Analysis of the 1-D MIKE SHE model revealed that soil moisture content was not sensitive to the *Averjanov N* parameter. A One-At-a-Time (OAT) SA (Morris' design) showed comparable conclusions. Therefore, *N* was excluded from the inverse optimisation. Both SA showed that K_s and θ_s of the A-horizon, K_s of the B-horizon and the depth *d* between the A- and B-horizon were the most important parameters in this study. It was concluded that both techniques are complementary and on the basis of both, sound conclusions concerning parameter sensitivity in hydrological modelling can be drawn. The main advantage of the Morris method was found to be the relatively low computational cost compared to the Monte Carlo SA and its ability to generate a 'qualitative' idea about the individual parameter interactions (or non-linear effects). Advantage of the Monte Carlo SA is the possibility for the quantification of the sensitivity of parameters on the basis of which the parameters can be ranked.

The Shuffled Complex Evolution (SCE) algorithm was adopted for the optimisation or autocalibration of the UZ soil parameters in the MIKE-SHE model. Initially, the same objective function as in the SA, i.e. total RMSE, was set in the SCE algorithm. Hence, we were dealing with a single-objective calibration problem. The optimisation bounds were based on ranges found in the literature and were set very wide, i.e. no prior parameter measurements were included in the optimisation algorithm in any way. The SCE algorithm succeeded in finding optimal parameter sets for the MIKE-SHE model which simulate the soil moisture time series at the different depths at each location well. Effective or optimised parameter sets were compared to their measured equivalents. All parameter distributions were found significantly different at the 5 % significance level except for α of the A-horizon and K_s and θ_s of the B-horizon. From this single-objective

autocalibration, it was concluded that estimated parameters from laboratory and in-situ measurements differ from their effective equivalents needed in unsaturated zone modelling at the field scale. Additionally, it was investigated how much worse model fits were when using the measured parameter values rather than their effective equivalents. It was concluded that measured laboratory parameters are not capable of simulating reasonably the moisture content observations in the field. Hence the measured laboratory parameters were found to be useless as direct information for the model.

Different reasons were discussed that help to explain differences between 'effective' and measured parameters. The first and probably most important is the 'scaling problem'. Ideally, physical properties should be measured at the same scale as characterized by the processes described by the model. Scale differences in this study are obvious: laboratory measurements are carried out on undisturbed soil samples which have a volume of 100-cm^3, single ring pressure infiltrometer measurements on a surface of 25 cm^2 and the model domain has an area of 1 m^2 and a depth of 6 m. A second possible cause for the large gap between effective and measured parameters may have to do with the different measurement techniques used in this study. *Reynolds et al., 2000* and *Herman et al., 2003* found that using different measurement techniques even at the same scale (or sample size) can yield different conductivity estimates. Additional uncertainty is present in the observed daily soil moisture content time series and this uncertainty is consequently propagated in the estimation of the effective parameters. A third possible reason for the big gap is the question whether the global optimum of the objective function has been reached by the autocalibration algorithm. In this study, the risk of missing the global optimum has been minimised by the use of a global optimisation method, i.e. the Shuffled Complex Evolution algorithm. A last possible reason that can cause differences between effective and measured parameters has to do with the uncertainty incorporated in any kind modelling exercise. This uncertainty can be further divided in three main categories of uncertainty: (a) parameter uncertainty, which is the main topic of this PhD research, (b) model structure uncertainty and (c) input uncertainty (e.g. uncertainty in rainfall and evapotranspiration). Under different physical (soil type, slope, etc.) and climatic conditions, by using other observation types (e.g. runoff, soil water heads), and by applying other numerical models, it is possible that differences between measured and effective parameters are smaller or larger than

observed in this study. Though, as argued throughout the thesis, we believe that this difference between measured and effective parameters is likely to exist in all hydrological modelling to a smaller or larger extent.

From this, it was questioned whether measuring parameters is worthwhile if they differ from the effective parameters needed by our models anyway? It could thus be argued that it is a just a waste of time and money and we better use the available computer power to autocalibrate the parameters within wide literature ranges. To validate or contest this, the usefulness of the estimated parameters as prior information in effective parameter estimation was investigated. Therefore, a joint probability distribution of the measured parameters was calculated and subsequently incorporated as prior information in an SCE inverse optimisation and a GLUE analysis. For the SCE algorithm, prior information was incorporated by a penalty term as a second objective. This then corresponded to a multi-objective calibration with one objective being the goodness-of-fit to the observations (RMSE) and the other objective being the distance of a parameter set from the measured joint parameter probability distribution. Again, the SCE algorithm succeeded in finding optimal parameter sets for the MIKE-SHE model which simulate the soil moisture time series well. As could be expected, the trade-off between the goodness-of-fit and the distance to prior measurements was found to be large, i.e. big difference in goodness-of-fit between the mean parameter set of the prior joint probability distribution and the optimised effective parameter set. Although a large trade-off was observed, the resulting Pareto front was found to be very sharp. This means that incorporating prior information in the SCE algorithm could be achieved by relaxing only slightly the goodness-of-fit. Doing this, effective or optimised parameter sets were found close to their measured equivalents while their resulting goodness-of-fit to the observations was only slightly worse. Hence, the effective parameter sets may be more physically feasible to the field conditions than effective parameter sets from a SCE optimisation without prior information. An SCE optimisation with the incorporation of prior information as outlined in this work, efficiently utilized all relevant information from the different measurements made, i.e. soil moisture content observations as well as prior parameter measurements. The validation of the model was proven successful as differences between RMSE of the calibration and the validation period are very small. Although slightly higher RMSE values are found using the

effective parameters with the prior, the dynamics of the soil moisture content at all depths are represented better with the prior than without the prior information. This increase in dynamics is a result of the higher effective conductivities obtained when incorporating prior information in the objective function.

Thereafter, a GLUE analysis using a uniform random sampling strategy across the specified parameter range from literature and a GLUE analysis using the joint probability distribution of the measured laboratory parameters were compared. Including prior information into a GLUE analysis was again found to be useful because (i) more parameters sets are classified as behavioural and hence are available for the estimation of the uncertainty bounds and (ii) the uncertainty bounds comprise the observed data better. On top of that, behavioural parameter sets are more physically feasible as they are much closer to measured parameters. Both, the prior measured parameter distributions as well as the correlation amongst parameters were found to be useful and beneficial to include in the GLUE analysis. Incorporating prior information in a GLUE analysis was able to reduce the amount of model evaluations needed for the same amount of behavioural parameter sets.

It is true that **effective** parameters were found **different** from the **measured** ones when doing a **'blind' optimisation**, i.e. an inverse modelling with wide literature parameter bounds. And even though the **prior information** was observed to be useless as direct model input, the incorporation of prior information in both the **SCE** and the **GLUE** algorithm showed that this prior information is **not useless**. The PhD research showed that the measuring of parameters although being very expensive (time and money), is useful but that care should be taken interpreting the measured parameter values. Even if it is found useless as direct model input, incorporating prior parameter measurements in an automated parameter estimation strategy is useful. It may either result in more 'physically feasible' effective parameter sets (SCE algorithm) or reduce the number of simulations needed (GLUE).

To conclude this PhD research, the importance of the quality of the rainfall time series on hydrological modelling and on effective parameter estimates was briefly examined. It was shown that the temporal resolution of rainfall is extremely important for the correct simulation of cumulative runoff over a year but hardly influences the simulation

of daily soil moisture content values at different depths over a year. Therefore, an easy-to-use and powerful tool of incorporating rainfall intensity into daily rainfall records for the estimation of infiltration and/or runoff volumes over long time periods was developed. The developed procedure is easily understandable and very easy to apply compared to disaggregation techniques of daily rainfall to a finer temporal resolution which all use very sophisticated statistical techniques. It was concluded that such techniques are not required when one is interested in the simulation of cumulative hydrological variables over months/years.

For the investigation of the importance of the temporal resolution of rainfall on effective parameter estimates, an SCE optimisation algorithm was set up for the estimation of K_s using different temporal rainfall resolutions. As observations, the simulated daily runoff using 10 minute input rainfall data (= reference run) was taken. The SCE succeeded in finding an effective K_s value that resulted in relatively high model efficiency (against reference run) using daily rainfall records. Even though the relatively high model efficiency, the dynamics were poorly mimicked. Additionally, effective K_s was found to be a function of the temporal rainfall resolution i.e. effective K_s using daily rainfall input records was found to be smaller than the K_s used in the reference model. Disaggregation of the daily rainfall records according to the presented procedure, resulted in an effective K_s very close to the reference K_s.

For large catchment models with many parameters, an autocalibration using daily rainfall records could probably find an effective parameter set that produces an acceptable fit with a reasonable match of the dynamics. Although validating this requires more research, disaggregating the daily rainfall according to the procedure presented will probably increase the efficiency of the (auto)calibrated model. Effective parameters of the autocalibrated model using daily rainfall records are for sure less 'realistic' than effective parameters resulting from the model with the 10 minute or the disaggregated rainfall time series. As said earlier, although more research on this topic is needed to validate some of these conclusions, this PhD research shows that reliability of the estimated effective parameters does not depend only on commonly mentioned factors such as type and quality of the observations, the way the model describes the

different processes, optimisation algorithm, … but also on the quality of the rainfall time series, and most likely time series of other input variables.

8.2. Innovative aspects of the study and recommendations for future research

From the problems encountered during and after the set-up of the experiment, some recommendations for similar future experimental research were suggested in Chapter 2. We believe that innovative about the experimental set-up is the way the TDR system worked. The methodology developed for the analysis of waveforms captured with longer cable lengths was evaluated as very successful. The size of the experimental hillslope (80 by 20 m) is also larger than sizes of other hillslope experimental sites mentioned in literature. Single-ring pressure infiltrometer measurements as such have existed since almost 2 decades. Though, the analysis of the measurements for the estimation of the field saturated hydraulic conductivity developed in this study, is believed to be innovative and certainly preferable over the classical approach. The methodology results in robust estimates of the field saturated hydraulic conductivity. Though robust estimates are obtained, care must be taken interpreting its value as shown by *Reynolds et al. (2000)*. Those authors illustrated that hydraulic conductivity estimates using different measurement techniques may differ. In this respect, future research is needed to contest or confirm these findings and suggest possible explanations, keeping in mind the scale issue.

The parameter identifiability problem forms the major topic of many hydrological studies in literature since little over a decade. The contributing aspect to the existing literature of this study lies within the way this study combines the measuring of parameters with inverse modelling techniques. The study shows that combining both more efficient in the estimation of effective parameters than when they are applied individually. The PhD research presents methods of incorporating prior measured parameter information in two different parameter estimation strategies, i.e. GLUE and SCE algorithms. Considering the distance from the prior measured parameter information as an objective in the objective function and consequently solving the

problem in a multi-objective calibration framework, is according to our knowledge innovative. The research confirms that measuring parameters although being highly time and money consuming is worthwhile but that at the same time care should be taken using the prior measured parameters as direct model input. Future research concerning the incorporation of prior measured parameter information in the SCE and GLUE algorithms, as performed in this study, is required to confirm the findings of this study. It is desirable that the methods of incorporating prior measured information in SCE and GLUE algorithms are repeated for different scales and types of models.

From these conclusions, it is suggested that future research is needed concerning both parameter measurement techniques and optimisation algorithms. As mentioned earlier, development of new in-situ and laboratory measurement techniques for the estimation of model parameters at different scales is crucial. For larger scales, remote-sensing techniques such as satellite images, radar images or air photographs offer perspectives. In this respect, upscaling and downscaling research can also help in the estimation of parameters at scales needed by the model on the basis of parameter estimates made at a smaller (upscaling) or larger (downscaling) scale. The inverse modelling algorithm used in this study, the SCE algorithm, is probably the most robust algorithm currently available for highly non-linear systems such as an unsaturated zone model. Though, more research is needed to incorporate some uncertainty analysis in global inverse optimisation algorithms. The GLUE algorithm as applied in this study, is capable of estimating some uncertainty bounds on the simulated model. Drawbacks of this method are the rather subjective character and the amount of model simulations needed. Future research attempting to develop a robust global optimisation algorithm capable of performing an uncertainty analysis is required.

The end of the PhD research deals with the importance of the quality of the rainfall time series on hydrological modelling and on effective parameter estimates. Although only briefly discussed, it was included in this text because of its importance and because very few or no literature can be found dealing with this problem. The presented procedure of incorporating rainfall intensity into daily rainfall records needs to be tested at the catchment scale and for the simulation of different hydrological variables. It is believed that even for catchment models, temporal resolution of rainfall is important for the

simulation of river discharge as well as for the estimated values of the effective parameters. To confirm this, research is needed investigating the effect of the temporal resolution of rainfall and evapotranspiration on effective parameter estimations at different scales.

References

A

Allen, R., L. Pereira, D. Raes and M. Smith, 1998. Crop evapotranspiration (Guidelines for computing crop water requirements). FAO Irrigation and Drainage Paper, No. 56. Rome, Italy, 297p.

Angulo-Jaramillo, R., J.P. Vandervaere, S. Roulier, J.L. Thony, J.P. Gaudet and M. Vauclin, 2000. Field measurement of soil surface hydraulic properties by disc and ring infiltrometers: A review and recent developments. *Soil & Tillage Research*, 55, 1-29.

Ankeny, M.D., M. Ahmed, T.C. Kaspar and R. Horton, 1988. Design for automated tension infiltrometer. *Soil Sci. Soc. Am. J.*, 552, 893-896.

Averjanov, S.F., 1950. About permeability of subsurface soils in case of incomplete saturation. In English Collection, Vol. 7. As quoted by P. Ya Palubarinova, 1962. The theory of ground water movement (English translation by I.M. Roger DeWiest. Princeton University Press, Princeton, NJ), 19-21.

B

Bagarello, V. and G. Provenza, 1996. Factors affecting field and laboratory measurements of saturated hydraulic conductivity. *Trans. ASAE.*, 39, 153-159.

Baker, J.M. and R.R. Allmaras, 1990. System for automating and multiplexing soil moisture measurement by time-domain reflectometry. *Soil Sci. Soc. Am. J.*, 54, 1-6.

Bard, Y., 1974. Non-linear parameter estimation, Academic, San Diego, California.

Bashford, K.E., K.J Beven and P.C. Young, 2002. Observational data and scale-dependent parameterizations: Explorations using a virtual hydrological reality. *Hydrol. Proc.*, 16, 293-312.

Beven, K. and P. Germann, 1982. Macropores and water flow in soils. *Water Resour. Res.*, 18, 1311-1325.

Beven, K., 1989. Changing ideas in hydrology – the case of physically based models. *J. Hydrol.*, 105, 157-172.

Beven, K. and A. Binley, 1992. The future of distributed models: model calibration and uncertainty prediction. *Hydrol. Proc.*, 6, 265-277.

Beven, K., 1993. Prophecy, reality and uncertainty in distributed hydrological modelling. *Adv. Water Resour.*, 16, 41-51.

Beven, K., 2001. Rainfall-runoff modelling: the Primer. John Wiley & Sons, New York, 372p.

Beven, K. and J. Freer, 2001. Equifinality, data assimilationand uncertainty estimation in mechanistic modelling of complex environmental systems using the GLUE methodology. *J. Hydrol.*, 249, 11-29.

Beyazgül, M., Y. Kayama and F. Engelsman, 2000. Estimation methods for crop water requirements in the Gediz Basin of western Turkey. *J. Hydrol.*, 229, 19-26.

Bierkens, M.F.P, P.A. Finke and P. De Willigen, 2000. Upscaling and downscaling methods for environmental research. Developments in plant and soil sciences, Vol. 88. Kluwer Academic Publishers, 190p.

Blöschl, G. and M. Sivapalan, 1995. Scale issues in hydrological modelling: a review. *Hydrol. Proc.*, 9, 251-290.

Boulet, G., J.D. Kalma, I. Braud and M. Vauclin, 1999. As assessment of effective land surface parameterisation in regional scale water balance studies. *J. Hydrol.*, 217, 225-238.

Bouma, J., 1981. Soil morphology and preferential flow along macropores. *Agric. Water Manag.*, 3, 235-250.

Boyle, D.P., H.V. Gupta and S. Sorooshian. 2000. Toward improved calibration of hydrological models: Combining the strengths of manual and automatic methods. *Water Resour. Res.*, 36, 3663-3674.

C

Carsel, R.F. and R.S. Parrish, 1988. Developing joint probability distributions of soil-water retention characteristics. *Water Resour. Res.*, 24, 755-769.

Choisnel, E., O. de Villele and F. Lacroze, 1992. Une approche uniformisée du calcul de l'évapotranspiration potentielle pour l'ensemble des pays de la communauté européenne. Commission de Communautés Européennes, Bruxelles-Luxembourg, 176p.

Christensen, S., 1997. On the strategy of estimating regional-scale transmissivity fields. *Groundwater*, 35, 131-139.

Christiaens, K. and J. Feyen, 2002. Constraining soil hydraulic parameter and output uncertainty of the distributed hydrological MIKE-SHE model using the GLUE framework. *Hydrol. Proc.*, 16, 373-391.

Conover, W. J., 1980. Practical nonparametric statistics. John Wiley & Sons, New York, 493p.

Cooper, V.A., V.T.V. Nguyen and J.A. Nicell, 1997. Evaluation of global optimization methods for conceptual rainfall-runoff model calibration. *Wat. Sci. Tech.*, 36, 53-60.

Cressie, N.A.C., 1993. Statisistics for spatial data. John Wiley & Sons, New York, 900p.

D

Dawdy, D.R. and T.O Donnell, 1965. Mathematical models of catchment behavior, *J. Hydraul. Div.*, 91(HY4), 113-137.

De Lima, M.I.P. and J. Grasman, 1999. Multifractal analysis of 15-min and daily rainfall from a semi-arid region in Portugal. *J. Hydrol.*, 220, 1-11.

de Vos, J.A., 1997. Water flow and nutrient transport in a layered silt loam soil. Ph.D. thesis. Wageningen Agricultural University, Wageningen, The Netherlands, 287p.

Demarée, G.R., M. De Corte, S. Derasse, M. Devorst and Ch. Trapenard, 1998. Een Kranige honderdjarige: De Hellmann-Fuess pluviograaf van het Koninklijk Meteorologisch Instituut te Ukkel (Belgium). *Water*, 100.

Deutsch, C. and A. Journal, 1992. GSLIB, Geostatistical Software Library and User's Guide. Oxford University Press, NY, 340p.

Duan, Q., 1992. The Shuffled Complex Evolution (SCE) method: Concept representation. Appendix to the SCE-UA software code.

Duan, Q., S. Sorooshian and V.K. Gupta, 1992. Effective and efficient global optimisation for conceptual rainfall-runoff models. *Water Resour. Res.*, 28, 1015-1031.

Duan, Q., V.K. Gupta and S. Sorooshian, 1993. A shuffled complex evolution approach for effective and efficient global minimization. *J. Optim. Theory and Appl.*, 76, 501-521.

Duan, Q., S. Sorooshian and V.K. Gupta, 1994. Optimal use of the SEC-UA global optimisation method for calibrating watershed models. *J. Hydrol.*, 158, 265-284.

Dunne, T. and L.B. Leopold, 1983. Water in environmental planning. W.H. Freeman, New York.

Durner, W., 1994. Hydraulic conductivity estimation for soils with heterogeneous pore structure. *Water Resour. Res.*, 30, 211-223.

E

Econopuly, T.W., 1987. Adaptability of a daily disaggregation model to the Midwestern Unites States. MSc-thesis, University of Arizona, Tucson, AZ, USA, 132p.

Edwards, W.M., L.D. Norton and C.E. Redmond, 1988. Characterising macropores that affect infiltration into non-tilled soil. *Soil Sci. Soc. Am. J.*, 52, 483-487.

Elrick, D.E., W.D. Reynolds and K.A. Tan, 1989. Hydraulic conductivity measurements in the unsaturated zone using improved well analyses. *Groundwater Monit. Rev.*, 9, 184-193.

Elrick, D.E. and W.D. Reynolds, 1992. Advances in Measurement of soil physical properties: Bringing theory into practice. *SSSA Special Publication*, 30, 1-24.

Elrick, D.E. and W.D. Reynolds, 1992. Methods for analyzing constant head well permeameter data. *Soil Sci. Soc. Am. J.*, 56, 320-323.

Elrick, D.E., G.W. Parkin, W.D. Reynolds and D.J. Fallow, 1995. Analysis of early-time and steady-state single-ring infiltration under falling head conditions. *Water Resour. Res.*, 31, 1883-1893.

F

Faeh, A.O., 1997. Understanding the processes of discharge formation under extreme precipitation: A study based on the numerical simulation of hillslope experiments. Mitteilung der Versuchsanstalt für Wasserbau, Hydrologie und Glaziologie, Zürich, Nr. 150.

Faeh, A.O., S. Scheerer and F. Naef, 1997. A combined field and numerical approach to investigate flow processes in natural macroporous soils under extreme precipitation. *Hydr. and Earth Syst. Sci.*, 4, 787-800.

Famiglietti, J., J.W. Rudnicki and M. Rodell, 1998. Variability in surface moisture content along a hillslope transect: Rattlesnake Hill, Texas. *J. Hydrol.*, 210, 259-281.

Ferré, P.A., D.L. Rudolph and R.G. Kachanoski, 1996. Spatial averaging of water content by time domain reflectometry: Implication for twin rod probes with and without dielectric coatings. *Water Resour. Res.*, 32, 271-279.

Franchini, M., G. Galeati and S. Berra, 1998. Global optimization techniques for the calibration of conceptual rainfall-runoff methods. *Hydrol. Sci. J.*, 43, 443-458.

Franks, S.W., P. Gineste, K.J. Beven and P. Merot, 1998. On constraining the predictions of a distributed model: The incorporation of fuzzy estimates of saturated areas into the calibration process. *Water Resour.Res.*, 34, 787-797.

Freer, J., K.J. Beven and B. Ambroise, 1996. Bayesian estimation of uncertainty in runoff prediction and the value of data: An application of the GLUE approach. *Water Resour.Res.*, 32, 2161-2173.

G

Gan, T.Y. and G.F. Biftu, 1996. Automatic calibration of conceptual rainfall-runoff models: Optimisation algorithms, catchment conditions and model structure. *Water Resour.Res.*, 32, 12, 3513-3524.

Gardner, W.R., 1958. Some steady-state solutions of unsaturated moisture flow equations with application to evaporation from a water table. *Soil Sci.*, 85, 228-232.

Grayson, R.B., I.D. Moore and T.A. McHahon, 1992a. Physically based hydrologic modelling. 1: A terrain-based model for investigative purposes. *Water Resour. Res.*, 28, 2639-2650.

Grayson, R.B., I.D. Moore and T.A. McHahon, 1992b. Physically based hydrologic modelling. 2: Is the concept realistic? *Water Resour. Res.*, 28, 2651-2658.

Grayson, R.B., A.W Western and F.H.S. Chiew, 1997. Preferred states in spatial soil moisture patterns: Local and nonlocal controls. *Water Resour. Res.*, 12, 2897-2908.

Gupta, V.K. and S. Sorooshian, 1985. The relationship between data and the precision of parameter estimates of hydrologic models. *J. Hydrol.*, 81, 57-77.

Gupta, V.K., S. Sorooshian and P.O. Yapo, 1998. Towards improved calibration of hydrological models: Multiple and non-commensurable measures of information. *Water Resour. Res.*, 34, 751-763.

Gupta, H.V., S Sorooshian and P.O. Yapo, 1999. Status of automatic calibration for hydrological models: Comparison with multilevel expert calibration. *J. Hydrol. Eng.*, 4, 135-143.

Gyasi-Agyei, Y., 1999. Identification of regional parameters of a stochastic model for rainfall disaggregation. *J. Hydrol.*, 223, 148-163.

H

Heimovaara, T.J. and W. Bouten, 1990. A computer controlled 36-channel time domain reflectometry system for monitoring soil water contents. *Water Resour. Res.*, 26, 2311-2316.

Heimovaara, T.J., 1993a. Time domain reflectometry in soil science: theoretical backgrounds, measurements and model. Doctoral Thesis Universiteit van Amsertdam with ref. ISBN 90-6787-036-6.

Heimovaraa, T.J., 1993b. Design of Triple-Wire time Domain Reflectometry Probes in Practice and Theory. *Soil Sci. Soc. Am. J.*, 57, 1410-1417.

Heimovaara, T.J., A.G. Focke, W. Bouten and J.M. Verstaten, 1995. Assessing temporal variations in soil water composition with time domain reflectometry. *Soil Sci. Soc. Am. J.*, 59, 689-698.

Heinen, M. and P.A.C. Raats, 1990. Evaluation of two models describing the steady discharge from a constant head well permeameter into unsaturated soil. *Soil Sci.*, 150, 401-412.

Herkelrath, W.N., S.P. Hamburg and F. Murphy, 1991. Automatic real-time monitoring of soil moisture in a remote field area with time domain reflectometry. *Water Resour. Res.*, 27, 857-864.

Herman, S., J. Mertens, A. Timmerman and J. Feyen, 2003. Comparison of tension infiltrometer, single-ring pressure infiltrometer and soil core K_{sat} estimates on a sandy loam hillslope. EGS-AGU-EUG Joint Assembly, Nice, France, April 06-11.

Hershenhorn, J., and D.A. Woolhiser, 1987. Disaggregation of daily rainfall. *J. Hydrol.*, 95, 299-322.

Hillel, D., 1980. Applications of soil physics. Academic Press, New York, New York, USA.

Hooke, R. and T.A. Jeeves, 1961. Direct search solutions of numerical and statistical problems. *Journ. Assoc. Comput. Mach.*, 8, 212-229.

I

Ibbitt, R.P., 1970. Systematic parameter fitting for conceptual models of catchment hydrology. Ph.D. dissertation, Imperial College of Science and Technology, University of London, London, England.

J

Jacques, D., 2000. Analysis of water flow and solute transport at the field scale. Ph.D.-thesis Nr. 454, Faculty of Agricultural and Applied Biological Sciences, K.U.Leuven, Belgium, 255p.

Johnson, M.E. 1987. Multivariate statistical simulation. John Wiley & Sons, New York, 230 p.

Johnson, N.L. and S. Kotz., 1970. Distributions in statistics: Continuous Univariate Distributions. Vol. 1, Houghton Mifin Company, Boston, Massachusetts, USA.

Johnson, P.R. and D. Pilgrim, 1976. Parameter optimisation of watershed models. *Water Resour. Res.*, 12, 477-486.

Johnson, R.A. and D.W. Wichern, 1992. Applied Multivariate Statistical Analysis. Prentice-Hall International Editions, Englewood cliffs, USA.

Journal, A.G. and C. Huijbregts, 1978. Mining geostatistics. Academic Press, New York, USA.

Jury, W.A., 1985. Spatial variability of soil physical parameters in solute migration: A critical literature review. EPRI EQ-4228 Project 2485-6, Riverside, CA, USA.

Jury, W.A., D. Russo, G. Sposito and H. Elabd, 1987. The spatial variability of water and solute transport properties in unsaturated soil. I. Analysis of property variation and spatial structure with statistical models. *Hilgardia*, 55, 1-32.

Jury, W.A., D. Russo, G. Sposito and H. Elabd, 1987. The spatial variability of water and solute transport properties in unsaturated soil. II. Scaling models of water transport. *Hilgardia*, 55, 33-56.

K

Kihupi N. 1990. Extension of one-dimensional water balance simulation models to heterogenous soil systems with special reference to macroporous soils. Ph.D.-thesis Nr. 189, Faculty of Agricultural and Applied Biological Sciences, K.U.Leuven, Belgium, 149p.

Kite, G.W. and P. Droogers, 2000. Comparing evapotranspiration estimates from satellites, hydrological models and field data. *J. Hydrol.,* 229, 3-18.

Klute, A., 1986. Water Retention: Laboratory Methods. In 'Methods of Soil Analysis. Part 1. Physical and Mineralogical Methods, Second Edition', A. Klute (ed.). Agronomy, No. 9, Part 1, 2nd edition.

Kristensen, K.J. and S.E. Jensen, 1975. A model for estimating actual evapotranspiration from potential evapotranspiration. *Nordic Hydrology*, 6, 170-188.

Kuczera, G., 1982. On the relationship of the reliability of parameter estimation and hydrologic time series data used in calibration. *Water Resour. Res.,* 18, 146-154.

Kuczera, G., 1997. Efficient subspace probabilistic parameter optimization for catchment models. *Water Resour. Res.*, 33, 177-185.

L

Lamb, R., K.J. Beven and S. Myrabo, 1998. Use of spatially distributed water table observations to constrain uncertainty in a rainfall-runoff model. *Adv. Water Resour.*, 22, 305-317.

Lauren, J.G., R.J. Wagenet, J. Bouma, and J.H.M. Wosten, 1988. Variability of saturated hydraulic conductivity in a glossaquic hapludalf with macropores. *Soil Sci.*, 145, 20-28.

Levenberg, K., 1944. A method for the solution of certain problems in least squares. *Quarterly Applied Math*, 2, 164-168.

Logsdon, S.D., L. Allmaras, L. Wu, J.B. Swann and G.W. Randall, 1990. Macroporosity and its relation to saturated hydraulic conductivity under different tillage practices. *Soil Sci. Soc. Am. J.*, 54, 1096-1101.

Luce, C.H. and T.W. Cundy, 1994. Parameter identification for a runoff model for forest roads. *Water Resour. Res.*, 30, 4, 1057-1069.

M

Madsen, H., 2000. Automatic calibration and uncertainty assessment in rainfall-runoff modelling. 2000 Joint conference on Water Resources Engineering and Water Resources Planning and Management, Hyatt Regency Minneapolis, USA, July 30-August 2.

Madsen, H., G. Wilson and H.C. Ammentorp, 2002. Comparison of different automatic strategies for calibration of rainfall-runoff models. *J. Hydrol.*, 261, 48-59.

Madsen, H. and M. Kristensen, 2003. Autocal: a generic tool for automatic calibration, sensitivity analysis and scenario management of numerical models. Model documentation and user guide, Internal report of the Danish Hydraulic Institute.

Madsen, H., 2003. Parameter estimation in distributed hydrological catchment modelling using automatic calibration with multiple objectives. *Adv. Water Resour.* 26, 205-216.

Mallants, D., D. Jacques, M. Vanclooster, J. Diels and J. Feyen, 1996. A stochastic approach to simulate water flow in a macroporous soil. *Geoderma*, 70, 299-324.

Mallants, D., B.P. Mohanty, A. Vervoort, and J. Feyen, 1997a. Spatial analysis of saturated hydraulic conductivity in a soil with macropores. *Soil Techn.*, 10, 115-131.

Mallants, D., Tseng, P.H., Toride, N., Timmerman, A. and J. Feyen, 1997b, Evaluation of multimodal hydraulic functions in characterizing a heterogeneous field soil, *J. Hydrol.*, 195, 172-199

Marquardt, D., 1963. An algorithm for least squares estimation of nonlinear parameters. *SIAM Journal Applied Math.*, 11, 431-441.

Masri, S.F., G.A. Bekey and F.B. Safford, 1976. An adaptive random search method for identification of large scale nonlinear systems. Proceedings of the 4th IFAC symposium on identification and system parameter estimation. North-Holland, Amsterdam.

McLaughin, D. and L.R. Townley, 1996. A reassessment of the groundwater inverse problem. *Water Resour. Res.*, 32, 1131-1161.

Mertens, J., D. Raes and J. Feyen, 2002a. Incorporating rainfall intensity into daily rainfall records for simulating runoff and infiltration into soil profiles. *Hydr. Proc*, 16, 731-739.

Mertens, J., D. Jacques, J. Vanderborght and J. Feyen, 2002b. Characterisation of the field-saturated hydraulic conductivity on a hillslope: In situ single ring pressure Iinfiltrometer measurements. *J. Hydrol.*, 263, 217-229.

Mertens, J., H. Madsen, M. Kristensen, D. Jacques and J. Feyen, 2003a. Sensitivity of soil parameters in unsaturated zone modelling and the relation between effective, laboratory and in-situ estimates. Submitted to *Hydr.Proc.*

Mertens, J., H. Madsen, L. Feyen, D. Jacques, and J. Feyen, 2003b. Including prior information and its relevance in the estimation of effective soil parameters in unsaturated zone modelling. Submitted to *J. Hydrol.*

Meyer, P.D., M.L. Rockhold and G.W. Gee, 1997. Uncertainty analyses of infiltration and subsurface flow and transport for SDMP sites. NUREG/CR-6565. Pacific Northwest National Laboratory prepared for U.S. Nuclear Regulatory Commission.

Mohanty, B.P., M.D. Ankeny, R. Horton and R.S. Kanwar, 1994. Spatial analysis of hydraulic conductivity using disc infiltrometers. *Water Resour. Res.*, 30, 2489-2498.

Morris, M.D., 1991. Factorial sampling plans for preliminary computational experiments. *Technometrics*, 33, 161-174.

Mualem, Y., 1976. A new model predicting the hydraulic conductivity of unsaturated porous media. *Water Resour. Res.*, 12, 513-522.

N

N. N., 1996. MATLAB®, High-Performance numeric computation and visualisation software. Users Guide, The Math Works Inc.

Nash, J.E. and J.V. Sutcliffe, 1970. River flow forecasting through conceptual models, Part 1: A discussion of principles. *J. Hydrol.*, 10, 282-290.

Nelder, J.A. and R. Mead, 1965. A simplex method for function minimization. *Comput. J.*, 7, 308-313.

P

Philip, J.R., 1985. Approximate analysis of the borehole permeameter in unsaturated soil. *Water Resour. Res.*, 21, 1025-1033.

Press, W., P. Flannery, S.A. Teukolksky and W.T. Vetterling, 1986. Numerical recipes, Cambridge University Press, New York, USA.

Pronzato, L., E. Walter, A. Venot and J.F. Lebruchec, 1984. A general purpose global optimizer: implementation and applications. *Mathematics and Computers in Simulation*, 26, 412-422.

R

Radwan, M., 2002. 'River water quality modelling as water resources management tool at catchment scale', Doctoral dissertation, Faculty of Engineering, K.U.Leuven, Belgium

Raes, D., 2002. ETO - calculation of reference evapotranspiration software (http://www.iupware.be). Faculty of Agricultural and Applied Biological Sciences, K.U.Leuven, Belgium

Refsgaard, J.C. and B. Storm, 1995. MIKE SHE. In: Singh (Ed.). Computer models of watershed hydrology. Water Resources Publications, Colorado, USA, 809-846.

Refsgaard, J.C., 1997. Parameterisation, calibration and validation of distributed hydrological models. *J. Hydrol.*, 198, 69-97.

Refsgaard, J.C., Butts, M.B. 1999. Determination of grid scale parameters in catchment modelling by upscaling local scale parameters. *Modelling of transport processes in soils. Ed. by Feyen, J. & K. Wiyo*, p. 650-665

Reynolds, W.D., D.E. Elrick and G.C. Topp, 1983. A reexamination of the constant head well permeameter method for measuring saturated hydraulic conductivity above the water table. *Soil Sci.*, 136, 250-268.

Reynolds, W.D., D.E. Elrick and B.E. Clothier, 1985. The constant head well permeameter: Effect of unsaturated flow. *Soil Sci.*, 139, 172-180.

Reynolds, W.D. and D.E. Elrick, 1990. Ponded infiltration from a single ring. Part 1. Analysis of steady flow. *Soil Sci. Soc. Am. J.*, 54, 1233-1241.

Reynolds, W.D., B.T. Bowman, R.R Brunke, C.F. Drury and C.S. Tan, 2000. Comparison of tension infiltrometer, pressure infiltrometer and soil core estimates of saturated hydraulic conductivity. *Soil Sci. Soc. Am. J., 64,* 478-484.

Richards, L.A., 1931. Capillary conduction of liquids through porous mediums. *Physics*, 1, 318-333.

Richardson, C.W. and D.A. Wright, 1984. WGEN: A model for generating daily weather variables. USDA-ARS, ARS-8, 83p.

Rosenbrock, H.H., 1960. An automatic method for finding the greatest or least value of a function. *Computer Journal*, 3, 175-184.

Russo, D. and W.A. Jury, 1987a. A theoretical study of the estimation of the correlation scale in spatially variable fields: 1. Stationary fields. *Water Resour. Res,* 23, 1257-1268.

Russo, D. and W.A. Jury, 1987b. A theoretical study of the estimation of the correlation scale in spatially variable fields: 2. Nonstationary fields. *Water Resour. Res*, 23, 1269-1279.

Russo, D., I. Russo and A. Laufer, 1997. On the spatial variability of parameters of the unsaturated hydraulic conductivity. *Water Resour. Res.*, 33, 947-956.

S

Saltelli, A., K. Chan and E.M. Scott, 2000. Sensitivity analysis. Wiley Series in Probability and Statistics. John Wiley & Sons, New York, 477p.

Schaap, M.G., F.J. Leij and M. Th. Van Genuchten, 1998. Neural network analysis of hierarchical prediction of soil hydraulic properties. *Soil Sci. Soc. Am. J.*, 62, 847-855.

Schwab, G.O., D.D. Fangmeier DD and W.J. Elliot, 1996. Soil and water management systems. John Wiley & Sons, New York, 371p.

Sorooshian, S., V.K. Gupta and J.L. Fulton, 1983. Evaluation of maximum likelihood parameter estimation techniques for conceptual rainfall-runoff models: Influence of calibration data variability and length on model credibility. *Water Resour. Res.,* 19, 251-259.

Sorooshian, S., Q. Duan and V.K. Gupta, 1993. Calibration of rainfall-runoff models: Application of global optimisation to the Sacramento Soil Moisture accounting model. *Water Resour. Res.*, 29, 1185-1194.

Sooroshian, S. and V.K. Gupta, 1995. Model calibration. In: Singh (Ed.). Computer models of watershed hydrology. Water Resources Publications, Colorado, USA. 809-846.

Spear, R.C. and G.M. Hornberger, 1980. Eutrophication in peel inlet. II: Identification of critical uncertainties via generalized sensitivity analysis. *Water Resour. Res.*, 14, 43-49.

Steenhuis, T., M. Winchell, J. Rossing, J.A. Zollweg and M.F. Walter, 1995. SCS runoff equation revisited for variable-source runoff areas. *J. of Irrig. and Drain. Eng..*, 234-238.

Stephens, D.B., K. Lambert and D. Watson, 1987. Regression models for hydraulic conductivity and field test of the borehole permeameter. *Water Resour. Res.*, 23, 2207-2214.

T

Thyer, M., G. Kuczera and B.C. Bates, 1999. Probabilistic optimisation for conceptual rainfall-runoff models: A comparison of the Shuffled Complex Evolution and simulated annealing algorithms. *Water Resour. Res.*, 35, 767-773.

Topp, G.C., J.L. Davis and A.P. Annan, 1980. Electromagnetic determination of soil water content: Measurement in coaxial transmission lines. *Water Resour. Res.*, 16, 574-582.

Topp, G.C. and J.C. Davis, 1985. Measurement of soil water content using time-domain reflectometry (TDR): A field evaluation. *Soil Sci. Soc. Am. J.*, 49, 19-24.

U

United Stated Department of Agriculture, Soil Conservation Service. 1985. National Engineering Handbook, Section 4: Hydrology.

V

van Genuchten, M.Th., 1980. A closed-form equation for predicting the hydraulic conductivity of unsaturated soils. *Soil Sci. Soc. Am. J.*, 44, 892-898.

van Genuchten, M.Th., Leij, F.J. and S.R. Yates, 1991. The RETC Code for Quantifying the Hydraulic Functions of Unsaturated Soils. U.S. Salinity Laboratory, U.S. Department of Agriculture, Riverside, California, USA, 85p.

Vanderborght, J., A. Timmerman and J. Feyen, 2000. Solute transport for steady-state and transient flow with and without macropores. *Soil Sci. Soc. Am. J.*, 64, 1305-1317.

Vauclin, M., D.E. Elrick, J.L. Thony, G. Vachaud, Ph. Revol and P. Ruelle, 1994. Hydraulic conductivity measurements of the spatial variability of a loamy soil. *Soil Technol.*, 7, 181-195.

Vazquez, R. and J. Feyen, 2003. Effect of potential evapotranspiration estimates on effective parameters and performance of the MIKE SHE-code applied to a medium-size catchment. *J. Hydr.*, 270, 309-327.

Vrugth, J.A., W. Bouten, H.V. Gupta and S. Sooroshian, 2002. Toward improved identifiably of hydrologic model parameters: The information content of experimental data. *Water Resour. Res.*, 38, 12, 1-13.

W

Wang, Q.J., 1991. The genetic algorithm and its application to calibrating conceptual rainfall-runoff models. *Water Resour. Res.*, 9, 2467-2471.

Weiler, M., F. Naef and C. Leibundgut, 1998. Study of runoff generation on hillslopes using tracer experiments and physically based numerical model. *IAHS Publications*, 248, 353-360.

White, R.E., 1985. The influence of macropores on the transport of dissolved and suspended matter through soil. *Ad. Soil Sci.*, 3, 95-121.

Willems, P., 2000. 'Probabilistic immission modelling of receiving surface waters', Doctoral dissertation, Faculty of Engineering, K.U.Leuven, October 2000.

Wu, L., J.B. Swan, J.L. Nieber and R.R. Allmaras, 1993. Soil-macropore and layer influences on saturated hydraulic conductivity measured with borehole permeameters. *Soil Sci. Soc. Am. J.*, 57, 917-923.

X

Xu, C.Y. and V.P. Singh, 1998. Dependence of evaporation on meteorological variables at different time-scales and intercomparison of estimation methods. *Hydr. Proc*, 12, 429-422.

Xu, C.Y. and V.P. Singh, 2000. Evaluation and generalization of radiation-based methods for calculating evaporation, *Hydr. Proc*, 14, 339-349.

Y

Yapo, P.O., V.K. Gupta and S. Sorooshian, 1996. Calibration of conceptual rainfall-runoff models: Sensitivity to calibration data. *J. Hydrol.*, 181, 23-48.

Yapo, P.O., V.K. Gupta and S. Sorooshian, 1998. Multi-objective global optimisation for hydrologic models. *J. Hydrol*., 204, 83-97.

Z

Zavattaro, L., N. Jarvis and L. Persson, 1999. Use of similar media scaling to characterise spatial dependence of near saturated hydraulic conductivity. *Soil Sci. Soc. Am. J.*, 63, 486-492.

Zhu, J. and B.P. Mohanty, 2002. Upscaling of soil hydraulic properties for steady state evaporation and infiltration. *Water Resour. Res.*, 38, 1178-1189.

References

Appendix A

The multivariate normal density

The multivariate normal density is a generalisation of the univariate normal density to $p \geq 2$ dimensions. Recall the univariate normal distribution, with mean μ and variance σ^2, has the probability density function:

$$f(x) = \frac{1}{\sqrt{2\pi\sigma^2}} e^{\frac{-[(x-\mu)/\sigma]^2}{2}} \qquad -\infty < x < +\infty \qquad \text{(A.1)}$$

A plot of this function yields the familiar bell-shaped curve shown in Fig. A.1. Also shown in the figure are approximate areas under the curve within ± 1 standard deviation and ± 2 standard deviations of the mean. These areas represent probabilities and thus, for the normal random variable *X*,

$$P(\mu - \sigma \leq X \leq \mu + \sigma) \cong 0.68$$
$$P(\mu - 2\sigma \leq X \leq \mu + 2\sigma) \cong 0.95$$

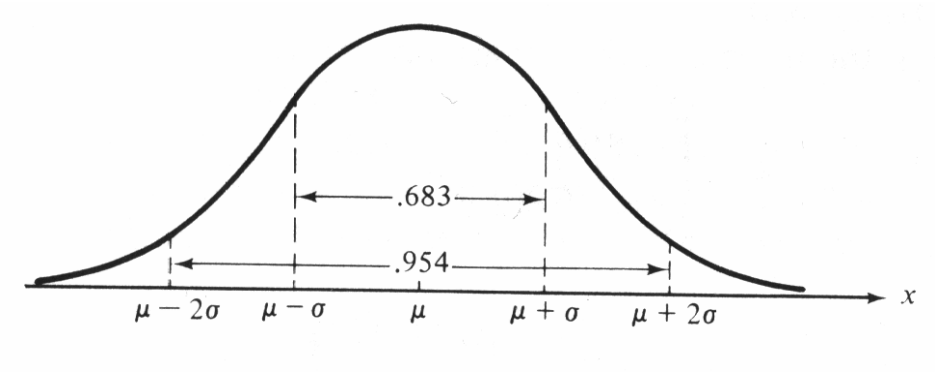

Figure A.1 A normal density with mean μ and variance σ and selected areas under the curve (after Johnson and Wichern, 1992)

It is convenient to denote the normal density function with mean μ and variance σ^2 by $N(\mu,\sigma^2)$. Therefore, $N(10,4)$ refers to the function with $\mu = 10$ and $\sigma = 2$. This notation is extended to the multivariate case below.

The term

$$\left(\frac{x-\mu}{\sigma}\right)^2 = (x-\mu)(\sigma^2)^{-1}(x-\mu) \qquad \text{(A.2)}$$

in the exponent of the univariate normal density function measures the squared distance from x to μ in standard deviation units. This can be generalized for a p x 1 vector x as:

$$(x-\mu)' \sum^{-1} (x-\mu) \qquad \text{(A.3)}$$

The p x 1 vector μ represents the expected value of the random vector X, and the p x p matrix Σ is its variance-covariance matrix. The covariance matrix can be written as $\Sigma = \begin{bmatrix} \sigma_{11} & \sigma_{12} \\ \sigma_{21} & \sigma_{22} \end{bmatrix}$. We shall assume the symmetric matrix Σ is positive definite, so the expression in Eq. A.3 is the squared generalized distance from x to μ..

The multivariate normal density is obtained by replacing the univariate distance Eq. A.2 by the multivariate generalized distance of Eq. A.3 in the density function of Eq. A.1. When this replacement is made, the univariate normalizing constant $(2\pi)^{-1/2}(\sigma^2)^{-1/2}$ must be changed to a more general constant that makes the ***volume*** under the surface of the multivariate density function unity for any p. This is necessary because in the multivariate case, probabilities are represented by volumes under the surface over regions defined by intervals of the x_i values. It can bee shown that this constant is $(2\pi)^{-p/2}|\Sigma|^{-1/2}$, and consequently a p-dimensional normal density for the random vector $X = [X_1, X_2, \ldots, X_p]'$ has the form:

$$f(x) = \frac{1}{(2\pi)^{p/2}\left|\sum\right|^{1/2}} e^{-(x-\mu)'\sum^{-1}(x-\mu)/2} \qquad \text{(A.4)}$$

where $-\infty < x_i < \infty$, $i = 1, 2, \ldots, p$. We shall denote this p-dimensional normal density by $N_p(\mu, \Sigma)$, which is analogous to the univariate case.

From the expression in Eq. A.4 for the density of a p-dimensional normal variable, it should be clear that the paths of x values yielding a constant height for the density are ellipsoids. That is, the multivariate normal density is constant on surface where the squared distance $(x-\mu)'\sum^{-1}(x-\mu)$ is constant. These paths are called **contours**. An example of two bivariate ($p = 2$) normal distributions is shown in Fig. A.2. More information on how to sample from a multivariate normal distributions and additional properties of the multivariate normal distribution can be found in *Johnson and Wichern, 1992*.

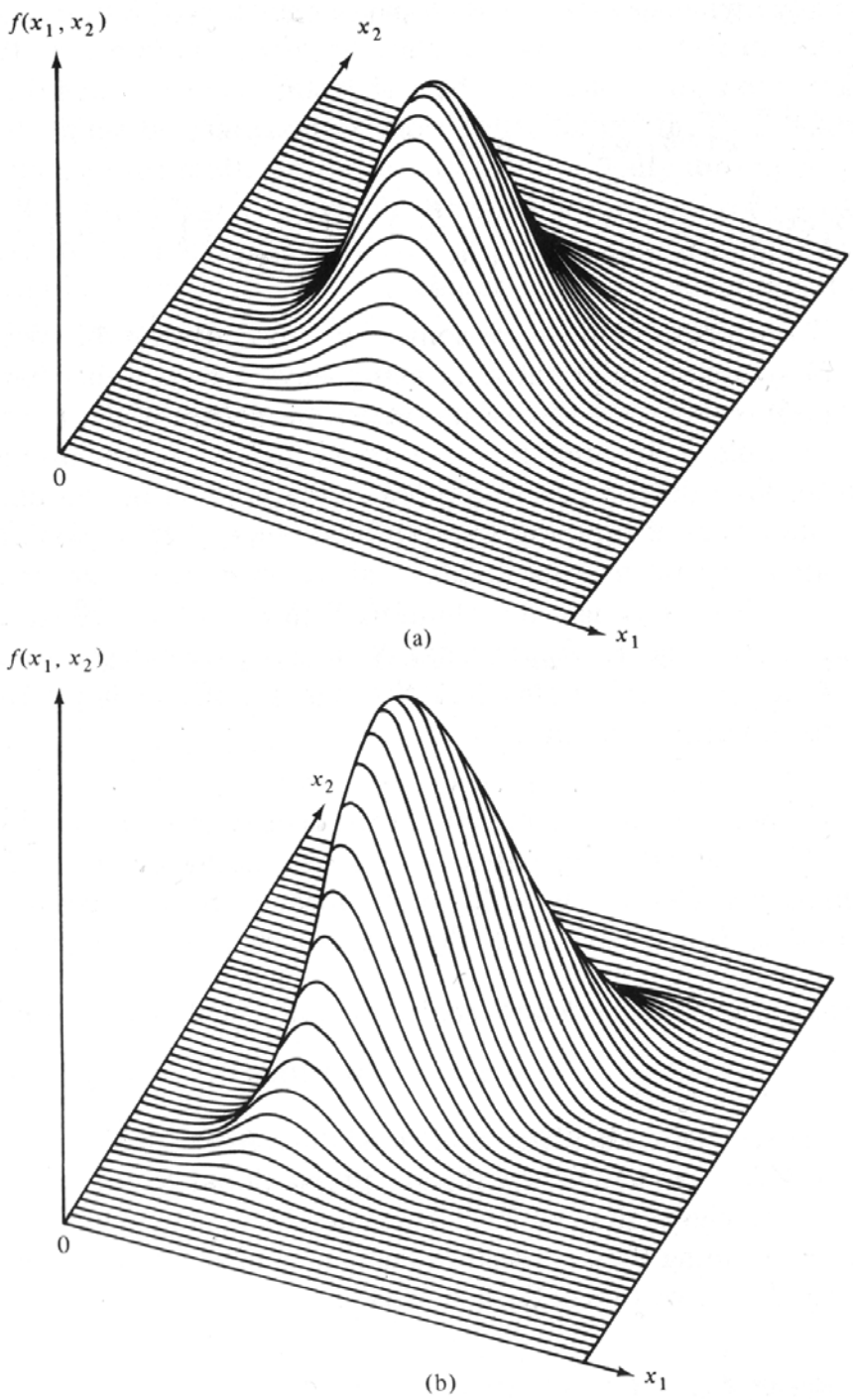

Figure A.2 Two bivariate normal distributions. (a) $\sigma_{11} = \sigma_{22}$ *and* $\rho_{12} = 0$ *(b)* $\sigma_{11} = \sigma_{22}$ *and* $\rho_{12} = 0.75$ *(with* $\rho_{12} = \sigma_{12}/(\sqrt{\sigma_{11}}\sqrt{\sigma_{22}})$*)*

Appendix B

Model Validation

As discussed in 6.4.3, the model verification was performed for the 9 locations along the middle transect (x = 10) of the hillslope. Simulated moisture content values using the effective parameters from the SCE with and without prior information for both the calibration and the validation period at these 9 locations are plotted below.

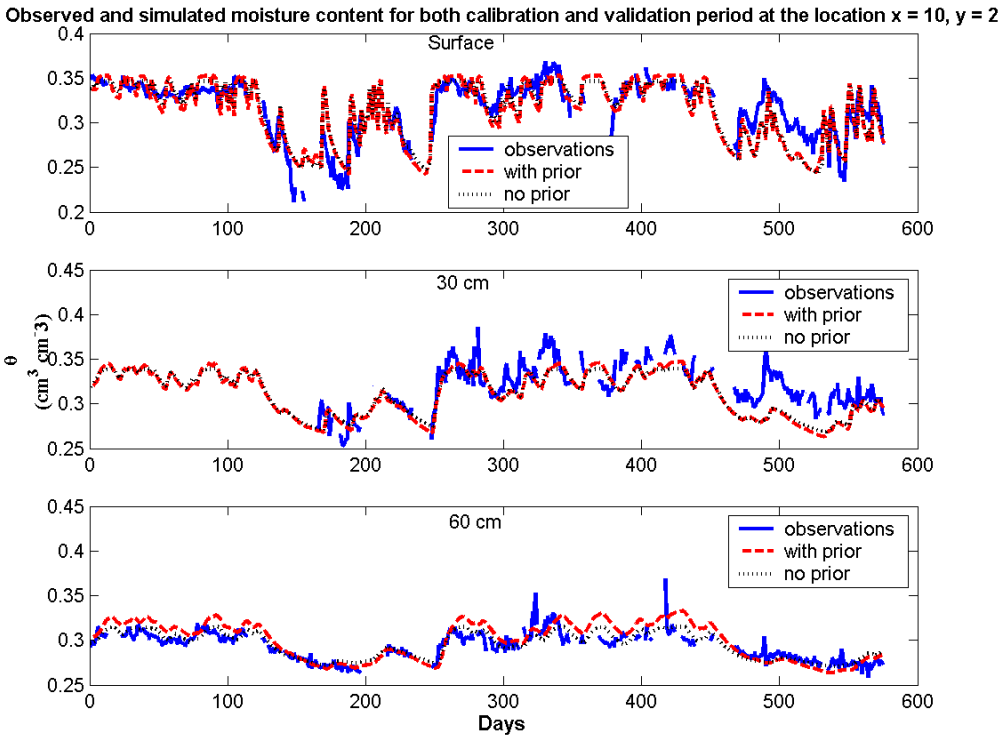

Observed and simulated moisture content for both calibration and validation period at the location x = 10, y = 10

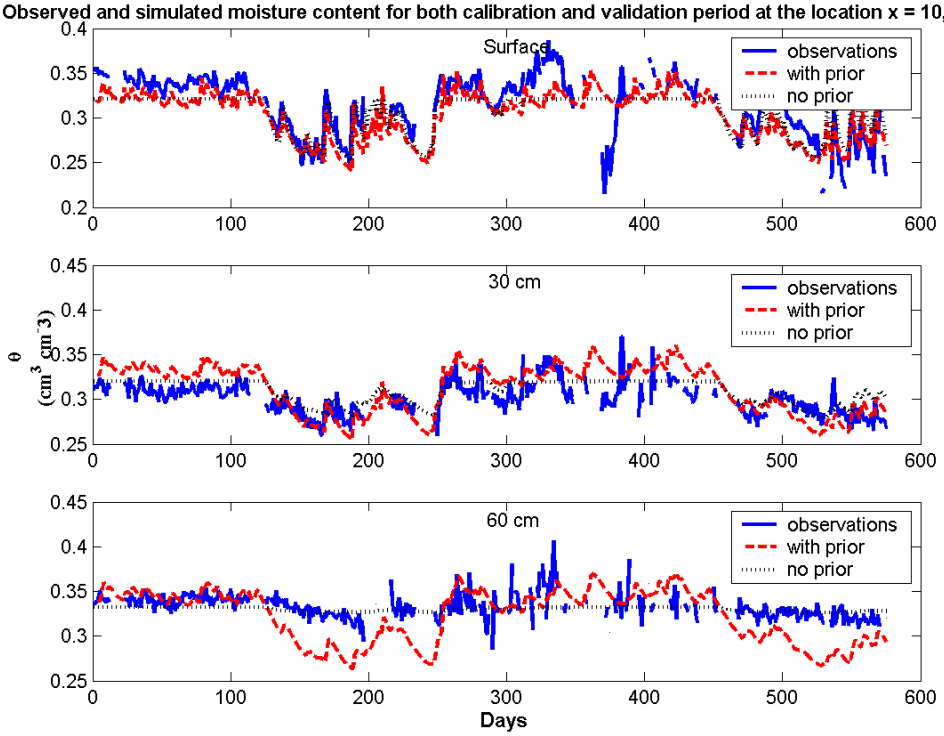

Observed and simulated moisture content for both calibration and validation period at the location x = 10, y = 20

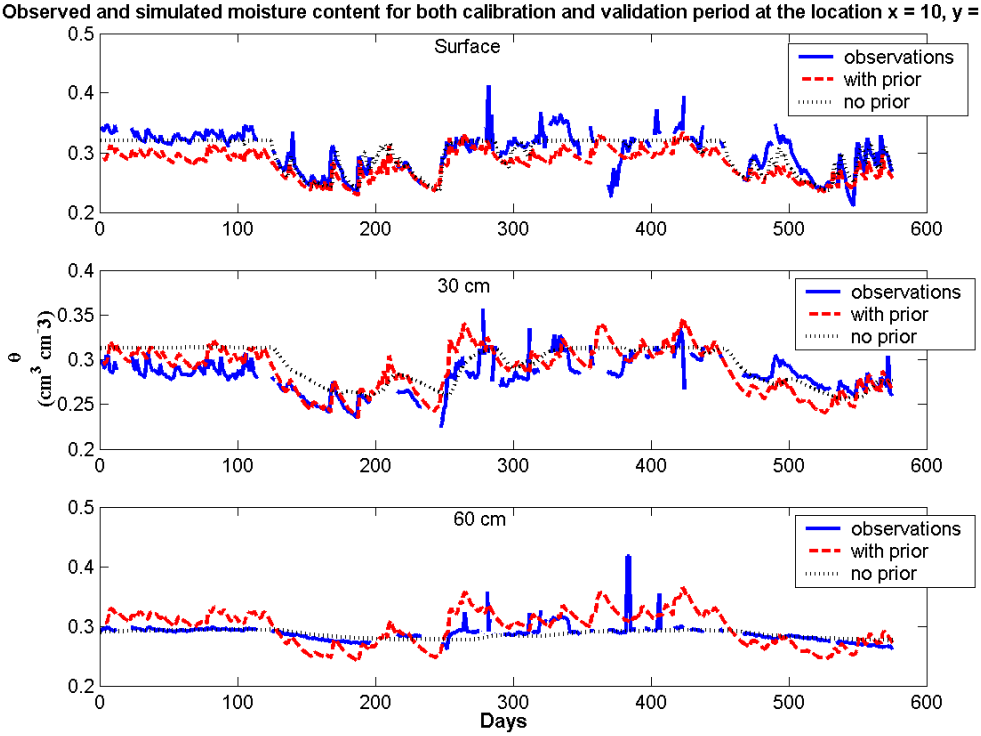

Observed and simulated moisture content for both calibration and validation period at the location x = 10, y = 30

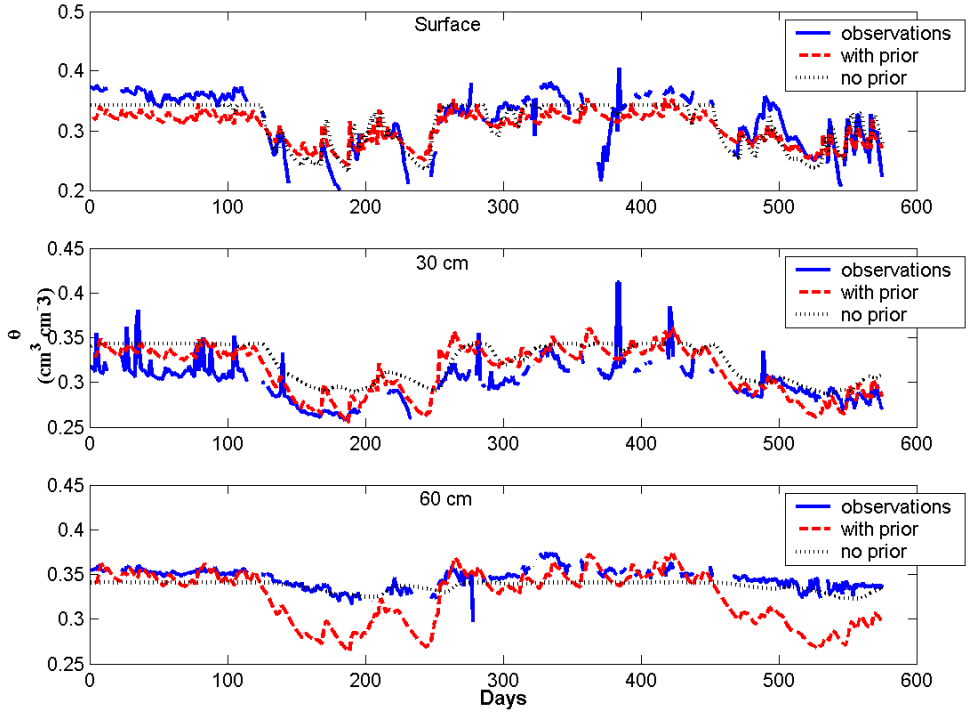

Observed and simulated moisture content for both calibration and validation period at the location x = 10, y = 40

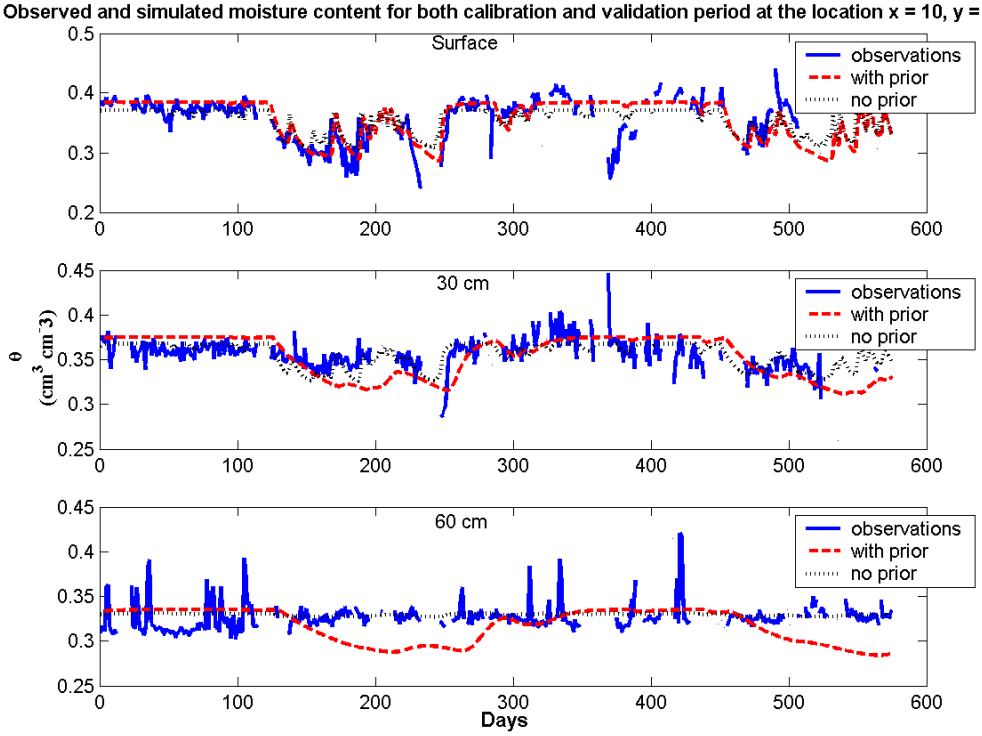

Observed and simulated moisture content for both calibration and validation period at the location x = 10, y = 50

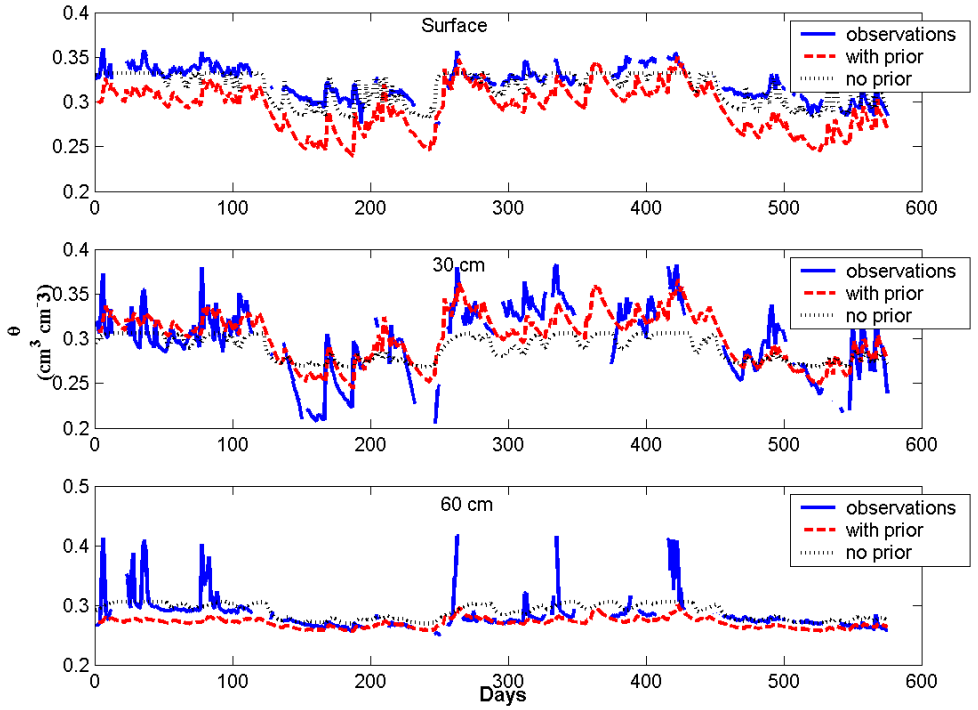

Observed and simulated moisture content for both calibration and validation period at the location x = 10, y = 60

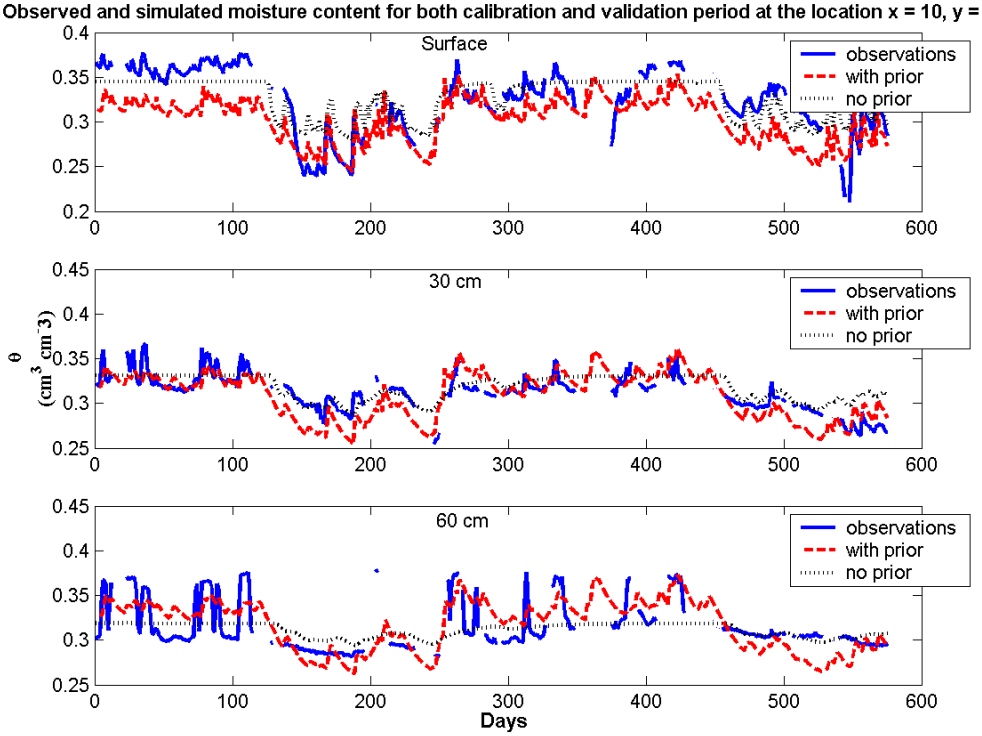

Observed and simulated moisture content for both calibration and validation period at the location x = 10, y = 70

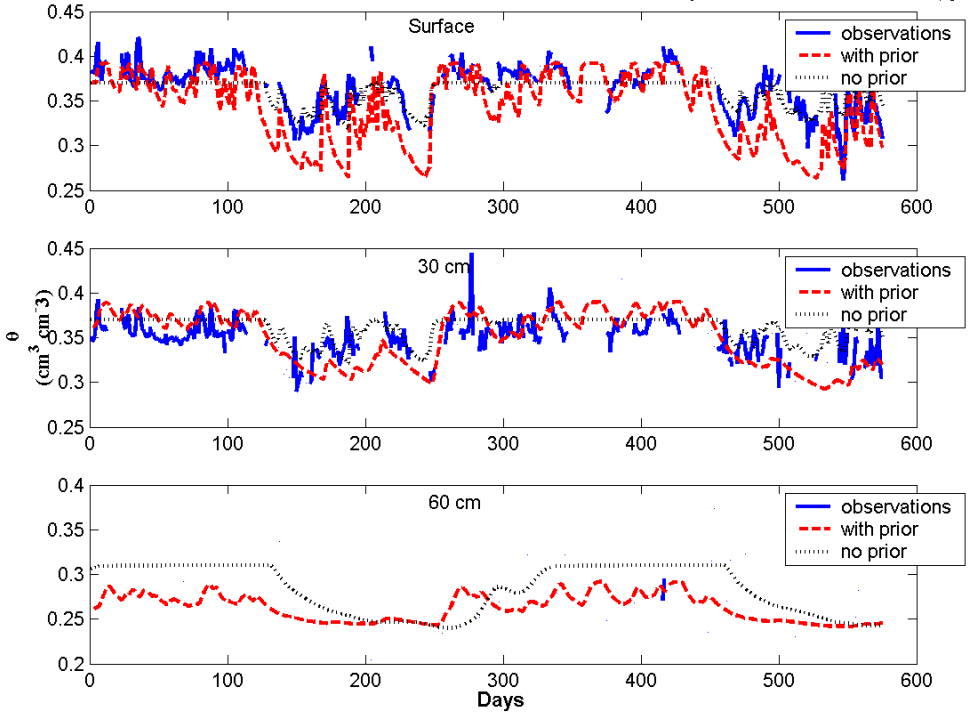

Observed and simulated moisture content for both calibration and validation period at the location x = 10, y = 78

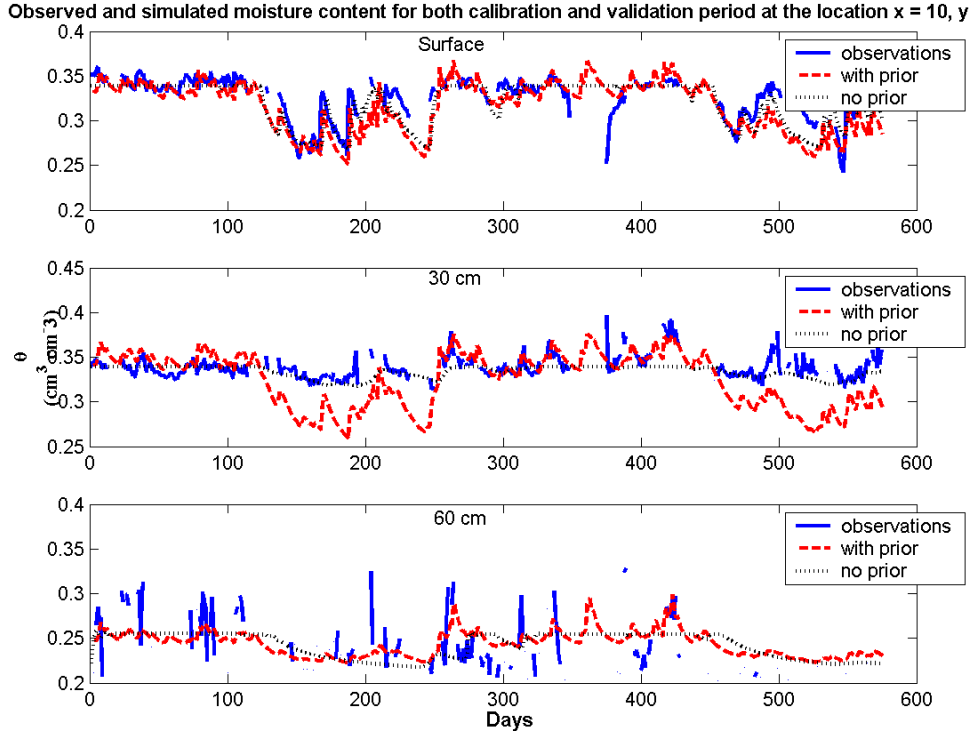

List of Publications

A. Papers in International Peer-Reviewed Journals

Mertens, J., D. Raes and J. Feyen, 2002. Incorporating rainfall intensity into daily rainfall records for simulating runoff and infiltration into soil profiles. *Hydr. Proc*, 16, 731-739.

Mertens, J., D. Jacques, J. Vanderborght and J. Feyen, 2002. Characterisation of the field-saturated hydraulic conductivity on a hillslope: In situ single ring pressure Iinfiltrometer measurements. *J. Hydrol.*, 263, 217-229.

Mertens, J., H. Madsen, M. Kristensen, D. Jacques and J. Feyen, 2003. Sensitivity of soil parameters in unsaturated zone modelling and the relation between effective, laboratory and in-situ estimates. Submitted to *Hydr.Proc.*

Mertens, J., H. Madsen, L. Feyen, D. Jacques, and J. Feyen, 2003. Including prior information and its relevance in the estimation of effective soil parameters in unsaturated zone modelling. Submitted to *J. Hydrol.*

B. Presentations At International Congresses, Symposia, and Workshops: Abstract only or not published

Herman S., Mertens J., Timmerman, A. and J. Feyen. Comparison of tension infiltrometer, single-ring pressure infiltrometer and soil core K_{sat} estimates on a sandy loam hillslope. In: Geophysical Research Abstracts of the XXVIII General Assembly of the European Geophysical Society, Nice, France, 6-11 April 2003, Abs. Nr. EAE03-A-02662.

Mertens, J., G. Govers, D. Raes, G. Wyseure and J. Feyen, 2001. Experimental set-up for the characterisation of the parameter space of a physically-based distributed rainfall-runoff model. In: Geophysical Research Abstracts of the XXVI General Assembly of the European Geophysical Society, Nice, France, 25-30 March 2001, p. 2960

Mertens, J., D. Raes. and J. Feyen, 2001. Disaggregation of daily rainfall records for simulating surface runoff and infiltration into soil profiles. In: Geophysical Research Abstracts of the XXVI General Assembly of the European Geophysical Society, Nice, France, 25-30 March 2001, p. 2586

Mertens, J., D. Jacques, J. Vanderborght, and J. Feyen, 2002. Characterisation of the field-saturated hydraulic conductivity on a hillslope: in-situ single ring pressure infiltrometer measurements. In: Geophysical Research Abstracts of the XXVII General Assembly of the European Geophysical Society, Nice, France, 21-26 April 2002, Abs. Nr. EGS02-A-02262.

Mertens, J., Madsen H., Kristensen M., Jacques, D., and J. Feyen. Parameter estimation strategies in unsaturated zone modelling and the relation between effective, laboratory and in-situ estimates. International Study Group on Inverse Modelling (ISGIM) 2003 meeting, Inverse methods in vadose zone hydrology, Bavaria, Germany, 5 April 2003.

Mertens, J., Madsen H., Kristensen M., Jacques, D., and J. Feyen. Sensitivity of soil parameters in unsaturated zone modelling and the relation between effective, laboratory and in-situ estimates. In: Geophysical Research Abstracts of the XXVIII General Assembly of the European Geophysical Society, Nice, France, 6-11 April 2003, Abs. Nr. EAE03-A-00818.

C. Books and Chapters in Books

Mertens, J. , D. Raes, and J. Ceuppens, 1999. Salinity in the rice schemes of the Senegal Delta. NATURA, The Nectar Programme, Thematic field WATER, Module 4: Deficit irrigation and re-use of non-convential water, Case study, Institute for Land and Water Management, K.U.Leuven.

D. Internal Reports and Other Publications

Mertens, J., 1998. Study of the fluctuation of the watertable in the Senegal Delta, Eindwerk Bio-Ingenieur, K.U. Leuven, p. 103

Mertens, J. and P. Peeters, 1999. Flood control of the Vondelbeek catchment using a Real-Time Fuzzy Logic controller, Eindwerk Masters in Water Resources Engineering: Hydrology, K.U. Leuven en V.U. Brussel, p. 106